UNIVERSITÀ DEGLI STUDI DI MILANO-BICOCCA
DIPARTIMENTO DI FISICA G. OCCHIALINI

CORSO DI DOTTORATO IN FISICA E ASTRONOMIA
CICLO XXVII

Fast neutron measurements for fusion and spallation sources applications

Carlo Cazzaniga

Supervisor: prof. Riccardi Claudia

Thesis Advisor: dr. Tardocchi Marco

Coordinator of PhD school: prof. Chirico Giuseppe

Academic Year 2013-2014

Il sole, con tutti quei pianeti
che gli girano attorno e da lui dipendono,
può ancora far maturare una manciata di grappoli d'uva
come se non avesse nient'altro da fare nell'universo.
– Galileo Galilei

Contents

List of papers

This thesis is based on the following papers, which are referred to in the text by their Roman numerals:

I. Cazzaniga, C., Nocente, M., Rebai, M., Tardocchi, M., Calvani, P., Croci, G., ... Gorini, G. (2014). "A diamond based neutron spectrometer for diagnostics of deuterium-tritium fusion plasmas." *Review of Scientific Instruments, 85(11), 11E101.*

II. Cazzaniga, C., Sundèn, E. A., Binda, F., Croci, G., Ericsson, G., Giacomelli, L., ... Contributors, J. E. (2014). "Single crystal diamond detector measurements of deuterium-deuterium and deuterium-tritium neutrons in Joint European Torus fusion plasmas." *Review of Scientific Instruments, 85(4), 043506.*

III. Cazzaniga, C., Nocente, M., Tardocchi, M., Fazzi, A., Hjalmarsson, A., Rigamonti, D., ... Gorini, G. (2014). "Thin YAP: Ce and $LaBr_3$: Ce scintillators as proton detectors of a thin-film proton recoil neutron spectrometer for fusion and spallation sources applications." *Nuclear Instruments and Methods in Physics Research Section A: Accelerators, Spectrometers, Detectors and Associated Equipment, 751, 19-22.*

IV. Cazzaniga, C., Tardocchi, M., Croci, G., Frost, C., Giacomelli, L., Grosso, G., ... Gorini, G. (2013). "First measurement of the VESUVIO neutron spectrum in the 30â80 MeV energy range using a Proton Recoil Telescope technique." *Journal of instrumentation, 8(11), P11008.*

V. Cazzaniga, C., et al., V. "A Telescope Proton Recoil spectrometer for fast neutron beamlines.", *submitted to Progress of Theoretical and Experimental Physics*

VI. Cazzaniga, C., Croci, G., Giacomelli, L., Grosso, G., Nocente, M., Tardocchi, M., ... Weller, A. (2013). "$LaBr_3$ scintillator response to admixed neutron and γ-ray fluxes." *Nuclear Instruments and Methods in Physics Research Section A: Accelerators, Spectrometers, Detectors and Associated Equipment, 732, 384-387.*

VII. Cazzaniga, C., Nocente, M., Tardocchi, M., Croci, G., Giacomelli, L., Angelone, M., ... Contributors, J. E. (2013). "Response of $LaBr_3$ (Ce) scintillators to 2.5 MeV fusion neutrons." *Review of Scientific Instruments, 84(12), 123505.*

VIII. Cazzaniga, C., et al. "Response of $LaBr_3$ (Ce) scintillators to 14 MeV fusion neutrons." *To be submitted to Review of Scientific Instuments*

Papers not included in this thesis

- Nocente, M., Fazzi, A., Tardocchi, M., Cazzaniga, C., Lorenzoli, M., Pirovano, C., ... Gorini, G. (2014). "Experimental investigation of silicon photomultipliers as compact light readout systems for γ-ray spectroscopy applications in fusion plasmas." *Review of Scientific Instruments, 85(11), 11E108.*

- Croci, G., Cazzaniga, C., Claps, G., Tardocchi, M., Rebai, M., Murtas, F., ... Gorini, G. (2014). "Characterization of a thermal neutron beam monitor based on gas electron multiplier technology." *Progress of Theoretical and Experimental Physics, 2014(8), 083H01.*

- Croci, G., Albani, G., Cazzaniga, C., Cippo, E. P., Schooneveld, E., Claps, G., ... Gorini, G. (2014). "Diffraction measurements with a boron-based GEM neutron detector." *EPL (Europhysics Letters), 107(1), 12001.*

- Fazzi, A., Nocente, M., Tardocchi, M., Varoli, V., Gorini, G., Lorenzoli, M., ... Cazzaniga, C. (2013, October). "A large area SiPM array coupled to a LaBr 3 crystal for a TPR spectrometer." *In Nuclear Science Symposium and Medical Imaging Conference (NSS/MIC), 2013 IEEE (pp. 1-4). IEEE.*

- Croci, G., G. Claps, R. Caniello, C. Cazzaniga, G. Grosso, F. Murtas, M. Tardocchi et al. "GEM-Based thermal neutron beam monitors for spallation sources." *Nuclear Instruments and Methods in Physics Research Section A: Accelerators, Spectrometers, Detectors and Associated Equipment (2013).*

- G Croci, C Cazzaniga, M Tardocchi, R Borghi, G Claps, G Grosso, F Murtas and G Gorini, "Measurements of γ-ray sensitivity of a GEM based detector using a coincidence technique" *2013 JINST 8 P04006*

- M. Nocente, M. Angelone, C. Cazzaniga, I. Chugunov, R.C. Pereira, G. Croci, D. Gin, G. Grosso, A. Neto, A. Olariu, S. Olariu, M. Pillon, A. Shevelev, J. Sousa, M. Tardocchi and G. Gorini "Gamma-ray measurements and neutron sensitivity in a fusion environment." *Proceedings of the 1st International Conference on "Fusion for Neutrons and Subcritical Nuclear Fission", Varenna, 2011*

- Nocente, M., Garcia-Munoz, M., Gorini, G., Tardocchi, M., Weller, A., Akaslompolo, S., ... Tardini, G. (2012). "Gamma-ray spectroscopy measurements of confined fast ions on ASDEX Upgrade." *Nuclear Fusion, 52(9), 094021.*

Abstract

In recent years there has been increasing interest in MeV range neutrons for applied physics studies. This encompasses both thermonuclear fusion experiments, where neutrons are the carriers of the energy released by the fusion reactions, and spallation sources, where there is need to mimic fast atmospheric neutrons to study effects on micro-electronics components. In both research domains there is demand for the development of dedicated instrumentation, which should combine high resolution and high counting rate (MHz) spectroscopy capabilities.
This thesis presents detector solutions based on Single crystal Diamond Detectors (SDDs) and Telescope Proton Recoil spectrometers (TPR). These devices were studied in mock up laboratory tests, as well as in dedicated measurements at nuclear accelerators, at the ISIS spallation neutron source and at the JET tokamak.
While there are certainly commonalities in the measurement requirements of fast neutrons at fusion and spallation facilities, specific distinctions shall also be remarked, which imply different drivers for the detector design. For diagnosing a fusion plasma, one has to measure at high resolution the details of a quasi-monoenergetic spectrum, which is peaked at 14 MeV for deuterium-tritium (DT) and at 2.5 MeV for deuterium plasmas. In a future fusion reactor, energy will be released via the d + t $\rightarrow$ n + α reaction, that occurs in a tokamak between deuterium and tritium in a plasma state. High resolution (<5% FWHM) is needed for neutron spectroscopy because the spectral shape of the neutron emission lines contains information on physical parameters such as the ion temperature or the presence of minority fast fuel ion population; high counting rates (>1 MHz) is crucial in order to provide time resolved measurements on a msec time scale, which is needed to study plasma phenomena such as magneto-hydrodynamic instabilities.
Unlike a tokamak, the neutron spectrum of a spallation source extends over several orders of magnitude, from thermal energies up to the energy of the proton accelerator (800 MeV for ISIS). The majority of beam-lines are dedicated to neutron scattering in the cold (<1 meV), thermal ($\approx$ 25 meV) or epithermal (>1eV) range, as of principal interest for condensed matter studies. Beam-lines dedicated to exploit the fast neutron component (>10 MeV) are however being built, especially in view of those experiments aimed at studying the effect that atmospheric neutrons induce on micro-electronics. For these applications, a neutron spectrum as close as possible to the atmospheric one should be achieved, with the added benefit of significantly increased neutron fluxes. For the design of such beam-lines, the neutron energy spectrum and the spatial distribution of its flux are presently determined on the basis of Monte Carlo calculations that are meant to reproduce the complexity of nuclear and intra-nuclear neutron-matter interactions up to 800 MeV. The accuracy of such modelling however relies heavily on physical assumptions on the interactions, which are often based on poorly known cross sections. Clearly, direct measurements of the fast neutron spectrum actually achieved at a beamline are highly desired, especially to verify the capability of the facility to reproduce the target atmospheric spectrum and to evaluate the accuracy of the simulations, thus shading light on the complex physics of fast neutron interactions with matter. Development of dedicated instrumentation

for fast neutron beam-monitoring is needed in particular for the initial operations of ChipIr, the new ISIS beam-line dedicated to irradiation test of electronic chips. Here measurements have to cope with high instantaneous counting rates (>1 MHz) due to the pulsed nature of the spallation source.
A new diamond based neutron spectrometer has been designed in this thesis for neutron emission spectroscopy studies on fusion deuterium-tritium plasma experiments and spallation sources. The detector features a dedicated electronic chain that combines in a single detector high counting rate capabilities (>1 MHz) and high energy resolution (<3% at 14 MeV neutron energy). So far electronic chains were optimized either for spectroscopy or counting rate capability, but not both at the same time. The response function of a prototype single pixel detector to 14 MeV neutrons has been measured at the Frascati Neutron Generator (FNG) by observation of the 8.3 MeV peak from the $^{12}C(n,\alpha)^{9}Be$ reaction occurring between 14 MeV neutrons and ^{12}C nuclei in the detector. The measured energy resolution (2.5% FWHM) meets the requirements for neutron spectroscopy applications in deuterium-tritium plasmas.
A pilot project of SDD installation at JET was started during this thesis. First simultaneous measurements of Deuterium-Deuterium (DD) and DT neutrons from deuterium plasmas using a SDD are presented. The deposited energy spectrum from DD neutrons is successfully reproduced by means of Monte Carlo calculations of the detector response function and simulations of neutron emission from the plasma, including background contributions. The results are of special interest in view of the development of compact neutron spectrometers for fusion applications, which could be installed in camera systems of present and future high power fusion experiments, where traditional neutron spectrometers based on the time of flight or magnetic proton recoil techniques would not be usable due to space constraints.
The same detector has been used to characterize the fast component of the neutron spectrum of dedicated beam-lines at spallation sources, such as ChipIr at ISIS, which started operations in 2014. In this respect, a first exploratory measurement is presented, which shall be regarded as a basis for future detailed measurements to be carried out in 2015, aiming at a full development of diamond detectors as monitors for fast neutron beam-lines.
TPR spectrometers have also been developed and used to complement information from diamond detectors. Two different TPR designs have been experimentally studied, based on silicon (Si) or inorganic crystal as proton detectors. A Si-YAP (inorganic crystal) TPR concept has been tested on the VESUVIO beam line at ISIS, where recoil protons, converted using a plastic target, were measured by a proton spectrometer, which used a 2.54 cm thick YAP scintillator and a 500 μm thick silicon detector in coincidence. The two detectors measured the full proton recoil energy and the partial deposited energy in transmission, respectively. With the TPR prototype, the VESUVIO fast neutron spectrum was measured up to 120 MeV and results were in good agreement with Monte Carlo simulation of the beam-line.
A second TPR concept completely based on inorganic scintillators has been explored by measurements of the YAP and $LaBr_3$ light yield to protons in the range 4-8 MeV. The experiments were performed at the Uppsala tandem proton accelerator and are of particular interest for a TPR aimed at measuring fusion deuterium-tritium neutrons, as Si detectors may not be able to cope with the high neutron fluxes expected in fusion devices of the next generation. Two thin inorganic scintillators based on YAP and $LaBr_3$ crystals (1" diameter x 0.1" height) have been used for proton measurements in Uppsala. A comparable good energy resolution for the two detectors was shown, better than 2% (FWHM) for 8 MeV protons, which well matches the requirements for an inorganic crystal based TPR for fusion applications. The fast scintillation time of YAP and $LaBr_3$ crystals (less than 30 ns) makes them interesting candidates for operation at high counting rates.
A final part of this thesis has been devoted to the assessment of the background induced by fast

2.5 and 14 MeV neutrons on scintillation detectors. The framework of the investigation was the capability to operate inorganic scintillators, intentionally developed for γ-ray spectroscopy of fusion plasmas, in the harsh, neutron rich environment of next step machines. In fact, in the context of γ-ray measurements for tokamak applications, neutrons are no more the carriers of information, but rather a background source that interferes with the measurements. From an instrumental point of view, it is thus essential to understand the fast neutron response of gamma-ray detectors, especially $LaBr_3$, which was shown to combine good energy resolution (about 3% at 662 keV) and counting rate capabilities exceeding 1 MHz. In this thesis, measurements of the response of a $LaBr_3$ scintillator to 14 MeV and 2.5 MeV neutrons irradiation are presented and explained by means of a dedicated MCNP model. Several reactions are found to contribute to the measured response, with a key role played by neutron inelastic scattering and (n,2n) reactions on ^{79}Br, ^{81}Br and ^{139}La isotopes.
In conclusion, the results presented in this thesis represent a step forward in the development of instrumentation for fast neutron detection of relevance for applications to fusion plasmas and spallation sources. In particular, these results show that common techniques can be adopted to combine good energy resolution (a few percent) and high counting rate capabilities in a single instrument, although the detailed detector design must be tailored to the measurement needs of each individual research field.

Chapter 1

Introduction

Misura ciò che è misurabile, e rendi misurabile ciò che non lo è.
– Galileo Galilei

1.1 Introduction to fast neutrons detection

Due to the sheer fact that a neutron has no electric charge and, for this reason, a very week electromagnetic interaction with matter, a neutron detector always fulfil two major tasks, conversion of the neutrons into secondary particles (usually charged particles), and detection of this secondary radiation within an active volume.
This thesis presents neutron measurements of interest for nuclear fusion experiments and fast neutron beam lines at spallation sources. The focus is on fast neutrons in the *low energy* (E_n<20 MeV) and *intermediate energy* (20 MeV <E_n<1 GeV)range; fusion neutrons have energy of 2.5 MeV and 14 MeV, considering Deuterium-Deuterium (DD) or Deuterium-Tritium (DT) experiments [1], respectively, while spallation neutrons have a wide spectrum up to hundreds of MeV [2].
Neutron detection techniques can be very different with respect to the application and to the neutron energy range. This introduction start with considerations on thermal neutron detection, for two reasons: same methods can be exploited for fast neutrons and most standard fast neutron measurements and dosimetry are based on neutron moderation.
Exothermic nuclear reactions are needed for thermal neutron detection, since they carry to little kinetic energy to induce ionization. More possibilities are open for MeV neutrons, and detectors can be based also on heavy ion recoil and endothermic reactions.

1.1.1 Thermal neutron detection using nuclear reactions and fast neutron counters based on neutron moderation

Reactions suitable for thermal neutron detection feature high cross section and a positive (and possibly large) Q value. The Q value of a reaction is defined as the difference between the masses at rest of the reactants and the masses of the products. A positive Q value means that the products are lighter than the reactants, and the energy difference is released as additional kinetic energy. Only a limited number of isotopes present suitable reactions to be exploited for thermal neutron detection. Tab.1.1 lists the most commonly used reactions, with their cross section quoted at 25 meV, Q values, and relative isotopic abundance. All this parameters are important in evaluating the effectiveness of a detector and its affordability, with particular emphasis on the following considerations:

- High cross section and isotopic abundance implies high efficiency.
- High Q value makes easier the detection, allowing for better discrimination from γ-ray background.
- Reaction with charged products (as the first three listed in the Tab.1.1 and plotted in Fig1.1) are usually preferred with respect to reactions emitting γ-rays, because ideally all the reaction products should deposit all their energy in the detector.

Reaction	Q value	Isotope concentr.	σ (at 25 meV)
$n + {}^{3}He \rightarrow p + {}^{3}H$	0.765 MeV	1.4 E-4 %	5300 b
$n + {}^{6}Li \rightarrow {}^{4}He + {}^{3}H$	4.78 MeV	7.5%	940 b
$n + {}^{10}B \rightarrow {}^{7}Li + {}^{4}He$	$\simeq 2.5MeV$	20%	3800 b
$n + {}^{113}Cd \rightarrow {}^{114}Cd + \gamma$	$\simeq 8MeV$	12%	21 kb
$n + {}^{157}Gd \rightarrow {}^{1158}Gd + \gamma$	$\simeq 8MeV$	16%	255 kb
$n + {}^{235}U \rightarrow fission fragments$	$\simeq 200MeV$	0.7%	505 b

Table 1.1: Parameters of the most commonly used reactions for thermal neutron detection.

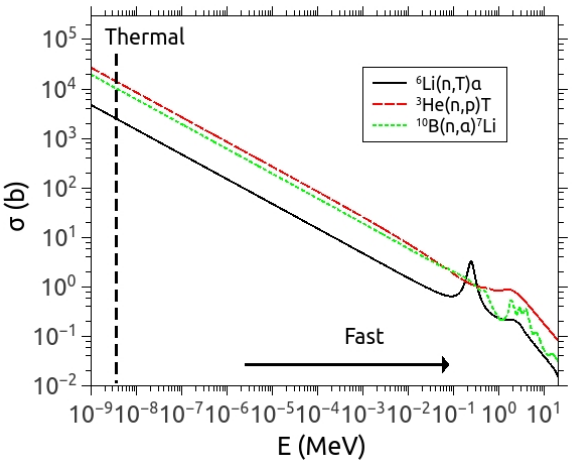

Figure 1.1: Cross sections of reactions of interest for neutron detectors as a function of the neutron energy.

Fig.1.1 shows the cross sections of reactions commonly used for neutron detectors as a function of the neutron energy. A nice review of thermal and fast neutron detectors is presented in Ref.[3], where different methods and techniques are discussed. The selected reactions present very high cross section values at thermal energies, quickly decreasing with the increasing energy of the incoming neutron. The cross section value falls as the $1/v$ law ($E^{-1/2}$).
For this reason, a thermal neutron detector can be used for MeV neutrons with a drop in the efficiency of more than three orders of magnitude. This problem can be overcome by surrounding the thermal neutron detector with a moderator material, hence providing an increased detection efficiency. By optimizing the thickness of the moderator (usually polyethylene) one can select the energy range where the detector is more efficient, as it was shown for the first time by Bramblett, Ewing and Bonner (see Ref.[4]).
The so called Bonner spheres[5, 6, 7] are neutron counters with different moderator thickness, that, with suitable deconvolution algorithms[8], can provide some information about the neutron

energy distribution. Although the spectroscopic capability of Bonner spheres is moderate by comparison with other fast neutron spectrometers (they feature a poor energy resolution due to the similarity of response functions available[8]) they are widely used for two principal reasons: first, they can measure over a very wide range of orders of magnitude in the neutron spectrum (the only spectrometer presently available which will cover the energy range from thermal to the GeV region), and second, the response function of a $\simeq 12$" diameter sphere is very similar to the fluence-to-dose curve for total human body exposure[3], making the bonner sphere a good detector for neutron dosimetry.

1.1.2 Fission counters

Detectors based on fission reaction can be dedicated to thermal neutron measurements using isotopes with large cross sections, as ^{235}U (see Tab.1.1), ^{233}U or ^{239}U. A major advantage of fission detectors is the high Q value of fission reactions ($\simeq 200$ MeV), which guarantees an easy discrimination of signal to background. Fission chambers are gas detectors that, thanks to their capability of operating in large neutron fluxes are often used for in-core operation in fission reactors, or, as discussed below, for beam monitoring in fusion and spallation sources.
As a matter of fact, fission counters can be easily adapted to fast neutron by choosing an isotope with threshold fission cross section, as ^{238}U, which detects neutron with E_n>1 MeV. In Fig.1.2 the cross section of ^{235}U and ^{238}U are reported and one can notice that they can be alternatively used for thermal and fast neutron detection, respectively.

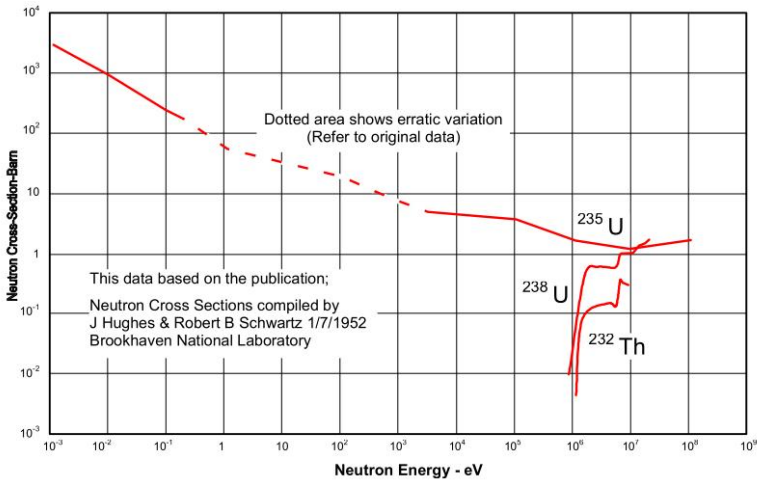

Figure 1.2: Fission cross sections of interest for neutron detectors as a function of the neutron energy.

1.1.3 Fast neutron detection using reactions on Carbon nuclei

In recent years, the technological development of artificially grown single crystal diamond detectors has encouraged the possibility of exploiting endothermic reactions of neutron with Carbon for fast neutron detection. In particular in this thesis the application of diamond detectors to fusion and spallation sources will be discussed. Neutron detection in SDDs is based on the collection of electrons and holes generated in the detector active volume by charged particles produced via neutron-induced nuclear reactions on ^{12}C. Here we present the cross sections of the reactions that allows for fast neutron detection.
The main reactions occurring in carbon are reported in Fig.1.3 for *low energy* neutrons. Due to

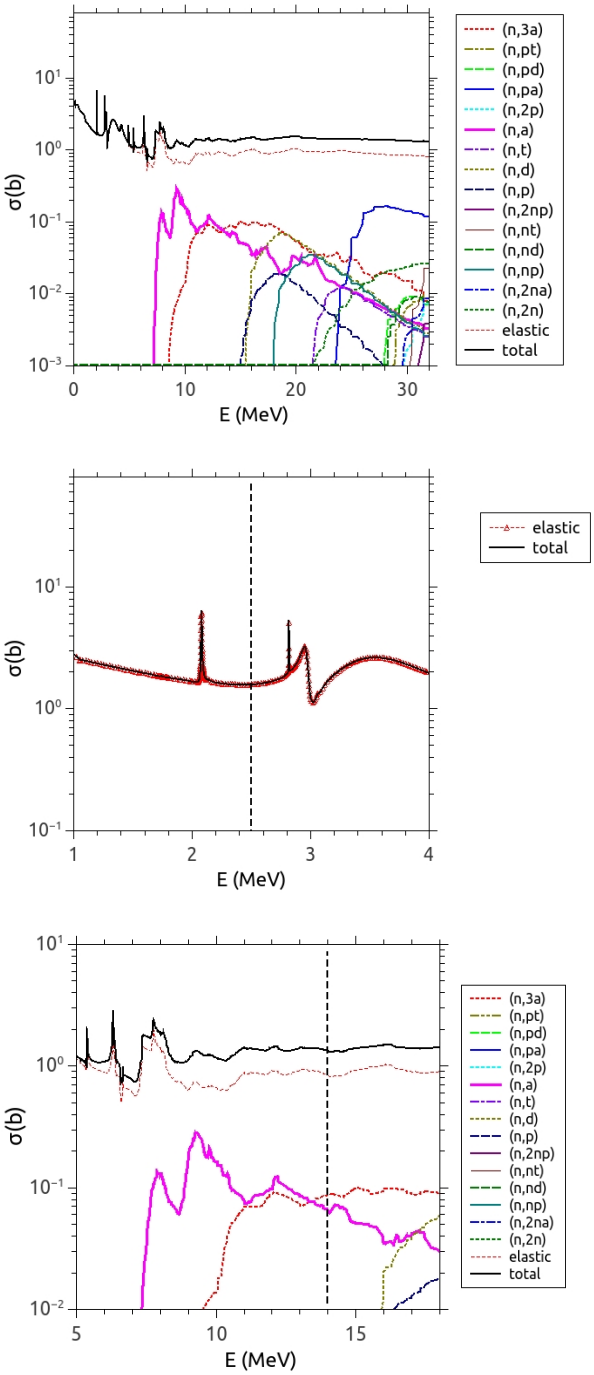

Figure 1.3: ^{12}C cross sections in the *low energy* range of interest for fast neutron detection with diamonds. On the top, all cross section in the *low energy* range. In the middle, cross sections for E_n<4 MeV, of interest for DD neutron measurements. In the bottom, cross sections for 5 MeV <E_n<18 MeV,of interest for DT neutron measurements. Dashed lines indicates 2.5 MeV and 14 MeV values for the middle and for the bottom, respectively.

the variety of available reactions, the nature of the diamond response function is very different according to the neutron energy. For neutron spectroscopy of DD neutron only the elastic scattering is available. For neutron spectroscopy above 6 MeV the most interesting reaction

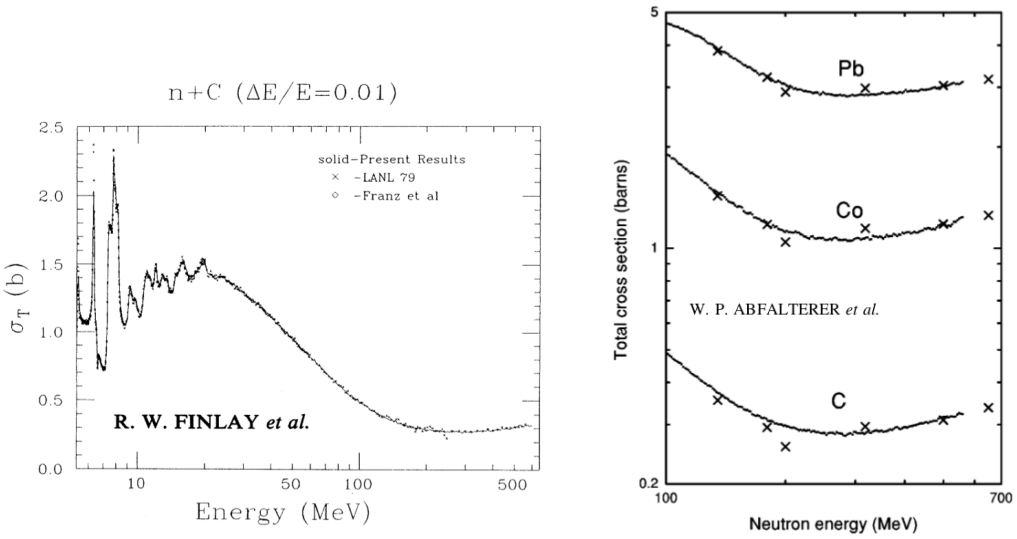

Figure 1.4: ^{12}C total cross section in the *intermediate energy* range of interest for fast neutron detection with diamonds. On the left, cross section from Ref.[9] for E_n<600 MeV. On the right, cross section from Ref.[10] for E_n<800 MeV.

channel is the $^{12}C(n,\alpha)^9Be$ where the deposited energy, ideally, equals the incoming neutron minus the reaction Q-value, therefore giving rise to a peak for DT neutron spectroscopy.
The quantitative interpretation of spectroscopy measurements at spallation sources is somehow limited, with respect to the fusion neutron case, by the incomplete knowledge of the neutron-carbon interaction cross sections above 20 MeV. The ^{12}C total cross section in the *intermediate energy* range, is presented in Fig.1.4 (see Refs. [9, 10]). This cross section includes nuclear cross section as in Fig.1.3 as well as intra-nuclear cascade cross sections.
One can have a first estimation of a diamond detection total efficiency using the following approximated formula

$$\epsilon_{tot} = 1 - \exp(-n\sigma_{tot}(E)d) \tag{1.1}$$

where n is the atom density, σ is the cross section, and d is the detector thickness. Considering $d = 500\mu m$ for the diamond detectors used in this thesis and $n = 176.2 \cdot 10^{21} cm^{-3}$ for diamond ($\rho = 3.5 g/cm^3$), we obtain $\epsilon_{tot} \simeq 1.1\%$ for 2.5 and 14 MeV. This values decrease moderately at intermediate energies: $\epsilon_{tot} \simeq 0.4\%$ at 500 MeV. On the other hand, if for the 14 MeV case we consider only the $^{12}C(n,\alpha)^9Be$ reaction, we calculate $\epsilon_{n,\alpha} \simeq 0.06\%$.

1.1.4 Ion recoil for fast neutron detection

Fast neutron detectors are commonly based on recoil of light nuclei. Elastic scattering of fast neutrons transfer to light nuclei enough energy to induce a signal in a detector. According to the scattering kinematics [3] the energy E_R transfered to the *recoil nucleus* follow the relation

$$E_R = \frac{4A}{(1+A)^2} cos^2(\theta) E_n \tag{1.2}$$

where θ is the recoil angle in the laboratory system and A is the atomic number. From eq.(1.3) one can understand that a larger fraction of energy is given to light nuclei, fixed the angle, with a maximum for $A = 1$. For a given nucleus the maximum energy transfer is for *head-on* collision ($\theta = 0$):

$$E_{R,max} = \frac{4A}{(1+A)^2} E_n \tag{1.3}$$

which corresponds to $E_{R,max} = E_n$ for hydrogen, and $E_{R,max} = 0.284 \cdot E_n$ for carbon. Detectors based on scattering on hydrogen are commonly used, and they consist mostly of organic scintillators [11, 12]. Proton recoil scintillators present a characteristic *box-like* response function to mono-energetic neutron: a countinuum ranging from 0 to E_n. As it will be shown later, a similar *box-like* response function is featured by diamond detectors, when $E_n < 4MeV$, with differences due to the different features of the differential cross sections $\frac{d\sigma}{d\Omega}(E)$.
Similarly to the bonner spheres case, a detector based on ion recoil (a plastic scintillator or a diamond detector operating at $E_n < 4MeV$) can give moderate spectroscopic information, when unfolding algorithms are applied. Limitations are given by the detailed knowledge of the response functions and by its stability versus changing variables (temperature, magnetic fields, fluxes, etc..).

On the other hand, *direct spectroscopy* can be performed using the Telescope Proton Recoil

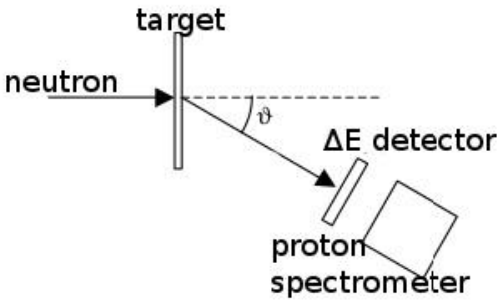

Figure 1.5: Schematics of the PRT experimental setup (not to scale).

(TPR) techniques. In the TPR neutrons are converted into protons in a thin hydrogenated target via elastic scattering, and only protons at a selected angle are detected. The Target ought to be thin with respect to the range of the protons that one aim to measure. In this manner one can retrieve the neutron energy by the simple relation derived from eq.(1.2):

$$E_n = \frac{1}{cos^2(\theta)} E_p \tag{1.4}$$

Recoil protons are detected with a $\Delta E - E$ detector system for background suppression, with a configuration similar to what is shown in Fig.1.5. The first detector is thin and measure only a small fraction of the proton energy. The second detector must be thick enough to stop the proton and measure its full energy E. The geometry of the detectors guarantees that coincidence particles are coming from the target, and $-E$ correlation allows for particle discrimination. Several parameters contribute to the efficiency and energy resolution: the target thickness, the solid angle covered by the detector, the energy resolution of the proton spectrometer.
Efficiency and energy resolution of a TPR spectrometer will be discussed in more details in Chap.3. Here we underline the fact that efficiency of a TPR is eventually due to the differential elastic scattering cross section of neutron on hydrogen. We introduce the empirical fit of the scattering cross section as a function on neutron energy as suggested by Marion and Young [13]

$$\sigma_{el}(E_n) = \frac{4.83}{E_n[MeV]} - 0.578 barns \tag{1.5}$$

In general, a characteristic of a TPR is the low efficiency (usually in the order of 10^{-5}), which is due to two reasons: (1) the target (thin for the protons not to loose too much energy) allows

for a typical efficiency of conversion of the order of $10^{-3} - 10^{-4}$ and (2) the detection solid angle must be small enough to minimize the error on $cos^2\theta$ (see eq.1.3).

1.1.5 Historical Remark

Having recently celebrated 80 years from the discovery of the neutron, made in 1932 by Chadwick[14], it is worth to remark that the discovery itself was driven by an experiment involving recoil of light nuclei. There is not space in these lines to emphasise the importance of this discovery for our understanding of Nature and for technological applications, but only to underline the success of a smart explanation of a rather simple experiment.
In the experiment, the unknown radiation from an α-Be source was converted using thin layers of different materials. Recoil nuclei were recorded using a ionization chamber. If, as it was firstly proposed, these recoil nuclei were due to a Compton scattering of a *quantum radiation* (i.e. γ-rays), it was not possible for energy and momentum to be conserved. The results were easily explained by the brilliant proposal of the existence of a *neutron*.

These experiments have shown that the radiation ejects particles from hydrogen, helium, lithium, beryllium, carbon, air, and argon. The particles ejected from hydrogen behave, as regards range and ionising power, like protons with speeds up to about $3.2 \cdot 10^9$ *cm. per sec. The particles from the other elements have a large ionising power, and appear to be in each case recoil atoms of the elements. [...] These results, and others I have obtained in the course of the work, are very difficult to explain on the assumption that the radiation from beryllium is a quantum radiation, if energy and momentum are to be conserved in the collisions. The difficulties disappear, however, if it be assumed that the radiation consists of particles of mass 1 and charge 0, or neutrons.*

Chadwick (1932)[14]

1.1.6 New challenges in neutron detection: welcome to the digital era

The development, started in early '90s, of high-speed Analog-to-Digital Converters (ADC) opened a wide range of new possibilities in nuclear measurements techniques, and they demonstrated in many cases significant advantages over analog systems. They are particularly useful for applications where good resolution (few %) spectroscopy is needed at high counting rates (MHz), as the applications investigated in this thesis. A traditional analog spectroscopic chain has shaping constants in the μsec time scale. On the other hand, this thesis presents spectroscopy results obtained with signals with width in the $10nsec$ time scale.
The ADC acquires multiple sample of the pulse (that we call $V(t)$) during its duration and converts these samples into a sequence of digital values that represent the voltage level (V_i).

Sampling frequency Sampling frequency is the speed at which the ADC converts the input signal to digital values. The sampling frequency of a high-speed digitizer is based on the sample clock that tells the ADC when to convert the instantaneous analog voltage to the digital values. The choice of the sampling frequency for a given application is driven by the Nyquist-Shannon theorem, which states: "If a signal V(t) contains no frequencies higher than f_{nyq} it is completely determined by giving its ordinates at a series of points spaced $\Delta t = 1/(2f_{nyq})$ apart" [15]. In other words, there is no additional information at sampling at a rate greater than twice the highest frequency component of the signal.

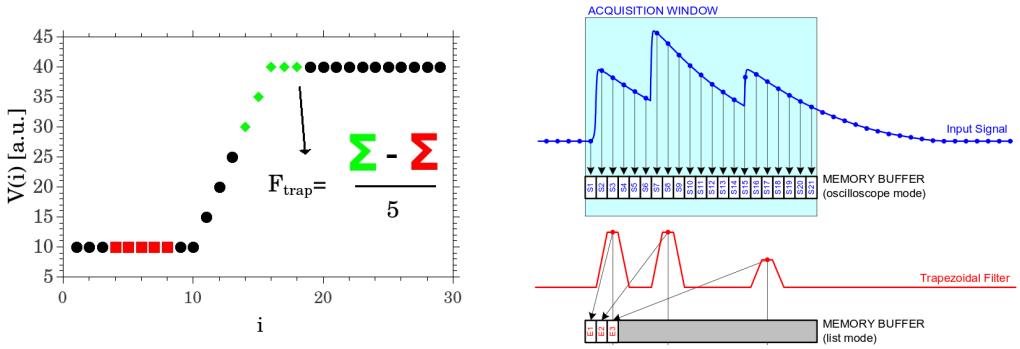

Figure 1.6: Schematic representation of the *trapezoidal filter algorithm*. On the left, a visual representation of how $F_{trap}(i)$ is calculated (eq.1.8) by the difference of mean values of two windows of length G separated by a distance L. On the right, a visual representation of how three pulses are analysed in a signal (blu line) thanks to a trapezoidal filter (red line). Figure on the right taken from Ref.[21].

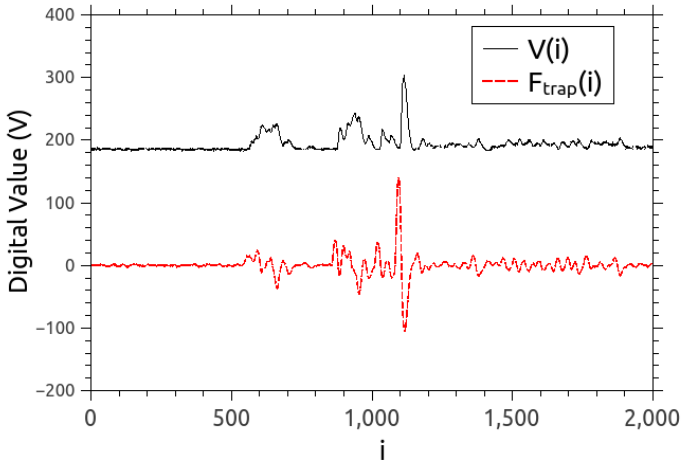

Figure 1.7: Examples a *trapezoidal filter* applied to fast signals.

ADC Resolution The resolution of an ADC is determined by how many parts the maximum signal can be divided into, which correspond to 2^n for an n-bit ADC. For example, a 12 bit ADC has a number of *codes* of $2^{12} = 4096$. Therefore, our best resolution is 1 part out of 4096, or 0.0244% of the full scale.
The choice of the ADC Resolution for a given application is driven by the signal to noise ratio of the electronic chain: the fundamental idea is that even if the ADC returns, say, an eight-bit value, the significance of the result can be reduced because of noise so that fewer of the bits are significant [16].

Fitting Algorithms One of the main advantages of digital acquisition is that, after the conversion to digital data, the information can be extracted by *off-line* (or *post-mortem*) analysis. This can involve fitting algorithms that have a degree of complexity too high to run *on-line*. In this thesis (*Papers VI, VII and VIII*) I made use of a fitting algorithm for Pulse Height analysis of pulses from inorganic scintillators developed by the Milano spectroscopy group and presented in Ref.[17]. Other algorithms can be dedicated, for example, to enhance the timing

performance of a digital system [18, 19] or for particle discrimination via pulse shape analysis [20].

Filters Digital filters are algorithms that shape the signal pulse. The shaping $F(t)$ of an analog signal can be mathematically represented by the convolution of the signal $V(t)$ with a shaping impulse *response function* $H(t)$. For a finite response function of length L this correspond to

$$F(t) = \int_{t-L}^{t} V(t') \cdot H(t - t')dt' \tag{1.6}$$

where it is assumed that only event in the past, with respect to a certain time t, can give a contribution.
The discrete representation of eq.1.6, valid for digital signal can be expressed as

$$F(i) = \sum_{j=i-L}^{i} V(j) \cdot H(i - j) \tag{1.7}$$

where $F(i)$ represents the new sequence of values that derives form the original sequence of values $V(i)$. In particular in this thesis a *trapezoidal filter* has been used (*Papers II, IV and V*), and its matematical representation is given by

$$F_{trap}(i) = \frac{1}{G}\left[\sum_{j=i-G}^{i} V(j) - \sum_{j=i-(L+2G)}^{i-(L+G)} V(j)\right] \tag{1.8}$$

where G and L are two parameters of the filter. The *trapezoidal filter algorithm* produces a new sequence of value F_{trap} calculated (eq.1.8) by the difference of mean values of two mobile windows of length G separated by a distance L. A visual representation is given in Fig.1.6. The *trapezoidal filter algorithm* is particularly useful when more pulses are close enough that one sits on the tail of the other (i.e. high rates applications). In this case, if the information is given by the pulse amplitude, after the trapezoidal filtering the information is given by maxima in the filtered sequence of values, as it is visually represented Fig.1.6 (on the right taken from Ref.[21]).
The trapezoidal filter is usually applied for signals with a fast rise time and a long tail, as it is the case for signals shown in Fig.1.6. It can however be applied to fast signals, when the parameters (G and L) are correctly chosen. This is the case for signal used in this thesis. In particular, the parameter L has to be equal to the signal rise time τ_{rise}, and the parameter G has to be much lesser then the decay time τ_{fall}. An example of the *trapezoidal filter* applied to fast signals is shown in Fig.1.7, where $L = \tau_{rise} = 10$ and $G = 2 << \tau_{fall}$ (every sampling point here corresponds to 1 ns). It is worth to notice that the filtered function is no longer a trapezoid, but an *undershoot* is introduced by the fast tail. Nevertheless, the information on the Pulse Height is given by maxima in the filtered sequence of values.

1.2 Introduction to Nuclear Fusion applications

1.2.1 The tokamak

Plasmas with temperatures in the keV range are necessary for producing fusion energy on the Earth. The toroidal device where the high temperature plasma is confined by magnetic fields (with toroidal and poloidal components) is called the *tokamak* (figure 1.8). A comprehensive review of tokamak properties is given in Ref.[22].
Fusion research has selected as best candidate the d + t $\rightarrow \alpha$ + n reaction (figure 1.8) for its high reactivity ($< \sigma v >$) at temperatures in the keV range and high Q value. In a d + t $\rightarrow \alpha$ + n reaction occurring in a DT plasma confined by a tokamak, the released 17.5 MeV energy per reaction are shared between the neutron and the α - particle in inverse proportion to their mass: the lighter neutron carries 14 MeV, while the four times more massive α - particle has the remaining 3.5 MeV.

Fusion products. Both the α -particle and the neutron are fundamental for different reasons. The neutron is unaffected by the magnetic fields that confine the plasma and leaves the tokamak. It is useful because (1) its kinetic energy can be converted to thermal energy by an *ad-hoc* designed blanket surrounding the tokamak [24] and because (2) it can *breed* the Tritium (the reactor fuel) via reactions with Lithium [25, 26]. The α - particle on the other hand remains confined in the plasma. Its role is vital for the self-sustainment of fusion reactions. α - particles, that are produced at an energy much higher than the average deuterium and tritium temperatures, need to transfer their energy to the reacting ions by slowing down in the bulk plasma to get the reaction going. This self heating has to be high enough to compensate for inevitable power losses.

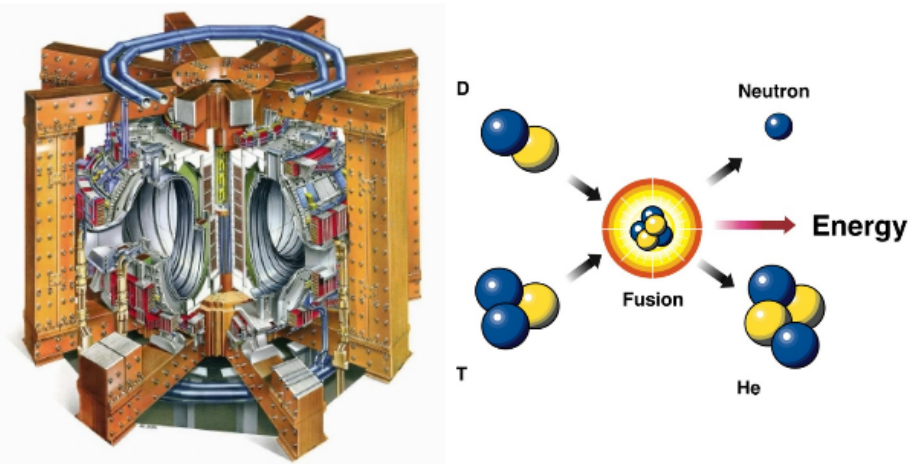

Figure 1.8: Illustration of a section of the JET tokamak [23] (on the left) and of the d + t $\rightarrow$ α + n reaction occurring in a DT plasma.

Plasma heating. To create a thermonuclear fusion plasma requires heating the fuels with auxiliary systems:

- **Ohmic Heating or Current Drive** From an electrotechnic point of view, a tokamak is a huge transformer. A current is driven into the coils around the central pole of the torus,

that act as the primary loop. A large current is induced in the plasma, the secondary loop. This plasma current produces heat, just as a wire warms up when an electric current flows through it. Other mechanisms can be used to drive a current in a tokamak, as the Lower Hybrid Current Drive [27]. Tokamaks largely rely on plasma current not only for heating, but also for the poloidal magnetic field.

- **Neutral Beam Injection (NBI)** High energy neutral particle beams injected into the plasma transfer their energy as they collide with the plasma ions [28, 29]. A particle beam is generated by accelerating ions with high voltage. Since the charged particles cannot penetrate the magnetic field around the plasma, they are turned into neutral atoms just before injection. The JET NBI system can produce neutral with kinetic energy up to 125 keV [30].

- **Radio-Frequency (RF) Heating** The plasma particles have different resonance frequencies, depending on their mass and charge and the magnetic field strength at their location. Therefore the heating can be applied selectively to a defined group of particles in a defined location in the plasma, by injecting radiation at just the right frequency. This is known as Ion-Cyclotron Resonance Heating (ICRH), or Electron-Cyclotron Resonance Heating (ECRH), depending if the frequency is set to resonate with positive ions or electrons, respectively.

- **Self-heating via d + t $\rightarrow \alpha$ + n reactions** For a fusion power reactor, the alpha particles fusion power must exceed, during steady operation, by more then 10 times the auxiliary heating power. *Burning plasma* physics will require study to gain sufficient knowledge to be able to design a prototype reactor. The ITER project has an overall programmatic objective "to demonstrate the scientific and technological feasibility of fusion energy for peaceful purposes" [32].

Fast ions. Good confinement of alphas is essentially required in realizing a nuclear fusion reactor. The fusion alpha particles and the ions accelerated to high energies by auxiliary systems (e.g. NB, RF) can modify the macro-behaviour of the plasma. In particular, they can interact with fluid-type (MHD) modes in the plasma causing them to grow (become unstable), and the non-linear development of such modes may cause the loss of the energetic particles [33, 34]. Uncontrolled instabilities are a major threat for a thermonuclear reactor, as they can limit the fusion performance or even cause abrupt losses of the plasma itself, called disruptions, which can cause damage to the first wall due to high power deposition.
A high power, large volume deuterium-tritium plasma is an intense source of neutrons and γ-rays, which can be used for fast ions diagnostics as discussed in Ref.[35].

1.2.2 Neutron measurements at tokamaks

In a tokamak the neutron emission is peaked at 14 MeV for deuterium-tritium (DT) and at 2.5 MeV for deuterium plasmas. As a matter of fact, in recent years, and therefore during this thesis, no tokamak has performed operations with DT plasmas, but only deuterium plasma. In a deuterium plasma 2.5 MeV neutron are emitted by the d + d $\rightarrow$ ^{3}He + n . A competing reaction is the d + d $\rightarrow$ ^{3}H + p (with 50% breanching ration) presenting no neutron emission, but responsible from the breeding of some tritium, which in turn gives a small (in the order of 1%) DT emission also in a deuterium plasma (*Paper II*).
Measuring fusion neutrons gives essential informations for the control of a fusion plasma. Neutron diagnostics can play different roles as neutron yield monitors, cameras and spectrometers[36].

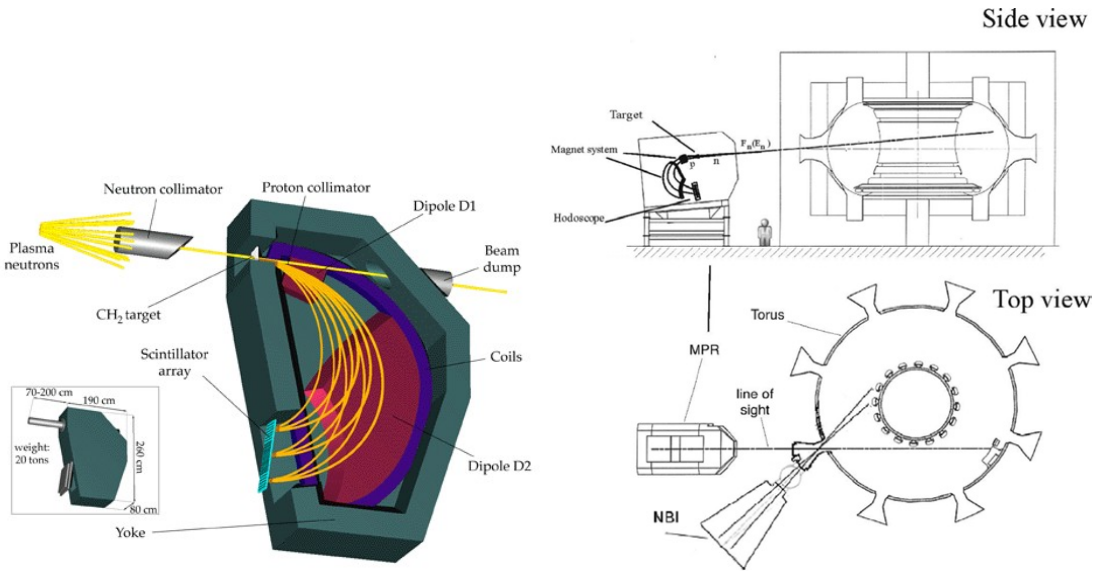

Figure 1.9: On the left, schematics of the Magnetic Proton Recoil spectrometer Upgrade (MPRu) installed at JET for DT plasmas. On the right the line of sight is shown with a side and top view of the JET tokamak. Figures taken from Ref.[50].

Neutron yield monitors Detectors to monitor the neutron inclusive flux are installed on most fusion plasma devices [37]. These measure the uncollimated flux which can be related to the total neutron yield, $Y_n(t)$, given appropriate calibration [38, 39, 40]. At JET the Fission Chambers and the Activation System methods have maintained the neutron measurement capability since 1984 with accuracies of 8-10%. The Fission Chamber (FC) neutron monitors comprise 3 pairs of moderated ion chambers containing ^{235}U and ^{238}U (see Ref.[40]). In this thesis we used measurements of $Y_n(t)$ from the JET fission chambers in *Papers II and VII*.

Neutron cameras A tomographic diagnostics is based on measurements of the neutron flux in arrays of collimators (cameras) whose lines of sight intersect the plasma in the poloidal plane. For a good tomographic reconstruction it is preferred to have two perpendicular cameras each with good radial coverage. Using a neutron camera, profiles of different types of plasma parameter information can be extracted. Neutron cameras are present in todays tokamaks, name JET [41, 42] and MAST [43], and are in view for ITER [44]. The quality of the information and the parameters that can be measured depend, obviously, by the performances of the neutron detectors of the camera. For example, information is added if detectors have spectroscopic capabilities.

Neutron emission spectroscopy For diagnosing a fusion plasma, one has to measure at high resolution (a few %) the details of a quasi-monoenergetic spectrum, which is peaked at 14 MeV for deuterium-tritium (DT) and at 2.5 MeV for deuterium plasmas. High counting rates (>1 MHz) are a key requirement for studying the interaction among fast ions and MHD instabilities on next step tokamaks on the msec time scale.
Concerning the neutron emission lines of a plasma, if the reactants had no velocity the neutron energy would be constant and exactly equal to 14.0 MeV and 2.45 MeV for the DT and DD reaction, respectively. When (which is always true) the reactants are not at rest, the energy of the products is shifted by a quantity that depends on the reactants kinetic energy and on the emission direction of the neutrons. This effect is responsible for the Doppler broadening

effects in the neutron emission. In a thermal plasma (with a Maxwellian velocity distribution and ion temperature T_i) the neutron line is of nearly Gaussian shape with a thermal Doppler broadening. The FWHM of the peak is proportional $\sqrt{T_i}$, which can be directly used to measure T_i [45].
However a fusion plasma is seldom at thermal equilibrium; when external heating is present in the form of NBI, ICRH or self heating, the fuel ion energy distribution develops non-Maxwellian components and even anisotropies with respect to the magnetic field direction. The neutron spectrum carries information on the reactants energy distribution, as demonstrated with dedicated work carried out mostly at the JET tokamak [50, 53].
In addition to information on the fast fuel (d and t) ion distribution, NES measurements can also provide insights into other minority, non-fuel fast ion population via the so-called *knock-on* processes [46]. A review of diagnosis of physical parameters of fast particles in high power fusion plasmas with high resolution neutron spectroscopy was recently presented in Ref.[47].

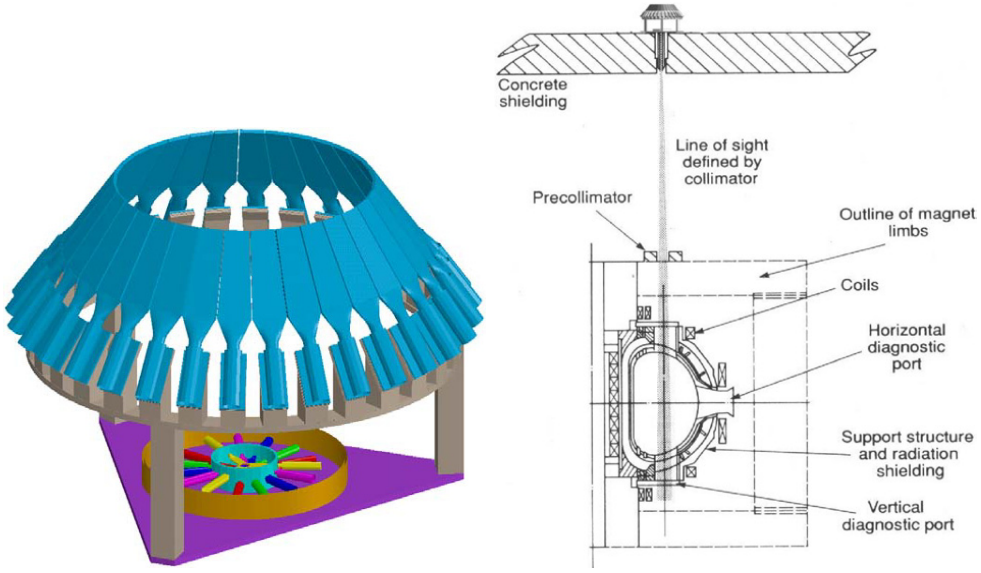

Figure 1.10: On the left, picture of the TOFOR neutron spectrometer installed at JET for D plasmas. On the right the details of the line of sight are shown. Figures taken from Ref.[52] and Ref.[47]

1.2.3 Instrumentation for high resolution neutron spectroscopy

At JET, a Magnetic Proton Recoil (MPR) spectrometer has been used for 14 MeV neutron measurements at 5% resolution, providing information of unprecedented detail on neutron emission from the plasma [48, 49, 50]. Collimated neutrons impinge on a thin foil, where a small fraction of the neutrons undergo elastic nuclear scattering on hydrogen nuclei (protons). A magnetic field separates the recoil protons according to their energy. Finally, the positions of the protons are actively measured in a position sensitive scintillator array placed in the curved focal plane of the magnet (the hodoscope). An illustration of the MPR working principle is presented in Fig.1.9. In the same figure, on the right, the tangential line of sight of the MPR (crossing twice the plasma core) is shown.
At JET the TOFOR spectrometer is optimized for 2.5 MeV neutrons, whose energy is measured with the Time of Flight technique [51, 52, 53, 54]. TOFOR uses plastic scintillator detectors, with the first (S1) placed in a collimated beam of neutrons, a fraction of which is detected

through the proton recoils produced in the scattering process. The second detector (S2) is placed a known distance L away from S1 and records a fraction of the scattered neutrons, again through proton recoils. S1 gives the start signal and S2 the stop one. A schematics of the TOFOR detector is presented in Fig.1.10. In the same figure, on the right, the vertical line of sight of the TOFOR is shown.

In Fig.1.11 results of the MPR and TOFOR spectrometers are shown. One can notice how the neutron emission spectrum changes due to physical parameters related to different plasma heating scenarios. In particular, during the ohmic phase the neutron emission is thermal (i.e.the peak is almost gaussian) with a spectral broadening due to a temperature of 2.3 keV, for JET DT discharge 42759, as measured by the MPR spectrometer. During the ICRH phase of the same discharge the peak is larger due to an increased temperature of 4.7 keV [55]. A tail (in the red circle) appears due to a fast ion population with a measured equivalent temperature of about 200 keV. On the right in Fig.1.11, measured time of flight spectra by the TOFOR spectrometer for the JET Deuterium discharge 74952 collected during the NBI (red) and ICRH (blu) phases [56, 57, 58].

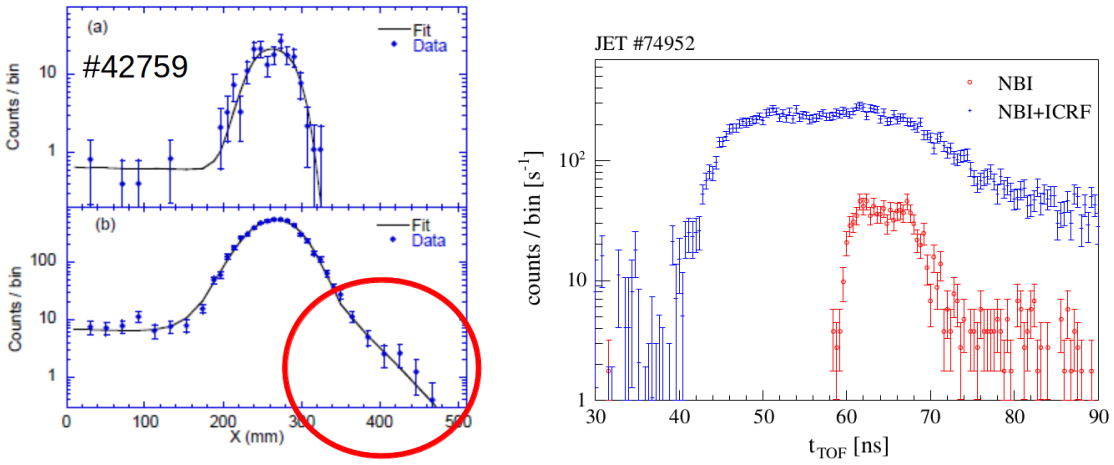

Figure 1.11: On the left, proton recoil spectra measured by the MPR spectrometer for the JET DT discharge 42759 collected during the Ohmic (top) and ICRH (bottom)phases, shown together with the best fit to the data. The neutron energy increases along the hodoscope x-axis. Figure taken from Ref.[47]. On the right, measured time of flight spectra by the TOFOR spectrometer for the JET Deuterium discharge 74952 collected during the NBI (red) and ICRH (blu)phases. Figure taken from Ref.[56].

1.2.4 Compact spectrometers

The spectrometers that have given so far the best results (the TOFOR and the MPR) are heavy and bulky so, of course, it is tempting to explore how to reduce the size. For example, the significant dimensions (several tens of meter) and weight (about 20 ton, plus 60 ton of shielding) of the instrument do not make the MPR technique particularly suitable for applications where there are space limitations, such as arrays of neutron detectors arranged in a camera system. Development of compact spectrometers has been focused on *liquid scintillators*, *diamond detectors* and *Thin-film Proton Recoil*.

At this point a distinction must be addressed. A *genuine spectrometer* present a direct correspondence between the measured signal and the energy of the neutron. In other words, for a mono-energetic neutron emission the response function of the spectrometer is ideally a delta

function, which is broadened in the real measurement by the finite energy resolution of the spectrometer.
On the other hand, in a detector with *moderate spectroscopic capability* the response function of mono-energetic neutrons is complex and present broad structures. As this is an intrinsic characteristic of the detector, one has tried to compensate for the broad spectral information content in the data by the development of advanced data unfolding techniques [60]. The accuracy of the reconstructed neutron spectrum is affected by the knowledge of the response function (which can be perturbed by detector instability [59]) and by the statistics of the measurements. These compact spectrometers with *moderate spectroscopic capability* are not an alternative to genuine neutron spectrometers.

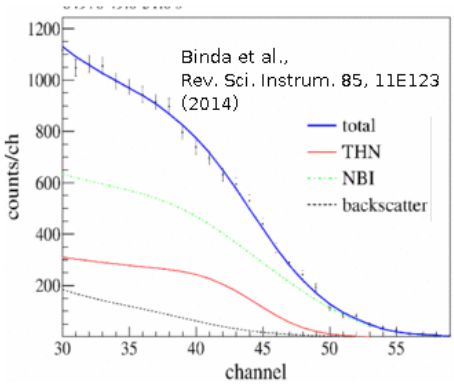

Figure 1.12: Pulse height spectrum measured with a NE213 compact spectrometer from a JET deuterium discharge collected during the NBI phase. The components are the thermal component (red solid line), the beam-thermal component (dashed-dotted green line), and the backscatter component (dashed black). The sum of the components is the blue bold line. Figure taken from Ref.[64]

Liquid scintillators Interest has been developed to explore the use of detectors, such as liquid scintillators for use as *compact spectrometers* with *moderate spectroscopic capability* in neutron cameras.
Spectrometers based on NE213 liquid scintillating material are commonly used to characterize neutron (n) emissions either from sources or produced at accelerator facilities [61]. Since NE213 is also sensitive to gamma (γ) radiation, in neutron measurements in mixed n-γ-fields the capability of neutron and the gamma discrimination via pulse shape analysis is an advantage for these detectors[62].
A NE213 was installed at JET on the same line of sight of the MPR spectrometer (see Fig.1.9) by the Uppsala university group [64]. Pulse height spectrum measured with a NE213 compact spectrometer from a JET deuterium discharge collected during the NBI phase is presented in Ref.[64] and shown in Fig.1.12. In Ref.[64] it is shown how applying a forward fitting procedure using modeled spectral components one can extract information on the plasmas (in this case the fraction of thermal neutron emission).
The diamond detector presented in this thesis was installed on the same collimated line of sight of the MPR and NE213 detector, and a comparison of the data is discussed (see *Paper II*).

Diamond detectors Single crystal diamond detectors (SDDs) feature advantages such as radiation resistance and low sensitivity to magnetic fields and γ-ray background, which make them interesting candidates for operation in the harsh environment of a high power tokamak.

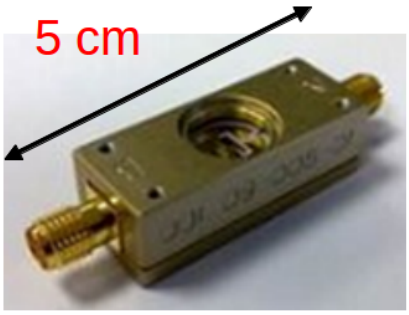

Figure 1.13: Picture of the prototype diamond detector installed at JET on a collimated line of sight.

A diamond is a *genuine spectrometer* for 14 MeV neutrons, thanks to the $^{12}C(n,\alpha)^{9}Be$ reaction, while it presents *moderate spectroscopic capabilities* for 2.5 MeV neutrons, when the pulse height spectrum is determined by elastic recoil on carbon.
Previous proof-of-principle measurements of 14 MeV neutrons with natural diamond detectors were performed in tokamak experiments with deuterium-tritium (DT) plasmas and are reported in [65, 66]. The use of artificially grown SDDs for applications to neutron measurements in fusion plasmas is recent and was so far focused on the determination of the time traces of 14 MeV neutron emission from trace tritium experiments at JET [67].
In this work it is presented the design of a new system based on a matrix of 12 SDD pixels, each equipped with independent high voltage supply and read-out electronics, designed for 14 MeV neutron spectroscopy applications in plasmas of deuterium-tritium (DT). The matrix is proposed for installation at JET on a collimated vertical line of sight in view of the next DT campaign. The results of a calibration at the Frascati Neutron Generator with 14 MeV neutrons impinging on a prototype single pixel detector are also presented, focusing in particular on the measured response function and energy resolution *(Paper I)*. A prototype single pixel diamond detector (see Fig.1.13) has been installed at JET during this thesis. The feasibility of neutron spectroscopy with SDDs has been demonstrated by measurement of the 2.5 MeV neutron spectrum from JET deuterium plasmas, together with 14 MeV neutrons from triton burn up emission *(Paper II)*.

TPR The Telescope Proton Recoil (TPR) spectrometer could be an interesting alternative for a compact *genuine spectrometer*.
The TPR detection principle is based on neutron-to-proton conversion via elastic scattering on hydrogen nuclei at a given angle in a plastic thin foil. The scattered proton energy can be easily measured and converted back to the incoming neutron energy, provided that the recoil angle is known.
A preliminary design of a non-magnetic TPR detector for fusion plasma diagnostics has been presented in Ref.[68]. Here it is shown through calculations that TPR could attain an energy resolution close to that of the MPR, combined with an increased efficiency of $2.9 \cdot 10^{-4} n \cdot cm^2$ and compact dimensions. The design of Ref.[68] used silicon detectors as proton spectrometers, given their excellent energy resolution and fast signals. In particular, a proton energy resolution better than 2% would be ideal for a TPR system, so that the overall energy resolution of the spectrometer, that gains contributions also from the finite aperture of the recoil solid angle and the thickness of the scattering foil, could still be about 5%.

In this thesis the possibility of a TPR based on inorganic scintillators has been investigated *(Paper III)*

1.2.5 γ-ray spectroscopy

Gamma-ray spectroscopy is among the diagnostics proposed to measure confined energetic ions in a high performance burning plasma, where the plasma behaviour is dominated by supra-thermal ions [69]. Energetic particles in the MeV range are naturally present in a burning deuterium-tritium plasma due to the main fusion reaction d + t $\rightarrow$ α + n and to auxiliary heating schemes. In a high power fusion device, γ-ray emission results from interactions between the energetic ions and impurities that are naturally found in the plasma [70, 47, 71]. Advanced γ-ray instrumentation is today installed at JET, in particular, a HpGe detector and $LaBr_3$ scintillator (see Fig.1.14). Parameters of the fast ion energy distribution can be obtained by combining information on the intensity and shape of characteristic peaks of γ-ray reactions occurring in the plasma [72, 73] as demonstrated with high energy resolution measurements in present tokamak devices [74, 75, 76] (see Fig.1.14 on the right).

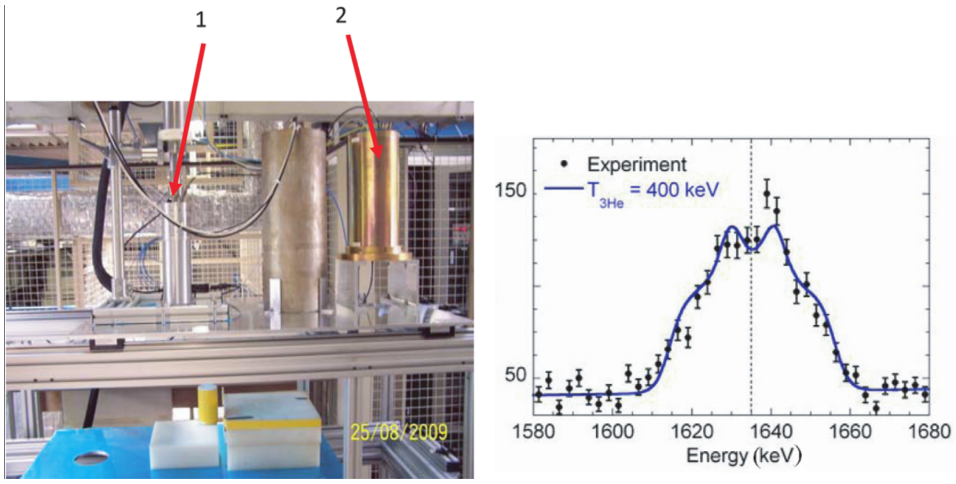

Figure 1.14: On the left, γ-ray spectroscopy instrumentation operating at JET, (1) an HpGe detector and (2) a $LaBr_3$ scintillator. On the right, experimental peak shapes for the 1635 keV lines from the reaction $^{12}C(^3He, p\gamma)^{14}N$ measured at JET with the HpGe spectrometer [75] .The blue line represents a fit to the data for a tail temperature of the fast ^3He population of 400 keV. Figure taken from Ref.[75].

Unlike present devices, γ-ray measurements in next step tokamaks, such as ITER, will have to be performed at MHz counting rates, still with high energy resolution, and under significant irradiation from 2.5 and 14 MeV neutrons produced by the main fusion reactions, d + d $\rightarrow$ ^{3}He + n in deuterium plasmas and d + t $\rightarrow$ α + n in deuterium-tritium. Dedicated solutions therefore need to be developed. A recent scintillator material, $LaBr_3$ [77, 78, 79], meets many of the requirements for γ-ray measurements at ITER. Unlike a HpGe detector, this scintillator is resilient to neutron damage. High counting rate γ-ray measurements up to a few MHz were also shown at nuclear accelerators without any significant degradation of the energy resolution [80]. Before this thesis, the effect of 2.5 and 14 MeV neutron irradiation on the detector had not yet been studied in detail. One study where the response of a 1.5" $LaBr_3$ (Ce) detector to neutrons produced by a conventional 241Am/9Be source was presented [81]. However, this result cannot be easily extrapolated for applications in fusion plasmas, due to the very different neutron spectrum of 241Am/9Be from that of deuterium and deuterium-tritium reactions.

In this thesis we present dedicated measurements of the $LaBr_3$ (Ce) response to 2.5 MeV and 14 MeV neutrons (*Papers VI, VII and VIII*). The experiments were carried out at neutron accelerators and at tokamak devices with deuterium plasmas. The results are analyzed using a MCNP model to identify the main processes contributing to the observed response. Implications of the results for γ-ray measurements in a deuterium-tritium plasma of ITER are discussed.

1.3 Introduction to fast neutron beam lines for chip irradiation

1.3.1 Spallation neutrons

The spallation process occurs when energetic particles (e.g., protons, deuterons, neutrons, pions, muons, etc.) interact with an atomic nucleus (the *target* nucleus). When the projectile kinetic energy is larger than about 100 MeV per nucleon, the de Broglie wavelength of the incident particle is shorter than the radius of the nucleus, allowing the incident particle to interact with individual nucleons. The initial intra-nuclear collision leads to a series of direct reactions (intra-nuclear cascade) whereby individual nucleons are expelled at high energies. Those can in turn interact with other target nuclei, leading to a multiplication effect. As a second step of the process, the original nucleus, after the collision, is left in an excited state. It subsequently relaxes to ground state by *evaporating* nucleons, mostly neutrons at low energies (MeV range). The spallation process is depicted in Fig.1.15, showing two stages of the process (intra-nuclear cascade and evaporation) [82].

Spallation and fission differ in several ways. One difference is in the number of neutrons

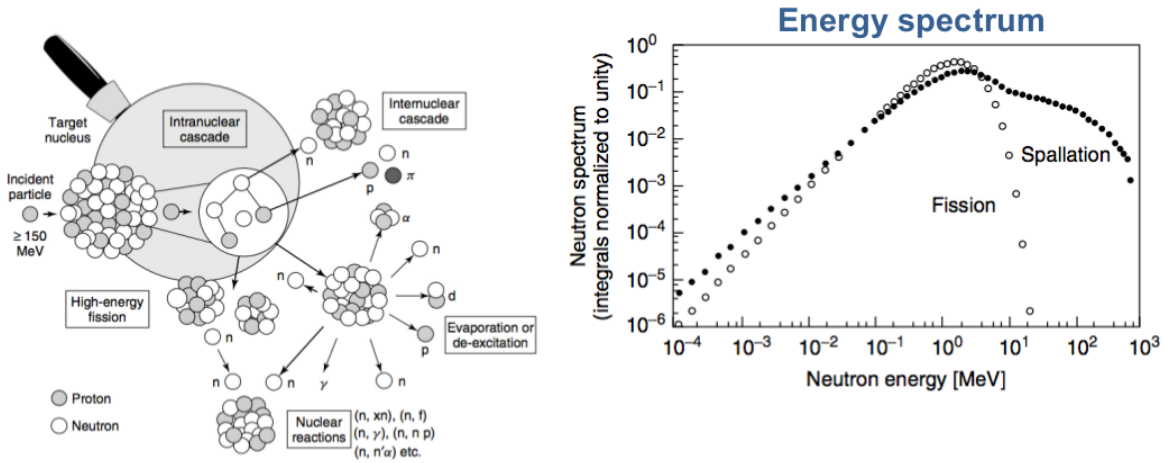

Figure 1.15: On the left, schematic representation of the spallation process. On the right, a typical neutron emission spectrum from spallation in comparison with a fission one.

produced per single event, about 2.5 for fission, dozens for spallation. On average, spallation neutrons have higher energies than fission neutrons (see Fig.1.15 on the right). In a spallation source, high-energy secondary neutrons approach the energy of the incident particle. The moderation process (by means of pre-moderators, moderators, reflectors) lowers the energy of fast neutrons down to thermal or cold energy. Because of advances in high-power accelerator technology, spallation became an important alternative method to fission for producing high fluxes of neutrons for a variety of applications.

Galactic cosmic rays are a natural source of spallation neutrons. They reach the earth's atmosphere and collide with atomic nuclei in air, creating cascades of interactions and reaction products, including neutrons. Some of these neutrons reach the ground. The neutron flux at the sea level is $\simeq 20 n/cm^2/h$ above 1 MeV. In Fig.1.16, the atmospheric neutron spectrum is shown; which was measured by means of the extended-energy multi-sphere neutron spectrometer (Bonner sphere), from Ref.[83].

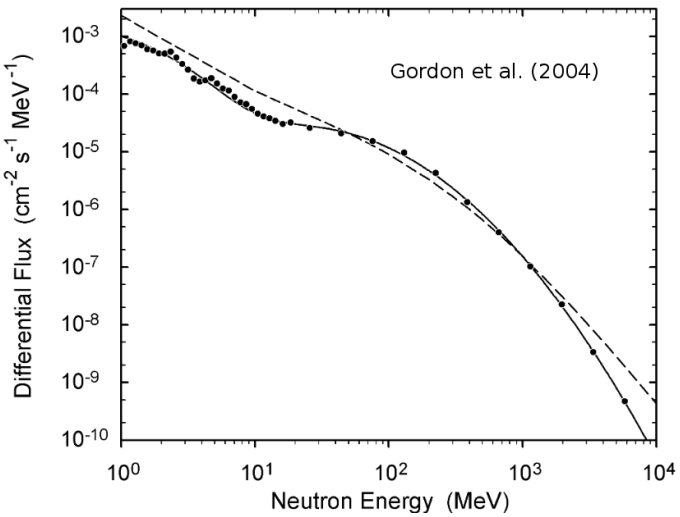

Figure 1.16: Measured atmospheric neutron spectrum, taken from Ref.[83]. The data points are the reference spectrum from the measurements, the solid and dashed curves are models (see Ref.[83].

1.3.2 Single Events Effects induced by atmospheric neutrons

Electronic devices are exposed to various types of radiation, such as energetic α particles, protons, neutrons and muons. The radiation may produce effects in electronics with consequences from temporary loss of data (*soft* errors) to catastrophic failure (*hard* errors). These effects in microelectronics are called Single Event Effects (SEEs)(see [84, 85, 86]).

As the name implies a single event effect is due to a single radiation event. The most common type of radiation-induced error is the *soft* error. The error is *soft* when the device (e.g. a memory) is not permanently damaged, and will store new data correctly. Soft errors include many types of different failure modes. In the commercial microelectronics devices for ground application the most common soft error is the Single Event Upset (SEU). SEUs are errors in which an individual memory component is directly corrupted by radiation. It consists of a flip in the logic state of a single bit.

Atmospheric radiation is a major concern to the reliability of micro-electronic devices. Due to the constantly decreasing dimensions and increased functionality of integrated circuits, SEEs must be considered when designing a digital system. Because of their intense flux and high Linear Energy Transfer, in the terrestrial environment neutrons represent the most important part of cosmic radiation producing single event effects [87]. The neutron flux, and then the rate of SEE, is 300 times higher at flight altitudes[88, 89].

Neutrons, being uncharged, do not directly generate ionization in silicon, but they interact elastically and inelastically with the nuclei in the chip material producing charge particles. At high energies, inelastic collisions are more effective and may lead to a series of direct reactions, called intra-nuclear cascades, which are characterized by the ejection of individual nucleons and heavy ions that more likely induce SEE into the device.

The probability of a SEE (cross section) is energy dependent and characteristic of the microelectronic chip

$$\sigma_{SEE}(E) = \frac{number\ of\ fails}{particles\ per\ unit\ area} \tag{1.9}$$

If the SEE cross section and the neutron spectrum are known, the Single event Effects Rate

(SER) can be easily calculated as

$$SER = \int \sigma_{SEE}(E) \left(\frac{d\phi(E)}{dE} \right) dE \tag{1.10}$$

A typical $\sigma_{SEE}(E)$ is characterised by a onset threshold energy and slow rise to a plateau value, according to the Weibull approximations [90, 91]. Fig.1.17 (taken from Ref.[92]) shows a selection of SEE cross sections for different effects and different systems, reviewed in Ref[92]. One can notice a wide range of energy threshold for different effects. Between them, cases A and D represent curves close to the extremes expected for most phenomena in most devices of interest. From this plot one can understand the importance of testing micro-electronics in a wide energy range up to hundreds of MeV. Testing electronics only with low energy neutrons would render the test meaningless with respect to SEE with high energy thresholds.
Another interesting discussion on the energy dependence of SEE cross sections can be found in Refs.[93, 94]. Examples of normalized Weibull approximation of cross-section, for values representative of SRAM (top) and DRAM (bottom) bit upsets are shown in In Fig.1.18, taken from Ref.[93]. The higher cutoff energy for DRAM indicates a larger critical charge is required to upset a DRAM cell than an SRAM cell.

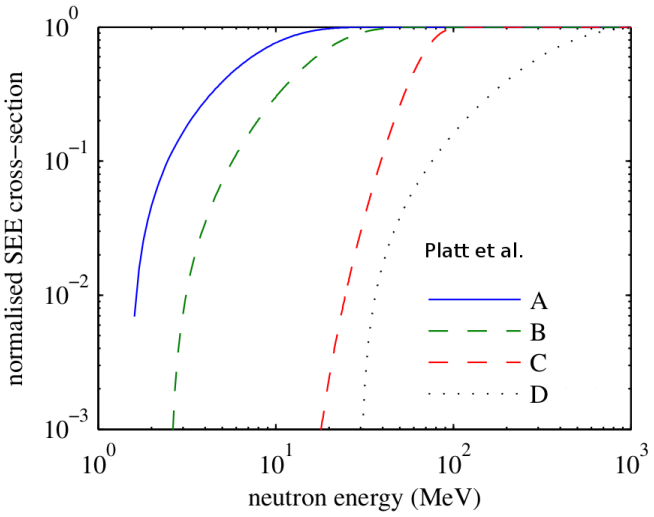

Figure 1.17: Selected SEE cross section functions for different effects and different systems (A,B,C and D) with a wide range of energy thresholds E_t. Figure taken from Ref.[92] .

1.3.3 Accelerated irradiation testing at spallation sources

Experiments with atmospheric neutrons at ground level and at different altitudes can be carried out, but due to low intensity, they require very long periods of data acquisition. Therefore, neutron sources represent an opportunity due to the availability of high intensity fluxes, which allow for accelerated irradiation experiments. A few dedicated facilities are available around the world, such as LANSCE [95] and TRIUMF [96], in order to investigate the SEEs incidence on chips. In Figure 1.19 the atmospheric neutron flux is compared to neutron facilities spectrum. LANSCE is a multidisciplinary facility for science and technology. At the Los Alamos Meson Physics laboratory, a 800 MeV high-power linear accelerator is used to accelerate both protons and negative hydrogen ions with pulsed beam. The resulting neutron spectrum is rather similar to that of neutrons produced in the atmosphere by cosmic rays, but with a neutron flux 10^8

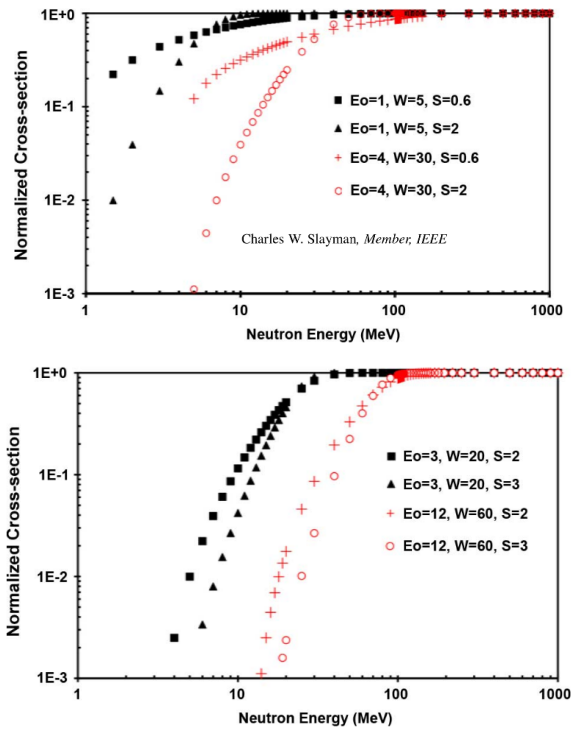

Figure 1.18: Examples of normalized Weibull approximation of cross-section, for values representative of SRAM (top) and DRAM (bottom) bit upsets. E_0, S and W are parameters of the Weibull function. Figure taken from Ref.[93] .

times higher than the natural one at sea level.
Irradiation tests of semiconductor devices are also performed at the Neutron Irradiation Facility (NIF) of TRIUMF, Vancouver, Canada. NIF is mainly dedicated to testing avionics and ground-based electronic systems. The neutrons are produced by an intense proton beam from a 500 MeV cyclotron, striking an aluminum beam stop immersed in a cooling water tank. NIF has an energy spectrum well matched to the atmospheric one, although somewhat softer than the one at LANSCE.
Below we will present the fast neutron beam-lines operating at ISIS. In particular, the new beam-line ChipIr has been built at the ISIS neutron source of the Rutherford Appleton Laboratory (UK) [103, 104] for neutron irradiation experiments on electronic and avionic devices and systems. The spectrum shown in Fig.1.19 refers on the pre-existing VESUVIO beam line. One of the key characteristics of SEE-inducing neutron fields is the distribution of neutrons by energy, defined by the differential neutron flux, $\left(\frac{d\phi(E)}{dE}\right)$ (see eq.1.10). Inevitably, each facility simulates the neutron field induced by cosmic rays with limited fidelity.
The practical problem is that $\sigma_{SEE}(E)$ (eq.1.9) cannot be easily measured because of the absence of suitable mono-energetic neutron fields. Therefore the purpose of accelerated testing in white neutron beams is to use measurable quantities to estimate an integral cross-section in a synthetic field and use this information to extrapolate an integral cross-section for the atmospheric field. It is clear that this analysis is more accurate if the synthetic spectrum is close to the atmospheric one and/or if the two spectra are well known.
The integral neutron flux is normally provided by facility beam monitoring and today is typically known to an uncertainty of about 10%. The threshold energy is commonly taken to be 10 MeV, under the assumption that the contribution of lower energy neutrons to the event rate is

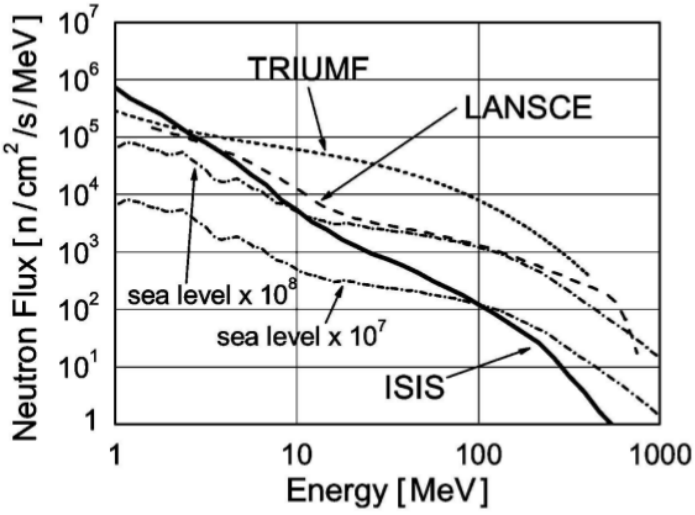

Figure 1.19: Neutron flux above 1 MeV in different neutron facilities compared with the atmospheric one, taken from Ref.[105]

.

small [92].

1.3.4 Fast neutrons beam lines at ISIS

Before the ChipIr beam was available, fast neutron irradiation tests have been performed at ISIS on the VESUVIO beam-line, located in the Target Station 1 (TS1). The VESUVIO beam-line, featuring a 300K water moderator, was designed to have an under-moderated spectrum for studies in the eV energy range. Spallation neutrons, before the moderators, have a wide energy spectrum, ending at the energy of the proton beam (800 MeV). This configuration provides VESUVIO with an intense tail of fast neutrons ($5 \cdot 10^4$ neutrons cm^{-2} sec^{-1} with $E_n > 10MeV$), which has been exploited in recent years for micro-electronics irradiation [102, 105].
As one can notice from Fig.1.19, the VESUVIO neutron spectrum is considerably softer with respect to TRIUMF, LANSCE and the atmospheric one, due to the moderator and to the Be reflector.
The new beam-line ChipIr has been built at the ISIS neutron source of the Rutherford Appleton Laboratory (UK) [103, 104] for neutron irradiation experiments on electronic and avionic devices and systems. ChipIr is designed to feature a fast neutron spectrum that mimics the atmospheric one, up to hundreds of MeV, with approximately $10^8 - 10^9$ times higher intensity with respect to the ground level and approximately $10^6 - 10^7$ with respect to normal flight altitude.
In particular, ChipIr will increase the high energy component of the spectrum using a channel cut out of the current beryllium reflector. An *ad-hoc* neutron transport system has been designed for optimization of the neutron spectrum for the specific application. ChipIr will provide a flux above 1 MeV in the order of 10^7 n cm^{-2} s^{-1}. That means 150 times more intense then the present ISIS-TS1 flux and 25 times more than the neutron flux at LANSCE.
The user community has proposed two modes of operation: a collimated neutron beam within a containment blockhouse (this is a standard approach adopted by other facilities), and a beam line that additionally provides a large, reasonably isotropic flood of neutrons by the use of ad-

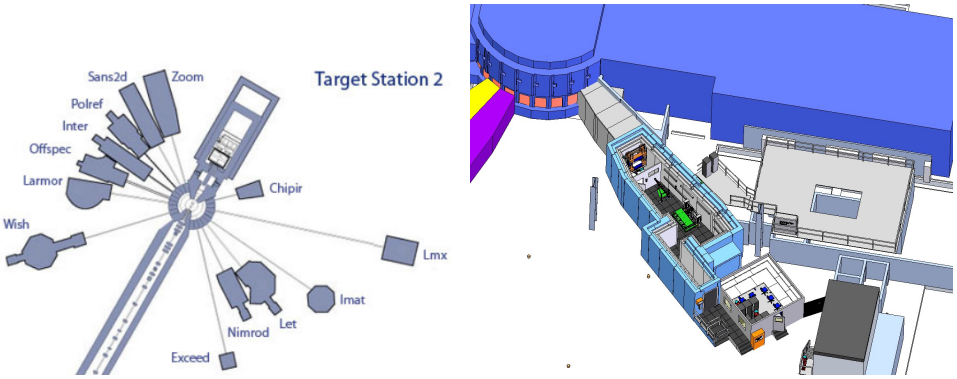

Figure 1.20: On the left, schematic representation of the Target Station 2 (TS2) at ISIS. On the right, CAD model of the ChipIr beam line.

ditional movable secondary scatterers. The last option will be unique to ChipIr and allow very large systems to be tested.
An important task for ChipIr design is the development of a neutron beam monitor for flux measurements in the MeV energy range.
The neutron energy spectrum and the flux spatial distribution of fast neutron beam-lines (e.g. ChipIr and VESUVIO) are determined on the basis of Monte Carlo calculations that try to reproduce the complexity of nuclear and intra-nuclear interactions up to 800 MeV. Direct measurements of these quantities are needed for the characterization of the neutron flux, to benchmark the simulations, and for a better understanding of the underlying physics of this kind of facilities.

1.3.5 Fast neutron instrumentation for spectroscopy and dosimetry

Different kinds of fast neutron detectors have been used to characterize the fast neutron flux:

- Irradiation foils [105]
- Bonner spheres [106]
- Thin-film breakdown counters [107]

and several are proposed for fast neutron ($E_n > 10MeV$) flux monitoring and imaging:

- Diamond detectors
- Gas Electron Multiplier detectors [108, 109, 110, 111]

A Telescope Proton Recoil spectrometer (TPR) was developed for a direct measurement of the fast neutron spectrum.

Diamond detectors SDDs can be exploited as fast neutron detectors for fast neutron beam-lines. In particular, they can be used as fast neutron beam monitors with moderate spectroscopic capabilities. Here the issues are very different with respect to the application to fusion plasmas. On fusion applications, one has to measure with high resolution the details of a quasi-monoenergetic spectrum. The presence in the response function of the $^{12}C(n,\alpha)^{9}Be$ peak allows for a direct measurement of the features of the 14 MeV emission peak. On the other hand, on a spallation beam-line, the neutron spectrum ranges for several orders of magnitude

from thermal energies up to the energy of the proton accelerator (800 MeV for ISIS). For this reason the response functions of the detector is more complex, since the contribution of elastic and inelastic scattering, besides the reactions with charged products (see Fig.1.3), can not be easily discriminated. Moreover, above a few dozens of MeV the range in diamond of charged products becomes comparable with the detector thickness (500 μm) and finite size effect start to play an important role in the response function. If one can achieve an accurate knowledge of the response functions, the neutron spectrum of the beam line would be retrieved by deconvolution analysis. The evaluation of SDDs response functions has been the subject of dedicated tests at accelerator facilities [97, 98], and results were compared with Monte Carlo Simulations[97]. At the time of the writing of this thesis, the comprehension of the response functions is not yet adequate enough for a deconvolution process. More work will be needed both on experimental and simulation side. Nevertheless, this does not mean that the direct measurement of the deposited energy in the diamond can not yet give important informations. On the contrary, the following advantages derives from a spectroscopic measurement with SDD.

- Since all reactions are endothermic and the detector has good energy resolution, one can be sure that counts above a certain energy threshold are due to fast neutrons above a certain energy.
- Electrons, and then γ-rays can be discriminated by pulse height.
- Moderate spectroscopic capabilities can be enough to diagnose changes in the deposited energy spectrum measured on different beam-lines, and on different configurations of the same beam line, as a direct consequence of changes in the neutron spectrum.

Eventually the best approach for using SDDs at a pulsed spallation source like ISIS may be to combine pulse height analysis (as done in ordinary spectroscopy) with Time of Flight analysis (ToF). In principle ToF analysis and pulse height analysis provide the same information on the neutron energy spectrum with limitations due to e.g. the fine time structure of the ISIS pulsed beam (the time spread of the proton pulse is not negligible) or the pulse height energy resolution of the SDD. By combining both analyses in one bi-parametric measurement one can overcome some of the limitations intrinsic in the use of time of flight analysis or pulse height analysis independently. Diamond detectors were tested in recent years by the Milano spectroscopy group at the VESUVIO beam line at ISIS [99, 100, 101].
In this thesis I present the first neutron measurements on the new ChipIr beam line. This work will be continued with the next experimental campaign in 2015. During the period pf this PhD thesis, I also characterized for the first time the fast neutron component of the PRISMA beam-line at ISIS using diamond detectors. Finally, experimental work was dedicated to the understanding of polarization effects and detector stability, for development of SDD technology as beam monitors of fast neutron at spallation sources.

TPR A TPR spectrometer is a candidate *genuine* spectrometer for measurements of the neutron energy spectrum without need of deconvolution algorithms. An easier data interpretation, however, comes at the price of increased experimental difficulties in operating coincidence techniques in a high flux environment.
During the period of this PhD thesis, a prototype TPR spectrometer was first tested on the VESUVIO beam line, and results are reported in *Paper IV*. In those preliminary measurements, a lithium glass scintillator was used for the transmission measurements (ΔE measurement), together with a 1" thick YAP crystal was used as proton spectrometer (E measurement).
As a further development (*Paper V*), the lithium glass scintillator has been replaced by a silicon

detector for ΔE measurements. The second solution allows for better background discrimination due to a better energy resolution on the ΔE. The Silicon fast signals are well suited to cope with the high instantaneous rates. The measurements performed with the TPR spectrometer in its final detector configuration on the VESUVIO beam-line are reported.

Chapter 2

Single crystal Diamond Detectors

Io stimo più il trovar un vero,
benché di cosa leggera,
che 'l disputar lungamente delle massime questioni
senza conseguir verità nessuna.
– Galileo Galilei

2.1 Overview

The applications of Single crystal Diamond Detectors (SDDs) are rapidly growing, ranging from UV detection [112, 113] for astrophysics and plasma physics, to minimum ionizing particle detection in particle physics experiments [114, 115], X-ray detection for radiology and radiotherapy [116, 117, 118], and proton beam sensors [119]. SDD applications for fast neutron measurements include neutron emission monitors and neutron spectrometers.
Neutron detection is based on the collection of the electrons/holes pairs produced by charged particles generated by neutron reactions with carbon nuclei. The most important reactions producing charge particles are the elastic channel, the $^{12}C(n,\alpha)^{9}Be$ reaction (the Q-value is -5.7 MeV) and the $^{12}C(n,n')3\alpha$ reaction (the Q-value is -7.3 MeV).

2.2 Design and realization of diamond based neutron spectrometers

A single SDD pixel prototype and a 12 pixel matrix were designed as neutron spectrometers and built at the CNR-ISM institute in Rome (Italy) based on the experience of X-ray detectors and dosimeters [117]-[124] (See Fig.2.1). The single pixel SDD was used for neutron measurements, whose results are presented hereby. At the time of the writing of this paper the 12 pixels matrix is being assembled and will be evaluated with laboratory tests. Each pixel is made of a single-crystal *electronic grade* diamond sample (4.5 x 4.5 mm^2, 500 μm-thick, with boron concentration [B] <5 ppb, and nitrogen concentration [N] <1 ppb), provided by Element Six Ltd [125]. Aimed at removing any organic and metallic impurity, each sample was cleaned for 30 s in a boiling mixture (1:1:1) of nitric, sulfuric, and perchloric acid, then rinsed in deionized water. Ultrasound sonication was also used for debris removal. Ohmic contacts were obtained on top and bottom surfaces of the samples by subsequent sputtering depositions of a multilayer metal structure (patent pending), followed by a final gold layer deposition, in order to improve weldability with microwires. Aimed at maximizing contact homogeneity between pixels, the diamond samples were metalized all together in two sessions (one for the top and one for the bottom surfaces).

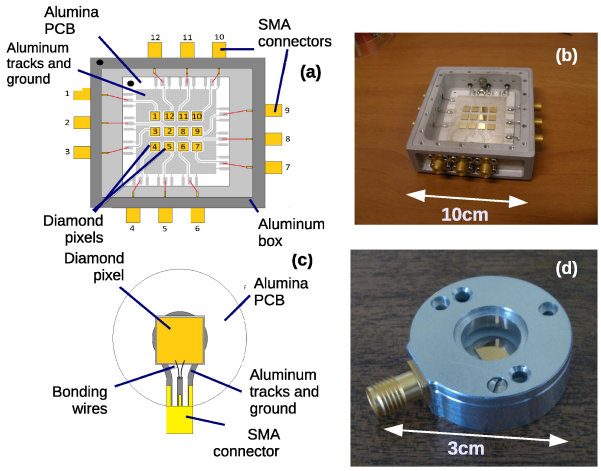

Figure 2.1: On the top, layout (a) and picture (b) of a neutron spectrometer based on a 12 pixel diamond matrix. On the bottom, layout (c) and picture (d) of a single pixel prototype. Figure taken from *Paper I*.

A dedicated 1 mm-thick alumina Printed Circuit Board (PCB) was designed and fabricated for the 12 pixel matrix. The bottom surfaces of the diamond samples were glued with a thin layer of conductive silver paste on their respective pixel pad, whereas top surfaces were wire-bonded (by means of 25 μm thick Al/Si wires) on the ground plane. In order to reduce cross-talk effects, the ground plane surrounds completely each pixel pad, as well as each signal track. All the pads and signal tracks, as well as the ground plane, are aluminum-made, aimed at minimizing metal activation by neutrons. The alumina PCB is housed inside a properly designed and developed aluminum metal case, equipped with 12 SMA connectors for pixel biasing and signal collecting.

Signals from each pixel are amplified by a fast charge preamplifier CIVIDEC C6, which is a low-noise charge amplifier with a rise time of 3.5 ns and a gaussian pulse shape with a FWHM of 10 ns [126]. Fast electronics is needed in order to allow for high rate measurements by reducing the pile-up probability. On the other hand, electronics with fast signals (tens of ns) feature worst energy resolution with respect to conventional spectroscopic preamplifiers with typically decay time in the range 50-500 μs. As a matter of fact, due to the large number of electron-hole pairs produced by MeV particles with a 5.5 eV band-gap (about 10^6), we can state that the finite energy resolution of the SDD is entirely dominated by the electronics, with no contribution from Poisson statistics. CIVIDEC C6 was selected among other commercial and custom made preamplifiers, giving an energy resolution of 1.9% (FWHM) for 5.5 MeV alpha particles in vacuum and a counting rate capability in excess of 1 MHz (see *papers I and II*).

2.3 Experiments for fusion neutron applications

2.3.1 Measurements of 14 MeV neutrons at the Frascati Neutron Generator

Measurements of the response of the SDD single pixel prototype to 14 MeV neutrons were carried out at the Frascati Neutron Generator (FNG) [127]. FNG accelerates deuterium ions at 300 keV onto a tritiated-titanium target containing about $37 \cdot 10^{10}$ Bq of tritium. The detector was mounted at 90 deg with respect to the incoming deuterium beam. At this position the mono-energetic DT neutrons do not feature any energy shift due to the kinematics, and their spectrum has the minimum broadening, about 1% (FWHM). The detector was placed at a

distance of 25 cm from the target, where the neutron flux is about $10^6 cm^{-2} s^{-1}$. The CIVIDEC C6 preamplifier was connected to the detector through a 15 cm long low capacity cable. A four channel, 1 GS/s-10 bit CAEN waveform digitizer model DT5751 was used to record the signals [128]. A typical neutron signal measured at FNG is shown in Fig.2.2. One can notice that its full duration is below 30 ns. Digitized signals were analysed off-line by integrating their area (a dedicated algorithm with baseline subtraction was used) and the deposited energy spectra was reconstructed.

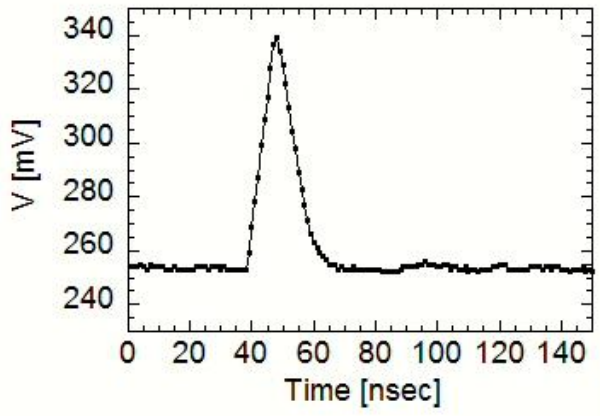

Figure 2.2: Pulse of a 14 MeV neutron recorded by a 10 bit / 1 GS/s digitizer. Figure taken from *Paper I.*

The deposited energy spectrum shown in Fig.2.3 integrates 780 seconds of measurement. Starting from high energy scale, it is possible to see the $^{12}C(n,\alpha)^9Be$ peak, the $^{12}C(n,n')3\alpha$ shoulder and the scattering continuum. The $^{12}C(n,\alpha)^9Be$ peak has a measured energy broadening of 2.7% FWHM. The energy resolution of the detector is therefore estimated to be 2.5% (FWHM), considering the 1% intrinsic broadening of the FNG DT spectrum. A zoom in log scale at higher deposited energies (7 MeV $< E_d <$ 14 MeV) shows the presence of $^{13}C(n,\alpha)^{10}Be$ peak. The intensity of this peak is 0.3% respect to the $^{12}C(n,\alpha)^9Be$. This is due to the fact that ^{13}C is only 1.1% of the natural carbon and the cross section is about 1/3 (22mb vs. 62mb) [129]. The continuous background at $E_d >$ 8.5 MeV can be due also to neutron interaction with other elements contained into the contacts. These events with deposited energy above the $^{12}C(n,\alpha)^9Be$ peak set the instrument sensitivity for diagnostics of energetic ion population in the fusion plasma to about 10^{-2} level with respect to the main bulk emission.
Another important feature for a neutron detector for diagnostics of fusion plasmas is the capability of discriminating direct neutrons from scattered ones. An improvement in the scattered to direct neutron ratio would enhance the imaging capability of a neutron camera system, and ease the interpretation and analysis of neutron calibrations in a tokamak. For DT neutron a straightforward possibility is to have an high energy threshold below the $^{12}C(n,\alpha)^9Be$ peak. It was found that the measured $^{12}C(n,\alpha)^9Be$ counts in the range 7 $MeV < E_d <$ 10 MeV are approximately 9.5% with respect to all the counts from other reaction channels (1.5 MeV $< E_d <$ 7 MeV).

In Fig.2.4 the counting time trace of the SDD is compared to the standard monitor of the FNG [127]. Here errors on the diamond measurements are due to the Poisson counting statistics and not shown because of the same size of the black dots. It is possible to notice the good agreement of the two traces. No instability effects were observed during these 14 MeV neutron irradiation measurements, which is a good indication for a straightforward use of a SDD for neutron emission diagnostics.

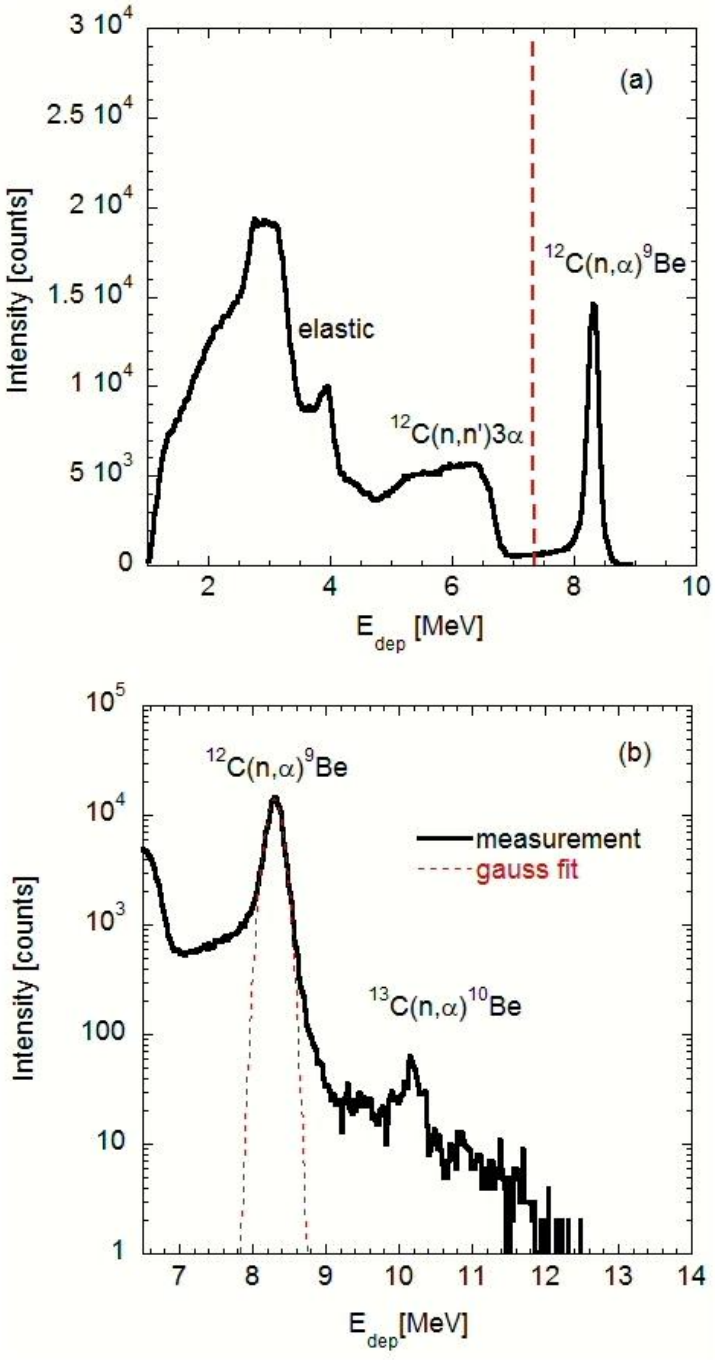

Figure 2.3: Deposited energy spectrum of mono-energetic 14 MeV neutrons (a). The dashed vertical line is the energy threshold applied to count only events of the $^{12}C(n,\alpha)^{9}Be$ peak. The same spectrum for 7 MeV $< E_d <$ 14 MeV is shown in log scale with a Gaussian fit to the $^{12}C(n,\alpha)^{9}Be$ peak (b). Figure taken from *Paper I*.

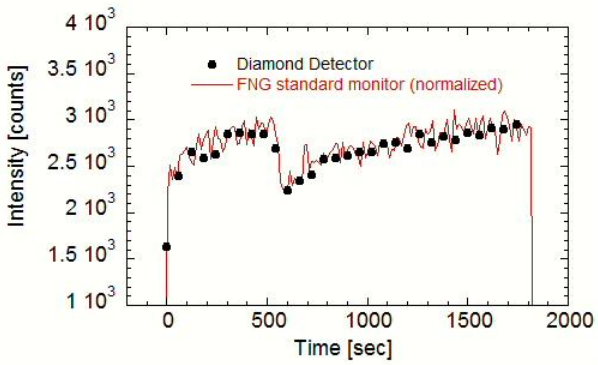

Figure 2.4: Counting time trace of a diamond detector compared with the standard monitor of the FNG. Figure taken from *Paper I*.

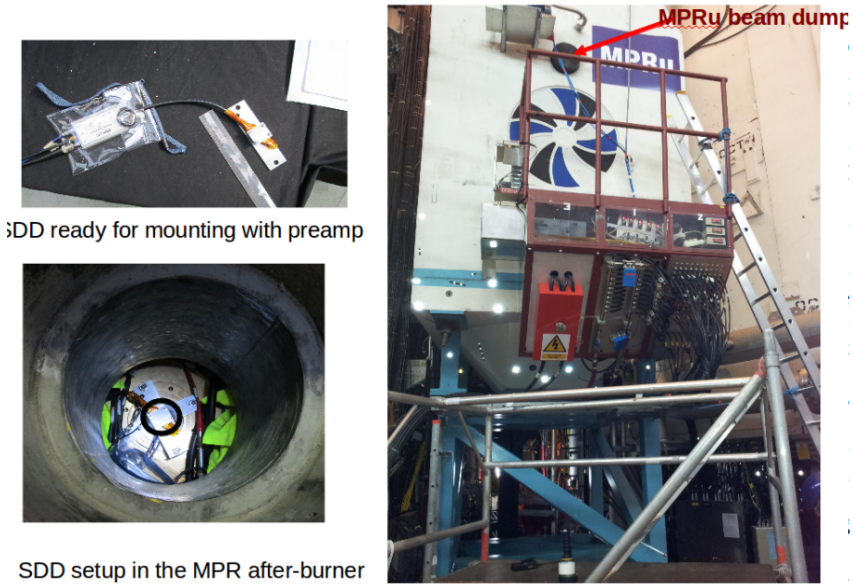

Figure 2.5: Pictures of the detector mounting with preamplifier on the detector table (top left) and inside the MPRu radiation shielding (bottom left). A picture of a back view of the MPRu is shown on the right. The diamond detector position is indicated with an arrow.

2.3.2 Experimental setup at the JET tokamak

An artificially grown SDD was installed in the JET Torus Hall on a collimated Line of Sight (LoS) shared with other neutron diagnostics, the MPRu proton-recoil neutron spectrometer and the NE213 scintillator. The installed diamond detector had a nominal active volume of the 4.7x4.7 mm^2 (surface area) x 0.5 mm (thickness) with 4.5 mm diameter aluminium electrical contacts.

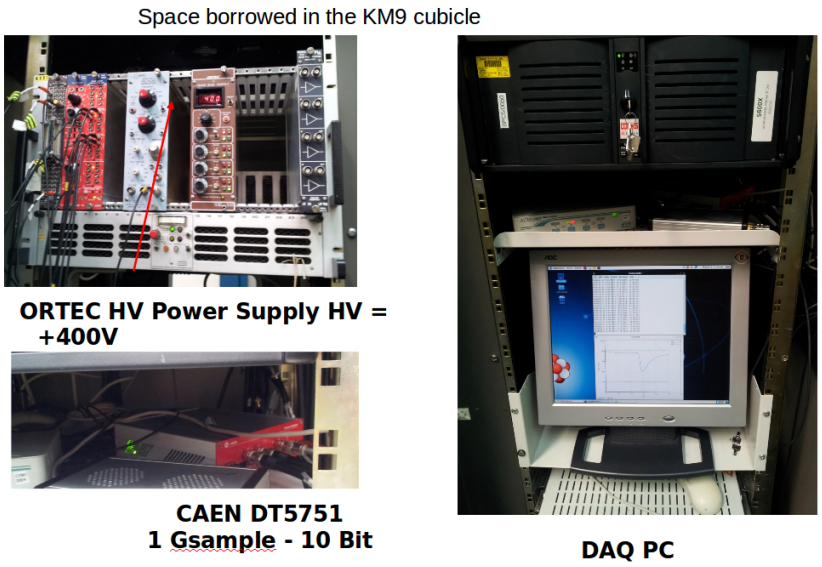

Figure 2.6: Pictures of the electronics mounted on the JET diagnostic hall for the setup of SDD measurements.

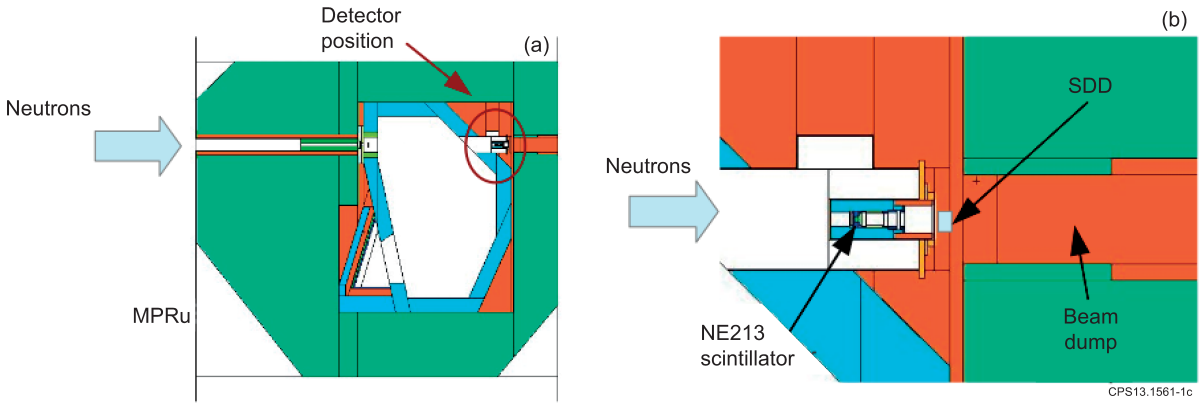

Figure 2.7: (a) Schematics of the SDD detector arrangement inside the radiation shielding of MPRu spectrometer. The direction of the neutrons produced by the plasma is indicated by the arrow. (b) Zoom of the detector position in front of the MPRu beam dump. Figure taken from *Paper II*.

Two separate read-out electronic chains (see Fig.2.8) were developed to measure, at the same time, DD (2.5 MeV) and DT (14 MeV) neutrons. This was needed since the energy deposition for DD neutrons, due to carbon recoil, is about 20 times less than the energy deposition of DT neutrons via the $^{12}C(n,\alpha)^{9}Be$ reaction. Both electronic chains shared a fast charge preamplifier CIVIDEC C6 [126] as a first amplification stage. The latter was placed about 20 cm away from

the diamond detector, without intercepting the neutron beam. A 120 meter BNC cable was laid down from the preamplifier to the JET Diagnostic Hall, where signals from the diamond detector were recorded. The signal FWHM from an α -particle of the calibration source, measured after the long BNC cable, was 20 ns (see Fig. 2.9). For 2.5 MeV neutron measurements a second amplification stage, consisting of a 20 dB current amplifier CIVIDEC C1, was installed right after the first preamplifier in the Torus Hall.

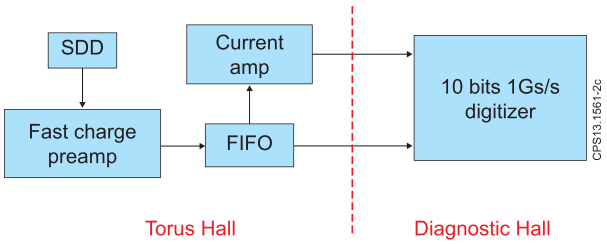

Figure 2.8: Schematics of the read-out electronics used for SDD measurements at JET. Figure taken from *Paper II*.

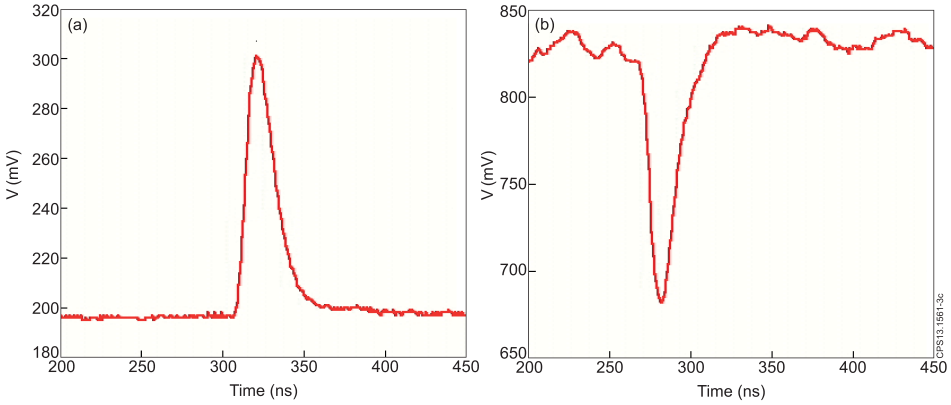

Figure 2.9: Signals from an α - particle of the calibration source after the BNC cable in the Diagnostic Hall (a) and from a 2.5 MeV neutron after the second amplification stage (see text for details) (b).

The signal of a 2.5 MeV neutron after the second amplification stage is shown in Fig.2.9. Clearly, there is a worse signal-to-noise ratio compared to the pulse from the calibration source, shown in Fig. 2.9. Nevertheless, the FWHM of the signal is still about 20 ns, which guarantees that the current amplifier did not introduce any significant shaping that could alter the fast temporal properties of the signal. Preserving fast signals is essential in view of high rate measurements in the JET DT campaign.
A four channel, 1 GHz, 10 bit CAEN waveform digitizer model DT5751 (input range: 0-1 V) was used to record the signals from both electronic chains in the Diagnostic Hall. The acquisition was triggered by the JET "pre"-signal, that is produced 40 s before each plasma discharge. The Pulse Height Spectrum (PHS) corresponding to each discharge was reconstructed off-line with a software based on a trapezoidal filter algorithm.
A calibration triple-α source (^{241}Am, ^{239}Pu and ^{244}Cm) was placed in front of the detector, providing a counting rate <10 Hz. A typical calibration spectrum, collected in 60 min without neutron emission from the plasma (see Fig.2.10). It has to be considered in the calibration a calculated energy loss in air of 0.39 MeV. An energy resolution (FWHM/E) of 2.2% can be measured at 5.2 MeV. This value is acceptable for fusion spectroscopy applications, as

it is smaller than the kinematic broadening of the thermal emission peak from DT plasmas (between 5% and 10% for plasma temperatures in the range 4-10 keV [45]). For 2.5 MeV neutron measurements, which correspond to a maximum of 0.8 MeV of deposited Energy, the energy resolution of the SDD is assumed to be 8%. This value was extrapolated from the resolution determined experimentally using a ^{137}Cs γ-ray source.

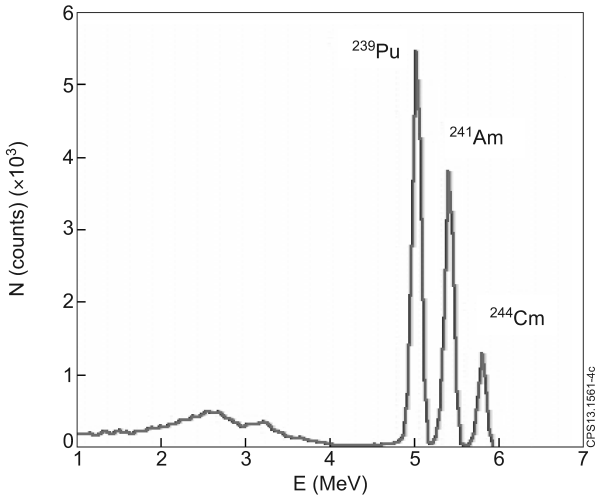

Figure 2.10: Energy spectrum of a calibration triple-α source measured with the SDD in the final setup at JET. Figure taken from *Paper II*.

2.3.3 Neutron measurements on JET deuterium plasmas

2.5 MeV neutron measurements have been performed in deuterium plasmas from July 2013 during the JET C31 campaign. A clear evidence that the signals measured by the SDD detector were due to fusion neutrons was obtained by comparing the counts measured by the SDD with the neutron yield observed by the standard JET neutron diagnostics. The result is shown in Fig.2.11, where each data point represents an individual discharge performed on the 13th of August 2013. The SDD measurements had a low energy threshold corresponding to a deposited energy $E_d = 0.3MeV$ and are shown in the Fig.2.11 versus the total neutron yield measured by the JET fission chamber diagnostics. There is clear linear correlation between the two set of data (correlation coefficient $R^2 = 0.9988$) with a proportionality constant of 4.5E-13. This small value results from the combined contribution of neutron transport from the plasma to the detector position and of the detector efficiency, which can be calculated to be about 1.4% for 2.45 MeV neutrons, based on the $n+^{12}C$ nuclear elastic scattering cross sections. A comparison between the counts recorded by SDD and a NE213 liquid scintillator (active volume 1 cm^2 x 1 cm) placed in front of the SDD along the same LOS is presented in Fig.2.11.b for the same set of discharges of Fig.2.11.a. Again, we find a very good correlation between the two set of data (R^2= 0.9986). The NE213/SDD efficiency ratio, derived from a linear fit to the data, is about 50/1.

The neutron emission time trace measured by SDD is compared with that from the JET fission chambers for a specific JET discharge (#84476) in Fig.2.12. The latter is a discharge with average Neutral Beam Injection (NBI) power of about 15 MW. Data for SDD are shown every 0.5 s to mitigate the statistical fluctuations arising from the low (a few hundred Hz) counting rates observed in deuterium plasmas at the detector location. The good agreement

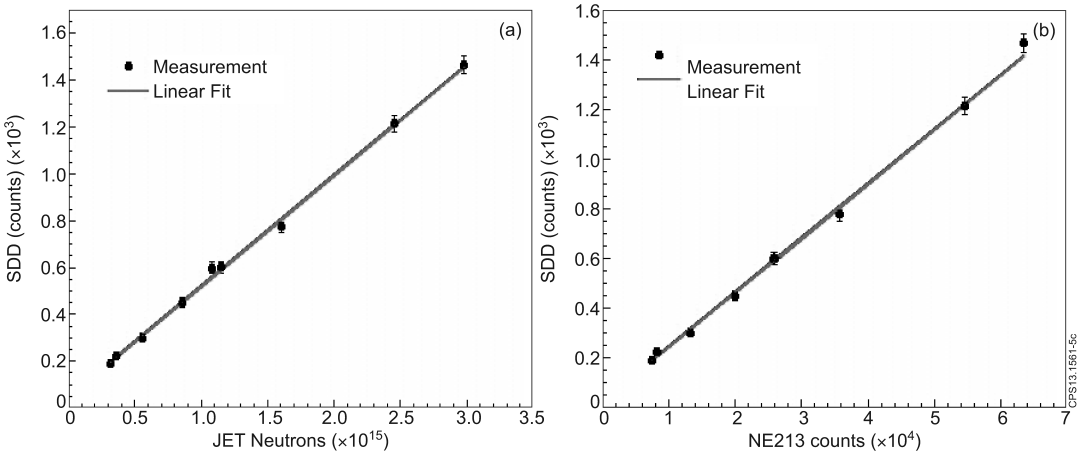

Figure 2.11: (a) Neutron counts measured by SDD versus the JET total neutron yield as derived from fission chambers. Each point corresponds to an individual discharge. (b) Neutron counts measured by SDD and by a NE213 liquid scintillator along the same line of sight. Figure taken from *Paper II*.

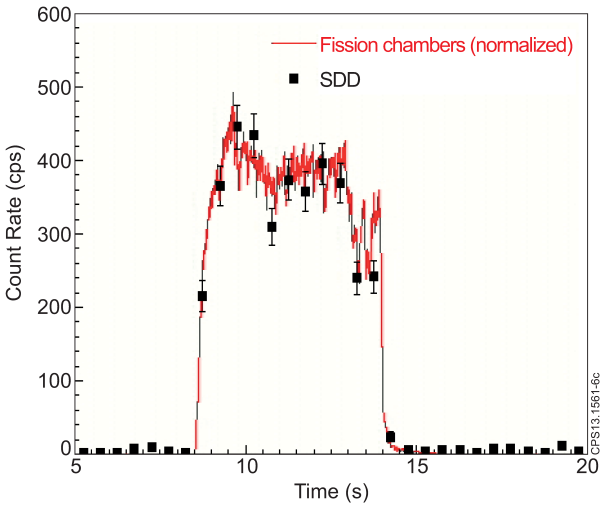

Figure 2.12: Time trace of neutron emission measured by SDD and by the JET fission chambers for discharge 84476. Figure taken from *Paper II*.

between the two set of data confirms the quality of the SDD measurements.
We now move to the analysis of the measured PHS from DD neutrons. This is shown for a single JET discharge (#84476) in Fig.2.13.a and for the sum of 45 similar discharges in Fig.2.13.b as a function of the charged particle energy released in the detector. All these experiments refer to deuterium plasmas with NBI power in the range 12 MW - 20 MW. Qualitatively, the PHS has the characteristic box shape expected from the energy distribution of the ^{12}C recoil ions. The shoulder of the PHS is at 0.69 MeV, which correctly corresponds to the maximum energy deposited by back-scattering of 2.5 MeV neutrons on Carbon (see eq.1.3). The broadening of the edge is due to the combined contribution of the finite detector energy resolution and of Doppler broadening from plasma kinematics (see below).

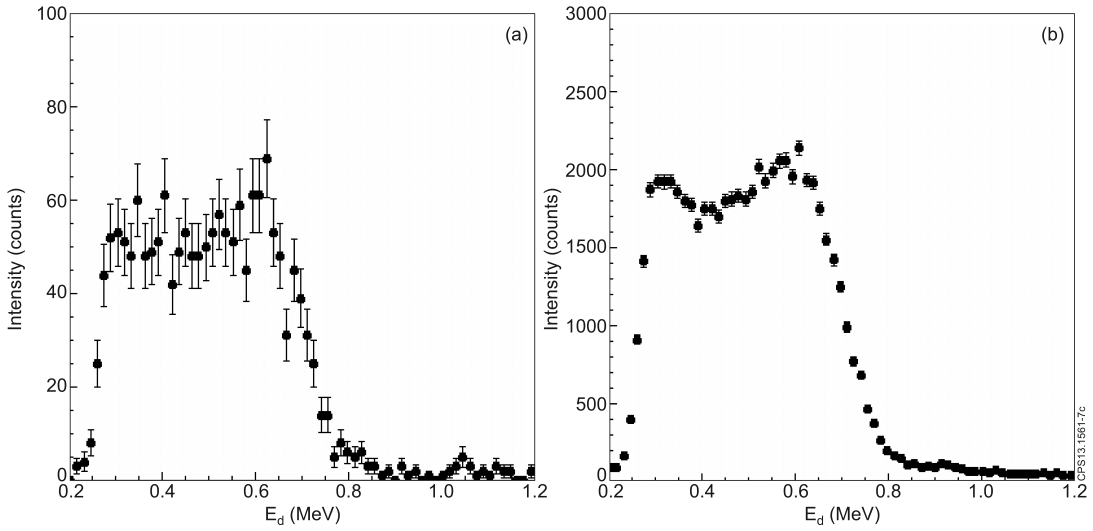

Figure 2.13: (a) Pulse height spectrum from DD fusion neutrons measured by SDD in discharge #84476 at JET, as a function of the charged particle energy released in the detector Ed (b) Pulse height spectrum from the sum of 45 similar JET discharges. Figure taken from *Paper II*.

A deuterium plasma offers the opportunity to also perform measurements of 14 MeV neutrons. These come from the burn up of tritons on deuterium. Tritons are produced by the d + d $\rightarrow$ ^{3}H + p reaction, which has about the same cross section as d + d $\rightarrow$ ^{3}He + n . At JET, the 14 MeV Triton Burn up Neutron emission (TBN) in deuterium plasmas is estimated to be about 1% of that at 2.5 MeV [130, 131, 132]. In order to observe TBN emission we summed a set of discharges performed at JET during more than 1 month of operations with the result shown in Fig.2.14.

Here, a very wide peak, centered at 8.5 MeV, can be observed; this peak is due to the 14 MeV TBNs, which interact via the $^{12}C(n,\alpha)^9Be$ reaction. The considerable width of the peak (about 2 MeV FWHM) reflects the triton slowing down distribution and is in good agreement with calculations for JET (see figure 7 of Ref.[130]). The fit is obtained by comparison of a Gaussian function in terms of Cash statistics [133]. It can be noted that a shoulder appears for $E_d < 8MeV$; this continuous is due to the $^{12}C(n,n')3\alpha$ reaction.

2.3.4 Quantitative analysis of the deposited energy spectrum

The measured PHS can be analyzed to separate different neutron emission components from the plasma. To this end, one must first determine the background due to the calibration source. This was measured, without plasma emission, for about 130 minutes with the results shown in

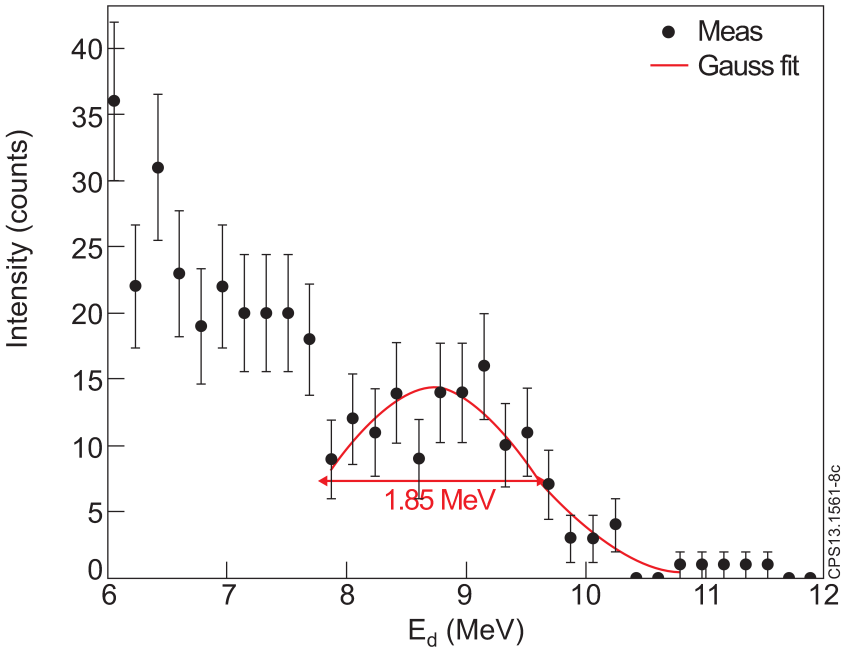

Figure 2.14: Measured pulse height spectrum from triton burn up neutrons in deuterium plasmas at JET. Data from all discharges during 1 month of operations at JET were summed. The FWHM of the (n,α) peak is indicated in the figure. Figure taken from *Paper II*.

Fig.2.17.

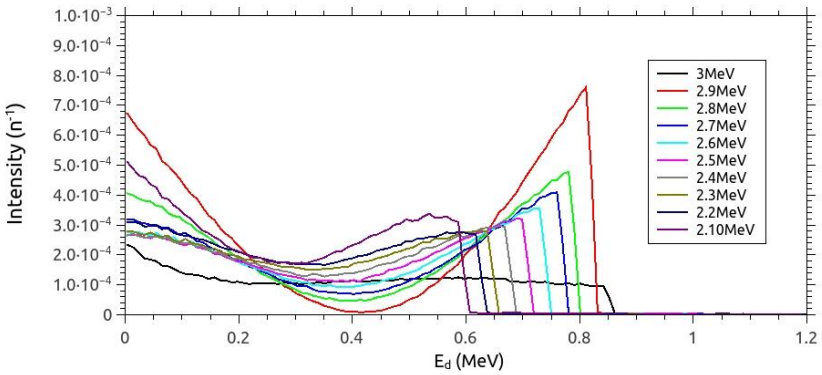

Figure 2.15: Response function of the SDD to mono-energetic neutrons.

A MCNP model was developed to simulate the detector response function to mono-energetic neutrons up to 4 MeV with an energy step of 100 keV. The model geometry consisted of the bare diamond volume and aluminum contacts. Mono-energetic neutrons are generated and headed on the detector front. The energy of the escaping neutron is then calculated for each neutron history. The deposited energy is obtained by subtracting incoming and out-coming energies of the neutron. Fig.2.15 shows the response functions calculated from 2 MeV to 3 MeV. It is worth to notice how the shape can change, from being box-like for neutron energies close to 2.5 MeV, to a far more peaked shape when one get closer to the resonance at 2.9 MeV.
The resulting response function was convoluted with simulations of increasing complexity of

the neutron emission spectrum from the plasma for comparison with measurements, as shown in Fig.2.18. As a first step, we assumed the neutron spectrum to uniquely consists of mono-energetic neutrons at E=2.45 MeV (green dashed curve). This however provides an unsatisfactory description of the measured PHS, both in the flat region corresponding to low recoil energies and for the high energy shoulder.

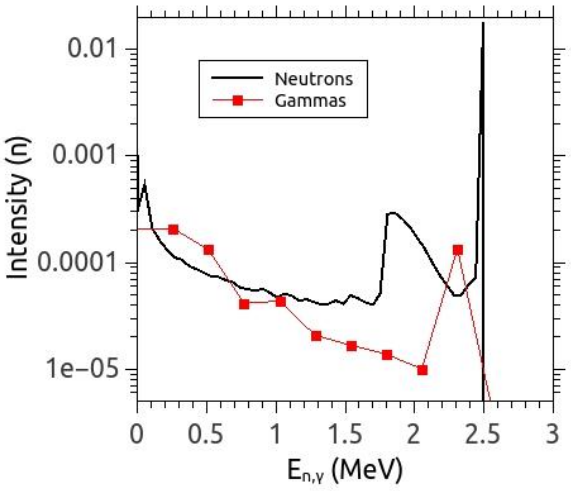

Figure 2.16: Scattered neutrons and gamma-rays energy distribution at the detector position calculated using a MCNP model of the MPRu line of sight.

As a second step, we used a more detailed model for neutron emission from NBI heated plasmas. In this model, neutron emission is described in terms of three components:

i the thermal, that arises from reaction within the thermal (Maxwellian) plasma population;

ii the beam-plasma, which originates from beam ions reacting with thermal ions;

iii and the beam-beam, that is due to fusion reactions among deuterons of the beam.

All of these components were calculated with the Monte Carlo code GENESIS, which can determine the neutron and γ-ray emission spectrum from the plasma using as input the reactant distribution functions [75, 134, 135]. A half-box model was adopted to represent the beam population [136]. The output from GENESIS was in turn validated by comparison with measurements from the TOFOR [52] neutron spectrometer for a few discharges.

As the summed spectrum of Fig.2.18 included plasmas with different NBI injection energies (ranging from 80 keV to 120 keV), separate simulations were correspondingly performed and then combined with weights proportional to the actual NBI power mix used in the experiments. The finite energy resolution of the SDD was taken into account by convolution with a Gaussian of FWHM=8%. This value was extrapolated from the resolution determined experimentally using a ^{137}Cs γ-ray source. The result of the fit is shown by the red curve in Fig.2.18. The high energy shoulder is now well described, but there is a significant excess of data in the low energy part of the spectrum that is not accounted for by the simulation.
This discrepancy can be solved by considering the background contributions from γ-rays and scattered neutrons to the measured spectrum. To this end, the MCNP model for MPRu (Fig.2.7) was used to calculate γ-ray production in the beam dump and the scattering of the incoming neutrons along the MPRu line of sight. Both scattered neutrons and γ-rays (simulated energy

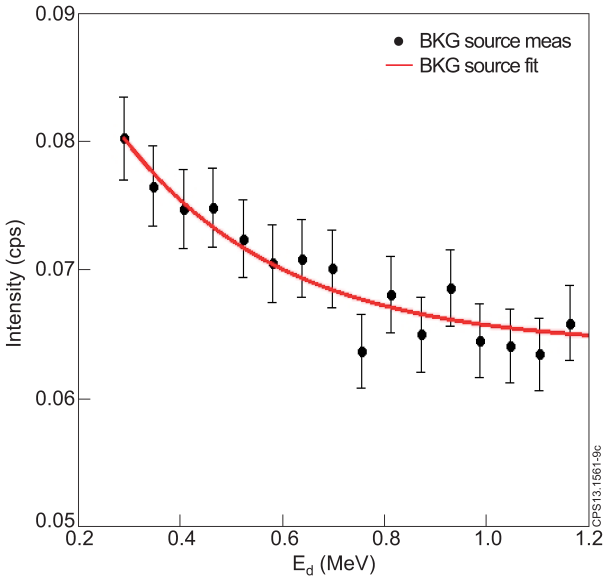

Figure 2.17: Background energy spectrum due to the calibration source normalized to the measurement time. Figure taken from *Paper II*.

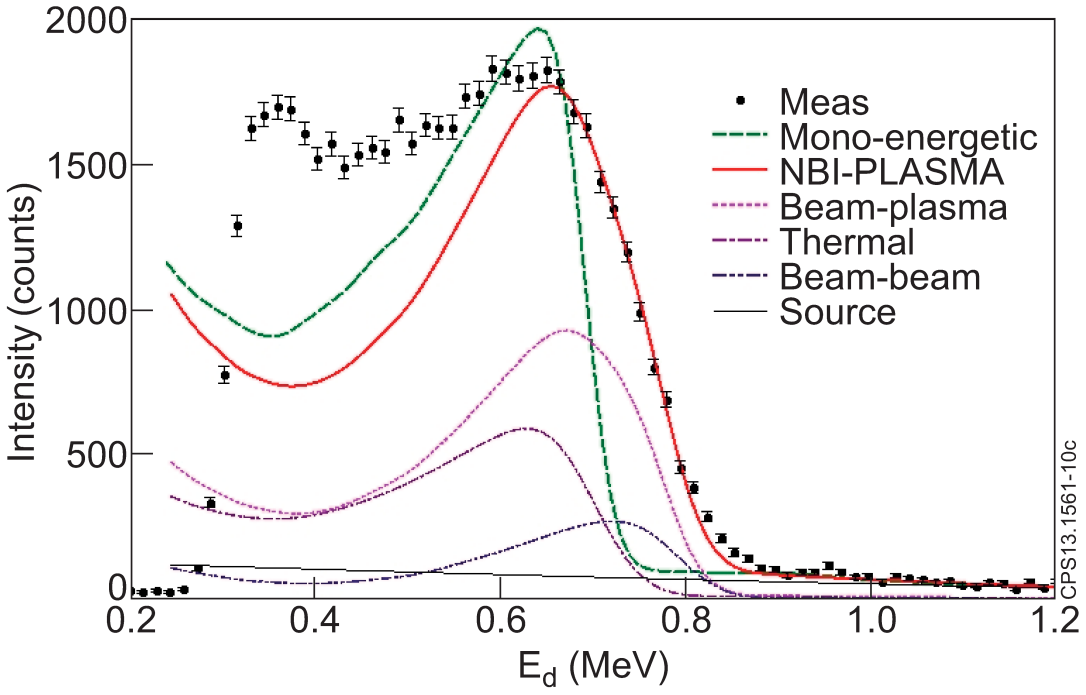

Figure 2.18: Measured SDD pulse height spectrum compared to simulations of the expected signal from different neutron emission models. The green dashed curve corresponds to mono-energetic neutrons at E=2.45 MeV. The solid red curve is instead the result of a neutron emission model for NBI injection, which includes thermal (pink dotted), beam-plasma (violet dotted) and beam-beam (blue dotted) reactions (see text for details). The background counting level from the triple-α calibration source is normalized to the measurement time. NBI-PLASMA is the sum of the four components Beam-plasma, thermal,Beam-beam and source. Figure taken from *Paper II*.

distributions are shown in Fig.2.16) come mostly from the polyethylene beam-dump, which is right after the diamond detector. The bump in the neutron scattered energy distribution starting at 1.8 MeV is due to back-scattering on carbon of CH_2. The main γ-ray line is due to neutron interaction on H of CH_2 .

The complete description of the measured data (solid line of Fig.2.19) thus included four contributions:

1. A primary component due to DD neutrons emitted from the plasma and that reach the detector

2. Scattered neutrons

3. γ-rays produced by the interaction of the primary neutrons with the MPRu LoS

4. Background events from the triple-α calibration source, normalized to measurement time.

These contributions are used for interpretation of the measured PHS as shown in Fig.2.19 in linear and log scale. Neutron scattering results in an excess of low energy neutrons that show up as a component of significant intensity up to $E_d = 0.5MeV$, with a rapid fall off at higher energies. γ-ray induced events in the SDD have a clear exponential shape.
Two normalization parameters only were determined by the fit, namely the absolute intensity of the primary neutron component and the amount of scattered neutrons. The scattered neutron/background γ-ray ratio was constrained to the value found by MCNP and confirmed by the NE213 measurements, which can distinguish signals from neutrons and γ-rays from their different pulse shapes. This allows for minimizing the number of free parameters in the fit. The background intensity from the triple-α source was known independently from a separate measurement and re-scaled to the actual measurement time during the plasma discharges.
With all four components included, we find a good agreement between measurements and data. In particular, neutron scattering amounts to 35% of the total, with background γ-rays contributing to about 20%. The contribution of the background components is mostly at low energies (say, $E_d < 0.5MeV$) negligible in the shoulder of the PHS, whose shape is completely determined by direct (primary) d+d neutrons.

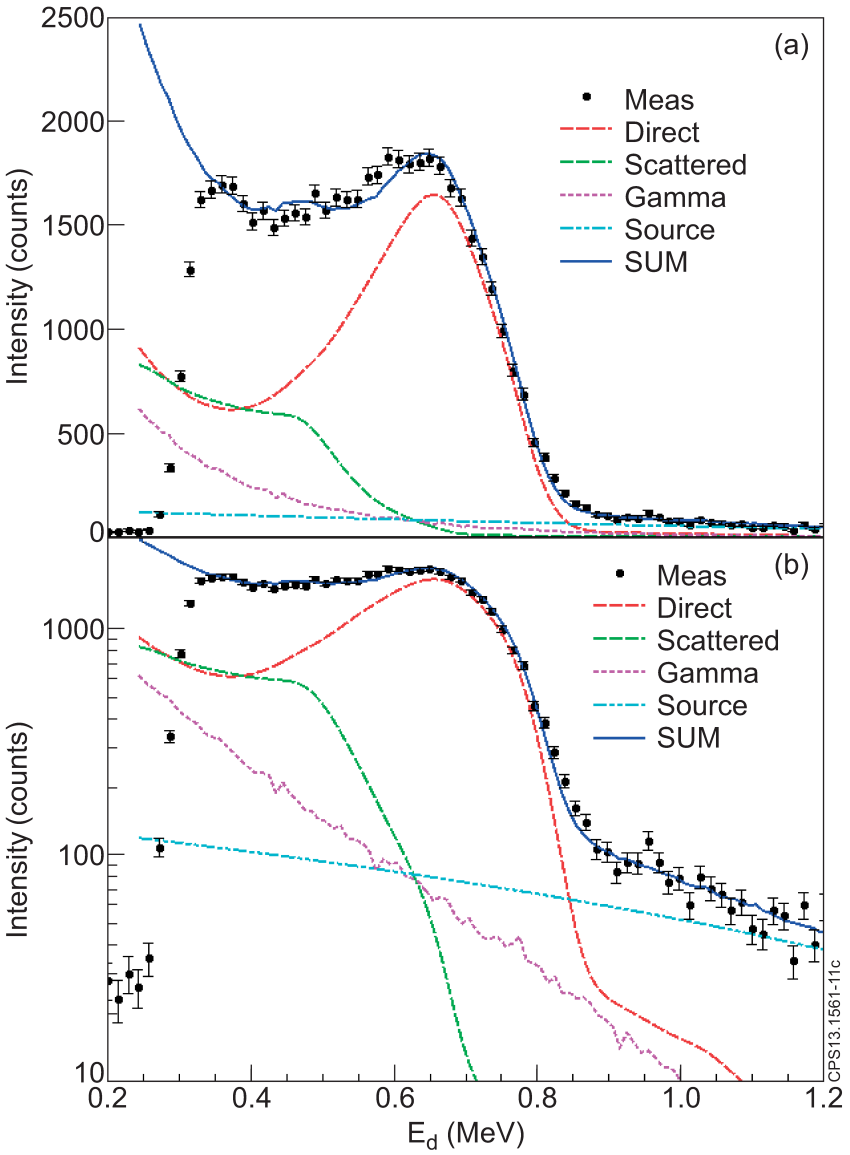

Figure 2.19: Measured PHS spectrum from a set of NBI plasmas as compared to simulations in linear (a) and logarithmic (b) scale. The simulated spectrum is the sum of four components: (1) a primary component due to d+d neutrons emitted from the plasma and that reach the detector; (2) scattered neutrons and (3) γ-rays produced by the interaction of the primary neutrons with the MPRu LoS ; (4) background events from the calibration source, normalized to measurement time. Figure taken from *Paper II*.

2.4 Experiments for spallation sources applications

2.4.1 Time-stability of a Single-crystal Diamond Detector for fast neutron beam diagnostic under alpha and neutron irradiation

Diamonds are known to be resistant to neutron irradiation. Nevertheless, measurements show transient effects during irradiation with ionizing particles. The decrease of detector counting rate is interpreted as due to a partial charge trapping, which modifies the electric field inside the detector. The so called *polarization effects* are strongly dependent on the nature of the interaction. Neutrons interact homogeneously in the whole detector volume whereas alpha particles, normally used as a calibration source, interact on the detector surface. Measurements have been carried out with both alpha particles, with a 37 kBq ^{241}Am calibration source, and neutrons at the ISIS neutron spallation source. We show that polarization effects are not permanent. The detector performances can in fact be promptly restored by changing the charge carrier type using, for instance, a High Voltage inversion.

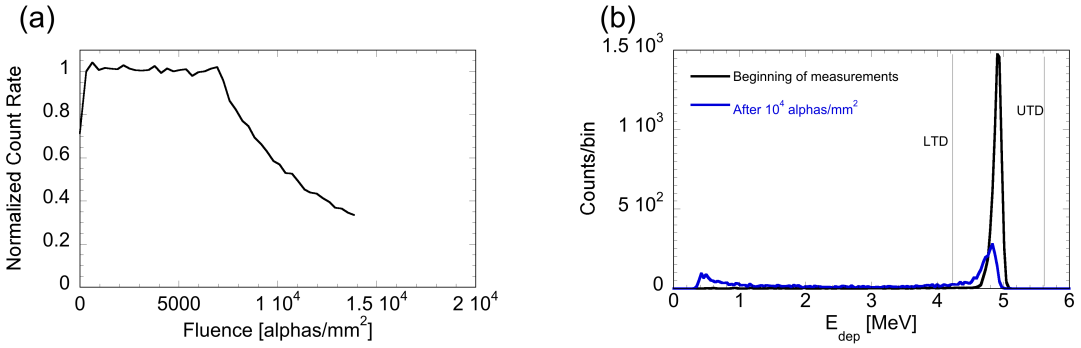

Figure 2.20: Stability (a) of the ^{241}Am alpha peak and degradation of the PH spectrum (b).

In order to study the time detector stability during the irradiation time, t_m, a time-resolved analysis of the spectrum in Fig.2.20.b was performed: as a significant parameter we used the full energy peak intensity. In practice, the peak integral between 4.3 MeV and 5.9 MeV was evaluated for constant time. At V_{bias}= +400 V alpha spectra have been acquired every 5 minutes for about 3 hours, the source count rate being 30 cps. Results of this analysis are reported in Fig.2.20, where the normalized count rate is reported as function of the source fluence rate. The full black line represents the detector stability obtained at V_{bias}= +400 V; the intensity is normalized considering the peak intensity of the first recorded spectrum. At V_{bias}=+400 V the SDD is peak intensity is constant, meaning that the SDD is stable, up to a fluence of $7 \cdot 10^3 \alpha/mm^2$ (about 1 hour); after that the intensity of the alpha peak rapidly decreases. This effect is called *polarization effect*. The irradiation time to get the detector fully polarized, *polarization time*, is related to the total counting rate, i.e. to the total charge deposited in the detector, and Vbias, which gives the electric field intensity into the detector bulk.

The time-stability of the SDD during the irradiation time (t_m) with neutrons was studied by counting during 290 seconds the number of signals whose amplitude was above the threshold of 150 mV (deposited energy equal to 6 MeV) (see Fig.2.21). The number of counts at different times is normalized with respect to the number of counts at the beginning of the measurement. The SDD behaviour is completely different from the one observed during alpha particle irradiation (Fig.2.20): the total counts decrease of 20 % in the first 50 minutes. After this transient

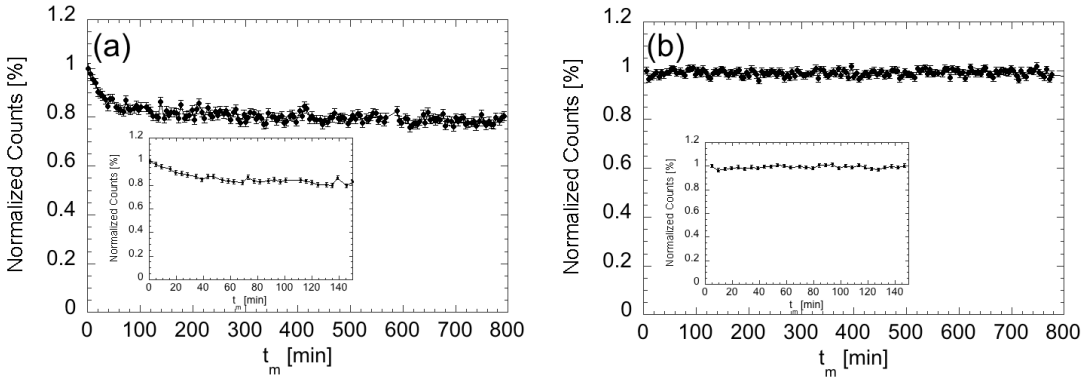

Figure 2.21: SDDs stability measured at the ISIS-VESUVIO beam line for two SDDs (see text).

time the counting rate is constant within 5%. In Fig. 3b the same plot is shown for the SDD-Al instead of the gold one. In this case the detector count rate is stable within 5% during the whole measurement.

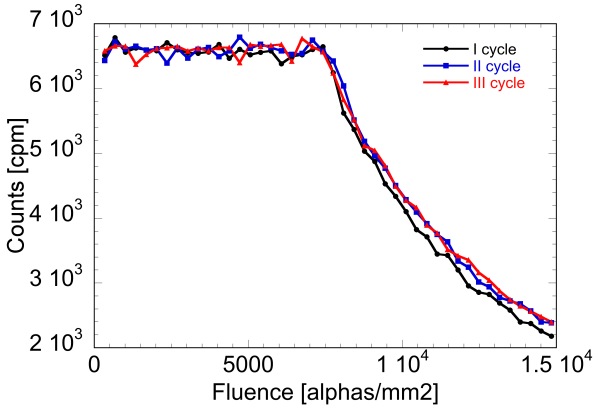

Figure 2.22: Stability of the Au-SDD under alpha particle irradiation, the source count rate was 110 cps. The polarization is induced by holes motion inside the detector, with a polarity inversion the detector properties are restored.

The V_{bias} switching off is not enough to completely restore the detector properties. On the other hand, if a polarity inversion of V_{bias} is performed, the signal and the electric field shape are restored. In Fig.2.22 an example of a cycle of polarity inversion is reported. Here, three cycles of polarity inversion were performed. The cycle consists of a periodic variation of Vbias: 45min at V_{bias}= +400 V , 30sec at V_{bias}= 0 V, 10min at V_{bias}= -400 V and then 30sec at V_{bias}= 0 V. Signals have been acquired during the +400 V regime, and the stability of the ^{241}Am peak is evaluated (as in section 2) during three HV-cycles. The source, placed near the bias contact, gives a rate of 110 cps and the fluence at which the detector is polarized is reproducible and equal to $7 \cdot 10^3/mm^2$.

A similar duty cycle was applied for the first time at ISIS. The cycle consists of a periodic variation of Vbias: 1 min at V_{bias}= +400 V, 5 sec at V_{bias}= 0 V, 30 sec at V_{bias}= -400 V and then 30sec at V_{bias}= 0 V.
Fig.2.23 shows the diamond detector time traces under neutron irradiation at ISIS with and without an HV duty cycle. Measurements were performed with the same diamond on different

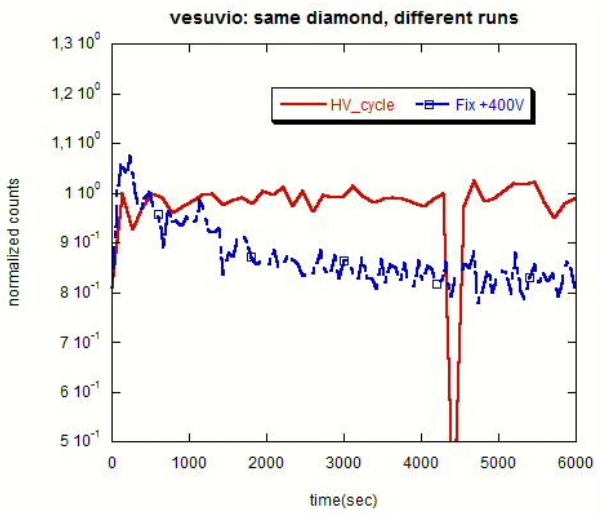

Figure 2.23: Diamond detector time traces under neutron irradiation at ISIS with and without an HV duty cycle. Measurements were performed with the same diamond on different runs of about 2 h.

runs of about 2 h. It is possible to appreciate that with a fixed bias the counting rate features a drop of 15% during the first hour. Using the HV duty cycle the counting rate remains constant during the whole irradiation time (when the ISIS beam was stable at 160 μA within a 5%), but for a quick drop around 4300 sec, after which the system recovers.
A further investigation is needed to understand intermittent failures of the system. Nevertheless, the HV duty cycle was demonstrated to be a good candidate technique to overcome the polarization problem on SDDs when operating on spallation sources.

2.4.2 Test of current preamplifiers for high instantaneous counting rates

Preamplifiers have been tested in order to cope with the high instantaneous flux expected on ChipIr (about $10^6 n/cm^2$ sec). A suitable preamplifier has to be as fast as possible in order to preserve the fast electric properties of the diamond. The Gain of the preamplifier has to match the application (neutrons of dozens of MeV), considering that the system in use is expected to be linear in the range 0-1 V. Tab.2.1 present the calibration of preamplifiers used for fast neutron experiments at ISIS with SDDs. It has been choosen so far to operate with commercially available preamplfiers. Fig.2.24 shows deposited energy spectra measured on PRISMA with a SDD using different preamplifiers in order to cover different energy ranges. A C6 pream cover lower energy range, but saturates at about 40 MeV, which correspond to 1 V of PH with this system. A C1 preamplifier allows for measurements at higher energies.

Preamp	1 MeV pulse height
C6	20 mV
C1	1.2 mV
C2	12 mV

Table 2.1: Calibration of pramplifiers used for fast neutron experiments at ISIS with SDDs.

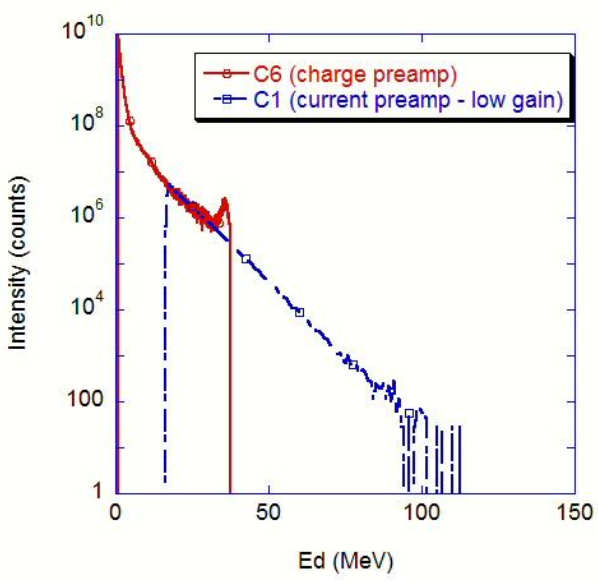

Figure 2.24: Deposited energy spectra measured on PRISMA with a SDD using different preamplifiers in order to cover different energy ranges.

2.4.3 Characterization of the PRISMA fast neutron flux using a SDD

PRISMA is an inverse geometry crystal-analyser spectrometer and high resolution diffractometer designed to measure excitations, critical scattering and diffuse scattering in single crystal samples, for measurements in the meV thermal energy range [137, 138]. This instrument is now decommissioned, and was exploited in this thesis as a detector testing position. The instrument shares the same line of sight with the ALF/ROTAX beam line, but it is closer to the spallation target (about 6 meters for PRISMA, 12 meters for ROTAX). For the normal use of the beam-line, a chopper is rotating in phase with the accelerator pulse, in order to cut away the fast neutron components of the spectrum, which are in general a source of background when operating in the thermal range. The chopper was set out of phase for this experiment, where we are interested in characterizing the fast neutron component of the spectrum.

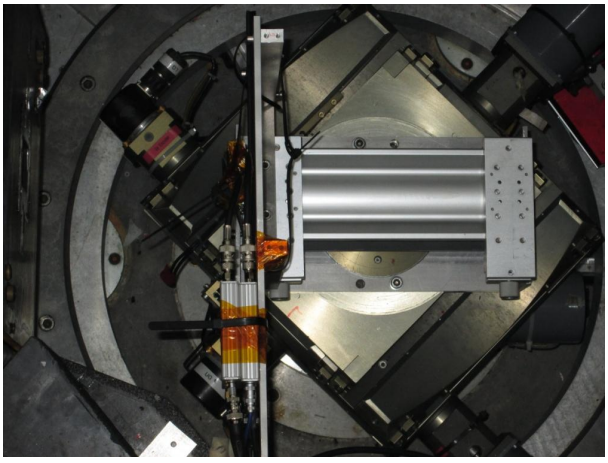

Figure 2.25: Picture of the detectors setup in the PRISMA beam-line.

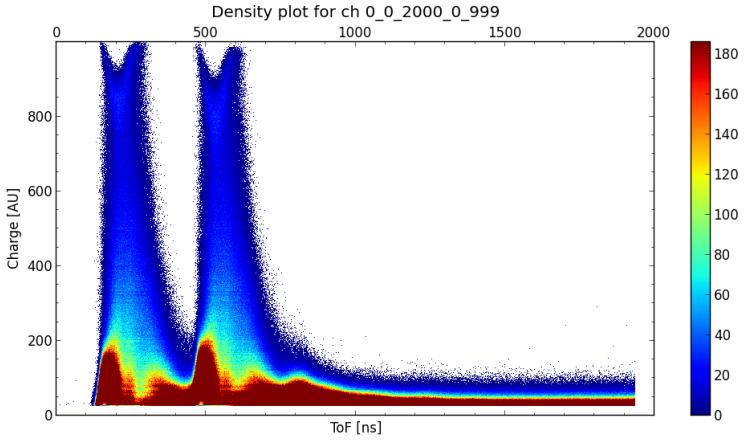

Figure 2.26: Bi-parametric contour plot of ToF and PH measured on PRISMA.

Fig.2.25 shows a picture of the detectors setup in the PRISMA beam-line. Two diamond detectors are mounted on a support and hold in the center of the neutron beam, coming from left to right in the picture. The C6 charge preamplifiers are also visible in the same picture. As explained above, the information of a neutron measurement with SDDs at a pulsed spallation source like ISIS are a combination of pulse height analysis (as done in ordinary spectroscopy) with Time of Flight analysis (ToF). Fig.2.26 shows the bi-parametric contour plot of ToF and PH measured on PRISMA. One can notice that the intensity distribution reflects here the double bunch structure of the ISIS proton pulse. These data can be reduced, by projection on the X or Y axis, and the deposited energy spectra (Fig.2.27) and ToF spectra (Fig.2.28) obtained. Deposited Energy spectrum measured on PRISMA is compared to other beam lines. The spectral shape above 7 MeV is almost identical to VESUVIO and ROTAX beam lines, while it is different at lower energies where γ-ray and scattered neutron play an important role. It is worth to notice that the neutron flux with $E > 10MeV$ of PRISMA is 5 times more intense with respect to the VESUVIO one. This result is of relevance for a possible use of PRISMA as a fast neutron irradiation point for detector testing or experiments for microchip irradiation. The 800 MeV proton beam has double bunch fine structure. The two proton bunches are about 70 ns wide (FWHM) and 322 ns apart, and their footprint can be seen in Fig.2.28, where the PRISMA and VESUVIO ToF spectra are compared. The VESUVIO beam-line is 11 meters, while PRISMA is only 6 meters long, and this result in shorter ToF for the same structures.

2.4.4 First experiments of fast neutron measurements on the ChipIr beam-line

First experiments were carried out to perform a preliminary characterization of the beam using diamond detectors.
As a first remark, we need to underline that ChipIr was not setup in its final configuration: the hole in the Be reflector will be cut only for 2015 operations, and therefore neutron transport on the beam-line is not yet optimized.

Fig.2.29 shows the schematics of the experimental setup for first fast neutron measurements on ChipIr. The signal from a SDD was split using a Fan-In-Fan-Out. One signal was fed to a 1Gsample digitizer for PH and ToF analysis. A copy of the signal was fed to a constant fraction discriminator, which in turn was sending logic signal to a counter. Similarly a Fission Chamber

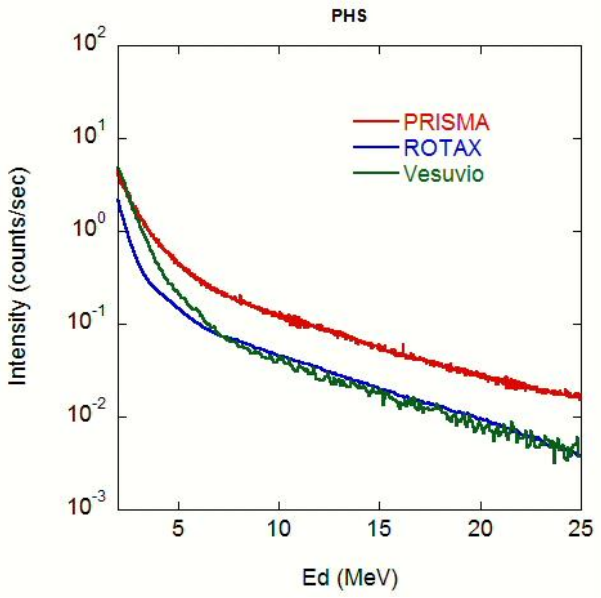

Figure 2.27: Deposited Energy spectrum measured on PRISMA compared to other beam lines.

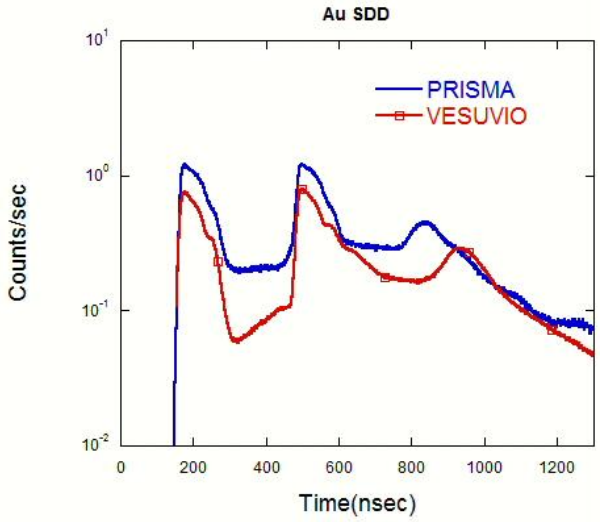

Figure 2.28: Time of Flight spectrum measured on PRISMA compared to VESUVIO.

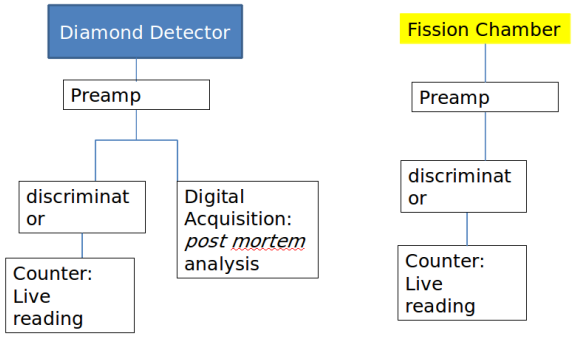

Figure 2.29: Schematics of the experimental setup for first fast neutron measurements on ChipIr.

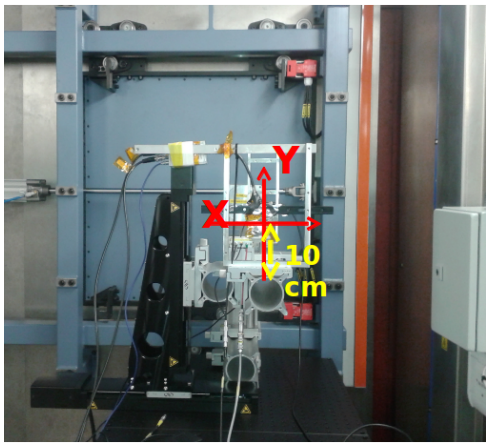

Figure 2.30: Picture of the experimental setup for first fast neutron measurements on ChipIr. SDDs are mounted on a X-Y movement system.

was used with a discriminator and a counter.
This measurement provides less information, but the results were available on-line during the experiments, without need for waiting for the post-mortem analysis. Two different threshold were used for the discriminator: 200 mV corresponding to about 10 MeV of deposited energy, and 400 mV, corresponding to about 20 MeV of deposited energy.

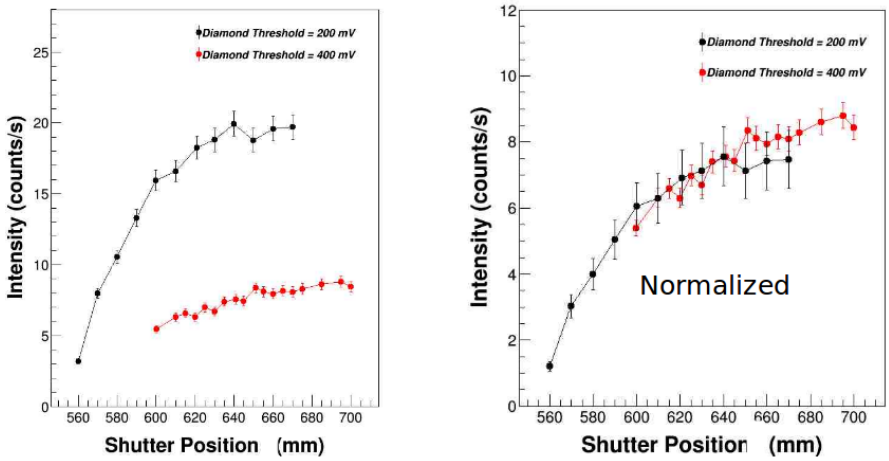

Figure 2.31: SDD count rate as a function of the shutter position using different thresholds.

Fig.2.30 shows a picture of the experimental setup. The SDDs are mounted on a X-Y movement system for a first attempt to map the ChipIr beam. The Fission Chamber is installed in a fixed position, to be used as a reference monitor during the profile scan. Fig.2.31 reports a measurement of the SDD count rate as a function of the shutter position using different thresholds. This measurements was needed for optimization of the shutter position, to define an effective opening for the following ChipIr operations. It was measured as expected an increasing neutron flux as the shuttering was opening, and a plateau is reached after 620 mm.

Fig.2.32 shows Partial ChipIr beam profiles measured by a SDD. The profiles could not be

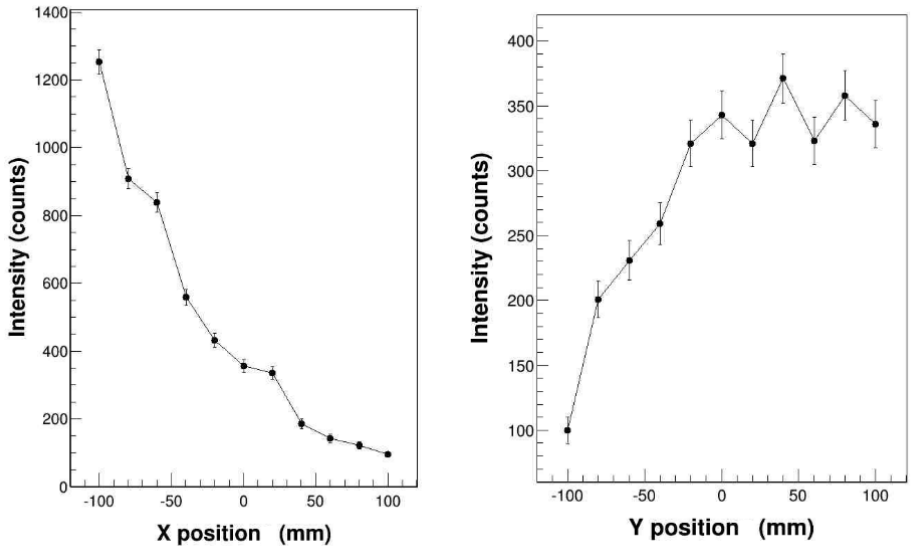

Figure 2.32: Partial ChipIr beam profiles measured by a SDD.

completed during this first measurements, because of the X-Y system setup. Further measurements will be needed in 2015 when ISIS will restart operations.
Fig.2.33 shows the Deposited Energy spectrum resulting from post-mortem analysis with the digitizer. The measured ChipIr spectrum is compared with measurement on VESUVIO with the same experimental setup and electronic chain. The spectral shape of the deposited energy spectrum is significantly different, with different slopes. In particular on VESUVIO it is clear the effect of the moderator with an enahanced component at low energy. Also at higher energy ($E > 10MeV$) the ChipIr spectrum has a harder spectrum. This is expected since, without moderator, the beam line is designed to stream the neutrons directly from the spallation target.

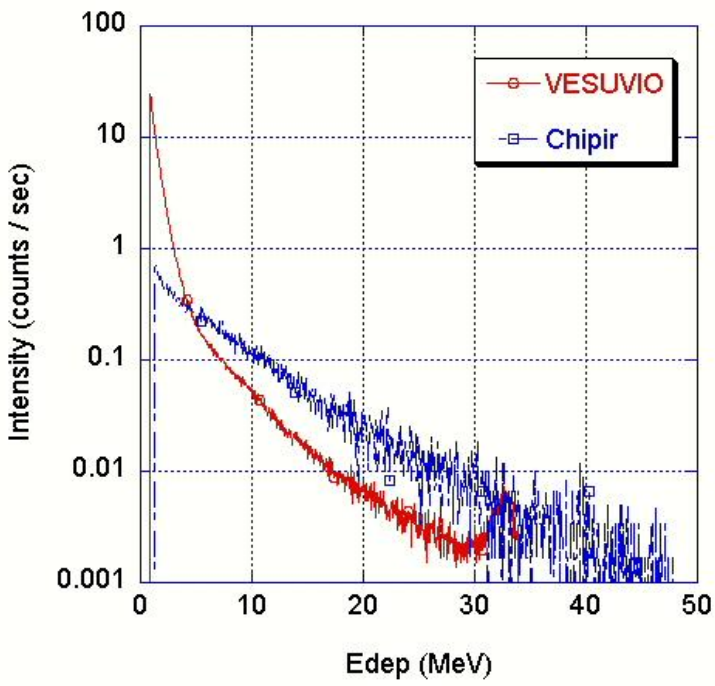

Figure 2.33: Deposited Energy spectrum measured on the ChipIr and VESUVIO beam-lines.

Chapter 3

Telescope Proton Recoil Spectrometers

E tutte queste cose furono scoperte e osservate pochi giorni or sono con l'aiuto d'un occhiale che io inventai.
– Galileo Galilei

3.1 Overview

The Telescope Proton Recoil (TPR) allows for a direct measurement of the fast neutron spectrum without using deconvolution algorithms, as illustrated in Chap.1, via eq.1.4. One of the prices to pay is the low efficiency of the spectrometer, typically in the orders of $10^{-7} - 10^{-5}$. The TPR is a consolidate technique in nuclear measurement, nevertheless, its design can vary a lot according to

i. The neutron energy range of interest.

ii. The energy resolution and the efficiency required by the applications.

iii. The background in the measurement environment.

In the design of a TPR, one has to consider the following issues

a. Proton detectors.

b. The target: passive or active hydrogenated material.

c. The geometrical parameters (target-detector distance, the recoil angle θ, the detector and the target solid angles Ω_D and Ω_T, the target thickness)

d. The vacuum system if needed.

In this thesis we considered a TPR for fusion application and a TPR for spallation sources. The two designs are different as explained in Chap.1. For diagnosing a fusion plasma, one has to measure at high resolution ($< 5\%$) the details of the 14 MeV line, and the counting rate has to be high (MHz) in order to follow the plasma on a msec time scale. On spallation sources the requirement on the energy resolution is less strict, but one has to handle a very high instantaneous counting rates due to the pulsed nature of the source and harsh measurement environment.
For both cases we choose a design with a passive polyethylene target and no vacuum system. An

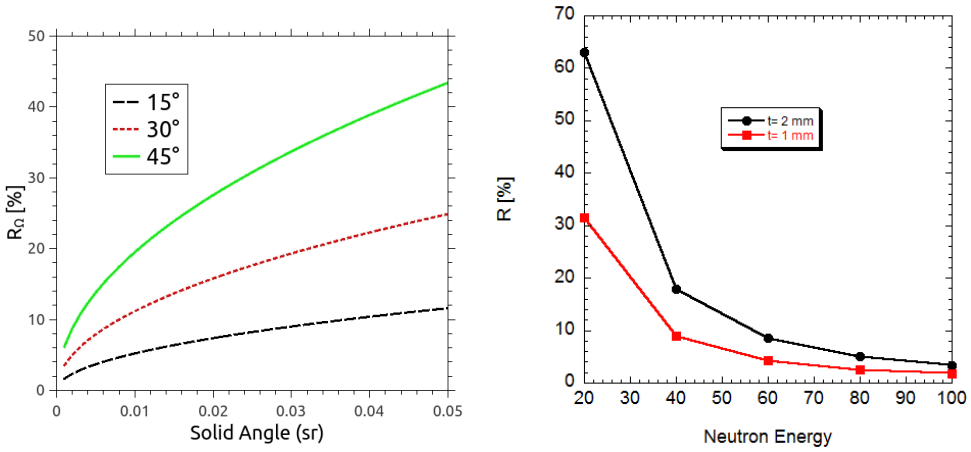

Figure 3.1: Calculated contribution to the energy resolution due to the detection solid angle Ω at selected recoil angles θ (left) and due to the target thickness t (at $\theta = 45$ deg)(right).

active target in fact would not cope with the high neutron fluxes expected for the applications. It has been calculated [147, 68] that the attenuation, at these energies, due to air at atmospheric pressure correspond to a contribution to the energy resolution smaller with respect to others. For fusion applications, the optimization of geometrical parameters was not a task of this thesis, and we refer to Ref.[68]. In this thesis we investigated the possibility of using fast scintillators (YAP and $LaBr_3$) as proton spectrometers (*Paper III*), with tests with laboratory sources and at proton accelerators.
For spallation sources, a TPR prototype was developed for measurement at the ISIS spallation source. We report the first results in the energy range 30 MeV $< E_n <$ 120 MeV (*Papers IV and V*).

3.2 Energy resolution and efficiency

Efficiency and energy resolution of the TPR system depend on several parameters that have to be optimized. The spectrometer resolution R is the combination of four effects

1. The target thickness t gives a contribution R_t to the resolution due to the energy loss of the protons exiting the polyethylene target.

2. The detector solid angle Ω_D with respect to the target centre gives a contribution R_{Ω_D} to the resolution, due to an uncertainty $\Delta\theta$ in the recoil angle.

3. The target solid angle Ω_T with respect to the detector centre gives a contribution R_{Ω_T} to the resolution, due to an uncertainty $\Delta\theta$ in the recoil angle.

4. The finite resolution of the proton spectrometer R_p.

and the TPR resolution is given by

$$R = \sqrt{R_t^2 + R_{\Omega_D}^2 + R_{\Omega_T}^2 + R_p^2} \tag{3.1}$$

in the hypothesis of uncorrelated contributions and approximated with equivalent gaussian functions. R_p is measured with calibration at proton accelerators, as presented below.
R_{Ω_D} and R_{Ω_T} can be analytically calculated as well as simulated with Monte Carlo codes.

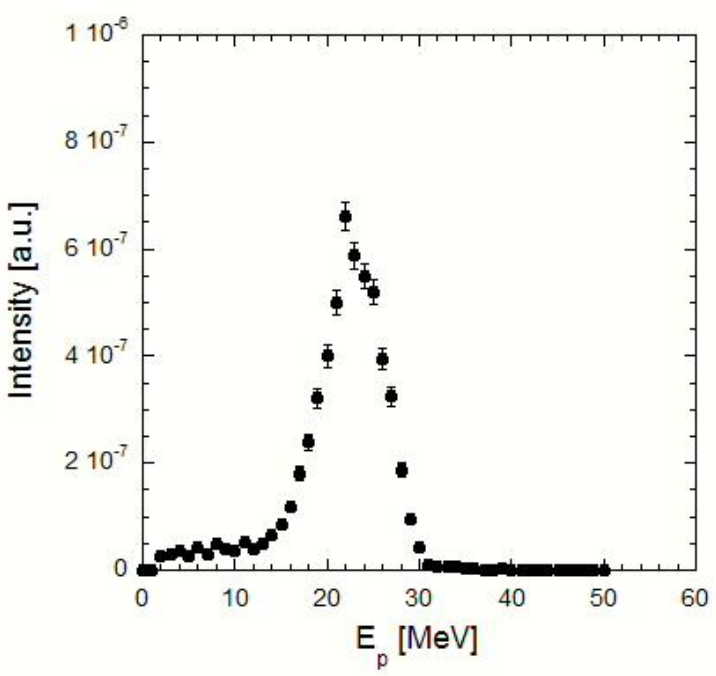

Figure 3.2: Simulated recoil proton energy distribution at the detector position for 50 MeV mono-energetic neutrons for the setup used at ISIS (see Section.3.4).Figure taken from *Paper IV*.

For the analytical calculation we refer to Ref.[139]. If one considers the detector and the target (at distance d) to have a circular area of radius r, the solid angle is $\Omega = \pi r^2/d^2$. Defining $\Delta\theta = arctan(r/d) = arctan(\sqrt{\frac{\Omega}{\pi}})$ we can estimate

$$\frac{\Delta E_n}{E_n} = \frac{cos^2(\theta - \Delta\theta) - cos^2(\theta + \Delta\theta)}{cos^2(\theta)} \tag{3.2}$$

This contribution is independent by the neutron energy, and it increases when θ is larger. This is due to the fact that the function $cos^2\theta$ has a larger derivative. Fig.3.1 presents on the left the resolution as a function of the solid angle at three selected recoil angles. It is clear that to optimize the resolution one would like to have a small recoil angle θ, which can be difficult because the proton detectors would come closer to the beam with the effect of increasing the background. Similarly one would like a small Ω_D and Ω_T, but this would clearly reduce the detector efficiency. Since eq.3.1 holds, it is clear that the optimum is having the target area equal to the detector area, and therefore $\Omega_D = \Omega_T$. Having one of the two considerably smaller then the other would reduce the detection efficiency without an improvement in the resolution, that would be dominated by the larger contribution.
R_t can be analytically calculated and simulated with Monte Carlo codes (SRIM, MCNP). For the analytical calculation we refer again to Ref.[139]. For a thin ($\Delta E_p << E_p$) target the proton energy loss in the target is proportional to the target thickness t

$$\Delta E_p = \left(\frac{dE}{dx}(E_p)\right) \cdot t \tag{3.3}$$

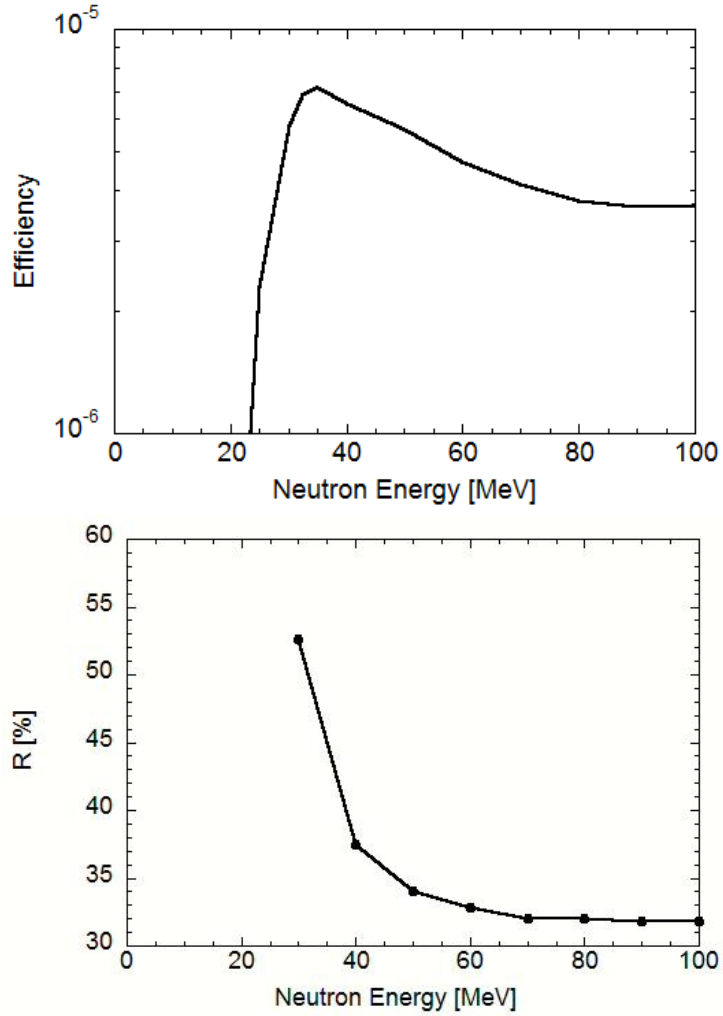

Figure 3.3: Simulated TPR efficiency (top) and energy resolution (bottom) for the setup used at ISIS (See details in Section.3.4). Figure taken from *Paper IV*.

The contribution due to the proton energy loss have a box-like shape that, which can be associated to an equivalent Gaussian width [139]. The contribution to the resolution becomes

$$R_t = \frac{2.35}{\sqrt{12}} \frac{\Delta E_p}{E_p} \tag{3.4}$$

If the approximation of thin target does not hold any more, eq.3.5 can not be used and the analythical representation is more complicated. A more time effective way of calculating the efficiency is via Monte Carlo methods. Fig.3.1 presents on the right the resolution as a function neutron energy (at $\theta = 45$ deg) for two selected target thickness. This contribution is dominant at lower energies. It is clear that reducing the target thickness improves the resolution at the expanse of a smaller efficiency (which for thin targets is linear with the thickness).
The efficiency ϵ of the TPR can be expressed by the equation

$$\epsilon = n \left(\frac{d\sigma}{d\Omega} \right) \Omega_D t \tag{3.5}$$

where n is the atom density and t the target thickness. For the ISIS prototype measurements an acceptable efficiency was obtained at the price of relatively poor energy resolution.
A MCNPX model was used to determine the TPR efficiency and energy resolution for monoenergetic neutrons for the ISIS prototype. In the model a collimated neutron beam is directed towards a polyethylene target foil. The system geometry was taken into account with sufficient level of detail, including the ΔE detector with thin entrance and exit aluminum windows and air along the proton flight path.At the proton detector position the proton energy distribution is given as output of the simulations. The proton energy distribution was calculated for several neutron energies; Fig.3.2 shows an example for 50 MeV neutrons. The computed efficiency is defined as the ratio between the number of protons arriving at the detector position and the number of neutrons hitting the target foil. The computed energy resolution is given by the FWHM of the proton energy distribution, using a fit assuming a Gaussian distribution. Fig.3.3 show the simulated efficiency and resolution as function of neutron energy.
It is worth to notice from Fig.3.3 that the efficiency is vanishing for under 20 MeV neutrons. They correspond to 10 MeV protons (according to eq.1.4), which are not energetic enough to reach the proton E detector, and are stopped either by the polyethylene foil itself, by the ΔE detector or by the air. Neutrons above 30 MeV correspond to protons above 15 MeV, which are energetic enough to reach the YAP detector. Efficiency for neutrons in the $30MeV < E_n < 100MeV$ range is dominated by the elastic scattering macroscopic cross section and it ranges (see Fig.3.3) from $7 \cdot 10^{-6}$ to $4 \cdot 10^{-6}$.
In Fig.3.3 one can notice a very poor resolution below 40 MeV. This is due to the fact that in this energy range energy resolution is dominated by the contribution of the thickness of the scattering foil. The resolution is rather flat above 50 MeV and it is about 30%. In this region the dominant effect is due to the detector-foil solid angle contribution. A significant improvement on the energy resolution is expected if, thanks to a better background reduction, one could choose a smaller scattering angle, because the proton recoil energy would increase according to eq.1.4.

3.3 Characterization of proton detectors

The detectors considered in this thesis for proton spectroscopy are:

- A 500 μm thick Silicon detector by Ortec [141] to be used as ΔE detector.

- Two thin YAP and $LaBr_3$ scintillators (1" x 2 mm) for E measurement of protons with $E_p < 20MeV$.
- A thick YAP scintillator (1" x 1") for E measurement of protons with $E_p < 100MeV$.

3.3.1 Characterization of Silicon Detectors

Silicon detectors are effective ΔE detectors because of their high resolution and fast signals.

- High resolution is guaranteed by the large number of information carriers (electron-hole pairs) that are produce per single interaction. The energy per electron-hole pair production is 3.62 eV.
- The electron and hole mobility allows, when a semiconductor is operated with a large enough electric field, for saturated velocities in the order of $10^7 cm/s$. This corresponds, for thickness $< 1mm$, to a signal of duration under 10 nsec.

As said above, a 500 μm thick Silicon detector by Ortec [141] has been used (Picture in Fig.3.4). To test the best spectroscopic capability of the detector, a measurement was set up with a traditional spectroscopic chain, which features a charge preamplifier Ortec-142-A, a shaping amplifier Ortec-570 with 1 μs shaping time, and a MAESTRO ADC [141]. The spectrum of a ^{241}Am alpha source has been measured in vacuum.

The Pulse Height spectrum (see Fig.3.5) present an energy resolution of 0.7% at the 5.485 MeV

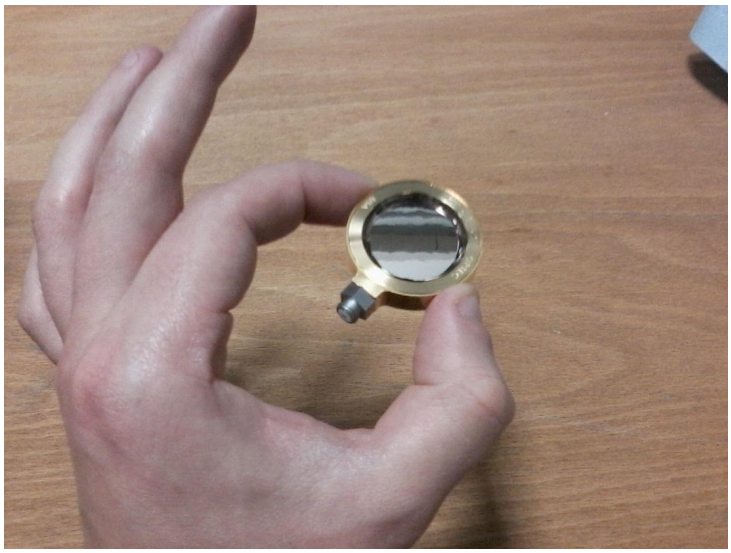

Figure 3.4: Picture of a 500 μm thick silicon detector.

peak of ^{241}Am. As a matter of fact, when the spectrum is analysed in log scale (see bottom of Fig.3.5), one can distinguish the four most intense α-lines of ^{241}Am: $\alpha_1 = 5.486$ MeV (84.5%), $\alpha_2 = 5.443$ MeV (13.0%), $\alpha_3 = 5.388$ MeV (1.6%) and $\alpha_4 = 5.545$ MeV (0.34 %), values from Ref.[151].

Although the spectroscopic chain gives the best results for energy resolution, it is not possible to exploit it for high rate applications, since it is too slow. Therefore, the possibility of using signals of duration < 10 nsec has been investigated. This can be achieved using a charge preamplifier that preserve the intrinsic time properties of the signal induced by the migration of electron-hole pairs in Silicon. The C2 preamplifier by CIVIDEC [126] has been used. Signals from the C2 preamplifier are fed into a 4 channel desktop digitizer with 1 GHz sampling

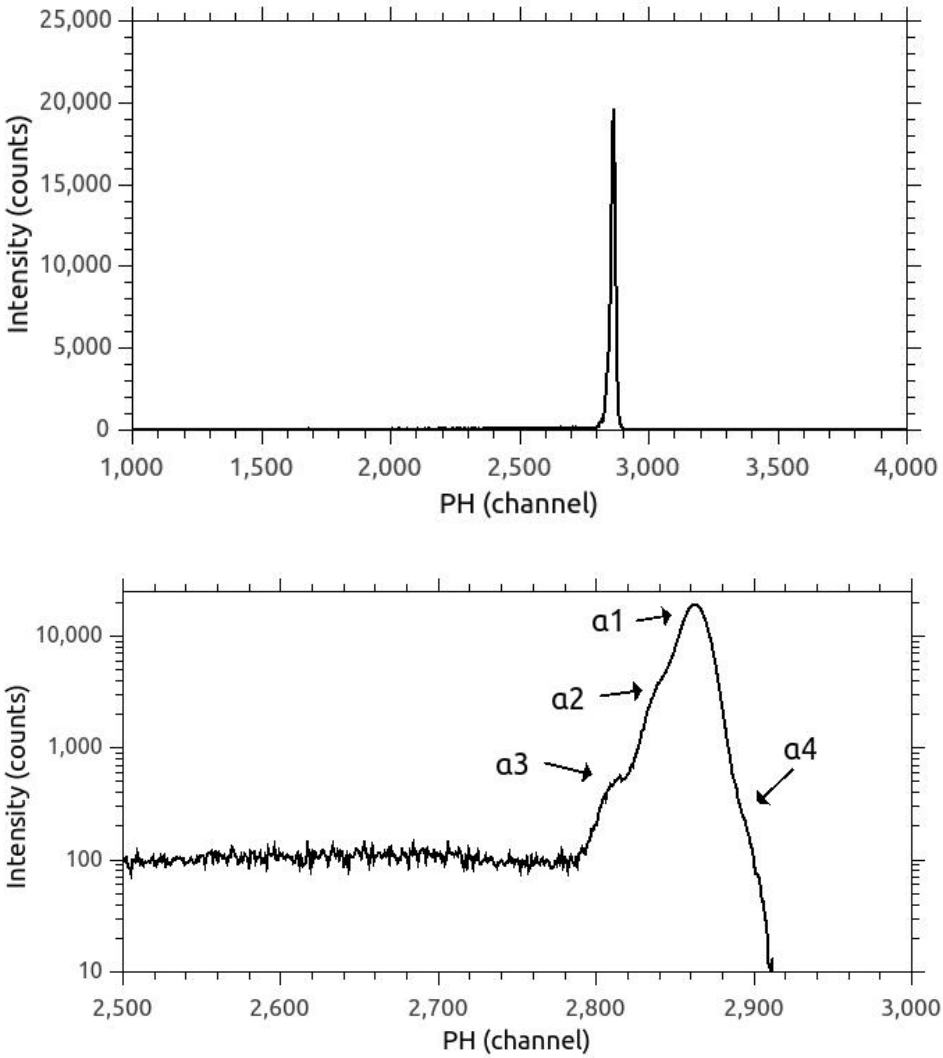

Figure 3.5: Alpha measurement with a ^{241}Am source in vacuum with spectroscopic electronic chain (top), and the same in log scale (bottom).

frequency, 0-1 V input range and 10 bit resolution [128].
The Pulse Height spectrum (see Fig.3.6) presents an energy resolution of 3.2% at the 5.485 MeV peak of ^{241}Am. This is clearly worst then the 0.7% of the spectroscopic chain, but it is suitable for a spectrometer that aims at an overall neutron energy resolution of about 5%.
Similarly we tried the fast charge preamplifier C6 [126]. This gives a slower signal $\simeq 30nsec$ with reflections, since this is optimize for detectors with smaller capacities (e.g. diamonds). A resolution of 3.2% is achieved, as shown in Fig.3.6.
After these tests we selected the C2 preamplifier to be used in the prototype TPR.
Proton measurements have been performed at the Legnaro Tandem-ALPI-PIAVE accelerator

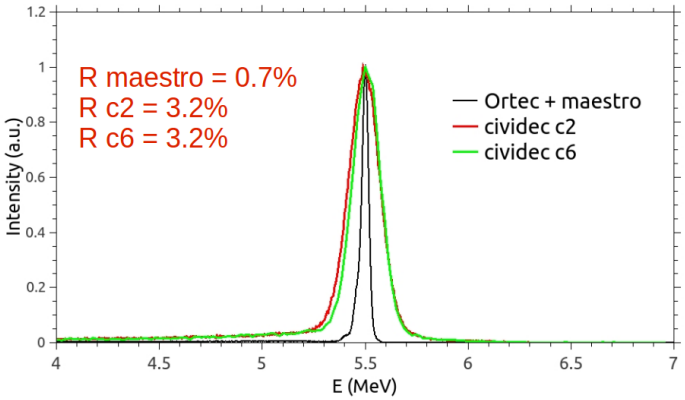

Figure 3.6: Alpha measurement in vacuum with spectroscopic and fast electronic chains.

[152]. Here The High Voltage Terminal exceeds 14.5 MV positive voltage as the maximum operational electrostatic value. Protons can be accelerated from 8 MeV to 28 MeV. Measurements have been performed at different energy values.
The Silicon detector was setup inside an interaction chamber, this has a cylindrical shape with a diameter of about 0.5 m. The proton beam enters from the aperture on one side of the chamber, along a diameter and perpendicularly to the chamber plane. The experiment was performed using a Rutherford scattering configuration [142] on a gold foil target ($\simeq 3\mu m$), which was necessary to significantly reduce the proton current on the detector, that would otherwise result in counting rates well beyond the MHz range that can be coped with by the device. A proton back-scattering angle on the gold foil of about 140 deg with respect to the proton beam was chosen.
Experimental difficulties were posed by the fact that it was the first time that protons were collimated on the specific beam line that has been used. Usually the experimental line is used with heavy ions. For this reason, a poor collimation on the gold scattering target was achieved, and the resulting peak is broadened, probably by protons scattering on other materials in the chamber. The measurement has to be considered as a first explorative attempt and will be repeated in 2015. The same is true for what is presented below, regarding tests of thin scintillators.
Nevertheless, if is not worth to consider the information on energy resolution to be reliable, we can still present results about the measured energy spectra. Those are shown for selected energies in Fig.3.7. as expected the deposited energy is larger for decreasing proton energy. The centroid of the peak is used to build the plot in Fig.3.8, where the measured deposited energy is shown as a function of the nominal proton energy. It is possible to notice the characteristic distribution, that derives from the Bethe formula [150].

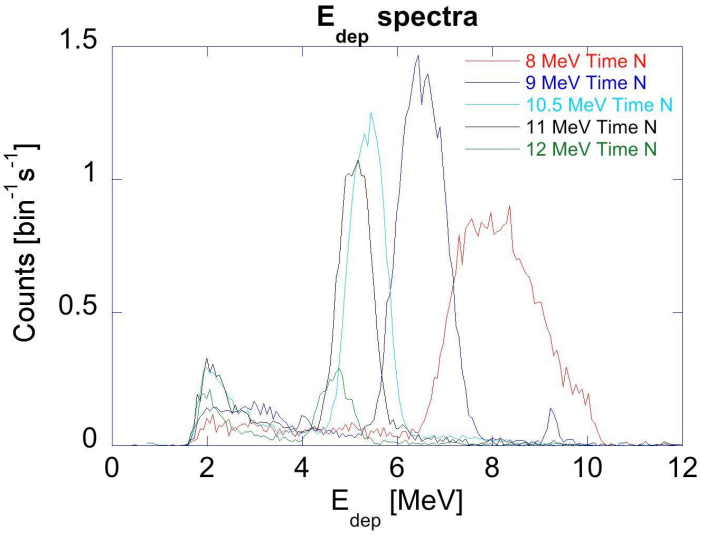

Figure 3.7: Deposited energy spectra measured at the Legnaro Tandem-ALPI-PIAVE accelerator with a fast electronic chain, selected for several proton energies.

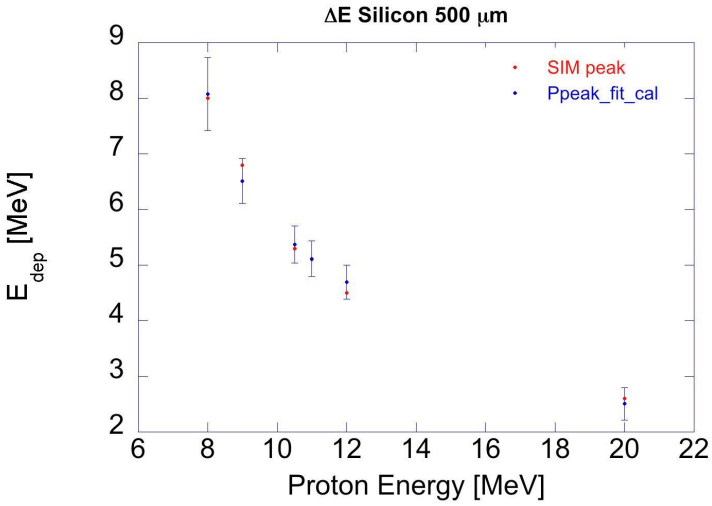

Figure 3.8: Proton measurement at the Legnaro Tandem-ALPI-PIAVE accelerator with a Silicon detector. The measured deposited energy is shown as a function of the nominal proton energy.

3.3.2 Characterization of fast inorganic scintillators

Thin YAP and $LaBr_3$ crystals

Two thin inorganic scintillators based on YAP and $LaBr_3$ crystals (1" diameter x 2 mm height, see picture in Fig.3.9) have been coupled to two eight dynode Photo Multiplier Tubes (PMTs), model R6231 by Hamamatsu [140]. Special care was taken in the case of $LaBr_3$ which, being hygroscopic, was encapsulated on all sides by the supplier, with a thin (125 μm) Be entrance window. This is where the proton beam was impinging in the experiment and was needed to minimize energy loss, that would otherwise not be tolerable in the thick encapsulating material. The ^9Be window was not needed for YAP, as this crystal is not hygroscopic. In this case, a thin (20 μm) aluminium layer was used for the purpose of light collection optimization only.

Figure 3.9: of a 2 mm thick YAP and $LaBr_3$ scintillators.

Detector characterization with laboratory γ-ray sources

The thickness of the two crystals is optimized to stop protons up to 20 MeV. For this reason the detectors have low efficiency to γ-rays, which are the main background source during the measurement. Nevertheless, the high density and high effective Z of the crystal allow distinguishing full-energy-peaks when the crystal is irradiated with laboratory γ-ray sources. An electronic chain devoted to energy resolution measurements and consisting of a ORTEC 570 amplifier and an ORTEC Multichannel Analyser was prepared [141]. These measurement are useful to determine the energy resolution of the two crystals to γ-rays in the MeV range, obtained from the FWHM of the full-energy peaks. A ^{137}Cs and ^{60}Co sources were used for this scope with the results summarized in Table 1 for YAP and $LaBr_3$. Here we note that the energy resolution found in the two cases does not significantly differ, especially above 1 MeV, where it is practically identical and has a value of 3.8%. This number can be compared to the expected light yield of 63000 photons-per-MeV of $LaBr_3$ [77] and 20000 to 25000 photons-per-MeV of YAP [143, 144, 145, 146], which would imply a much better resolution for $LaBr_3$. The difference can be qualitatively understood based on other contributions to the energy resolution. These are, for instance, variations in the luminescence and transparency characteristics of YAP depending on the concentration of the Ce doping and crystal phases [146]. Finally, there can be a further contribution due to non-homogeneous light collection over the crystal volume. This

can be minimized by optimizing the coupling of the crystal to PMT.
Fig.3.10 shows the measured γ-ray spectrum from a ^{60}Co calibration source using $LaBr_3$ and

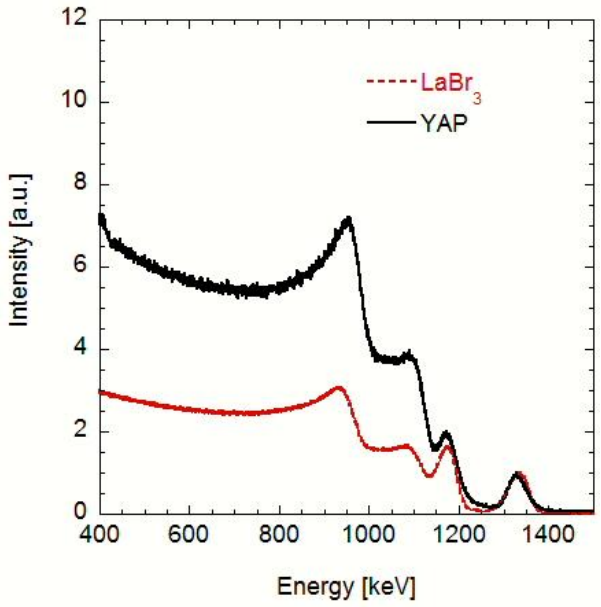

Figure 3.10: γ-ray spectra from a ^{60}Co γ-ray laboratory source measured with the thin $LaBr_3$ and YAP scintillators used in the proton measurements at Uppsala. Figure taken from *Paper III*.

YAP. The spectra are normalized to unity at the 1.33 MeV peak. In both cases, the two full energy peaks corresponding to 1.17 and 1.33 MeV γ-rays from ^{60}Co can be observed, which were used to determine the energy resolution values reported in Tab.3.3.2 Most of the events lie in the Compton shoulder, as expected from the limited thickness of the scintillators, that provides a peak-to-Compton ratio of about 1/4 for YAP and 1/2 for LaBr3.

Source	Peak Energy	$LaBr_3$ Resolution	YAP Resolution
^{137}Cs	0.66 MeV	4.2%	5.5%
^{60}Co	1.17 MeV	3.5%	3.8%
^{60}Co	1.33 MeV	3.7%	3.8%

Table 3.1: Energy resolution values (FWHM/E) measured with γ-ray sources for the thin $LaBr_3$ and YAP scintillators used in the proton experiment.

Proton measurements at the Uppsala tandem accelerator

The scintillators were irradiated with 4 to 8 MeV protons from a tandem accelerator at Uppsala University. The accelerator features an accelerating voltage up to 5 MV and can produce beams of protons as well as heavy ions. Fig.3.11 shows the setup of the experiment in Uppsala inside the proton interaction chamber, i.e. a metal cylinder with a diameter of about 0.5 m. The proton beam enters from the aperture on one side of the chamber, along a diameter and perpendicularly to the chamber s plane. The experiment was performed using a Rutherford scattering configuration [142] on a gold foil target ($\simeq 3\mu m$), which was necessary to significantly reduce the proton current on the detector, that would otherwise result in counting rates well

beyond the MHz range that can be coped with by the device. A proton scattering angle on the gold foil of about 45 deg with respect to the proton beam was chosen. The PMTs were operated with a negative High Voltage of 750 V and energy calibration was repeated in situ with ^{137}Cs and ^{60}Co .

The spectroscopic chain is the reference for energy resolution measurements, but it cannot

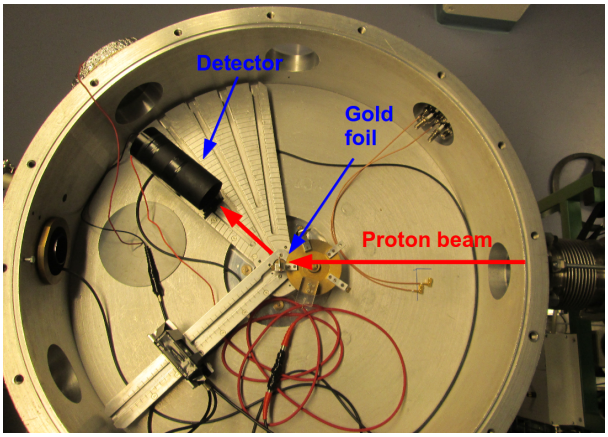

Figure 3.11: Experimental setup at the Uppsala tandem accelerator. The position of the detector and target (a gold-foil) for the Rutherford scattering experiment are indicated, together with the proton beam direction. Figure taken from *Paper III*.

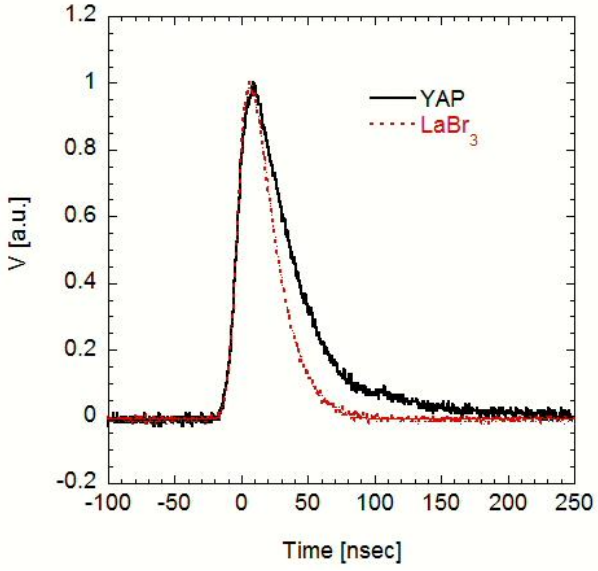

Figure 3.12: Measured YAP and $LaBr_3$ signals from the PMT anode. Figure taken from *Paper III*.

be used at high rates (MHz), since the shaped signals after the amplifier have a too long time constant (μsec). High rate measurements can however still be performed by direct digitization of the signal from the PMT anode using a digital acquisition system. Count rates up to a few MHz can be handled thanks to the fast scintillation time of YAP and $LaBr_3$ crystals, which is 27 and 16 nsec, respectively, with only a moderate degradation in the energy resolution, as demonstrated in Ref.[80]. The shapes of YAP and $LaBr_3$ signals after the PMT anode are compared in Fig.3.12. In particular, we can here notice a clear difference in the falling edges of

the two signals, which are due to the different time constant of the crystals. The rising edge is instead similar, as this part of the signal is dominated by the PMT response, which is the same for both scintillators.
Fig.3.13 compares proton energy spectra, normalized to peak height, measured with the thin $LaBr_3$ and YAP scintillators at the Uppsala tandem accelerator in the Rutherford scattering experiment described in section 2 and using a 8 MeV proton beam. The x-axis scale corresponds to the known proton beam energy corrected for the energy loss in the entrance window of each detector. This was calculated using MCNPX and was found to be larger (1.1 MeV) for the 125 μm Be window of $LaBr_3$ than in the case of the YAP Al window (0.2 MeV).
Different background levels can be also observed for the two measurements, due to the different position of the two detectors in the interaction chamber. In particular, YAP was closer to the proton beam dump.
Besides introducing a correction in the energy scale on the x-axis of the spectrum, the entrance

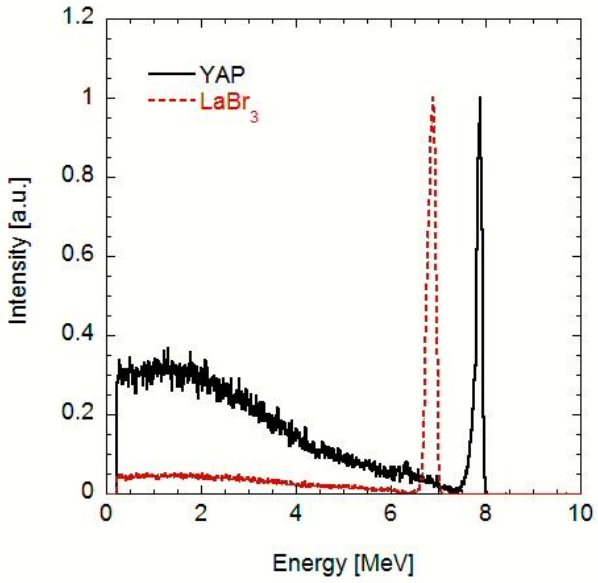

Figure 3.13: Proton energy spectra measured with thin $LaBr_3$ and YAP scintillators at the Uppsala tandem accelerator using a 8 MeV beam. Figure taken from *Paper III*.

windows also give a finite contribution to the detector energy resolution that sums up to those from statistics, electronic noise and intrinsic crystal effects, such as a non ideal light collection by the PMT. This finite contribution, which is relevant in the case of the $LaBr_3$ Be entrance window, proton straggling, and it is calculated by MCNPX to range from 8.8% to 1.2% MeV as the energy of the proton beam varies in the range 4 to 8 MeV.
The overall proton energy resolution of thin $LaBr_3$ and YAP scintillators measured for $4MeV < E_p < 8MeV$ are presented in Fig.3.14. The energy dependence of the resolution suggests a predominance of straggling effects for the $LaBr_3$ detector below 7 MeV. This is likely to be the reason why YAP outperforms LaBr3 for $E_p < 8MeV$. Finally, it is worth noticing that, based on our measurements, the energy resolution of both detectors is better than 2% for $E_p > 7MeV$, which is an excellent value and promising result in view of the design of a scintillator based TPR spectrometer for applications at fusion devices and spallation sources.

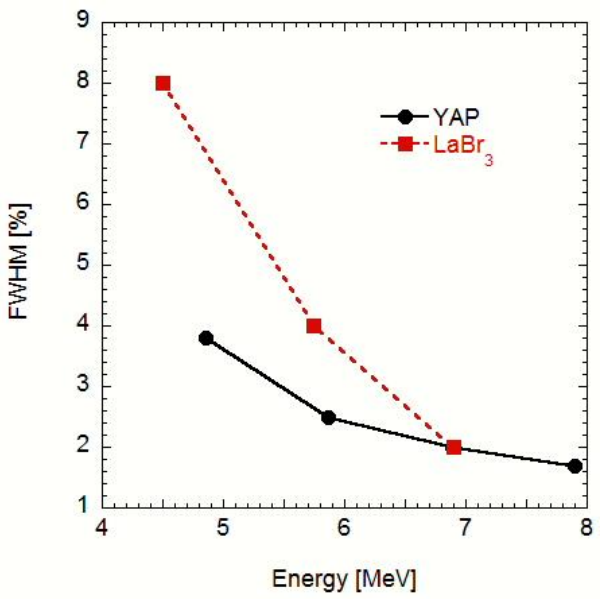

Figure 3.14: Energy resolution of thin $LaBr_3$ and YAP scintillators measured at the Uppsala tandem accelerator at different proton beam energies. Figure taken from *Paper III*.

Proton measurements at the Legnaro Tandem-ALPI-PIAVE accelerator

The scintillators were irradiated with 8 to 20 MeV protons at the Legnaro Tandem-ALPI-PIAVE accelerator.
Here a 1"x1" YAP scintillator was used along with the two thin YAP and $LaBr_3$ scintillators. As explained before, experimental difficulties in the proton beam collimation compromised the information on the energy resolution. Therefore, the measurements at the Legnaro Tandem-ALPI-PIAVE accelerator will be repeated in 2015.
Nevertheless, the measurements are useful for energy calibration of the system, in terms of relative proton/gamma light yield. The light yield of a scintillator crystal under proton irradiation is different from that measured with γ-rays of same energy due to quenching effects. For these relative measurements, the detectors were energy calibrated (in MeVee, MeV electron equivalent) with ^{137}Cs and ^{60}Co γ-ray sources. In Fig.3.15 the Pulse Height amplitude in MeVee (i.e. the centroid of the spectrum, found using a gaussian fit) measured by the two YAP and $LaBr_3$ scintillators is plotted as a function of the nominal proton energy. The most important information is that the light yield ratio proton/gamma is about 1 for the YAP scintillator, while it is measure to be about 75% for the $LaBr_3$ crystal.
The light collection for the YAP 1"x1" crystal is sensibly less then the 1"x2mm crystal. This fact is possibly explained by YAP self light absorption [146].

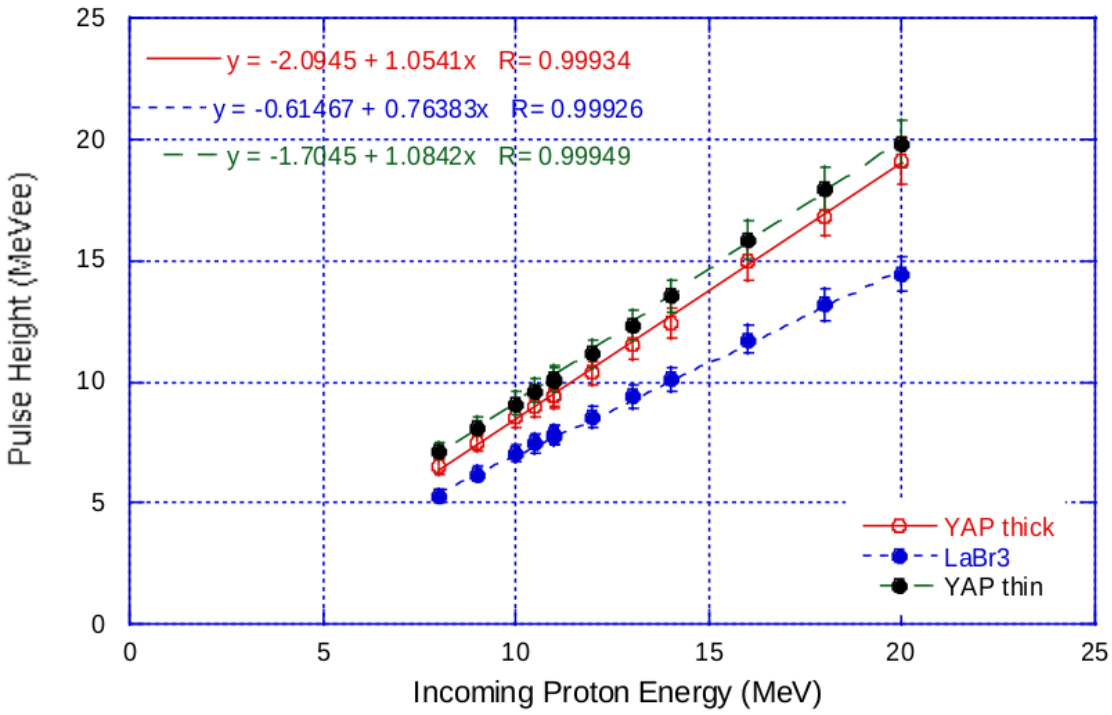

Figure 3.15: Pulse height amplitude in MeVee measured by the YAP and $LaBr_3$ scintillators as a function of the nominal proton energy.

3.4 Measurements of the fast neutron spectrum at the ISIS spallation source

Experimental setup

A picture of the experimental setup of the TPR spectrometer on the VESUVIO beam-line is shown in Fig.3.16. A 2 mm thick polyethylene foil intercepts the entire beam cross section (about 5 cm in diameter). The proton spectrometer is placed clear of the neutron beam at 19 cm from the target and at an angle of 45 deg with respect to the neutron direction. At this angle recoil protons have 1/2 of the corresponding neutron energy, due to the elastic scattering kinematics (eq.1.4). The geometry sets the efficiency and resolution of the spectrometer, and the current configuration was chosen as a compromise of the two.
The proton spectrometer is composed by a 500 μm thick silicon detector for ΔE measurement and a 2.54 cm thick YAP scintillator for E measurements. The YAP scintillator is thick enough to stop protons up to about 100 MeV [147]. Both detectors have a circular section with a diameter of 2.54 cm. The YAP crystal is coupled to a Hamamatsu R9420-100-10mod photo-multiplier-tube (PMT) [140], where a High Voltage (HV) of -600 V is applied. The Silicon Detector is coupled to a current preamplifier CIVIDEC C2 [126] with a HV of +170 V.
The YAP spectrometer was previously calibrated with gamma sources of ^{137}Cs and ^{60}Co . The ratio between the proton light yield to photon light yield is assumed to be 90% according to measurements performed at proton accelerators (Fig.3.15). The Silicon Spectrometer was calibrated using ^{241}Am alpha source and with protons from 10 to 20 MeV at the Legnaro tandem accelerator (Fig.3.8).
Signals from the two detectors are fed into a 4 channel desktop digitizer with 1 GHz sampling frequency, 0-1 V input range and 10 bit resolution [128]. Since at the ISIS neutron source the

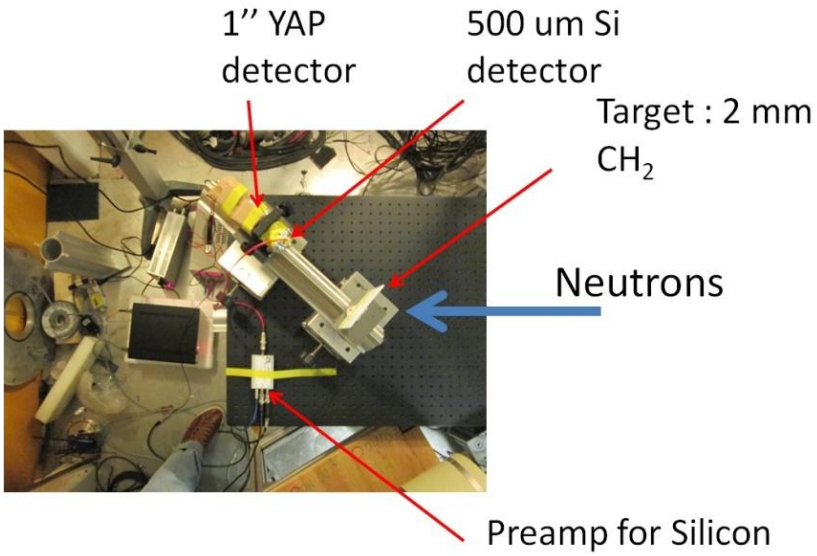

Figure 3.16: Picture of the experimental setup of a TPR spectrometer on the VESUVIO beamline of the ISIS spallation source. Figure taken from *Paper V*.

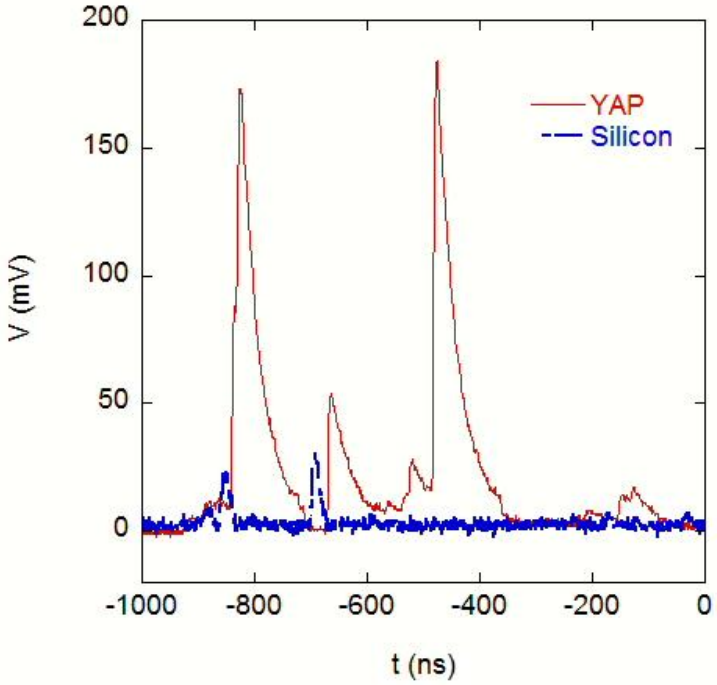

Figure 3.17: Example of signal pulses from the two detectors composing the TPR. The signal of the YAP is recorded directly after the PMT, while the Silicon signal is recorded after a current preamplifier. Figure taken from *Paper V*.

beam is pulsed with a repetition frequency of 50 Hz, the board trigger is set on a reference signal (T_0) generated by the proton extraction from the synchrotron. For each T0 a 3000 ns long waveform is stored for both detectors. Neutrons with $E_n > 10MeV$ fall inside this short time window. Fig.3.17 shows an example of the two detectors pulses recorded for the same T_0. The zero of the time scale is defined as the rising edge of the T_0 signal. Neutrons with $E_n > 10MeV$ are recorded into the "pre-trigger" (i.e. negative time in the figure), because they arrive before the T_0 signal. This is due to the electronics used to extract the T_0 signal at ISIS and it is suited for most of the instruments that work with a Time of Flight (ToF) in the ms time scale.
Due to the pulsed nature of the source, even if the global count rate is relatively low (the machine operates at 50 Hz), the instantaneous count rate is very high (> 1 MHz), more than one signal pulse can be present within 1 μs window and pile-up is an important issue. A fast scintillation time (27 ns for the YAP crystal), a dedicated voltage divider and analysis algorithms are needed to cope with high count rate, to guarantee a good energy resolution. The coincidence analysis is carried out off-line and includes Pulse Height (PH) and ToF spectral analysis. In the example of Fig.3.17, one can notice three E signals with PH > 50 mV (t = -825, -663 and -475 ns). Only the first two of these three have a corresponding ΔE signal from the Silicon detector, and can be associated to a recoil proton event.

Optimization of ΔE-E coincidence of TPR measurements

A proton recoil spectrometer could in principle use a single detector. Multiple detectors are used in coincidence to reduce the background of secondary particles induced by fast neutrons (i.e. γ-rays and charged particles) [148, 149]. The coincidence analysis of the TPR was optimized off-line. Two events, E and ΔE, are considered to be in coincidence if the time difference Δt of their maxima falls inside a selected Δt window. Any rising edge in the waveform with amplitude above a user-defined threshold is defined as event. In order to reduce the probability of random coincidences, the Δt window must be set as short as possible. The Δt window is not centered to zero, since different time delays are introduced by the PMT and the preamplifier. The center of the Δt window was found using a routine that counts the number of coincidence events as a function of Δt. The result is plotted in Fig.3.18. True coincidence events appear in a peak, which rises over a continuum of random coincidences. According to these results, the Δt window was centered at -27.5 ns with a 10 ns width.
A further tool for data reduction is given by the relation between E and ΔE. Fig.3.19 shows the ΔE-E contour plot of coincidence events measured by the TPR. Proton related events have the characteristic distribution due to the *Bethe formula* [150]. Energy thresholds are defined accordingly; threshold on E is 8 MeV, which is the minimum energy for a proton to be transmitted by the silicon. Threshold on ΔE is set above the electronic noise. Protons can be measured up to 60 MeV with this system. Above this value the ΔE signal is too small (PH is less than 10 mV).

Results

The results of the ToF and PH coincidence analysis are presented in Fig.3.20 and Fig.3.21, respectively. A measurement without the scattering target (*no target* in Fig.3.20 and Fig.3.21) was carried out to estimate the background level and it is shown for comparison normalized to the integrated beam current. The time distribution of the coincidence counts is due to the double bunch structure of the ISIS proton beam. Every proton bunch is 70 ns wide and for this reason neutron spectroscopy in the MeV range or above is impossible with ToF analysis alone, due to the 11 meters of flight path, because the energy resolution would be too poor.

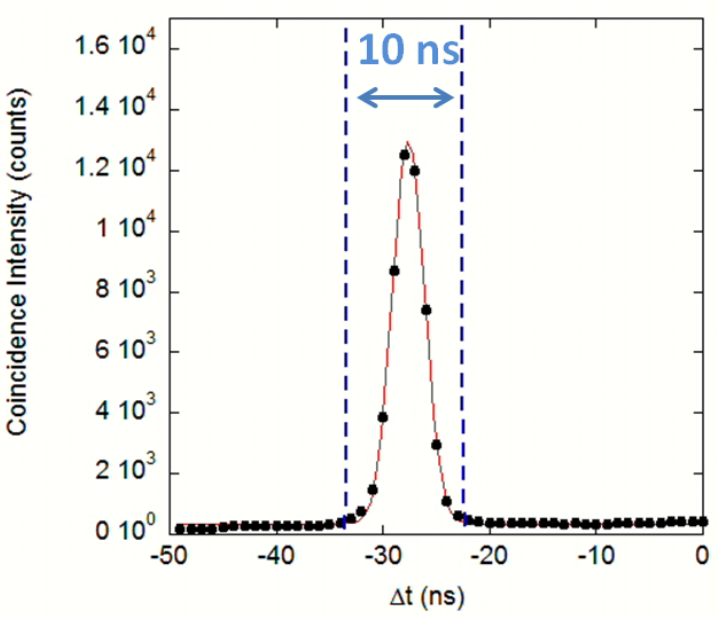

Figure 3.18: Coincidence events as a function of the time difference of YAP and Si events (E and ΔE). True coincidence events appear in a peak, which rises over a continuum of random coincidences. The continuous line is a Gaussian fit of the data. Dashed lines indicate the limit of the Δt window selected for the TPR measurements. Figure taken from *Paper V*.

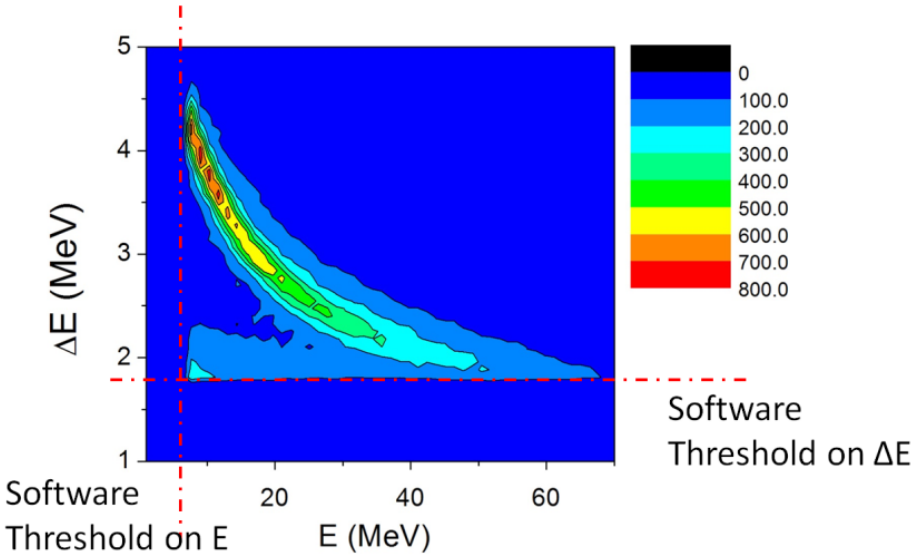

Figure 3.19: ΔE-E contour plot of coincidence events measured by the TPR. The chromatic scale (colors online) indicates the intensity of counts. Dashed lines indicate software energy threshold used for the off-line analysis. Figure taken from *Paper V*.

However, it is possible to distinguish a clear difference between measurements with and without the scattering foil. The peaks in the background measurement (no target) are almost symmetric in ToF, centered at a ToF compatible with γ-rays. For this reason, this background is called γ-flash, even if it could be due to at least four processes, (1) γ-rays from the target, (2) γ-rays induced by spallation neutrons (hundreds of MeV) with a velocity not distinguishable from light, (3) charged particles (including protons) induced by spallation neutrons and (4) charged particles (including protons) induced by γ-rays via photonuclear reactions. Among those (3) and (4) are the most likely because can produce a coincidence ΔE-E event, while (1) and (2) can contribute only via random coincidences.

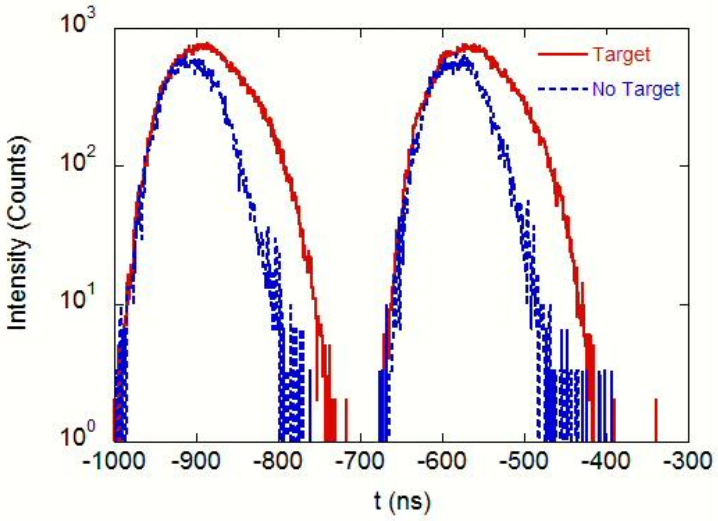

Figure 3.20: Time distribution of the coincidence counts with respect to the T0 signal of the accelerator. Comparison with a background measurement without the polyethylene target is shown. The difference between the two measurements is due to fast neutrons detected by the TPR spectrometer. Figure taken from *Paper V*.

The ToF structures are broadened at higher ToF when the scattering target is present. These events are compatible with proton recoil of fast neutrons with energy $20MeV < E_n < 120MeV$. In the PH Spectrum, shown in Fig.3.21, it is possible to notice that the normalized intensity almost doubles with the presence of the target, and the slope of the spectrum is different. The proton energy is defined as ΔE + E.
In order to retrieve the neutron spectrum the data have been analyzed following the step listed here:

i The background measurement was subtracted from the measured proton energy spectrum.

ii . The proton energy is corrected by adding the calculated energy loss in 19 cm of air [147].

iii The neutron energy scale is set according to the scattering kinematics (i.e. the proton energy scale is multiplied by a factor of 2 at 45 deg).

iv The neutron flux is found dividing the counts by the efficiency, which is a function of the neutron energy and by the area illuminated by the beam. The efficiency was calculated with MCNPX as presented above.

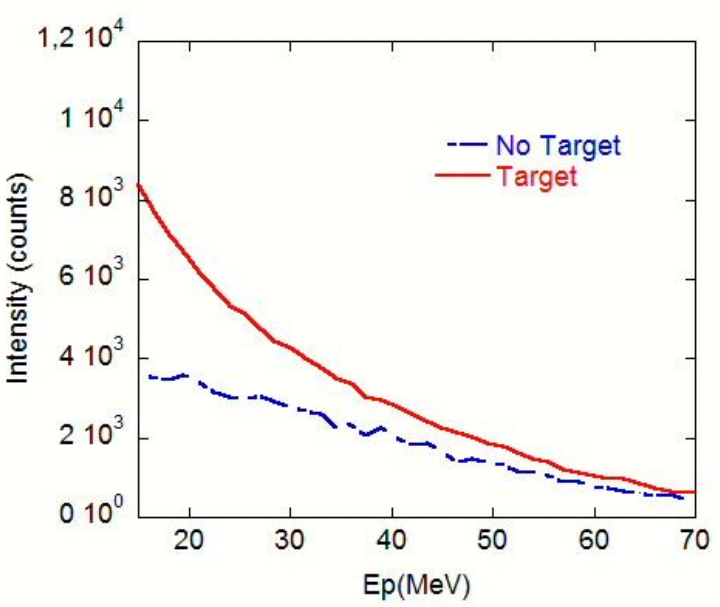

Figure 3.21: Recoil proton energy distribution of the coincidence counts and a background measurement without the polyethylene target. Figure taken from *Paper V*.

The resulting neutron spectrum is presented in Fig.3.22 together with the simulated neutron spectrum [105]. The intensity of the simulated spectrum was normalized to the measurement. The measured neutron flux in the energy range $30MeV < E_n < 120MeV$ is $(1.5 \pm 0.2) \cdot 10^4 s^{-1} cm^{-2}$, considering an average proton current of 160 μA. Extrapolating this result at lower energies, it corresponds to a neutron flux of $(7.6 \pm 0.9) \cdot 10^4 s^{-1} cm^{-2}$ for $E_n > 10MeV$, at 180 μA proton current. For comparison, the reference value for VESUVIO, reported in Ref.[105], is $(5.8 \pm 1) \cdot 10^4 s^{-1} cm^{-2}$ for $E_n > 10MeV$ at 180 μA proton current and the neutron flux measured by the TPR is compatible within 2σ. Ref.[106] and Ref.[107] report measurements of $(8.3 \pm 0.8) \cdot 10^4 s^{-1} cm^{-2}$ and $(8.5 \pm 1) \cdot 10^4 s^{-1} cm^{-2}$, respectively. To compare the different measurements of the flux see Tab.3.2.

Method	Neutron Flux ($s^{-1}cm^{-2}$)	Reference
TPR	$(7.6 \pm 0.9) \cdot 10^4$	*Paper V*
Activation foils	$(5.8 \pm 1) \cdot 10^4$	Ref.[105]
Bonner spheres	$(8.3 \pm 0.8) \cdot 10^4$	Ref.[106]
Breakdown counters	$(8.5 \pm 1) \cdot 10^4$	Ref.[107]

Table 3.2: Measurements, that can be found in literature, of the VESUVIO neutron flux in the energy range $E_n > 10MeV$ at 80 μA proton current.

It has to be reminded that the most important advantage of the TPR technique is the direct measurement of the energy spectrum, without the necessity of deconvolution algorithms. Concerning the spectral information, a good agreement between the measured and simulated neutron energy spectrum is found. As a discussion of the comparison between measurements and simulations, the following points must be addressed:

(a) The flux and spectrum measured by the TPR are an average over the 5 cm wide neutron beam area. The measurement was carried out at the back of the irradiation table (see

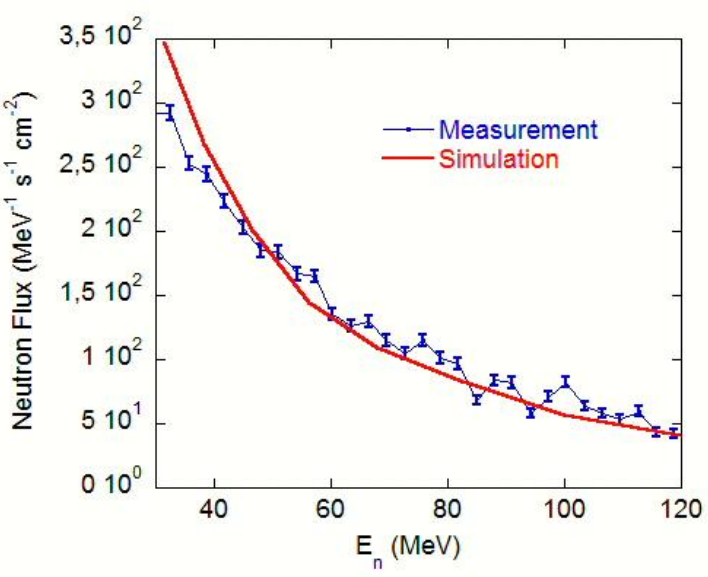

Figure 3.22: Neutron spectrum measured by the TPR compared to Monte Carlo simulation of the VESUVIO beam-line. Figure taken from *Paper V*.

Fig.3.16) and not in the center of the beam line tank. A correction for the distance resulting from the R^2 law allows a measurement on the table to be scaled to the centre of the tank [107].

(b) The quality of the simulations of the fast neutron transport can be affected by components of the beam line not included in the geometry and by lack of reliable nuclear cross sections above 20 MeV.

(c) Errors in the TPR measurement shown in Fig.3.22 are estimated based on the Poisson counting statistics. The error in the measured neutron flux is considering also an error of 10% in the energy calibration of the proton spectrometer. Future measurements at a proton accelerator can diminish this error.

Chapter 4

Response of γ-ray spectrometers to a fast neutron field

Ho amato le stelle troppo profondamente per avere paura della notte.
– Galileo Galilei

4.1 Overview

High resolution γ-ray spectrometers have been developed within a project, coordinated by the ENEA-CNR association, resulted in the installation in the JET roof laboratory of two large sizes (3"x6") $LaBr_3$ scintillators [17] and one High Purity Germanium semiconductor [47]. These γ-ray spectrometers are capable of achieving high energy resolution combined to high count rate capability [80].
ENEA-CNR has proposed the use of γ-ray spectrometers in the ITER Radial Neutron Camera. The spectrometers have been commissioned and have been collecting data in JET experimental campaigns. Results achieved during the past campaigns has shown the potentiality of the high resolution γ-ray spectroscopy in diagnosing fast minority ions (e.g ^3He and ^4He) accelerated by ICRH [75, 76]. It is of particular interest the possibility of diagnosing the alpha particle energy distribution in DT burning plasma experiments of next step tokamaks, such as ITER and DEMO [47, 154].
In this context, it is interesting to study the performance of the new spectrometers in high 14 MeV neutron fluxes, such as the one of the future JET DT campaign. High Purity Germanium semiconductors suffer by radiation damage caused by energetic neutrons (let say above a few MeV), whose effect is a degradation of the energy resolution. Damage can be recovered by a so called annealing procedure. $LaBr_3$ scintillators, on the other hand, are not damaged by neutrons but feature a sensitivity to neutrons which represents a source of background for the measurements of the γ-ray emission spectrum from the plasma. Suitable neutron attenuators must be designed with the aim of reducing the neutron flux with a minimum attenuation of the γ-ray flux.

4.2 Monte Carlo simulation of the $LaBr_3$ response functions to γ-rays

Two 3"x6" $LaBr_3$ (Ce) scintillator detectors have been installed at JET and used for γ-ray spectroscopy. Monte Carlo simulations of γ-ray spectroscopy measurements have been performed with the MCNPX code in order to characterize the detector response function. A

first simulation includes only the 3"x6" $LaBr_3$ crystal. Further simulations have been performed, adding one after another the surrounding components of the detector. The aim is to understand the relative effect of the different elements and materials. First we included the mu-metal shielding (80% nickel, 20% iron), the glass window (supposing the material composition is mainly SiO_3), and an Al cylinder to mimic the PMT body structure. The iron shielding has been included in the simulation only in a second time. The final detector layout is shown in Fig.4.1.

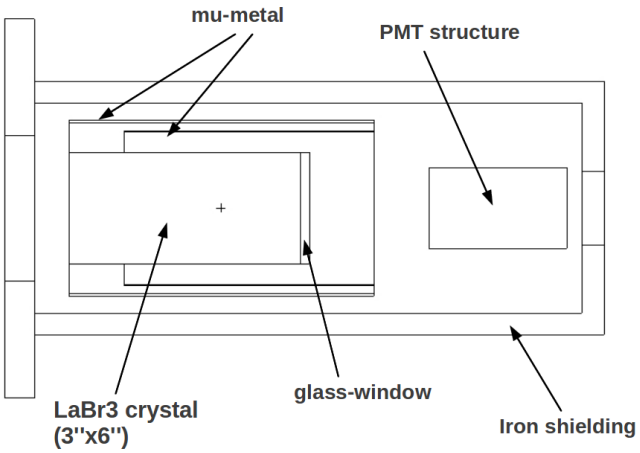

Figure 4.1: Detector layout used for MCNPX simulations.

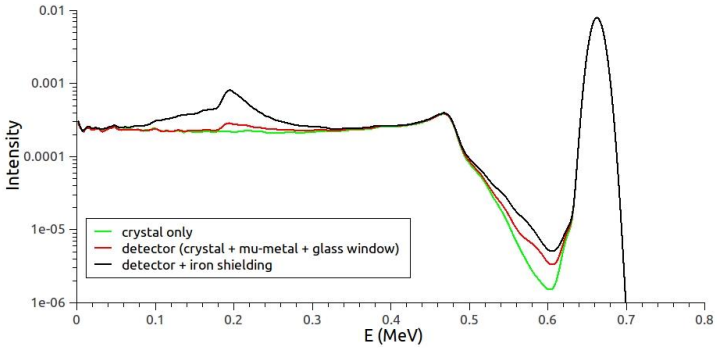

Figure 4.2: Simulated spectra of a ^{137}Cs radioactive source using a 3"x6" $LaBr_3$ scintillator. Different surrounding components are included (see Fig.4.1).

The simulated energy spectrum of a ^{137}Cs radioactive source changes as we add different elements in the geometry (see Fig.4.2). The spectra are normalized to the simulated events. A 3% energy resolution at 662 keV peak is taken to broad the spectra using a convolution algorithm. It is worth to notice how the full energy peak and the Compton-edge do not have any variation, while the difference is clear in the low energy part of the spectrum. The effect of added high Z material, such us the Iron magnetic shield, contributes to scatter additional radiation into the detector. The peak at 0.2 MeV is the backscattered peak due to γ-rays [3].

It is necessary to verify the agreement of the simulations with experimental data in order to prove the reliability of method and results. Energy calibration measurements have been carried out using ^{60}Co and ^{137}Cs radioactive sources for both KM6S1 and KM6S2. MCNPX

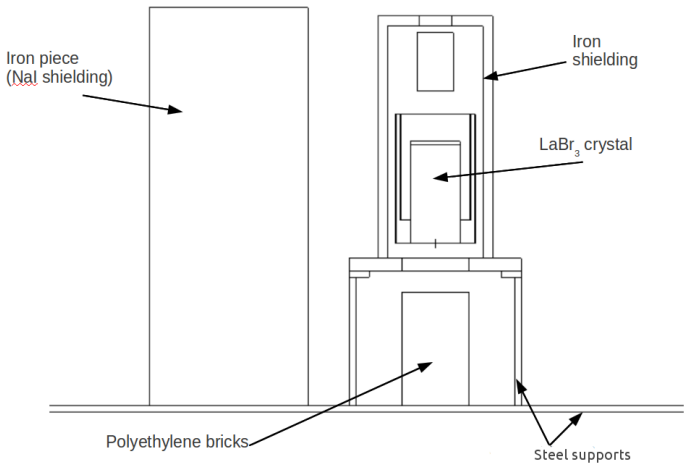

Figure 4.3: Layout of of KM6S1 JET setup for MCNPX simulations.

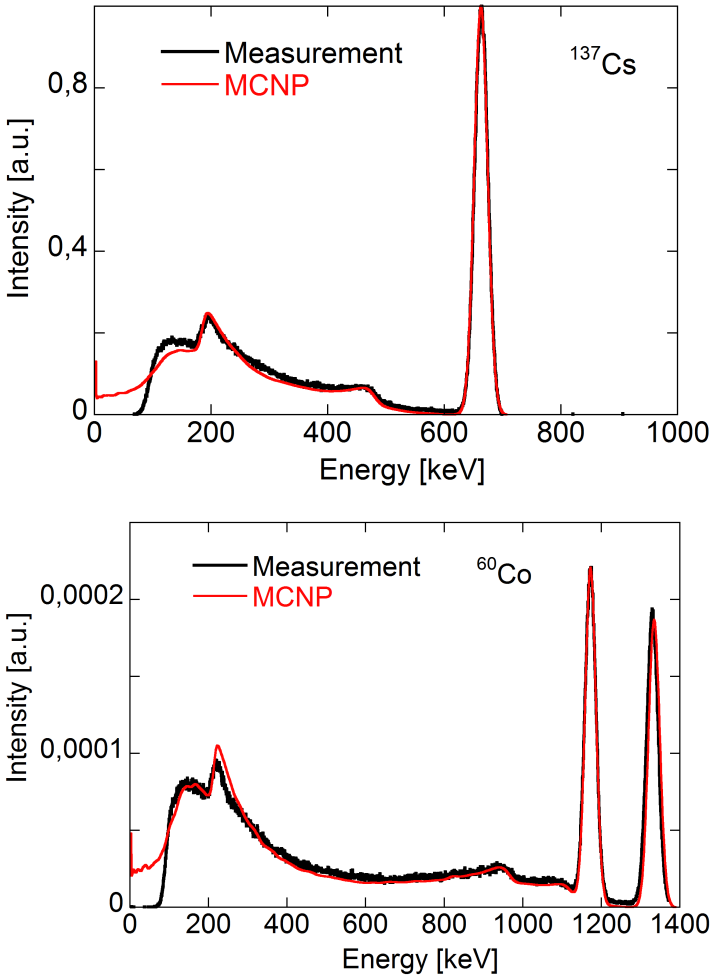

Figure 4.4: Simulated and measured spectra of ^{137}Cs and ^{60}Co radioactive sources for the KM6S1, a 3"x6" $LaBr_3$ scintillator. Data are normalized to full-energy-peak height. Figure taken from *Paper VI*.

simulations have been performed using a model of the JET setup in order to reproduce those measurements. The layout of KM6S1 is shown in Fig.4.3. Since High Z materials are important for scattering γ-rays, steel supports have been included as well as an iron cylinder standing by the detector. This cylinder represents, for the sake of simplicity, a NaI detector with his iron shielding. Polyethylene bricks ($(CH_2)_n$) are included because very close to the radiation sources.

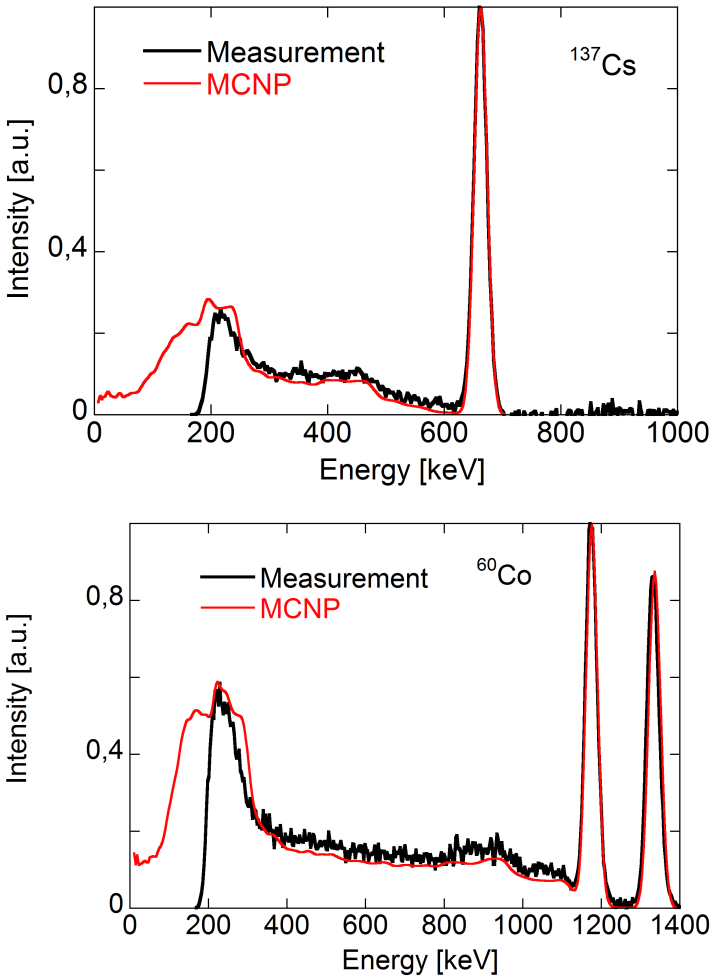

Figure 4.5: Simulated and measured spectra of ^{137}Cs and ^{60}Co radioactive source for the KM6S2, a 3"x6" $LaBr_3$ scintillator. Normalized to full-energy-peak height.

Here the radioactive sources were standing on a polyethylene bricks at 3.4 cm from the detector. A background measurement was necessary to be subtracted from the calibration measurement with ^{60}Co or ^{137}Cs source. In fact the $LaBr_3$ scintillator has an intrinsic background due to radioactive isotopes. The main contributions is due to 138La, which represents the 0.1% of the natural lanthanum. Since background structures can be quite complicated to be included in the simulation, subtracting the measured background from the calibration spectra is a more straightforward procedure. We show in Fig.4.4 the comparison of the measurement with simulation of spectra of a ^{60}Co and ^{137}Cs radioactive source respectively for the KM6S1. The same for KM6S2 is shown in Fig.4.5. A measured 4% energy resolution at 662 keV peak is taken to broad the simulated spectra using a convolution algorithm. Spectra are normalized to full-energy-peak height, and the integral over the all area gives the number of counts per

simulated event. These results show a good agreement of simulation with data. It has to be noticed the agreement both at the Compton-edge level and at the low energy back-scattering level. This gives a good reliability to MCNPX simulations used to study γ-ray spectroscopy problems, and particularly to the characterization of the $LaBr_3$ scintillator.

The complete detector model has now been used to simulate the response function for different energy γ-rays. MCNP simulations to all energies form 100 keV to 10 MeV have been performed, with 100 keV step. A collimated radiation source has been used. In Fig.4.6 the simulated spectra for selected γ-ray energies are shown. Features of these spectra are the single and double escape peaks, that are present when the incident γ-ray energy is above the threshold level of 1.022 MeV. Compton structures can be appreciated. This spectra do not consider the detector resolution, which can be added in a second time if needed.

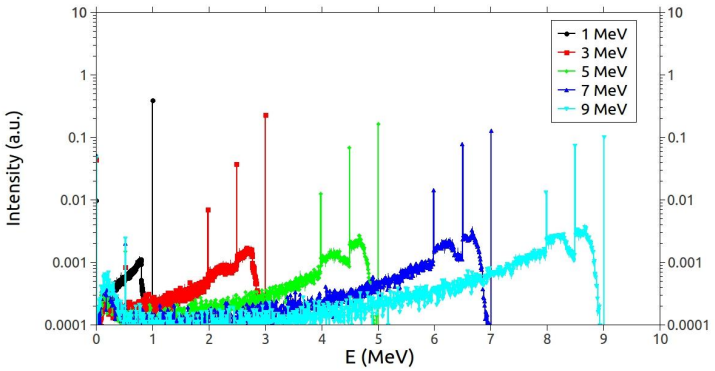

Figure 4.6: Simulated spectra for selected γ-ray energies for a 3"x6" $LaBr_3$ scintillator.

Since the spectra are normalized to the simulated events, it is possible to notice that the full-energy-peak efficiency get smaller as the energy of the photon increase. MCNP simulations have been performed in order to evaluate the efficiency as a function of the γ-ray energy. Results are shown in Fig.4.7.

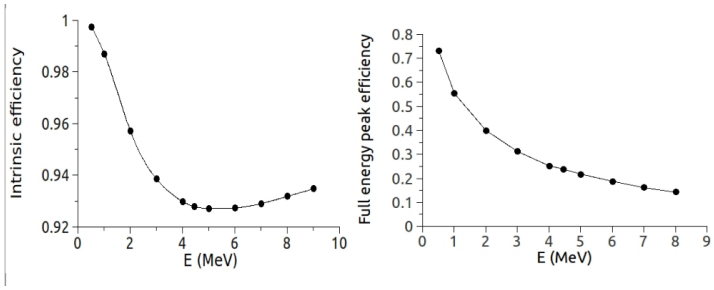

Figure 4.7: Simulated intrinsic efficiency (left) and full-energy-peak efficiency (right) as a function of the γ-ray energy for a 3"x6" $LaBr_3$ scintillator.

Intrinsic efficiency and full-energy-peak efficiency are defined respectively as number of events in the whole spectrum and number of events in the full-energy-peak divided by the number of photons incident on the detector. The 3"x6" $LaBr_3$ scintillator has a considerably high efficiency thanks to high effective Z, high density and big volume. Full-energy-peak efficiency is 25% at 4.44 MeV, which is the energy of γ-rays from the reaction of interest $^9Be(\alpha, n\gamma)^{12}C$.

4.3 Monte Carlo simulation of the HPGe response functions to γ-rays

HPGe detectors are standard equipment used in laboratory and industry for high resolution γ-ray spectroscopy. HpGe detector works on the principles of semiconductor detectors: e-/hole pairs are produced by ionizing radiations and are collected on the electrodes by the electric field. High energy resolution is achieved thanks to a particularly narrow band gap (band gap of Ge is only 0.7eV), which produce a large number of pairs, which represent the information carriers. Because of this narrow band gap, HPGe must be operated cold (77K), otherwise the leakage current would be to high to perform any measurement.
This physical requirement reflect on the detector shape and layout. It is necessary to keep the detector in a vacuum chamber for thermal insulation. The chamber has a thin aluminum wall to minimize the attenuation of low energy photons. It is also necessary to maintain a thermal contact through a copper junction. This is why a hole in the detector is needed. Closed-ended coaxial allows for large volume crystals. The final detector layout used for simulations is shown in Fig.4.8. MCNP simulations have been performed to evaluate the efficiency as a function

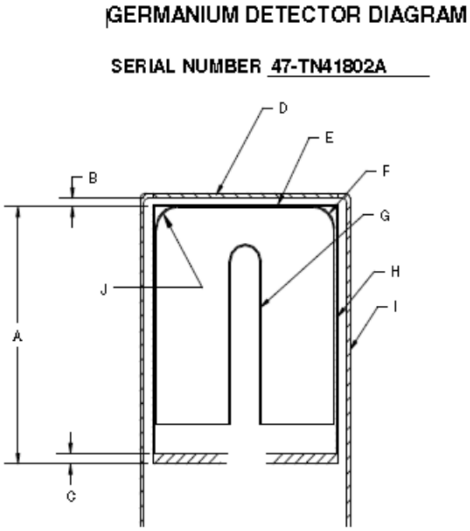

Figure 4.8: HPGe detector layout used for simulations (A = 130 mm).

of the γ-ray energy. Results are shown in Fig.4.7. Since the spectra are normalized to the simulated events, it is possible to notice that the full-energy-peak efficiency get smaller as the energy of the photon increase.
It is necessary to verify the agreement of the simulations with experimental data in order to prove the reliability of method and results. Energy calibration measurements have been carried out using ^{137}Cs and ^{60}Co radioactive sources. MCNPX simulations have been performed using a model of the JET setup of the detector, in order to put the point-like radiation source in the right position. Since High Z materials are important for scattering γ-rays, steel supports have been included.
MCNP simulations are used to study the response of a HPGe detector irradiated with ^{137}Cs and ^{60}Co radioactive sources (see Fig.4.9). A measured 2 keV energy resolution at 1332 keV peak is taken to broad the simulated spectra using a convolution algorithm. Spectra are normalized to full-energy-peak height, and the integral over the all area gives the number of counts per simulated event. We show the spectra obtained with the complete simulation (MCNP1), including nearby materials, and spectra with a simulation including the crystal only (MCNP2). These

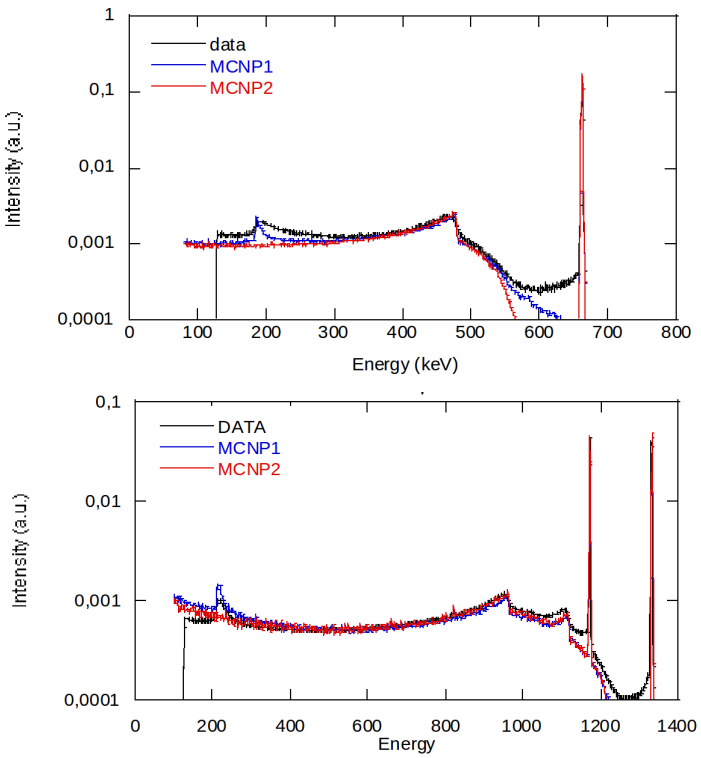

Figure 4.9: Simulated and measured spectra of ^{137}Cs (top) and ^{60}Co (bottom) radioactive sources for the HPGe detector. MCNP1 and MCNP2 are simulations considering the complete geometry and the crystal only, respectively.

results show a good agreement of simulation with data. It has to be noticed the agreement both at the Compton-edge level and at the low energy back-scattering level. This gives a good reliability to MCNPX simulations used to study γ-ray spectroscopy problems, and particularly to the characterization of the HPGe detector. Small difference is ascribed to multiple compton events likely caused by background γ-rays of higher energies and surrounding materials not included in the simulation.

4.4 Monte Carlo simulation of the $LaBr_3$ response to fusion neutrons

The response of the crystal to 2.5 and 14 MeV neutrons is due to nuclear interaction with the isotopes of $LaBr_3$. ^{79}Br and ^{81}Br compose Bromine with relative concentration of about 1:1, while ^{139}La is the only stable isotope of Lanthanum, and other isotopes are present only in traces. The interaction of fast neutron with these isotopes produces secondary particles, which in turn deposit their energy into the crystal, giving rise to recordable pulses. The cross sections for the production of secondary particles can be found in Fig.4.10. The response to 2.5 MeV neutrons is dominated only by inelastic scattering. Other channels contribute to the response to 14 MeV neutrons, since cross sections are above threshold at this energy. The most relevant of those is the (n,2n) reaction on ^{79}Br , ^{81}Br and ^{139}La . This reaction has a dual effect on the response. First, it contributes to the creation of γ-rays emitted by the excited nuclei, and secondly it produces a population of secondary neutrons, which can interact again with the crystal isotopes. Other cross sections are also significant for the production of charged particles, alpha, deuterons and protons. Among those the largest is the (n,np) reaction on ^{79}Br .

A MCNP model was implemented for the interpretation of experimental results. Mono-energetic 14 MeV neutrons are directed onto a 3"x3" $LaBr_3$. Mono-energetic 2.5 MeV neutrons are directed onto a 3"x6" $LaBr_3$. Different detector volumes are considered, since measurements were performed with different detectors. However, simulations of 14 MeV neutrons are performed also for a 3"x6" detector, which is what is currently installed at JET. A summary of the results of 14 MeV neutrons simulations is presented in Tab.4.1. For the case of 14 MeV neutrons on 3"x3" $LaBr_3$, 1.17 γ-rays and 0.45 secondary neutrons are emitted per neutron history. γ-rays are produced into the crystal and they have a large probability (close to 40%) to be detected, due to the large volume, high density and high Z of the scintillator. Charged particles are less likely to be produced, due to smaller cross sections, but, on the other hand, we can consider their detection efficiency to be 100%.

	$LaBr_3$ 3"x6"	$LaBr_3$ 3"x3"
gamma creation	1.87	1.18
neutron creation (n,2n)	$6.98 \cdot 10^{-1}$	$4.51 \cdot 10^{-1}$
proton creation	$1.53 \cdot 10^{-2}$	$9.54 \cdot 10^{-3}$
deuteron creation	$1.13 \cdot 10^{-3}$	$7.62 \cdot 10^{-4}$
alpha creation	$1.58 \cdot 10^{-3}$	$1.10 \cdot 10^{-3}$

Table 4.1: MCNP simulation summary of the response of a 3"x3" $LaBr_3$ crystal to 14 MeV neutrons. Results are normalized per neutron history.

Fig.4.11 shows on the other hand the energy distribution of γ-rays induced by 2.5 MeV mono-energetic neutrons simulated with MCNP for a 3"x6" $LaBr_3$ detector. The contribution of each individual isotope is shown separately. At this poin one has to consider the response

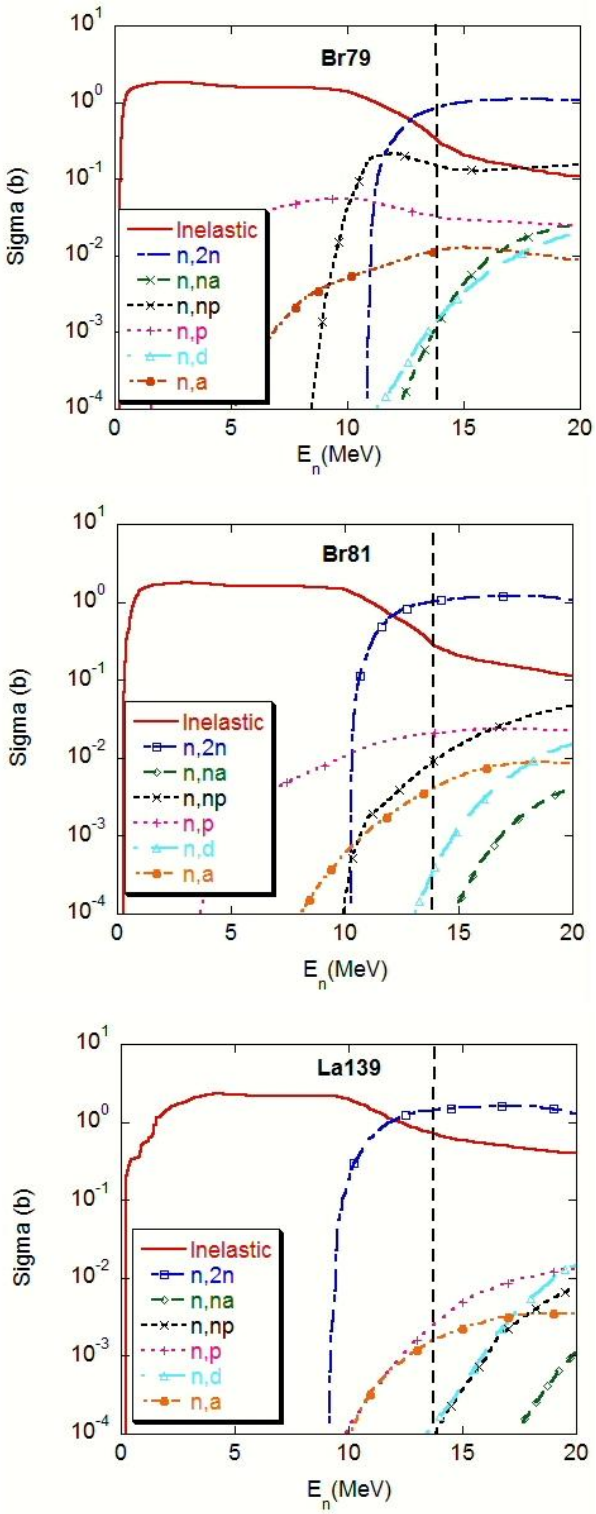

Figure 4.10: Neutrons cross sections on ^{79}Br , ^{81}Br and ^{139}La . Figure taken from *Paper VIII*.

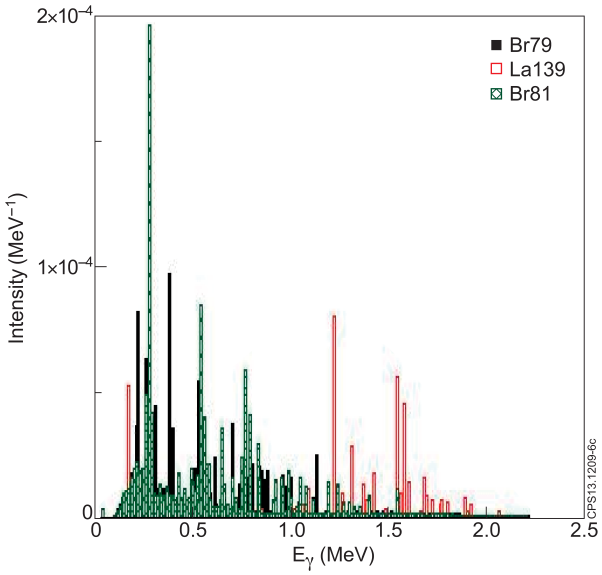

Figure 4.11: Energy distribution of γ-rays induced by 2.5 MeV mono-energetic neutrons simulated with MCNP for a $LaBr_3$ detector. The contribution of each individual isotope is shown separately. Figure taken from *Paper VII*.

function of the detectors to this emitted secondary particles. Fig.4.12 shows, for the 14 MeV case, the simulated deposited energy spectra for all the secondary particle of interest into a 3"x3" $LaBr_3$. γ-ray contribution is largely dominant for $E_d < 5MeV$. Charged particles are relevant for $E_d < 5MeV$. Considering a threshold of 0.35 MeV, the detector efficency to 14 MeV neutrons is 43%, taking into account the contribution of secondary γ-rays and secondary charged particles. For comparison, the efficiency of a 3"x6" $LaBr_3$ (Ce) to 2.5 MeV neutrons is found to be 76%. Eventually, the energy broadening due to the finite energy resolution of the detector is taken into account by convolution of the response with Gaussian functions. The energy resolution of 3.2% (FWHM/E) is considered to scale, according to the Poisson law, as $1/\sqrt{E}$.

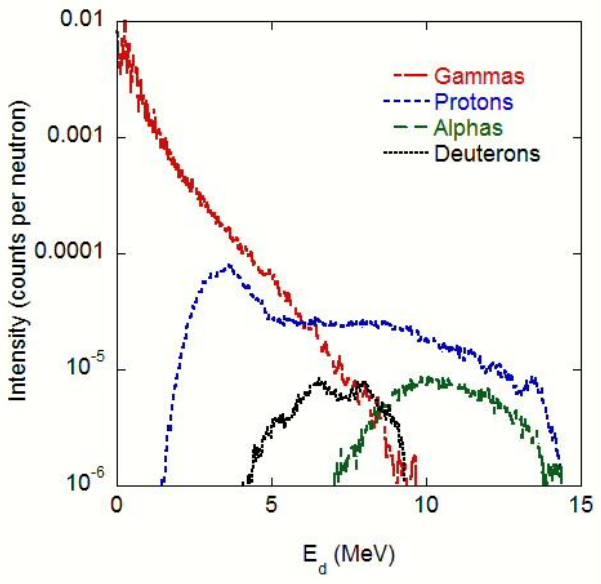

Figure 4.12: MCNP simulation of the deposited energy distribution of secondary particles into a 3"x3" $LaBr_3$ spectrometer during 14 MeV irradiation. Figure taken from *Paper VIII*.

4.5 Monte Carlo simulation of the HPGe response to fusion neutrons

In the simulations, neutrons with 2.5 MeV and 14 MeV energies are directed in a flat beam configuration towards the head of the detector (which is the top in Fig.4.8).
Counts in the detector are due to secondary particles emitted due to neutron interactions. It is found that several channels contribute to the measured response, the most relevant being neutron inelastic scattering on Ge nuclei (four stable isotopes are present in natural concentrations). Charged particles are also emitted for the 14 MeV case. Tab.4.2 summarize the MCNP simulations of secondary particles emission. Results are normalized per neutron history. Fig.4.13 shows the energy distribution of emitted γ-rays due to fusion neutrons interaction in a HPGe detector, simulated with MCNP.
If we consider the efficiency to charged particles detection to be about 100%, and the total efficiency to γ-rays in the MeV energy range to be about 60% (100% photopeak relative efficiency). We can estimate the efficiency to neutrons to be 52% for 2.5 MeV and 50% for 14 MeV.
A summary of the calculated efficiencies is presented in Tab.4.3, where the HPGe is compared to $LaBr_3$ detectors.

	2.5 MeV	14 MeV
gamma creation	$8.86 \cdot 10^{-1}$	$8.43 \cdot 10^{-1}$
neutron creation (n,2n)	$4.83 \cdot 10^{-1}$	1.22
proton creation	0.0	$1.82 \cdot 10^{-2}$
deuteron creation	0.0	$3.17 \cdot 10^{-6}$
alpha creation	0.0	$6.86 \cdot 10^{-4}$

Table 4.2: MCNP simulation summary of the response of the JET HPGe detector to 2.5 MeV and 14 MeV neutrons. Results are normalized per neutron history.

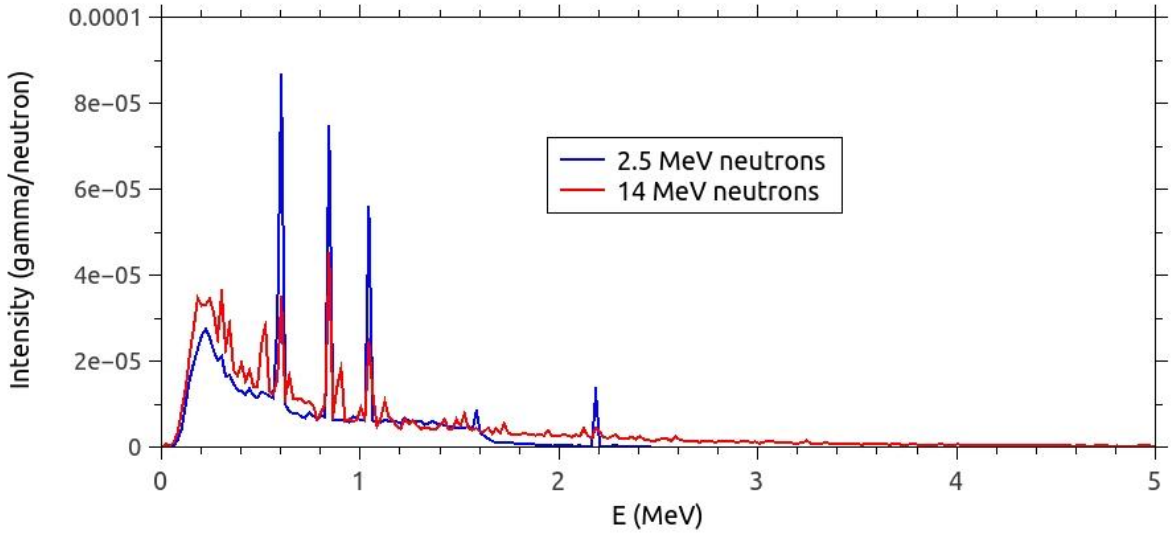

Figure 4.13: Energy distribution of emitted γ-rays due to fusion neutrons interaction in a HPGe detector, simulated with MCNP.

	2.5 MeV	14 MeV
$LaBr_3$ 3x6 (JET)	76%	70%
$LaBr_3$ 3x3	n.a.	43%
HPGe (JET)	52%	50%

Table 4.3: MCNP simulation summary of the counting efficiency to fusion neutrons for different γ-ray detectors.

4.6 Measurements of the response of $LaBr_3$ detector to mono-energetic neutrons and simulations banchmark

The response of $LaBr_3$ (Ce) to 2.5 MeV and 14 MeV neutrons has been measured at the Frascati Neutron Generator. 2.5 MeV neutron response was also measured at JET during deuterium plasma operations. The Frascati Neutron Generator (FNG) accelerates deuterium ions at 300 keV onto a tritiated-titanium target containing about $37{\cdot}10^{10} Bq$ of tritium, providing emission of 14 MeV mono-energetic neutrons. The $LaBr_3$ (Ce) crystal used for the measurements has a cylindrical shape with 3 inches diameter and 3 inches height, for 14 MeV measurements, and 3 inches diameter and 6 inches height, for 2.5 MeV measurements. The detector was placed at 1.25 m from the target. The detector was mounted at 90 deg with respect to the incoming deuterium beam. At this angle the mono-energetic 14 MeV neutron spectrum has the minimum broadening, corresponding to about 1%.

The light emitted by the scintillator was collected by a photo-multiplier tube and signals were fed directly into a 12 bit - 250 Msample/s digitizer. Each waveform above threshold was saved and analysed off-line using a dedicated algorithm. The pulse height spectrum was energy calibrated using laboratory ^{137}Cs and ^{60}Co sources. The energy resolution of this system is measured to be 3.2% at the 0.662 MeV line of ^{137}Cs .
The results of MCNP simulations are compared to the measurements. As a matter of fact, the detector at FNG does not have a collimated line of sight, and it is exposed to a more

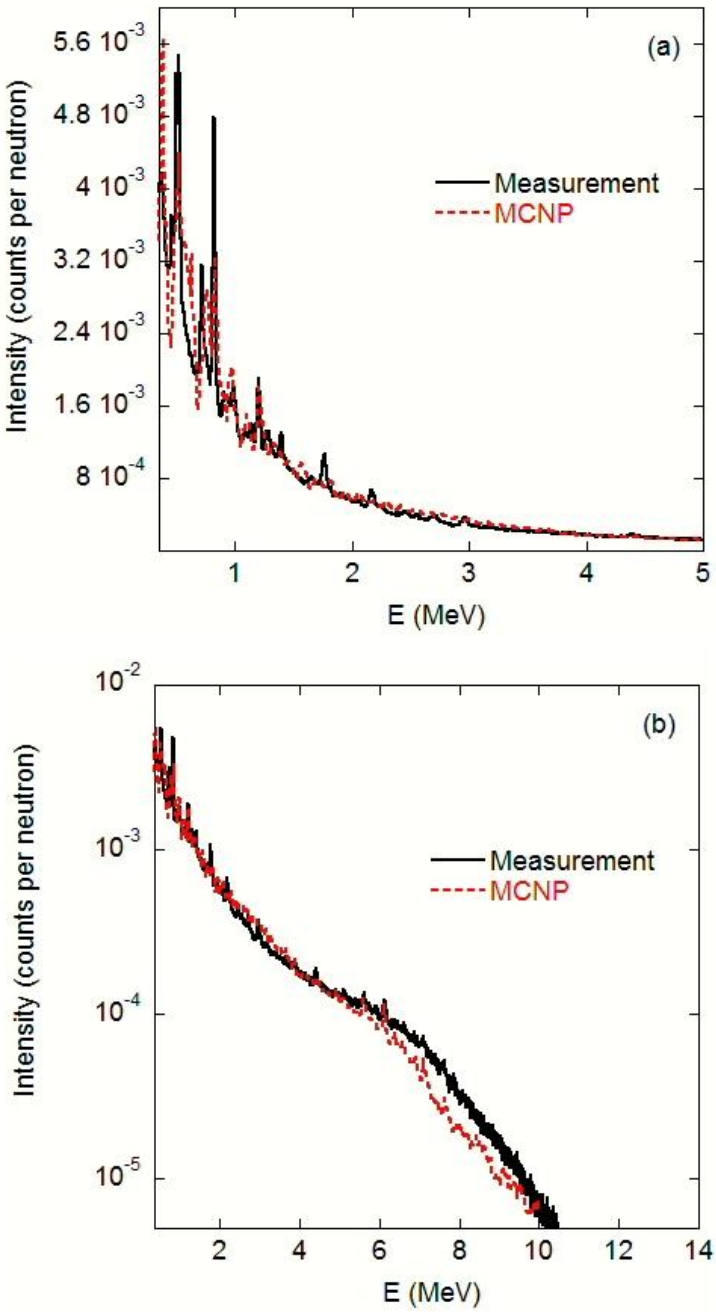

Figure 4.14: Measured and simulated energy spectra of the $LaBr_3$ response at FNG. In the simulation, the three components at FNG (direct neutrons, scattered neutrons, and background gammas) are considered. All the secondary particles (gamma, protons, deuterons and alphas) are considered. Figure taken from *Paper VIII*.

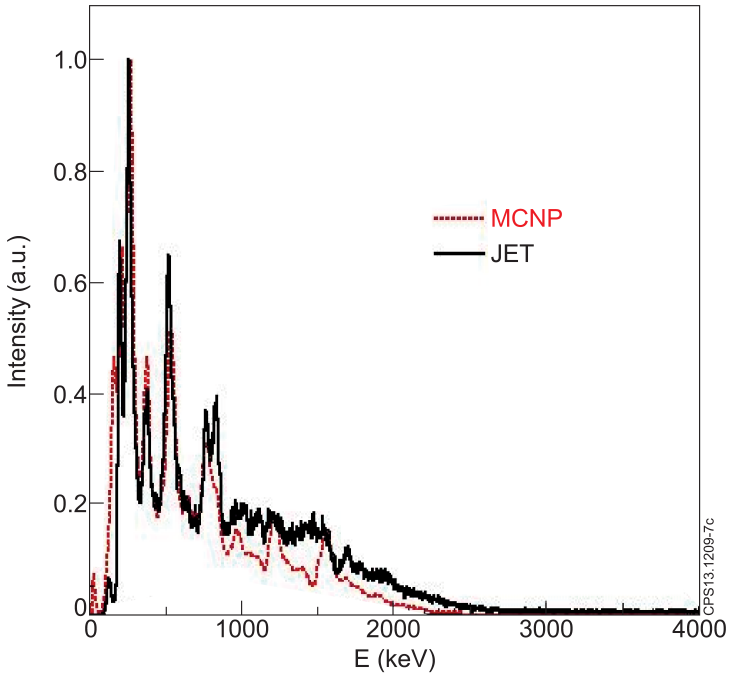

Figure 4.15: Response spectrum of a $LaBr_3$ (Ce) detector to 2.5 MeV neutrons simulated with MCNP and measured at JET. Figure taken from *Paper VII*.

complex admixed neutron and γ-ray field. Scattered neutrons with degradated energy and neutron-induced γ-rays reach the detector after interaction with the surrounding materials into the experimental hall. The energy distributions of scattered neutron and environmental γ-rays were calculated thanks to a MCNP model, which was provided by the FNG facility. The results of this calculation were then used as input for two new MCNP simulations of the response of the $LaBr_3$ detector to these scattered neutron and γ-ray field. The 2.5 MeV response measured at JET has used, because it has a collimated line of sight, and results are *cleaner* with respect to the FNG measurements.
Fig.4.14 and Fig.4.15 presents the comparison of simulations with experimental results for 14 MeV and 2.5 MeV, respectively. Simulations and measurements are consistent, as the same peaks and structures are found. The small differences observed are due to the following reasons. First of all, we have not included any other material in the simulation but the $LaBr_3$ crystal. Background γ-rays induced by neutron interactions with the tokamak main components and materials surrounding the detector are therefore not accounted for by the MCNP result. For example, the peak at 0.8 MeV can be attributed to the interaction of fast neutrons on iron, an abundant element in most tokamak structures. Similarly, we expect that environmental γ-rays induced by neutron interactions can fill the gaps in the energy region 1 to 1.5 MeV of the simulated spectrum. The second reason that could explain such differences is that the simulation considers only 2.5 MeV mono-energetic neutrons, and does not include other components of the neutron spectrum.
As a final test of the MCNP model, we can compare the predicted detector count rate as a function of the total neutron yield of JET with that measured (see Fig.4.16). Three different discharges have been considered with NBI powers up to 17 MW, corresponding to neutron yields as high as $4 \cdot 10^{15} n/s$. The results indicate that the measured counting rate is in agreement with the prediction. The dispersion of the data is likely due to the different neutron transport conditions, changing with the plasma, along the line of sight [153].

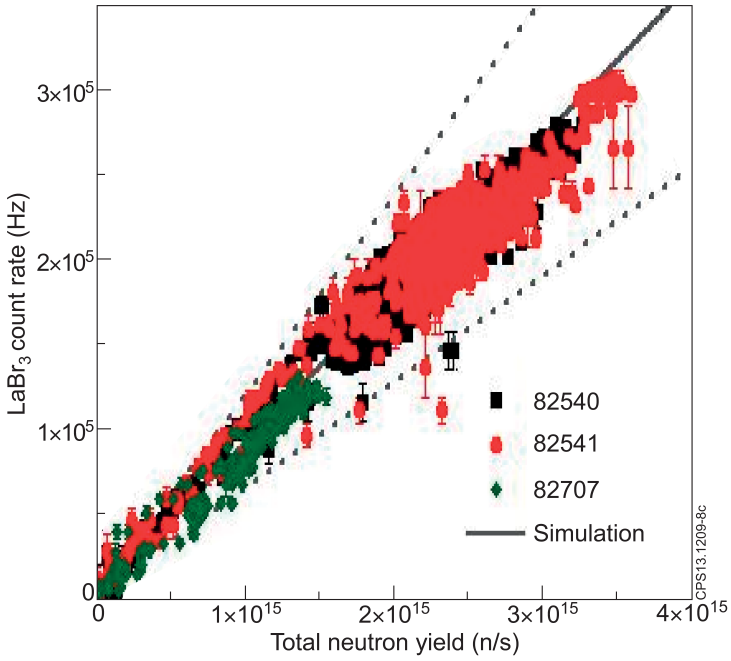

Figure 4.16: $LaBr_3$ (Ce) detector count rate as a function of the JET total neutron yield. Scattered points are from different JET discharges. The dashed lines correspond to the uncertainty on the slope for the linear relation between the $LaBr_3$ (Ce) counting rate and the JET neutron yield, as predicted by simulations. Figure taken from *Paper VII*.

4.7 Short lived activation induced by 14 MeV neutrons

Post-irradiation measurements have been carried out at FNG. These measurements are of interest for two reasons. Activation of a large volume crystal can pose problems for handling after a large neutron flux irradiation and, secondly, the production of short lived isotopes reflects into a build-up of the counting rate during the measurement itself.

$LaBr_3$ (Ce) was irradiated for about 1.5 h. The neutron yield was $1.5 \cdot 10^{10}$ neutrons per second, which resulted in a neutron fluence on the detector front surface of approximately $3.8 \cdot 10^6$ neutrons per second.

After the FNG was switched off, the measurement was started. In Fig.4.17 the counting rate as a function of the time is presented. One point is acquired every second.

According to the given interpretation, the short lived activation is due to ^{78}Br and ^{80}Br , which have a decay time of 540 s and 1500 s, respectively. ^{78}Br and ^{80}Br are produced by (n,2n) reactions on ^{79}Br and ^{81}Br . On the other hand, the (n,2n) reaction on ^{139}La produces ^{138}La, which has a half live of billions of years, and therefore cannot add any contribution on this time scale.

In Fig.6, the experimental data of count rate intensity (I) as a function of time (t) have been fitted by a double exponential decay with time constants $\tau_1 = 540s$ (^{78}Br) and $\tau_2 = 1500s$ (^{80}Br),

$$I = A \cdot \exp\left(-\frac{t}{\tau_1}\right) + B \cdot \exp\left(-\frac{t}{\tau_2}\right) + C \tag{4.1}$$

where A, B and C are the three free parameters of the fit. The A and B parameters define the initial concentrations of ^{78}Br and ^{80}Br . The free parameter C takes into account all active isotopes with $\tau >> 30min$. These can be isotopes of surrounding materials at FNG.

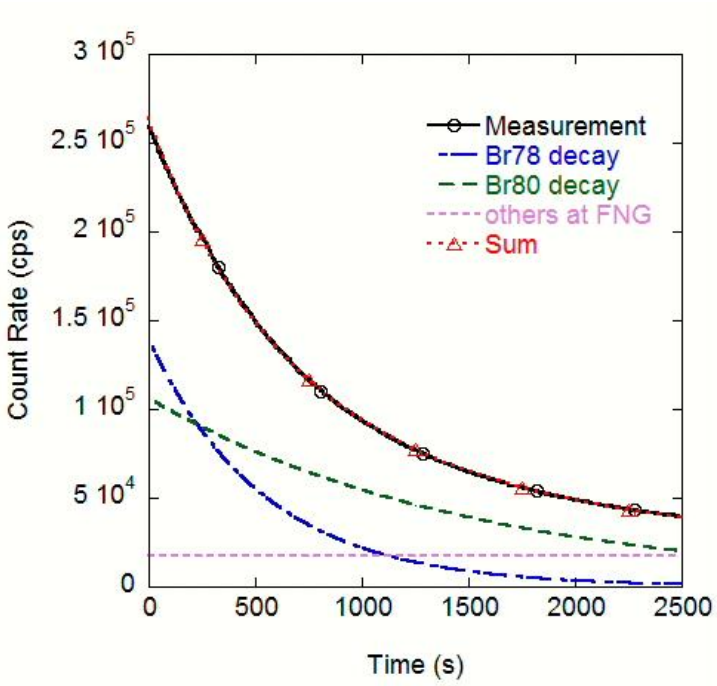

Figure 4.17: Post-irradiation measured count rate as a function of time. Measurement is fitted by a double exponential decay with time constants $\tau_1 = 540s$ (^{78}Br) and $\tau_2 = 1500s$ (^{80}Br). A constant free parameter takes into account all active isotopes with $\tau >> 30$ min at FNG. The Sum of the three contributions is compared with experimental data. Figure taken from *Paper VIII*.

4.8 Neutron attenuators

The possibility to implement a γ-ray camera system composed of an array of $LaBr_3$ (Ce) crystals is currently under study for ITER [154]. One of the main challenges is the background on the detector produced by high neutron fluxes up to $10^8 - 10^9 cm^{-2} s^{-1}$ at the detector position without neutron filters. The overall background count rate of the detector must also be kept sufficiently low, in order not to exceed its few MHz total count rate capability, leading to paralysis.
Further work needs to be addressed to the design of neutron attenuators that can reduce the overall detector load at an acceptable level to enable measurements. A promising attenuator candidate is ^6LiH, as both ^6Li and H, being light nuclei, are good neutron moderators and, having low Z, give low γ-ray attenuation. Besides, ^6Li is also a neutron absorber, with a capture cross section of $3 \cdot 10^3 b$ for thermal neutrons.At present at JET a ^6LiH attenuator is being designed for installation in a γ-ray spectroscopy line of sight.

In this thesis, simple CH_2 attenuators have been studied at JET. MCNP simulations have been performed to assess the attenuation of 2.5 and 14 MeV neutrons due to different thickness of CH_2 attenuators. Results are presented in Fig.4.19. Here we considered a flat neutron beam, and attenuator placed at 100 cm distance from the detector. Neutrons are counted only if energy is above 0.7 MeV, which is the minimum to induce inelastic scattering on $LaBr_3$.

At JET (2.5 MeV neutrons) two different attenuator slabs (10 cm each) have been used (see Fig.4.20). Similar discharges with 5.5 MW NBI are considered. Measured attenuation was 7 times for 1 slab and 16 times for 2 slabs. This compares with MCNP calcualtion, which is 5 times for 1 slab and 12 times for 2 slabs, but the response of the detector to the modified

JET DT neutron emission (s^{-1})	14 MeV neutron flux at detector position (s^{-1} cm^{-2})	Gamma-detectors counting rate (cps)	30 cm CH_2 / Gamma-detectors counting rate (cps)	80 cm CH_2 / Gamma-detectors counting rate (cps)
10^{+16}	$2.7 \cdot 10^{+4}$	$7 \cdot 10^{+5}$	$7 \cdot 10^{+4}$	$7 \cdot 10^{+2}$
10^{+17}	$2.7 \cdot 10^{+5}$	$7 \cdot 10^{+6}$ *(too high)*	$7 \cdot 10^{+5}$	$7 \cdot 10^{+3}$
10^{+18}	$2.7 \cdot 10^{+6}$	$7 \cdot 10^{+7}$ *(too high)*	$7 \cdot 10^{+6}$ *(too high)*	$7 \cdot 10^{+4}$
10^{+19}	$2.7 \cdot 10^{+7}$	$7 \cdot 10^{+8}$ *(too high)*	$7 \cdot 10^{+7}$ *(too high)*	$7 \cdot 10^{+5}$

Figure 4.18: Neutron induced counting rate on gamma-detectors at JET for different neutron emissions during the DT campaign.

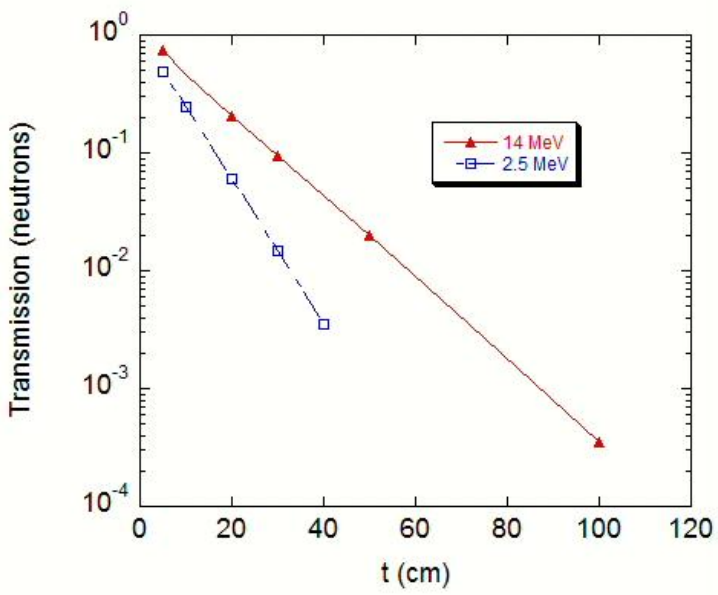

Figure 4.19: MCNP simulation of a CH_2 attenuators for 2.5 and 14 MeV neutrons.

neutron spectrum after the attenuator is still not considered in this simulation.
Based on these results, a simple assessment of the performance of gamma-detectors installed at JET during the next DT campaign can be done, considering expected fluxes and the efficiencies given above for 14 MeV neutrons. Here we consider the efficiency to neutrons to be the same (60%) for the two detectors. In the table (Fig.4.18) a counting rate is labelled as too high when the $LaBr_3$ cannot cope with it. It has been considered that the total neutron yield of JET can range from 10^{16} to 10^{19} during the DT campaign. The HPGe will indeed be paralyzed at much smaller fluxes with respect to the $LaBr_3$. Concerning the $LaBr_3$ detector, it can be concluded that 80 cm of CH_2 shielding is needed to be not limited by neutron flux.

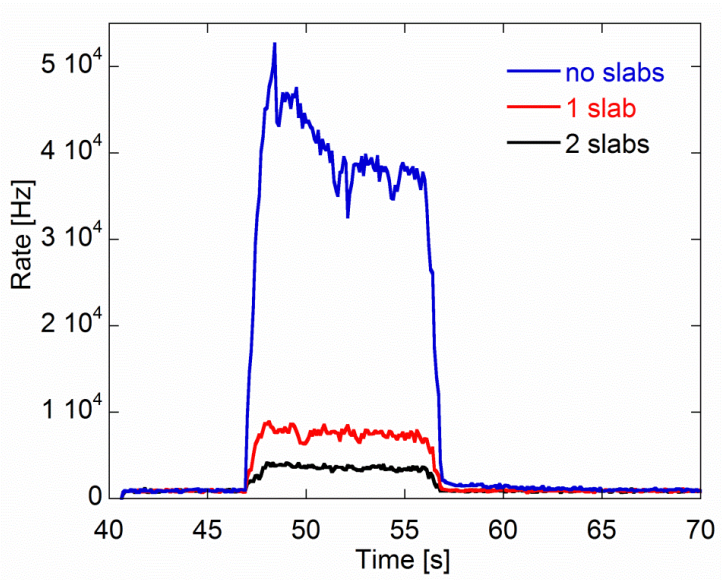

Figure 4.20: Measured counting rate at JET of a $LaBr_3$ detector with different neutron attenuators.

Chapter 5

Conclusions and Outlook

Ricordati che dietro ogni problema c'è un'opportunità.
– Galileo Galilei

This thesis presents results on fast neutron measurements applied to nuclear fusion and spallation sources. The novelty of the research activity was the development of instrumentation and methods for neutron detection with the capability to combine good energy resolution (a few percent) and high counting rates (> 1 MHz). These results can be summarised following the three parts of the thesis: Diamond Detectors, Telescope Proton Recoil spectrometers and γ-ray spectrometers. Based on these results new instruments will be installed at the JET tokamak, for plasma diagnostics during the next experimental campaigns, and at the ISIS spallation source, where the ChipIr beam-line dedicated to fast neutron irradiation will start full operations in 2015.

Concerning the application of Single crystal Diamond Detectors (SDDs) to fusion plasma diagnostics, the response of the single pixel SDD prototype to 14 MeV neutrons (*Paper I*) was measured at the Frascati Neutron Generator (FNG). Measurements showed a 2.5% energy resolution using fast electronics optimized for high counting rates, featuring a total signal length below 30 ns. Details of the response function to 14 MeV neutrons have been studied, with focus on the $^{12}C(n,\alpha)^{9}Be$ peak, which is of interest for spectroscopy of energetic ions in a fusion plasma.

First measurements at JET of the neutron spectrum from deuterium plasmas using a single crystal diamond detector were presented (*Paper II*). The observed neutron count rate was successfully correlated to data from other standard neutron rate diagnostics at JET. The deposited energy spectra were measured for both 2.5 MeV and burn-up 14 MeV neutrons. Monte Carlo simulations were used to determine the device response function and to interpret the measured pulse height spectrum in terms of components of neutron emission from NBI plasmas, including background contributions. A good agreement was found between calculations and measurements.

Concerning the application of SDDs to spallation sources, a SDD was used to characterise the fast neutron beam of PRISMA and VESUVIO beam-lines at the ISIS spallation source. Measurements have been performed to develop optimal solution for high rate measurements to be applied on the new ChipIr beam-line. In particular, different fast preamplifiers have been tested as well as a method of HV cycling to overcome polarization effects.

The SDD diamond was used for the first neutron measurements on the new ChipIr beam-line. Here preliminary tests where performed before the end of the ChipIr construction, which is at present still on going to optimize the fast neutron transport. A harder neutron spectrum was observed with respect to what measured on VESUVIO and PRISMA. This is indeed expected, since ChipIr has been designed with a line of sight on the spallation target without direct view

on the moderator.
For Fusion applications, a TPR concept based on fast inorganic scintillators has been studied, with laboratory characterizations and measurements at proton accelerators. Energy resolution measurements have been performed with thin (1"x0.1") $LaBr_3$ and YAP scintillators using protons between 1 and 8 MeV at the Uppsala Tandem accelerator (*Paper III*). The measurements have shown that both crystals are good candidate components for a TPR spectrometer for fusion and spallation source applications as they match the required energy resolution and fast scintillation time. In particular, our measurements show that a proton energy resolution better than 2% can be achieved at 8 MeV. These results extrapolate favourably at $E_p > 8MeV$, making $LaBr_3$ and YAP an effective alternative to silicon detectors for a TPR neutron spectrometer designed to deliver neutron spectra with an overall neutron energy resolution better than 5%.
A further characterization of the crystals at proton energies in the 10-30 MeV energy range was done at the Legnaro Tandem-ALPI-PIAVE accelerator, and preliminary results are presented. Measurements of the energy resolution will be repeated in 2015, due to experimental problems in the proton collimation. However, the preliminary measurements are useful to assess the relative electron/proton light yield for these crystals, which is close to 95% for the thin YAP and 75% for the $LaBr_3$. These results ar promising since they show a low light reduction when the crystals are irradiated with protons with respect to γ-ray interaction. It can be concluded that a thin YAP crystal is a cost effective solution to use in a TPR spectrometer.
Concerning the TPR for spallation sources, a first prototype was succesfully installed on the VESUVIO beam-line and measured the VESUVIO neutron spectrum in the 30-120 MeV neutron energy range. The optimization of the setup and off-line coincidence analysis was mostly devoted to reduce the intense background and distinguish recoil proton events.
The first measurements were performed with a Proton Recoil Telescope consisting of a thin plastic foil placed in the neutron beam and two scintillator detectors (*Paper IV*). This design was lately improved by using a silicon detector as ΔE detector. Good background discrimination was obtained with the present detector configuration, using in coincidence a 500 μm Silicon detector and a 2.5 cm thick YAP scintillator. Measurements of the neutron spectrum of the VESUVIO beam line are presented in the 30 MeV $< E_n <$ 120 MeV energy range, where the neutron flux was measured to be $(1.5 \pm 0.2) \cdot 10^4 s^{-1} cm^{-2}$ at 160 μA proton current. The measured spectrum shows a good agreement with Monte Carlo simulations of the VESUVIO beam line (*Paper V*).
Response functions of γ-ray spectrometers for the diagnostics of fusion plasmas have been studied. The detectors now in use at JET and of interest for next generation tokamaks are $LaBr_3$ scintillators and a HPGe detector. A MCNP model was developed and benchmarked with measurements with laboratory ^{137}Cs and ^{60}Co γ-ray sources. The MCNP model was adapted in order to simulate the response of the $LaBr_3$ crystal to fusion neutron, which was unknown, and firstly observed with measurements at neutron sources and tokamaks (*Paper VI*).
The response of $LaBr_3$ (Ce) scintillators to 2.5 (*Paper VII*) and 14 MeV (*Paper VIII*) neutrons has been measured at the FNG and at the JET tokamak. Measurements are used to benchmark Monte Carlo simulations. It is found that several channels contribute to the measured response, the most relevant ones being neutron inelastic scattering and (n,2n) reaction on ^{79}Br , ^{81}Br and ^{139}La . This reactions are responsible for the production of secondary γ-rays, which in turn deposit their energy into the $LaBr_3$ (Ce) crystal. A small contribution is due to the production of secondary charged particles, relevant only for 14 MeV neutrons. Considering all contributions, the counting efficiency of a 3"x3" $LaBr_3$ (Ce) to 14 MeV neutrons is found to be 43%. The efficiency of a 3"x6" $LaBr_3$ (Ce) to 2.5 MeV neutrons is found to be 76%. For 14 MeV neutrons, the (n,2n) reaction is also responsible for the production of the short lived ^{78}Br and ^{80}Br isotopes, whose decay is the main contribution to post irradiation measurements.

The results presented in this thesis represent a step forward in the development of instrumentation for fast neutron detection.
Following these results, and other studies by other groups, SDDs has been selected as promising candidates for a compact detector for use in camera systems of a burning plasma experiment, where there is limited space for implementation of more complex devices. SDDs feature compact dimensions and high rate capability. Moreover, the SDD does not suffer significant gain drifts at high counting rates and strong magnetic fields, which could instead be of major concerns for a scintillator detector. In deuterium plasmas, SDD allows for a good discrimination of direct (primary) and scattered neutrons. Such improvement in the scattered to direct neutron ratio would enhance the imaging capability of a neutron camera system, and ease the interpretation and analysis of neutron calibrations in a tokamak. In DT plasmas, SDD could allow for obtaining a spatially resolved spectroscopy information from the peak shape of the (n,α) reaction, providing detailed information on the fuel ion energy distribution in a high performance device. A 12-pixel SDD matrix has been designed and built for DT neutron emission measurements of the JET fusion plasma experiments. After characterization with laboratory α-sources and 14 MeV neutron source (in late 2014), this system will be installed at the JET tokamak for neutron spectroscopy measurements, with particular emphasis to the future DT campaign (at present scheduled for 2017).
SDDs are proposed for installation as fast neutron monitor of ChipIr. A matrix with 4-pixels of reduced dimensions ($\simeq 1mm^2$) is being designed to cope with the high instantaneous flux of ChipIr, that will start full operations in 2015 with the optimized neutron transport configuration. As future development of the diamond detector technology for application on ChipIr the following points have to be considered:

1. Study of the polarization effects, that determine transients that jeopardize the diamond time stability. A strategy to overcome this effects, based on HV cycling, has been identified. This can be of relevance also for fusion applications concerning long pulses of next step burning plasmas. In this thesis, during the measurements at the 14 MeV source the detector response was found to be stable during the irradiation time (20 minutes at 1 kHz counting rate), without showing any polarization effect (*Paper I*).

2. Study of the response functions for neutron energy above 20 MeV, and up ideally to hundreds of MeV. A more detailed knowledge of the response functions would improve the energy information that can be retrieved from the diamond measurement. This can be done with dedicated measurements at quasi-monoenergetic neutron sources, and with the development of dedicated Monte Carlo models.

Following the results presented in this thesis, future developments of the TPR projects are expected:

1. For fusion applications, the TPR concept based on scintillators will be compared to the one based on Silicon detectors, with new measurements at proton accelerators. The possibility of tests of a complete system at a 14 MeV neutron source is under study.

2. Based on the results obtained on the VESUVIO beam-line, a new system will be built to measure the neutron spectrum of the ChipIr instrument at the ISIS spallation source.

Concerning the response of γ-ray spectrometers to a fast neutron field, the results presented in this thesis are of relevance for the design of γ-ray detectors in burning plasma fusion experiments of the next generation, such as ITER, where capability to perform measurements in an intense 14 MeV neutron flux is required.

Acknowledgements

If the past three years, that I dedicated to this work, have been so enjoyable and have produce a few useful results, it is in large part credit of a long list of people that gave advice, contribution and support. Probably more then that, it is credit of all the people that with their time and passion helped me in this wonderful journey on the strenuous roads of experimental science.
For this reason, probably only half of the people that deserve it will find space on this page, and among those only half will receive half of the credit that I would like to give.
First of all I would like to thank my tutor Claudia, who, with liberal foresight, gave me the possibility to start and follow this project. She also gave me the opportunity to be teaching assistant in the course of experimental physics, which has been indeed a challenging and enjoyable task during my PhD.
Many thanks go to Marco, who firstly showed me the ropes of a laboratory for nuclear measurements, and then followed closely my work, always with new inputs, ideas and advices. His helpfulness, together with a cheerful mood, has been fundamental for the success of this work.
It goes almost without saying, a big thank to the mentor of the Milano neutron spectroscopy group, Giuseppe, who always supported my work. It is thanks to his dedicated guide that I could follow these projects and have many educational opportunities, traineeships at international laboratories, schools, conferences etc.
Thanks to Chris, who supervised my work at the ISIS spallation source and gave a fundamental support for my period abroad.
For the results of the scientific work presented in this thesis, and for the friendly working environment, I have to thank all the group in Milano-Bicocca and IFP-CNR that adopted me during these three years. In Particular, Massimo was an indispensable colleague during experimental campaigns, a good travel mate, and a guide for all my dilemmas about plasma physics and diagnostics. He was also essential in my learning curve of scientific writing, and favourite victim for internal revision of my papers. Gabriele showed me how much dedication is necessary for laboratory work and thought me a lot about gas detectors. Marica introduced me to the enchanted world of diamond detectors. Thanks to Luca for the help from JET with neutron and γ-ray instrumentation. Andrea and Tino have recently joined the Milano-Bicocca group and are already a vital part of it. Thanks to Alberto, Giovanni, Enrico and Giorgia.
A special credit must be given to colleagues of the Uppsala Univerity group, for the support on the installation of the Diamond Detector at JET, Göran and Federico, for MCNP simulations, Erik, and for TPR related experiments, Anders and Davide.
Thanks to Erich for the help form CERN on electronics. Luigino and Sara helped me with specific MCNP issues. Thanks to all the neutron people from JET, Brian, Sergei, Sean, et al. and people at ENEA in Frascati, Mario, Maurizio and Tonino. Thanks to Alberto for the collaboration with Milano-Politecnico.
Thanks to Daniele, Marco and Paolo for the collaboration on Diamond detectors.
Thanks to all the friends that have been closed during the past three years. I don't have the

space to list all the names, but each of you have a space in my hart if not on these pages.
A huge Thank You to my parents and all my family for the support and affection demonstrated me.
Thank you my beloved Amanda for the wonderful year that we spent together and the support demonstrated me while I was dedicating so much time and energy to this work.
I hope that my twenty-five readers will find something interesting in this thesis, but all the mistakes are mine.

Bibliography

[1] Almqvist, E. "Fast Neutrons from the T+ D and T+ Li Reactions." Canadian Journal of Research 28.4 (1950): 433-448.

[2] Hess, Wilmot N., et al. "Cosmic-ray neutron energy spectrum." Physical Review 116.2 (1959): 445.

[3] Knoll, Glenn F. "Radiation detection and measurement." Wiley. com, 2010.

[4] Bramblett, Richard L., Ronald I. Ewing, and T. W. Bonner. "A new type of neutron spectrometer." Nuclear Instruments and Methods 9.1 (1960): 1-12.

[5] East, L. V., and R. B. Walton. "Polyethylene moderated ^3He neutron detectors." Nuclear Instruments and Methods 72.2 (1969): 161-166.

[6] Johnson, T. L., et al. "Recent advances in Bonner sphere neutron spectrometry." Proceedings of the topical conference on theory and practices in radiation protection and shielding. Volumes 1-2. 1987.

[7] Jacobs, Gerard JH, and Rob LP van den Bosch. "Calibration measurements with the multisphere method and neutron spectrum analyses using the SAND-II program." Nuclear instruments and Methods 175.2 (1980): 483-489.

[8] Thomas, D. J., and A. V. Alevra. "Bonner sphere spectrometers - a critical review." Nuclear Instruments and Methods in Physics Research Section A: Accelerators, Spectrometers, Detectors and Associated Equipment 476.1 (2002): 12-20.

[9] Finlay, R. W., et al. "Neutron total cross sections at intermediate energies." *Physical Review C 47.1 (1993): 237.*

[10] Abfalterer, W. P., Bateman, F. B., Dietrich, F. S., Finlay, R. W., Haight, R. C., & Morgan, G. L. (2001). "Measurement of neutron total cross sections up to 560 MeV." *Physical Review C, 63(4), 044608.*

[11] Klein, Horst. "Neutron spectrometry in mixed fields: NE213/BC501A liquid scintillation spectrometers." Radiation protection dosimetry 107, no. 1-3 (2003): 95-109.

[12] Gagnon-Moisan, F., M. Reginatto, and A. Zimbal. "Results for the response function determination of the Compact Neutron Spectrometer." Journal of Instrumentation 7, no. 03 (2012): C03023.

[13] Marion, Jerry B., and Frank Coleman Young. "Nuclear reaction analysis." (1968).

[14] Chadwick, James. "Possible existence of a neutron." Nature 129.3252 (1932): 312.

[15] C.E. Shannon, "Communication in the presence of noise", Proceedings of the Institute of Radio Engineers, vol. 37, no. 1, 10, January 1949. Reprint as classic paper in: Proceedings of IEEE, vol. 86, No. 2, (February 1998).

[16] Crawley, H. B., McKay, R., Meyer, W. T., Rosenberg, E. I., Thomas, W. D. (1994). "A test bench for evaluating fast ADCs." Nuclear Instruments and Methods in Physics Research Section A: Accelerators, Spectrometers, Detectors and Associated Equipment, 342(2), 578-590.

[17] Nocente, M., et al. "Energy resolution of gamma-ray spectroscopy of JET plasmas with a LaBr3 scintillator detector and digital data acquisitiona)." Review of scientific instruments 81.10 (2010): 10D321.

[18] Hellesen, C., Skiba, M., Ericsson, G., Andersson Sundèn, E., Binda, F., Conroy, S., ... Weiszflog, M. (2013). "Impact of digitization for timing and pulse shape analysis of scintillator detector signals." Nuclear Instruments and Methods in Physics Research Section A: Accelerators, Spectrometers, Detectors and Associated Equipment, 720, 135-140.

[19] Skiba, Mateusz, et al. "Fully digital data acquisition system for the neutron time-of-flight spectrometer TOFOR at JETa)." Review of Scientific Instruments 83.10 (2012): 10D907.

[20] Marrone, S., et al. "Pulse shape analysis of liquid scintillators for neutron studies." Nuclear Instruments and Methods in Physics Research Section A: Accelerators, Spectrometers, Detectors and Associated Equipment 490.1 (2002): 299-307.

[21] Carlo Tintori "Digital Pulse Processing in Nuclear Physics" technical report, *http* : *//www.caen.it/documents/News/*20*/WP*2081*_DigitalPulseProcessing_Rev_*2.1*.pdf*

[22] Wesson J., "Tokamaks", 3rd edition, Clarendon Press (2004)

[23] http://www.efda.org/jet/

[24] Smith, Dale L., et al. "Blanket comparison and selection study." Fusion Tech 8.1 (1984): 1.

[25] Sahin, S., Tawfik A. Al Kusayer, and M. Abdul Raoof. "Preliminary design studies of a cylindrical experimental hybrid blanket with deuterium-tritium driver." (1986).

[26] Asaoka, Yoshiyuki, et al. "Requirements of tritium breeding ratio for early fusion power reactors." (1996).

[27] Hoang, G. T., et al. "A lower hybrid current drive system for ITER." Nuclear Fusion 49.7 (2009): 075001.

[28] Goldston, Robert J., et al. "New techniques for calculating heat and particle source rates due to neutral beam injection in axisymmetric tokamaks." Journal of computational physics 43.1 (1981): 61-78.

[29] Duesing, G., et al. "Neutral beam injection system." (1987).

[30] Ćirić, D., et al. "Performance of upgraded JET neutral beam injectors." Fusion Engineering and Design 86.6 (2011): 509-512.

[31] Keilhacker, M., and M. L. Watkins. "D-T experiments in the JET tokamak." Journal of nuclear materials 266 (1999): 1-13.

[32] Green, B. J. “ITER: burning plasma physics experiment.” Plasma physics and controlled fusion 45.5 (2003): 687.

[33] Wong, King-Lap. “A review of Alfvèn eigenmode observations in toroidal plasmas.” Plasma physics and controlled fusion 41.1 (1999): R1.

[34] Heidbrink W.W., Phys. Plasmas 15 (2008) 055501

[35] Nocente, M. (2012). “Neutron and gamma-ray emission spectroscopy as fast ion diagnostics in fusion plasmas” (Doctoral dissertation, Universitá degli Studi di Milano-Bicocca).

[36] Giacomelli, Luca, et al. “Advanced neutron diagnostics for JET and ITER fusion experiments.” Nuclear fusion 45.9 (2005): 1191.

[37] Jarvis O.N. 1994 Plasma Phys. Control. Fusion 36 209

[38] Angelone, M., et al. “Calibration of the neutron yield measurement system on FTU tokamak.” Review of scientific instruments 61.11 (1990): 3536-3539.

[39] Jarvis, O. N., et al. “Inâvessel calibration of the JET neutron monitors using a 252Cf neutron source: Difficulties experienced.” Review of Scientific Instruments 61.10 (1990): 3172-3174.

[40] Syme, D. B., et al. “Fusion yield measurements on JET and their calibration.” Nuclear Engineering and Design 246 (2012): 185-190.

[41] Marcus, F. B., et al. “Neutron emission profile measurements during the first tritium experiments at JET.” Nuclear fusion 33.9 (1993): 1325.

[42] Kaellne, J., and G. Gorini. “A neutron camera for burning plasmas.” Review of scientific instruments 63.10 (1992): 4545-4547.

[43] Cecconello, Marco, et al. “A neutron camera system for MASTa).” Review of Scientific Instruments 81.10 (2010): 10D315.

[44] Kaellne, Jan, et al. “Advanced neutron diagnostics for ITER fusion experiments.” JET-EFDA Workprogramme, 2005.

[45] Fisher W A, Chen S H, Gwinn D and Parker R R 1983 Phys. Rev. A 28 3121

[46] Nocente M, Gorini G, Kaellne J and Tardocchi M 2011 a Nucl. Fusion 51 063011

[47] Tardocchi, M., M. Nocente, and G. Gorini. “Diagnosis of physical parameters of fast particles in high power fusion plasmas with high resolution neutron and gamma-ray spectroscopy.” Plasma Physics and Controlled Fusion 55.7 (2013): 074014.

[48] H. Sjostrand et al., “New MPRu Instrument for Neutron Emission Spectroscopy at JET”, Review of Scientific Instruments 77, 10E717 (2006).

[49] E.Andersson Sundèn et al., “The thin foil magnetic proton recoil neutron spectrometer MPRu at JET”, Nucl. Instr. and Meth.. A 610 (2009) 682.

[50] G. Ericsson et al., “Neutron emission spectroscopy at JET - Results from the magnetic proton recoil spectrometer”, Review of Scientific Instruments 72 (2001) 759.

[51] Gorini, G., and J. Kaellne. “High count rate timeâofâflight spectrometer for DD fusion neutrons.” Review of scientific instruments 63.10 (1992): 4548-4550.

[52] Gatu Johnson, Maria, Luca Giacomelli, Anders Hjalmarsson, Jan Kaellne, Matthias Weiszflog, Erik Andersson Sundèn, Sean Conroy et al. "The 2.5-MeV neutron time-of-flight spectrometer TOFOR for experiments at JET." Nuclear Instruments and Methods in Physics Research Section A: Accelerators, Spectrometers, Detectors and Associated Equipment 591, no. 2 (2008): 417-430.

[53] Gatu Johnson, Maria, Luca Giacomelli, Anders Hjalmarsson, Matthias Weiszflog, E. Andersson Sundǹ, Sean Conroy, Goran Ericsson et al. "The TOFOR neutron spectrometer and its first use at JET." Review of scientific instruments 77, no. 10 (2006): 10E702-10E702.

[54] Hjalmarsson, Anders, Sean Conroy, Goeran Ericsson, Luca Giacomelli, Giuseppe Gorini, Hans Henriksson, Jan KÃllne, Marco Tardocchi, and Matthias Weiszflog. "The TOFOR spectrometer for 2.5 MeV neutron measurements at JET." Review of scientific instruments 74, no. 3 (2003): 1750-1752.

[55] Tardocchi, M., Conroy, S., Ericsson, G., Gorini, G., Henriksson, H., & Kaellne, J. (2002). "Neutron emission spectroscopy of radio frequency heated (D)T plasmas." Nuclear fusion, 42(10), 1273.

[56] Hellesen, Carl, et al. "Measurements of fast ions and their interactions with MHD activity using neutron emission spectroscopy." Nuclear fusion 50.8 (2010): 084006.

[57] Hellesen, Carl, et al. "Neutron emission generated by fast deuterons accelerated with ion cyclotron heating at JET." Nuclear fusion 50.2 (2010): 022001.

[58] Hellesen, Carl, et al. "Neutron spectroscopy measurements and modeling of neutral beam heating fast ion dynamics." Plasma Physics and Controlled Fusion 52.8 (2010): 085013.

[59] Marocco, Daniele, et al. "High count rate neutron spectrometry with liquid scintillation detectors." Nuclear Science, IEEE Transactions on 56.3 (2009): 1168-1173.

[60] Sundèn, Erik Andersson, et al. "Evaluation of spectral unfolding techniques for neutron spectroscopy." AIP Conference Proceedings. Vol. 988. No. 1. 2008.

[61] H. Klein and S. Neumann, Nucl. Instrum. Meth. A 476, 132 (2002).

[62] H. Klein, Radiat. Prot. Dosim. 107, 95 (2003).

[63] Giacomelli, L., et al. "Evaluation of a digital data acquisition system and optimization of n-γdiscrimination for a compact neutron spectrometer." Review of Scientific Instruments 82.1 (2011): 013505.

[64] Binda, F., et al. "Forward fitting of experimental data from a NE213 neutron detector installed with the magnetic proton recoil upgraded spectrometer at JETa)." Review of Scientific Instruments 85.11 (2014): 11E123.

[65] A. Krasilnikov et al., Review of scientific instruments 68, no. 1 (1997): 553-556.

[66] M. Pillon et al., Nucl. Instrum. and Meth. in Physics Research Section B 101, no. 4 (1995): 473-483.

[67] M. Angelone et al., Review of scientific instruments 76, no. 1 (2004): 013506.

[68] Conroy, Sean W., et al. "Neutron spectrometer for ITER using silicon detectors." Review of Scientific Instruments 79.10 (2008): 10E508-10E508.

[69] Fasoli, A., C. Gormenzano, H. L. Berk, B. Breizman, S. Briguglio, D. S. Darrow, N. Gorelenkov et al. "Physics of energetic ions." Nuclear Fusion 47, no. 6 (2007): S264.

[70] Kiptily, V. G., F. E. Cecil, and S. S. Medley. "Gamma ray diagnostics of high temperature magnetically confined fusion plasmas." Plasma physics and controlled fusion 48, no. 8 (2006): R59.

[71] Kiptily, V. G., F. E. Cecil, O. N. Jarvis, M. J. Mantsinen, S. E. Sharapov, L. Bertalot, S. Conroy et al. "γ-ray diagnostics of energetic ions in JET." Nuclear Fusion 42, no. 8 (2002): 999.

[72] Cecil, F. E., and David E. Newman. "Diagnostics of high temperature deuterium and tritium plasmas by spectrometry of radiative capture reactions." Nuclear Instruments and Methods in Physics Research 221, no. 2 (1984): 449-452.

[73] Proverbio, I., M. Nocente, V. G. Kiptily, M. Tardocchi, G. Gorini, and JET-EFDA Contributors. "The 12C (3He, pγ) 14N reaction cross section for γ-ray spectroscopy simulation of fusion plasmas." Review of scientific instruments 81, no. 10 (2010): 10D320-10D320.

[74] Nocente, M., M. Garcia-Munoz, G. Gorini, M. Tardocchi, A. Weller, S. Akaslompolo, R. Bilato et al. "Gamma-ray spectroscopy measurements of confined fast ions on ASDEX Upgrade." Nuclear Fusion 52, no. 9 (2012): 094021.

[75] Tardocchi, Marco, M. Nocente, I. Proverbio, V. G. Kiptily, P. Blanchard, Sean Conroy, M. Fontanesi et al. "Spectral Broadening of Characteristic γ-Ray Emission Peaks from 12C (3He, pγ)14 N Reactions in Fusion Plasmas." Physical review letters 107, no. 20 (2011): 205002.

[76] Nocente, Massimo, Marco Tardocchi, V. G. Kiptily, Patrick Blanchard, I. Chugunov, Sean Conroy, T. Edlington et al. "High-resolution gamma ray spectroscopy measurements of the fast ion energy distribution in JET 4He plasmas." Nuclear Fusion 52, no. 6 (2012): 063009.

[77] Van Loef, E. V. D., P. Dorenbos, C. W. E. Van Eijk, K. W. Kraemer, and H. U. Guedel. "Scintillation properties of $LaBr_3$:Ce3+ crystals: fast, efficient and high-energy-resolution scintillators." Nuclear Instruments and Methods in Physics Research Section A: Accelerators, Spectrometers, Detectors and Associated Equipment 486, no. 1 (2002): 254-258.

[78] Nicolini, R., F. Camera, N. Blasi, S. Brambilla, R. Bassini, C. Boiano, A. Bracco et al. "Investigation of the properties of a 1 "Ã 1 " LaBr3:Ce scintillator." Nuclear Instruments and Methods in Physics Research Section A: Accelerators, Spectrometers, Detectors and Associated Equipment 582, no. 2 (2007): 554-561.

[79] Giaz, A., Pellegri, L., Riboldi, S., Camera, F., Blasi, N., Boiano, C., ... Wieland, O. (2013). "Characterization of large volume 3.5 "Ã 8 " $LaBr_3$: Ce detectors." Nuclear Instruments and Methods in Physics Research Section A: Accelerators, Spectrometers, Detectors and Associated Equipment, 729, 910-921.

[80] Nocente, M., M. Tardocchi, A. Olariu, S. Olariu, R. C. Pereira, I. N. Chugunov, A. Fernandes et al. "High Resolution Gamma Ray Spectroscopy at MHz Counting Rates With LaBr Scintillators for Fusion Plasma Applications." Nuclear Science, IEEE Transactions on 60, no. 2 (2013): 1408-1415.

[81] Roberts, Oliver, Pankaj Joshi, David Jenkins, Bob Wadsworth, and Adam Tuff. "Neutron Response of 1.5" $LaBr_3$: Ce Crystal Scintillators for PARIS." (2008).

[82] Russell, G. J., E. J. Pitcher, and L. L. Daemen. “Introduction to spallation physics and spallation-target design.” AIP Conference Proceedings. IOP INSTITUTE OF PHYSICS PUBLISHING LTD, 1995.

[83] Gordon, M. S., et al. “Measurement of the flux and energy spectrum of cosmic-ray induced neutrons on the ground.” Nuclear Science, IEEE Transactions on 51.6 (2004): 3427-3434

[84] T. J. O’Gorman, J. M. Ross, A. H. Taber, J. F. Ziegler, H. P. Muhlfeld, C. J. Montrose, H. W. Curtis, and J. L. Walsh, “Field testing for cosmic ray soft errors in semiconductor memories,” IBM J. Res. Dev., vol. 40, p. 3, 1996.

[85] P. E. Dodd and L. W. Massengill, “Basic Mechanisms and modelling of single event upsets in digital microelectronics,” IEEE Trans. on Nucl. Sci., vol. 50, pp. 583 - 602, 2003.

[86] J. Ziegler and W. Lanford, “The Effect of Sea-Level Cosmic Rays on Electronic Devices” J. Appl. Phys., vol. 52, pp. 4305 - 4312, 1981.

[87] Ziegler, James F. “Terrestrial cosmic rays.” IBM journal of research and development 40.1 (1996): 19-39.

[88] Normand, Eugene. “Single event upset at ground level.” IEEE transactions on Nuclear Science 43.6 (1996): 2742-2750.

[89] Taber, A., and E. Normand. “Single event upset in avionics.” IEEE Transactions on Nuclear Science 40 (1993): 120-126.

[90] Weibull, W., “A statistical distribution function of wide applicability” J. Appl. Mech.-Trans. ASME, vol. 18, 3, 1951, pp. 293-297.

[91] Normand, E., and T. J. Baker. “Altitude and latitude variations in avionics SEU and atmospheric neutron flux.” Nuclear Science, IEEE Transactions on 40.6 (1993): 1484-1490.

[92] Platt, S. P., A. V. Prokofiev, and X. X. Cai. “Fidelity of energy spectra at neutron facilities for single-event effects testing.” Reliability Physics Symposium (IRPS), 2010 IEEE International. IEEE, 2010.

[93] Slayman, Charles W. “Theoretical correlation of broad spectrum neutron sources for accelerated soft error testing.” Nuclear Science, IEEE Transactions on 57.6 (2010): 3163-3168.

[94] Slayman, Charles. “Accuracy of various broad spectrum neutron sources for accelerated soft error testing.” SELSE6, Stanford University, Stanford, CA, March 23 24 (2010).

[95] http://lansce.lanl.gov/.

[96] http://www.triumf.ca/

[97] Rebai, M., et al. “Response of a single-crystal diamond detector to fast neutrons.” Journal of instrumentation 8.10 (2013): P10007.

[98] Pillon, M., et al. “Experimental response functions of a single-crystal diamond detector for 5â20.5 MeV neutrons.” Nuclear Instruments and Methods in Physics Research Section A: Accelerators, Spectrometers, Detectors and Associated Equipment 640.1 (2011): 185-191.

[99] Pietropaolo, A., et al. “Fission diamond detectors for fast-neutron ToF spectroscopy.” EPL (Europhysics Letters) 94.6 (2011): 62001.

[100] Rebai, M., et al. “Diamond detectors for fast neutron measurements at pulsed spallation sources.” Journal of instrumentation 7.05 (2012): C05015.

[101] Giacomelli, L., et al. “Pulsed neutron beam measurements with diamond detectors.” Nuclear Instruments and Methods in Physics Research Section A: Accelerators, Spectrometers, Detectors and Associated Equipment 720 (2013): 125-127.

[102] S. P. Platt,et al., “Charge-collection and single-event upset measurements at the ISIS neutron source,” IEEE Trans. Nucl. Sci., vol. 55, no. 4, pp. 2126â2133, Aug. 2008.

[103] S. Ansell and C. D. Frost, “A design of an irradiation beamline for Target Station 2, ISIS,” in Proc. 9th European Conf. Radiat. Effects Compon. Syst. (RADECS 2007), Sep. 2007, paper F-1.

[104] C. D. Frost, S. Ansell, and G. Gorini, “A new dedicated neutron facility for accelerated SEE testing at the ISIS facility,” in Proc. IEEE International Reliability Physics Symposium, 2009, pp. 952â955.

[105] Andreani, C., et al. “Facility for fast neutron irradiation tests of electronics at the ISIS spallation neutron source.” Applied physics letters 92.11 (2008): 114101-114101.

[106] Bedogni, Roberto, et al. “Characterization of the neutron field at the ISIS-VESUVIO facility by means of a bonner sphere spectrometer.” Nuclear Instruments and Methods in Physics Research Section A: Accelerators, Spectrometers, Detectors and Associated Equipment 612.1 (2009): 143-148.

[107] Smirnov, A. N., et al. “Application of thin-film breakdown counters for characterization of neutron field of the VESUVIO instrument at the ISIS spallation source.” Nuclear Instruments and Methods in Physics Research Section A: Accelerators, Spectrometers, Detectors and Associated Equipment 687 (2012): 14-22.

[108] Murtas, F., et al. “Triple GEM gas detectors as real time fast neutron beam monitors for spallation neutron sources.” Journal of instrumentation 7.07 (2012): P07021.

[109] Croci, G., et al. “nGEM fast neutron detectors for beam diagnostics.” Nuclear Instruments and Methods in Physics Research Section A: Accelerators, Spectrometers, Detectors and Associated Equipment 720 (2013): 144-148.

[110] Croci, G., et al. “nGEM neutron diagnostic concept for high power deuterium beams.” Journal of instrumentation 7.03 (2012): C03010.

[111] Croci, G., et al. “Measurements of γ-ray sensitivity of a GEM based detector using a coincidence technique.” Journal of Instrumentation 8.04 (2013): P04006.

[112] Almaviva, S., et al. “Extreme UV photodetectors based on CVD single crystal diamond in a p-type/intrinsic/metal configuration.” Diamond and related materials 18.1 (2009): 101-105.

[113] Mainwood, Alison. “Recent developments of diamond detectors for particles and UV radiation.” Semiconductor science and technology 15.9 (2000): R55.

[114] Pomorski, M., et al. “Characterisation of single crystal CVD diamond particle detectors for hadron physics experiments” physica status solidi (a) 202.11 (2005): 2199-2205.

[115] Adam, W., et al. “The development of diamond tracking detectors for the LHC.” Nuclear Instruments and Methods in Physics Research Section A: Accelerators, Spectrometers, Detectors and Associated Equipment 514.1 (2003): 79-86.

[116] Balducci, A., et al. “Radiological X-ray dosimetry with single crystal CVD diamond detectors.” Diamond and related materials 15.4 (2006): 797-801.

[117] Trucchi, D. M., et al. “Very Fast and Primingless Single-Crystal-Diamond X-Ray Dosimeters.” Electron Device Letters, IEEE 33.4 (2012): 615-617.

[118] Girolami, Marco, et al. “Diamond detectors for UV and X-ray source imaging.” Electron Device Letters, IEEE 33.2 (2012): 224-226.

[119] Margarone, D., et al. “Full characterization of laser-accelerated ion beams using Faraday cup, silicon carbide, and single-crystal diamond detectors.” Journal of Applied Physics 109.10 (2011): 103302.

[120] Bellucci et al., IEEE Electron Device Letters, 35 (2013) 695-697.

[121] Girolami, M., et al. “Radiation-assisted Frenkel-Poole transport in single-crystal diamond.” Applied Physics Letters 103.8 (2013): 083502.

[122] Trucchi, D. M., et al. “The influence of grain-boundaries on the electronic performance of CVD diamond films.” Diamond and related materials 14.3 (2005): 575-579.

[123] Conte, G., et al. “Grain boundary transport in x-ray irradiated polycrystalline diamond.” Journal of Applied physics 93.10 (2003): 6078-6083.

[124] Conte, Gennaro, et al. “Temporal response of CVD diamond detectors to modulated low energy Xâray beams.” physica status solidi (a) 201.2 (2004): 249-252.

[125] Element Six Ltd webpage, http://www.e6.com

[126] CIVIDEC webpage, http://www.cividec.at

[127] Martone, M., M. Angelone, and M. Pillon. “The 14 MeV frascati neutron generator.” Journal of nuclear materials 212 (1994): 1661-1664.

[128] webpage, http://www.caen.it

[129] Sudbrock et al., Radiochim. Acta 88, 829-832 (2000)

[130] Frenje, J., L. Ballabio, S. Conroy, G. Ericsson, M. Tardocchi, E. Traneus, J. Kaellne, and G. Gorini. “Neutron spectrometry of triton burn-up in plasmas of deuterium.” Plasma physics and controlled fusion 40, no. 7 (1998): 1211.

[131] Ballabio, L., J. Frenje, J. Kaellne, S. W. Conroy, G. Ericsson, M. Tardocchi, E. Traneus, and G. Gorini. “Measurement and interpretation of the spectrum of the triton burnup neutron emission from deuterium tokamak plasmas.” Nuclear fusion 40, no. 1 (2000): 21.

[132] Sjoestrand, Henrik, Giuseppe Gorini, Sean Conroy, Goeran Ericsson, Luca Giacomelli, Hans Henriksson, Anders Hjalmarsson et al. “Triton burn-up neutron emission in JET low current plasmas.” Journal of Physics D: Applied Physics 41, no. 11 (2008): 115208.

[133] Cash, Webster. “Parameter estimation in astronomy through application of the likelihood ratio.” The Astrophysical Journal 228 (1979): 939-947.

[134] Nocente, M., M. Garcia-Munoz, G. Gorini, M. Tardocchi, A. Weller, S. Akaslompolo, R. Bilato et al. "Gamma-ray spectroscopy measurements of confined fast ions on ASDEX Upgrade." Nuclear Fusion 52, no. 9 (2012): 094021.

[135] Chen, Z., M. Nocente, M. Tardocchi, T. Fan, and G. Gorini. "Simulation of neutron emission spectra from neutral beam-heated plasmas in the EAST tokamak." Nuclear Fusion 53, no. 6 (2013): 063023.

[136] Henriksson H. 2003 Neutron spectroscopy studies of heating effects in fusion plasmas PhD Thesis Acta Universitatis Upsaliensis No 861, Faculty of Sciences and Technology, Uppsala University

[137] Steigenberger, U., et al. "The development of the PRISMA spectrometer at ISIS." Nuclear Instruments and Methods in Physics Research Section B: Beam Interactions with Materials and Atoms 53.1 (1991): 87-96.

[138] Petrillo, C., et al. "A double crystal analyser system for the PRISMA spectrometer." Journal of Neutron Research 3.2 (1996): 93-103.

[139] G. Gorini, "Analytical model for characterization of the MPR spectrometer", UU-NF 95/1

[140] Hamamatsu online catalogue, http://www.hamamatsu.com/

[141] ORTEC online catalogue, http://www.ortec-online.com/

[142] E. Rutherford, "The Scattering of α and β Particles by Matter and the Structure of the Atom", Philosophical Magazine Series 6, vol. 21 May 1911, p. 669-688

[143] M. Moszyhski et al, "Properties of the YAP : Ce scintillator", Nuclear Instruments and Methods in Physics Research A 404 (1998) 157F 165

[144] M. Kapusta et al, "A high-energy resolution observed from a YAP : Ce scintillator", Nuclear Instruments and Methods in Physics Research A 421 (1999) 610â613

[145] A. Del Guerra et al, "Measurement of absolute light yield and determination of a lower limit for the light attenuation length for YAP:Ce crystal", IEEE TRANSACTIONS ON NUCLEAR SCIENCE, VOL 44, NO. 6, DECEMBER 1997

[146] T.B. de Queiroz et al, "Luminescence characteristics of YAP:Ce scintillator powders and composites", Optical Materials 32 (2010) 1480â1484

[147] J. F. Ziegler, SRIM - The Stopping and Range of Ions in Solids, http://www.srim.org/

[148] Pietropaolo, A., et al. "Characterization of the γbackground in epithermal neutron scattering measurements at pulsed neutron sources." Nuclear Instruments and Methods in Physics Research Section A: Accelerators, Spectrometers, Detectors and Associated Equipment 568.2 (2006): 826-838.

[149] Pietropaolo, A., et al. "γ-ray background sources in the VESUVIO spectrometer at ISIS spallation neutron source." Nuclear Instruments and Methods in Physics Research Section A: Accelerators, Spectrometers, Detectors and Associated Equipment 608.1 (2009): 121-124.

[150] M. S. Livingston and H. A. Bethe, Revs. Modern Phys. 9, 285 (1937)

[151] R.B. Firestone and L.P. Ekstroem, LBNL Isotopes Project - LUNDS Universitet, http://ie.lbl.gov/toi/

[152] Laboratori Nazionali di Legnaro, http://www.lnl.infn.it/index.php/en/accelerators-3/tandem-xtu

[153] Johnson, M. Gatu, Sean Conroy, Marco Cecconello, E. Andersson SundÃ©n, GÃ¶ran Ericsson, M. Gherendi, Carl Hellesen et al. "Modelling and TOFOR measurements of scattered neutrons at JET." Plasma Physics and Controlled Fusion 52, no. 8 (2010): 085002.

[154] Chugunov, I. N., et al. "Development of gamma-ray diagnostics for ITER." Nuclear fusion 51.8 (2011): 083010.

Synopsis of attached papers

The abstracts of the papers attached to this thesis have been collected in this section.

I. **A Diamond based Neutron Spectrometer for diagnostics of Deuterium-Tritium Fusion Plasmas**
Single crystal Diamond Detectors (SDD) are being increasingly exploited for neutron diagnostics in high power fusion devices, given their significant radiation hardness and high energy resolution capabilities. The geometrical efficiency of SDDs is limited by the size of commercially available crystals, which is often smaller than the dimension of neutron beams along collimated lines of sight in tokamak devices. In this work we present the design and fabrication of a 14 MeV neutron spectrometer consisting of 12 diamond pixels arranged in a matrix, so to achieve an improved geometrical efficiency. Each pixel is equipped with an independent high voltage supply and read-out electronics optimized to combine high energy resolution and fast signals (less than 30 ns), which are essential to enable high counting rate (>1 MHz) spectroscopy. The response function of a prototype SDD to 14 MeV neutrons has been measured at the Frascati Neutron Generator by observation of the 8.3 MeV peak from the $^{12}C(n,\alpha)^{9}Be$ reaction occurring between neutrons and ^{12}C nuclei in the detector. The measured energy resolution (2.5% FWHM) meets the requirements for neutron spectroscopy applications in deuterium-tritium plasmas.

II. **Single crystal Diamond Detector measurements of DD and DT neutrons in JET fusion plasmas**
First simultaneous measurements of DD and DT neutrons from deuterium plasmas using a Single crystal Diamond Detector are presented in this paper. The measurements were performed at JET with a dedicated electronic chain that combined high count rate capabilities and high energy resolution. The deposited energy spectrum from DD neutrons was successfully reproduced by means of Monte Carlo calculations of the detector response function and simulations of neutron emission from the plasma, including background contributions. The reported results are of relevance for the development of compact neutron detectors with spectroscopy capabilities for installation in camera systems of present and future high power fusion experiments.

III. **Thin YAP (Ce) and $LaBr_3$ (Ce) scintillators as proton detectors of a thin-film proton recoil neutron spectrometer for fusion and spallation sources applications**
Two thin inorganic scintillators based on YAP and $LaBr_3$ crystals (1" diameter x 0.1" height) have been used for proton measurements at the Uppsala tandem accelerator in the energy range 4-8 MeV. Measurements show a comparable good energy resolution for the two detectors, better than 2% (FWHM) for 8 MeV protons, which compares to 3.8% ($LaBr_3$) and 3.7% (YAP) obtained at the 1.3 MeV peak of a ^{60}Co γ-ray source. The main advantage of these crystals are a fast scintillation time (less than 30 ns), an excellent light yield and the capability to operate in large neutron background, which make them

ideal candidates as proton detectors of a thin-film proton recoil neutron spectrometer for application on fusion experiments and fast neutron spallation sources.

IV. **First measurement of the VESUVIO neutron spectrum in the 30-80 MeV energy range using a Proton Recoil Telescope technique**
Measurements of the fast neutron energy spectrum at the ISIS spallation source are reported. The measurements were performed with a Proton Recoil Telescope consisting of a thin plastic foil placed in the neutron beam and two scintillator detectors. Results in the neutron energy range 30 MeV $<E_n<$80 MeV are in good agreement with Monte Carlo simulations of the neutron spectrum

V. **A Telescope Proton Recoil spectrometer for fast neutron beam-lines**
Fast neutron measurements were performed on the VESUVIO beam-line at the ISIS spallation source using a new Telescope Proton Recoil spectrometer. Neutrons are converted into protons via elastic scattering on a plastic target. Recoil protons are measured by a proton spectrometer, which use in coincidence a 2.54 cm thick YAP scintillator and a 500 μm thick silicon detector, measuring the full proton recoil energy and the partial deposited energy in transmission, respectively. The VESUVIO fast neutron spectrum was measured up to 120 MeV and results are in good agreement with Monte Carlo simulation of the beam-line. This instrument is of particular interest for the characterization of the ChipIr beam-line at ISIS, which was designed to feature an atmospheric-like neutron spectrum for the irradiation of micro-electronics.

VI. **$LaBr_3$ scintillator response to admixed neutron and γ-ray fluxes**
Gamma ray spectroscopy is a promising method for diagnosing fast ions and confined alpha particles in a fusion plasma device. This application requires γ-ray detectors with high energy resolution (say a few percent for gamma ray energies in the range 1-5 MeV), high efficiency and high count rate capability, ideally up to a few MHz. Furthermore, the detector will have to withstand the high 14 MeV and 2.45 MeV neutron fluxes produced by the main fusion reactions between deuterium and tritium. Experimental results demonstrate that the requirements on energy resolution, efficiency and count rate can be met with a $LaBr_3$ scintillator detector equipped with fast digital data acquisition. The measured response of the detector to 2.45 MeV neutrons is presented in this paper and discussed in terms of the interaction mechanism between neutrons and detector.

VII. **Response of $LaBr_3$ (Ce) scintillators to 2.5 MeV fusion neutrons**
Measurements of the response of $LaBr_3$ (Ce) to 2.5 MeV neutrons have been carried out at the Frascati Neutron Generator and at tokamak facilities with deuterium plasmas. The observed spectrum has been interpreted by means of a MCNP model. It is found that the main contributor to the measured response is neutron inelastic scattering on ^{79}Br, ^{81}Br and ^{139}La. An extrapolation of the count rate response to 14 MeV neutrons from deuterium-tritium plasmas is also presented. The results are of relevance for the design of γ-ray diagnostics of fusion burning plasmas.

VIII. **Response of $LaBr_3$ (Ce) scintillators to 14 MeV fusion neutrons**
The response of $LaBr_3$ (Ce) to 14 MeV neutrons has been measured at the Frascati Neutron Generator. A MCNP model is used for the interpretation of experimental results. It is found that several channels contribute to the measured response, the most relevant being neutron inelastic scattering and (n,2n) reaction on ^{79}Br, ^{81}Br and ^{139}La. This reactions are responsible for the production of secondary γ-rays, which in turns deposit their energy into the $LaBr_3$ (Ce) crystal. A small contribution is due to the production of

secondary charged particles, relevant only at deposited energies E_d >5 MeV. Considering all contributions, the efficiency of a 3"x3" $LaBr_3$ (Ce) to 14 MeV neutrons is found to be 43%. The (n,2n) reaction is also responsible for the production of the short lived ^{78}Br and ^{80}Br isotopes, whose decay is the main contribution to post irradiation measurements. The results presented hereby are of relevance for the design of γ-ray diagnostics of fusion burning plasmas.

Paper I

A diamond based neutron spectrometer for diagnostics of deuterium-tritium fusion plasmas[a)]

C. Cazzaniga,[1,2,b)] M. Nocente,[1,2] M. Rebai,[1] M. Tardocchi,[2] P. Calvani,[3] G. Croci,[2] L. Giacomelli,[1] M. Girolami,[3] E. Griesmayer,[4] G. Grosso,[2] M. Pillon,[5] D. M. Trucchi,[5] and G. Gorini[1,2]

[1]*University of Milano Bicocca, Piazza della Scienza 3, Milano, Italy*
[2]*Istituto di Fisica del Plasma, Associazione EURATOM-ENEA-CNR, via Roberto Cozzi 53, Milano, Italy*
[3]*CNR-ISM, Research Area Roma 1, Via Salaria km 29.300, 00015-Monterotondo Scalo (Rm), Italy*
[4]*Atominstitut, Vienna University of Technology, Vienna, Austria*
[5]*Associazione EURATOM-ENEA sulla Fusione ENEA C.R. Frascati, Via E. Fermi, 45, 00044 Frascati (Roma), Italy*

(Presented 3 June 2014; received 29 May 2014; accepted 11 June 2014; published online 2 July 2014)

Single crystal Diamond Detectors (SDD) are being increasingly exploited for neutron diagnostics in high power fusion devices, given their significant radiation hardness and high energy resolution capabilities. The geometrical efficiency of SDDs is limited by the size of commercially available crystals, which is often smaller than the dimension of neutron beams along collimated lines of sight in tokamak devices. In this work, we present the design and fabrication of a 14 MeV neutron spectrometer consisting of 12 diamond pixels arranged in a matrix, so to achieve an improved geometrical efficiency. Each pixel is equipped with an independent high voltage supply and read-out electronics optimized to combine high energy resolution and fast signals (<30 ns), which are essential to enable high counting rate (>1 MHz) spectroscopy. The response function of a prototype SDD to 14 MeV neutrons has been measured at the Frascati Neutron Generator by observation of the 8.3 MeV peak from the ^{12}C(n, α)^{9}Be reaction occurring between neutrons and ^{12}C nuclei in the detector. The measured energy resolution (2.5% FWHM) meets the requirements for neutron spectroscopy applications in deuterium-tritium plasmas. [http://dx.doi.org/10.1063/1.4885356]

I. INTRODUCTION

Single crystal Diamond Detectors (SDD) can play an important role as compact neutron detectors with spectroscopy capabilities for use in camera systems of a burning plasma experiment, where there is limited space for implementation of more complex devices such as dedicated spectrometers for 2.5 and 14 MeV neutrons.[1–3] Furthermore, SDDs feature other advantages such as radiation resistance and low sensitivity to magnetic fields and γ-ray background, which make them interesting candidates for operation in the harsh environment of a high power tokamak.

The performance evaluation of SDDs as neutron spectrometers has been the subject of dedicated tests at accelerator facilities.[4–11] Neutrons are measured by means of their interactions with carbon nuclei in the detector, which include elastic and inelastic scattering, besides the ^{12}C(n,n′)3α and ^{12}C(n,α)^{9}Be reactions.[12] The latter process is the most interesting one for 14 MeV neutron measurements, since it results in a peak centred at $E_0 = 8.3$ MeV (which compares to a reaction Q value of −5.7 MeV). Neutron spectroscopy measurements with SDDs are especially concerned with measuring the shape of this (n,α) peak, as its width would be proportional to plasma temperature,[13] net of the added broadening from the instrument response function. Additional diagnostic capabilities may also be possible by resolving small (at the 10^{-2} level) high energy components appearing along the falling edge of the (n,α) peak,[14–17] as so far demonstrated at JET with *ad hoc* designed non-compact neutron spectrometers.[18–21]

Previous proof-of-principle measurements of 14 MeV neutrons with natural diamond detectors were performed in tokamak experiments with deuterium-tritium (DT) plasmas and are reported in Refs. 22 and 23. The use of artificially grown SDDs for applications to neutron measurements in fusion plasmas is recent and was so far focused on the determination of the time traces of 14 MeV neutron emission from trace tritium experiments at JET.[24] It is only very recently that the feasibility of neutron spectroscopy with SDDs has been demonstrated by measurement of the 2.5 MeV neutron spectrum from JET deuterium plasmas, together with 14 MeV neutrons from triton burn up emission.[25]

In this work, we present the design of a new system based on a matrix of 12 SDD pixels, each equipped with independent high voltage supply and read-out electronics, designed for 14 MeV neutron spectroscopy applications in plasmas of DT. Special care was taken in optimizing the electronic chain to combine high energy resolution and counting rate (>1 MHz) capabilities. The matrix is proposed for installation at JET on a collimated vertical line of sight in view of the next DT campaign. The results of an experiment at the Frascati Neutron Generator with 14 MeV neutrons impinging on

[a)]Contributed paper, published as part of the Proceedings of the 20th Topical Conference on High-Temperature Plasma Diagnostics, Atlanta, Georgia, USA, June 2014.

[b)]Author to whom correspondence should be addressed. Electronic mail: carlo.cazzaniga@mib.infn.it.

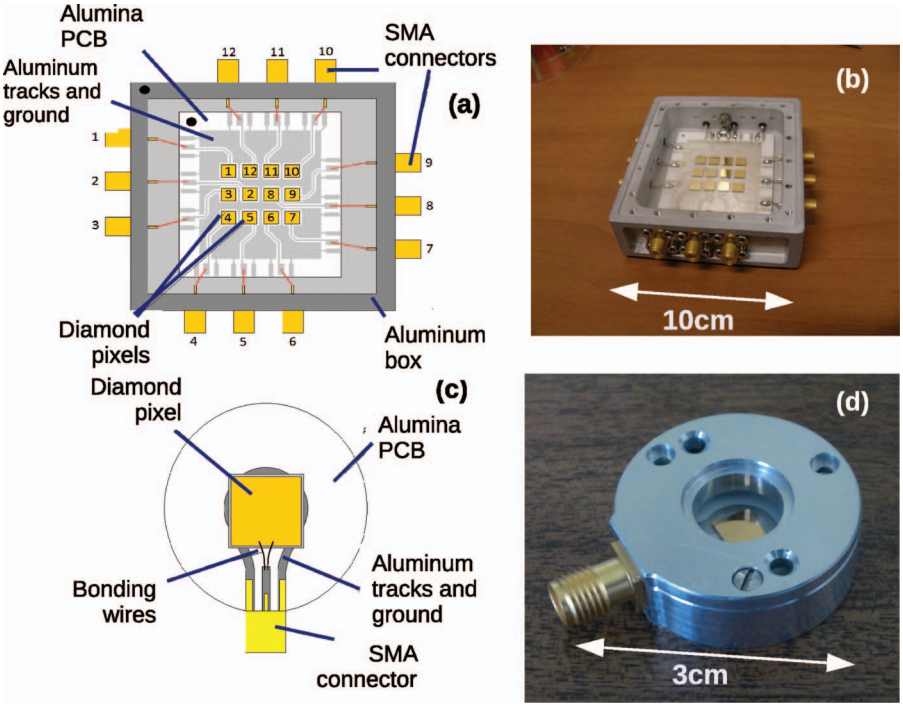

FIG. 1. On the top, layout (a) and picture (b) of a neutron spectrometer based on a 12 pixel diamond matrix. On the bottom, layout (c) and picture (d) of a single pixel prototype.

a prototype single pixel detector are also presented, focusing in particular on the measured response function and energy resolution.

II. DESIGN AND REALIZATION OF DIAMOND BASED NEUTRON SPECTROMETERS

A single SDD pixel prototype and a 12 pixel matrix were designed as neutron spectrometers and built at the CNR-ISM institute in Rome (Italy) based on the experience of X-ray detectors and dosimeters[26–32] (see Fig. 1). The single pixel SDD was completed and neutron measurement results are presented hereby. At the time of the writing of this paper the 12 pixels matrix is being assembled and will be evaluated with laboratory tests. Each pixel is made of a single-crystal "electronic grade" diamond sample (4.5×4.5 mm^2, 500 μm-thick, with boron concentration [B] <5 ppb, and nitrogen concentration [N] <1 ppb), provided by Element Six Ltd.[33] Aimed at removing any organic and metallic impurity, each sample was cleaned for 30 s in a boiling mixture (1:1:1) of nitric, sulfuric, and perchloric acid, then rinsed in deionized water. Ultrasound sonication was also used for debris removal. Ohmic contacts were obtained on top and bottom surfaces of the samples by subsequent sputtering depositions of a multilayer metal structure (patent pending), followed by a final gold layer deposition, in order to improve weldability with microwires. Aimed at maximizing contact homogeneity between pixels, the diamond samples were metalized all together in two sessions (one for the top and one for the bottom surfaces).

A dedicated 1 mm-thick alumina Printed Circuit Board (PCB) was designed and fabricated for the 12 pixel matrix. The bottom surfaces of the diamond samples were glued with a thin layer of conductive silver paste on their respective pixel pad, whereas top surfaces were wire-bonded (by means of 25 μm thick Al/Si wires) on the ground plane. In order to reduce cross-talk effects, the ground plane surrounds completely each pixel pad, as well as each signal track. All the pads and signal tracks, as well as the ground plane, are aluminum-made, aimed at minimizing metal activation by neutrons. The alumina PCB is housed inside a properly designed and developed aluminum metal case, equipped with 12 SMA (SubMiniature version A) connectors for pixel biasing and signal collecting.

Signals from each pixel are amplified by a fast charge preamplifier CIVIDEC C6, which is a low-noise charge amplifier with a rise time of 3.5 ns and a Gaussian pulse shape with a FWHM of 10 ns.[34] Fast electronics is needed in order to allow for high rate measurements by reducing the pile-up probability. On the other hand, electronics with fast signals (tens of ns) feature worst energy resolution with respect to conventional spectroscopic preamplifiers with typically decay time in the range 50–500 μs. As a matter of fact, due to the large number of electron-hole pairs produced by MeV particles with a 5.5 eV band-gap (about 10^6), we can state that the finite energy resolution of the SDD is entirely dominated by the electronics, with no contribution from Poisson statistics. CIVIDEC C6 was selected among other commercial and custom made preamplifiers, giving an energy resolution of 1.9% (FWHM) for 5.5 MeV alpha particles in vacuum.

III. MEASUREMENTS OF 14 MeV NEUTRONS AT THE FRASCATI NEUTRON GENERATOR

Measurements of the response of the SDD single pixel prototype to 14 MeV neutrons were carried out at the Frascati Neutron Generator (FNG).[35] FNG accelerates deuterium ions

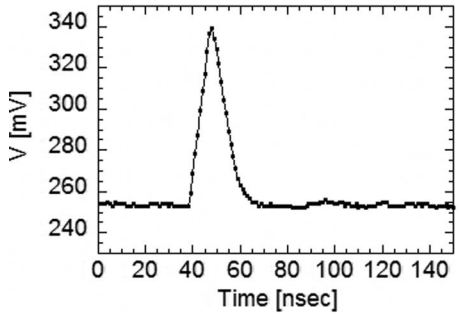

FIG. 2. Pulse of a 14 MeV neutron recorded by a 10 bit/1 GS/s digitizer.

at 300 keV onto a tritiated-titanium target containing about 37 $\times$ 10^{10} Bq of tritium. The detector was mounted at 90° with respect to the incoming deuterium beam. At this position the mono-energetic DT neutrons do not have any energy shift due to the kinematics, and their spectrum has the minimum broadening, corresponding to about 1%. The detector was placed at a distance of 25 cm from the target, providing a neutron flux of about 10^6 n cm^{-2} s^{-1}. The CIVIDEC C6 preamplifier was connected to the detector through a 15 cm long low capacity cable. A four channel, 1 GS/s-10 bit CAEN waveform digitizer model DT5751 was used to record the signals.[36] A typical neutron signal measured at FNG is shown in Fig. 2. One can notice that its full duration is below 30 ns. Digitized signals were analyzed *off-line* by integrating their area (a dedicated algorithm with baseline subtraction was used) and the deposited energy spectra built.

The deposited energy spectrum shown in Fig. 3 integrates 780 s of measurement. Starting from high deposited energy, it is possible to see the ^{12}C(n,α)^{9}Be peak, the ^{12}C(n,n′)3α shoulder and the scattering continuum. The (n,α) peak has a measured energy broadening of 2.7% FWHM. The energy resolution of the detector is therefore estimated to be 2.5% (FWHM), considering the 1% intrinsic broadening of the FNG DT spectrum. A zoom in log scale at higher deposited energies (7 MeV $<$ E_d $<$ 14 MeV) shows the presence of ^{13}C(n,α)^{10}Be peak. The intensity of this peak is 0.3% with respect to the ^{12}C(n,α)^{9}Be peak. This is due to the fact that ^{13}C is only 1.1% of the natural carbon and the cross section is about 1/3 (22 mb vs. 62 mb).[37] The continuous background at E_d $>$ 8.5 MeV can be due also to neutron interaction with other elements present into the contacts. These events with deposited energy above the ^{12}C(n,α)^{9}Be peak set the instrument sensitivity for diagnostics of energetic ion population in the fusion plasma to about 10^{-2} level with respect to the main bulk emission.

Another important feature for a neutron detector for diagnostics of fusion plasmas is the capability of discriminating direct from scattered neutron. An improvement in the scattered to direct neutron ratio would enhance the imaging capability of a neutron camera system, and ease the interpretation and analysis of neutron calibrations in a tokamak. For DT neutron a straightforward possibility is to have an high energy threshold below the (n,α) peak. It was found that the measured (n,α) counts in the range 7 MeV $<$ E_d $<$ 10 MeV are 9.5% with respect to all the counts from other reaction channels (1.5 MeV $<$ E_d $<$ 7 MeV).

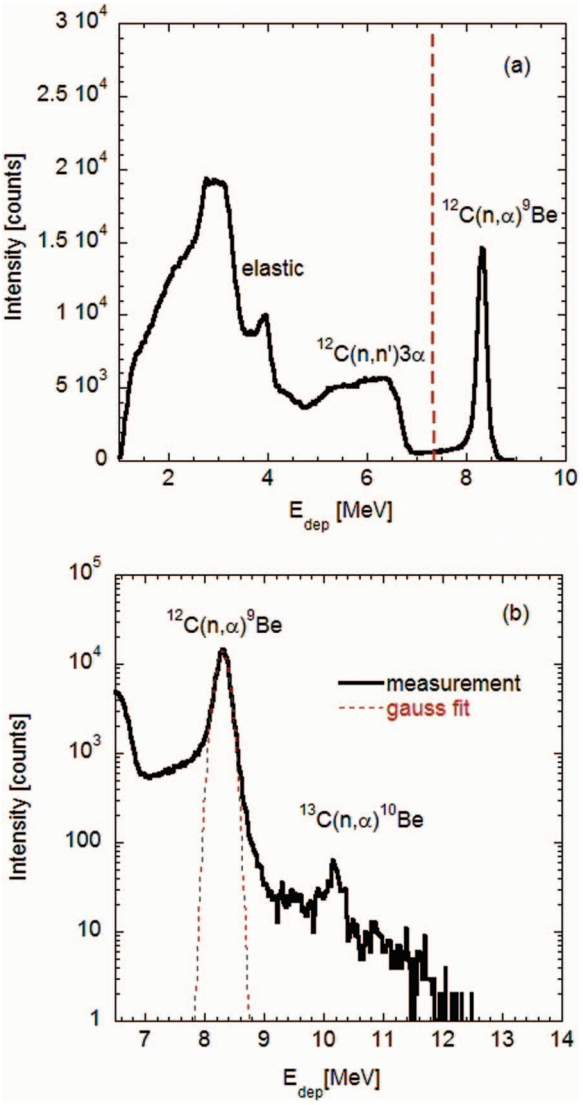

FIG. 3. Deposited energy spectrum of mono-energetic 14 MeV neutrons (a). The dashed vertical line is the energy threshold applied to count only events of the (n,α) peak. The same spectrum for 7 MeV $<$ E_d $<$ 14 MeV is shown in log scale with a Gaussian fit to the (n,α) peak (b).

In Fig. 4, the counting time trace of the SDD is compared to the standard monitor of the FNG.[35] Here, errors on the diamond measurements are due to the Poisson counting statistics and not shown because of the same magnitude of the

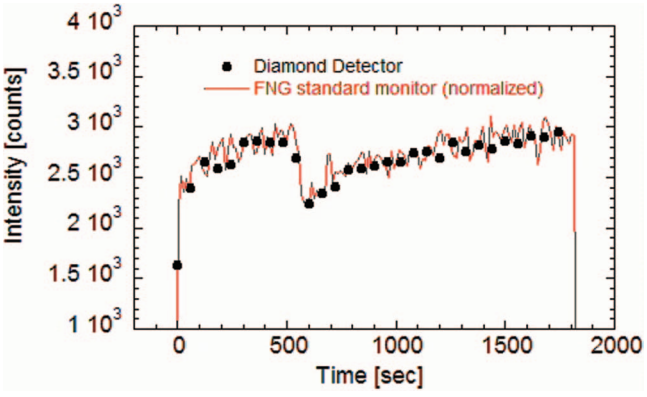

FIG. 4. Counting time trace of a diamond detector compared with the standard monitor of the FNG.

black dots. It is possible to notice the good agreement of the two traces. No instability effects were observed during these 14 MeV neutron irradiation measurements, which is a good indication for a straightforward use of a SDD for neutron emission diagnostics.

IV. CONCLUSIONS

Two SDD based neutron spectrometers (a single pixel and a 12-pixel matrix) have been designed and built for DT neutron emission measurements of fusion plasma experiments. The response of the single pixel SDD to 14 MeV was measured at FNG. Measurements showed a 2.5% energy resolution using fast electronics, optimized for high counting rates, featuring a total signal length below 30 ns. Details of the response function to 14 MeV neutrons have been studied, with focus on the $^{12}C(n,\alpha)^{9}Be$ peak, which is of interest for energetic ions studies in a fusion plasma. The detector response was stable during the irradiation time, without showing any instability effect. The 12 pixel SDD matrix, after characterization, will be installed at the JET tokamak for neutron spectroscopy measurements during the future DT campaign.

[1]H. Sjöstrand *et al.*, Rev. Sci. Instrum. **77**(10), 10E717 (2006).
[2]M. Gatu Johnson *et al.*, Rev. Sci. Instrum. **77**(10), 10E702 (2006).
[3]X. Zhang *et al.*, Rev. Sci. Instrum. **85**, 043503 (2014).
[4]A. Pietropaolo *et al.*, EPL **92**(6), 68003 (2010).
[5]L. Giacomelli *et al.*, Nucl. Phys. B, Proc. Suppl. **215**, 242–246 (2011).
[6]M. Rebai *et al.*, Nucl. Phys. B, Proc. Suppl. **215**, 313–315 (2011).
[7]A. Pietropaolo *et al.*, EPL **94**(6), 62001 (2011).
[8]M. Rebai *et al.*, J. Instrum. **7**(5), C05015 (2012).
[9]M. Pillon *et al.*, Nucl. Instrum. Methods Phys. Res., Sect. A **640**(1), 185–191 (2011).
[10]M. Rebai *et al.*, J. Instrum. **8**(10), P10007 (2013).
[11]L. Giacomelli *et al.*, Nucl. Instrum. Methods Phys. Res., Sect. A **720**, 125–127 (2013).
[12]Cross section database, see http://www.nndc.bnl.gov/.
[13]W. R. Faust and E. G. Harris, Nucl. Fusion **1**, 62 (1960).
[14]M. Nocente *et al.*, Nucl. Fusion **51**, 063011 (2011).
[15]Z. Chen *et al.*, Nucl. Fusion **53**, 063023 (2013).
[16]M. Nocente *et al.*, Nucl. Fusion **50**, 055001 (2010).
[17]M. Nocente *et al.*, Nucl. Fusion **53**, 053010 (2013).
[18]C. Hellesen *et al.*, Nucl. Fusion **53**, 113009 (2013).
[19]M. Tardocchi *et al.*, Plasma Phys. Controlled Fusion **55**, 074014 (2013).
[20]C. Hellesen *et al.*, Nucl. Fusion **50**, 084006 (2010).
[21]M. Gatu Johnson *et al.*, Nucl. Fusion **50**, 045005 (2010).
[22]A. Krasilnikov *et al.*, Rev. Sci. Instrum. **68**(1), 553–556 (1997).
[23]M. Pillon *et al.*, Nucl. Instrum. Methods Phys. Res., Sect. B **101**(4), 473–483 (1995).
[24]M. Angelone *et al.*, Rev. Sci. Instrum. **76**(1), 013506 (2005).
[25]C. Cazzaniga *et al.*, Rev. Sci. Instrum. **85**, 043506 (2014).
[26]D. M. Trucchi *et al.*, IEEE Electron Device Lett. **33**, 615–617 (2012).
[27]M. Girolami *et al.*, IEEE Electron Device Lett. **33**, 224–226 (2012).
[28]A. Bellucci *et al.*, IEEE Electron Device Lett. **34**, 695–697 (2013).
[29]M. Girolami *et al.*, Appl. Phys. Lett. **103**, 083502 (2013).
[30]D. M. Trucchi *et al.*, Diamond Relat. Mater. **14**, 575–579 (2005).
[31]G. Conte *et al.*, J. Appl. Phys. **93**, 6078–6083 (2003).
[32]G. Conte *et al.*, Phys. Status Solidi A **201**, 249–252 (2004).
[33]Element Six Ltd, see http://www.e6.com.
[34]CIVIDEC, see http://www.cividec.at.
[35]M. Martone *et al.*, J. Nucl. Mater. **212–215**, 1661–1664 (1994).
[36]CAEN, see http://www.caen.it.
[37]F. Sudbrock *et al.*, Radiochim. Acta **88**, 829–832 (2000).

Paper II

Single crystal diamond detector measurements of deuterium-deuterium and deuterium-tritium neutrons in Joint European Torus fusion plasmas

C. Cazzaniga,[1,2,a)] E. Andersson Sundén,[3] F. Binda,[3] G. Croci,[2] G. Ericsson,[3] L. Giacomelli,[1] G. Gorini,[1,2] E. Griesmayer,[4] G. Grosso,[2] G. Kaveney,[5] M. Nocente,[1,2] E. Perelli Cippo,[2] M. Rebai,[1] B. Syme,[5] M. Tardocchi,[2] and JET-EFDA Contributors[b)]
JET-EFDA, Culham Science Centre, Abingdon OX14 3DB, United Kingdom
[1]*Department of Physics "G. Occhialini," University of Milano Bicocca, Piazza della Scienza 3, Milano, Italy*
[2]*Istituto di Fisica del Plasma, Associazione EURATOM-ENEA-CNR, via Roberto Cozzi 53, Milano, Italy*
[3]*Department of Physics and Astronomy, EURATOM-VR Association, Uppsala University, Uppsala, Sweden*
[4]*Atominstitut, Vienna University of Technology, Austria*
[5]*Culham Centre for Fusion Energy, Culham OX143DB, United Kingdom*

(Received 31 January 2014; accepted 23 March 2014; published online 11 April 2014)

First simultaneous measurements of deuterium-deuterium (DD) and deuterium-tritium neutrons from deuterium plasmas using a Single crystal Diamond Detector are presented in this paper. The measurements were performed at JET with a dedicated electronic chain that combined high count rate capabilities and high energy resolution. The deposited energy spectrum from DD neutrons was successfully reproduced by means of Monte Carlo calculations of the detector response function and simulations of neutron emission from the plasma, including background contributions. The reported results are of relevance for the development of compact neutron detectors with spectroscopy capabilities for installation in camera systems of present and future high power fusion experiments. [http://dx.doi.org/10.1063/1.4870584]

I. INTRODUCTION

Single crystal Diamond Detectors (SDDs) are artificially produced by chemical vapor deposition.[1] In recent years they have been successfully used for fast neutron measurements in the MeV range mostly at spallation sources,[2–5] where spectral measurements were demonstrated in time of flight experiments. SDDs are interesting candidates also for measurements of the 2.5 MeV and 14 MeV neutron energy spectrum from fusion plasmas of tokamak experiments, particularly in next step devices, such as ITER. Here, advantage can be taken of the high neutron fluxes (10^9 n cm^{-2} s^{-1}), which enable measurements at high counting rates (MHz) and, thus, temporal resolution (a few ms). Besides, the compact dimensions and radiation resistance of SDDs make them particularly interesting as detectors for camera systems with spectroscopy capabilities, thanks to their high energy resolution (≈2% at 5 MeV).

As far as neutron spectroscopy applications of SDDs are concerned, a distinction must be made between neutrons of energy below and above 6 MeV, due to the different response function of the instrument in these energy ranges. Above 6 MeV, neutron spectroscopy is enabled by the ^{12}C(n,α)^{9}Be reaction (energy threshold: 6.17 MeV) between the incoming neutrons and carbon nuclei of the diamond crystal. The α particle energy is deposited in the device and results in a peak, whose mean position and shape depend on the incoming neutron energies. For example, 14 MeV neutrons from deuterium-tritium (DT) plasmas would be manifested as a peak at mean energy $E_0 = 8.5$ MeV with width proportional to the square root of the plasma temperature T.[6] Measurements of 14 MeV neutrons were performed in tokamak experiments with DT plasmas using natural diamond detectors and are reported in Refs. 7–9.

For neutron energies below 6 MeV, instead, the ^{12}C(n,α)^{9}Be reaction is forbidden by kinematics and the main reaction channel is neutron elastic scattering on ^{12}C nuclei. The ^{12}C recoil nuclei are stopped in the detector and, for a monochromatic neutron beam, their spectrum appears as a continuous distribution ending at the maximum recoil energy transferred to ^{12}C, which is proportional to the incoming neutron energy. Measurements of the SDD response in this energy range, as well as for $E_n > 6$ MeV, were performed at accelerator facilities and are reported in the literature.[10–12] The simultaneous detection of 2.5 and 14 MeV neutrons from a fusion plasma using a lithium coated SDD is reported in Ref. 13. In this experiment, the detection efficiency of the device was boosted by the ^{6}Li(n,α)T reaction in the coating which, however, resulted in a loss of spectroscopy information on 2.5 MeV neutrons.

In this work we present the first simultaneous spectroscopy measurements of 2.5 and 14 MeV neutrons from a deuterium-deuterium (DD) fusion plasma in a tokamak environment using a bare SDD. The measurements were performed at JET with a fast acquisition chain optimized for high rate applications and are interpreted in terms of components of the neutron emission spectrum together with the simulated SDD response function. Advantages of SDDs over other techniques based on compact detectors for neutron measurements in tokamak experiments are finally illustrated.

a)carlo.cazzaniga@mib.infn.it
b)See the Appendix of F. Romanelli *et al.*, Proceedings of the 24th IAEA Fusion Energy Conference 2012, San Diego, USA.

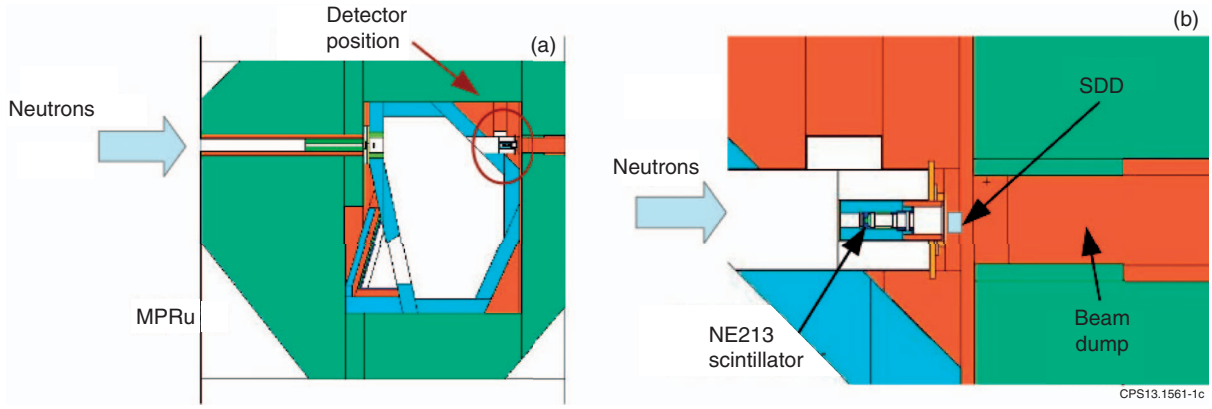

FIG. 1. (a) Schematics of the SDD detector arrangement inside the radiation shielding of MPRu spectrometer. The direction of the neutrons produced by the plasma is indicated by the arrow. (b) Zoom of the detector position in front of the MPRu beam dump.

II. EXPERIMENTAL SETUP

An artificially grown SDD was installed in the JET Torus Hall on a collimated Line of Sight (LoS) shared with other neutron diagnostics, the MPRu proton-recoil neutron spectrometer and the NE213 scintillator.[14–17] Fig. 1 shows the position of the detector inside the MPRu radiation shielding as in the MCNP model[18] used for the calculations presented in Sec. IV. The installed diamond detector had a nominal active volume of the 4.7 × 4.7 mm^2 (surface area) × 0.5 mm (thickness) with 4.5 mm diameter aluminium electrical contacts.

Two separate read-out electronic chains (see Fig. 2) were developed to measure, at the same time, DD (2.5 MeV) and DT (14 MeV) neutrons. This was needed since the energy deposition for DD neutrons, due to carbon recoil, is about 20 times less than the energy deposition of DT neutrons via the (n,α) reaction. Both chains shared a fast charge preamplifier CIVIDEC c6[22] as a first amplification stage. The latter was placed about 20 cm away from the diamond detector, without intercepting the neutron beam. A 120 meter BNC cable was laid down from the preamplifier to the JET Diagnostic Hall, where signals from the diamond detector were recorded. The signal FWHM from an α-particle of the calibration source, measured after the long BNC cable, was 20 ns (see Fig. 3(a)). For 2.5 MeV neutron measurements a second amplification stage, consisting of a 20 dB current amplifier CIVIDEC c1,[22] was installed right after the first preamplifier in the Torus Hall. Fig. 3(b) shows the signal from 2.5 MeV neutrons after the second amplification stage. Clearly, there is a worse signal-to-noise ratio compared to the pulse from the calibration source of Fig. 3(a), but the FWHM of the signal is still about 20 ns, which shows that the current amplifier did not introduce any significant shaping that could alter the fast temporal properties of the signal. Preserving fast signals is essential in view of high rate measurements in the JET DT campaign.

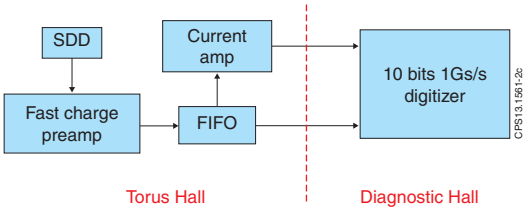

FIG. 2. Schematics of the read-out electronics used for SDD measurements at JET.

A four channel, 1 GHz, 10 bit CAEN waveform digitizer model DT5751 (input range: 0–1 V) was used to record the signals from both electronic chains in the Diagnostic Hall.[23] The acquisition was triggered by the JET "pre"-signal, that is produced 40 s before each plasma discharge. The Pulse Height Spectrum (PHS) corresponding to each discharge was reconstructed off-line with a software based on a trapezoidal filter algorithm.[24]

A calibration triple-α source (^{241}Am, ^{239}Pu, and ^{244}Cm) was placed in front of the detector, providing a counting rate $<$10 Hz. A typical calibration spectrum, collected in 60 min without neutron emission from the plasma, is shown in Fig. 4. It has to be considered in the calibration a calculated energy loss in air of 0.39 MeV. An energy resolution (FWHM/E) of 2.2% can be measured at 5.2 MeV. This value is acceptable for fusion spectroscopy applications, as it is smaller than the kinematic broadening of the thermal emission peak from DT plasmas (between 2% and 10% for plasma temperatures in the range 3–10 keV [6]). For 2.5 MeV neutron measurements, which correspond to a maximum of 0.8 MeV of deposited Energy, the energy resolution of the SDD is assumed to be 8%. This value was extrapolated from the resolution determined experimentally using a ^{137}Cs γ-ray source.

III. NEUTRON MEASUREMENTS ON JET DEUTERIUM PLASMAS

Neutron measurements (2.5 MeV) have been performed in deuterium plasmas from July 2013 during the JET C31 campaign. A clear evidence that the signals measured by the SDD detector were due to fusion neutrons was obtained by comparing the counts measured by the SDD with the neutron yield observed by the standard JET neutron diagnostics. The result is shown in Fig. 5, where each data point represents an individual discharge performed on 13 August 2013. The SDD measurements had a low energy threshold

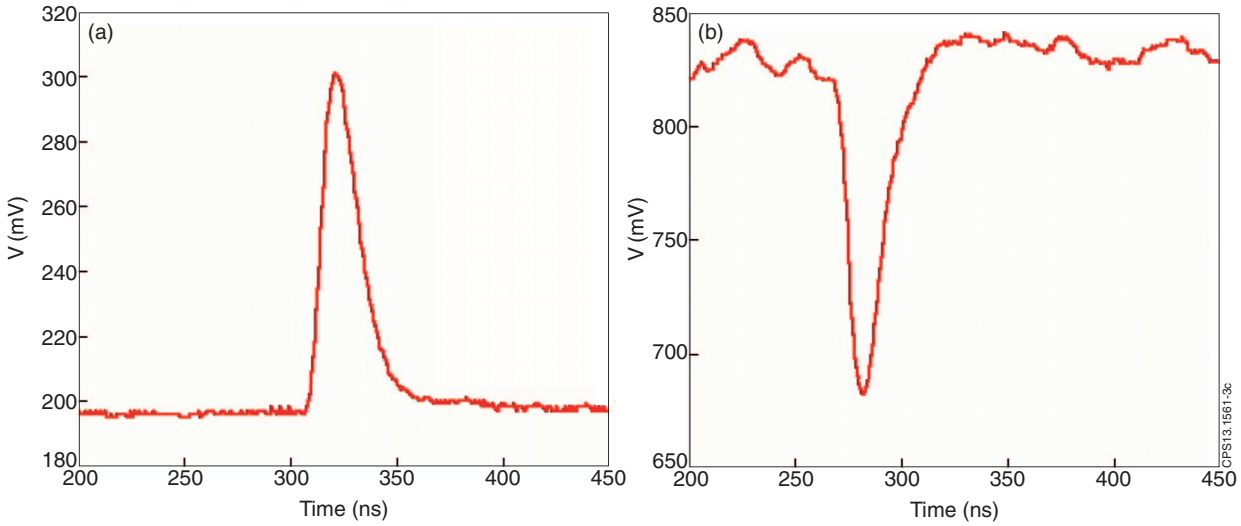

FIG. 3. Signals from an α particle of the calibration source after the BNC cable in the Diagnostic Hall (a) and from a 2.5 MeV neutron after the second amplification stage (see text for details) (b).

corresponding to a deposited energy $E_d = 0.3$ MeV and are shown in the figure versus the total neutron yield measured by the JET fission chamber diagnostics.[25] There is clear linear correlation between the two set of data (correlation coefficient $R^2 = 0.9988$) with a proportionality constant of 4.5×10^{-13}. This small value results from the combined contribution of neutron transport from the plasma to the detector position and of the detector efficiency, which can be calculated to be about 1.4% for 2.45 MeV neutrons, based on the $n+^{12}C$ nuclear elastic scattering cross sections.[26] A comparison between the counts recorded by SDD and a NE213 liquid scintillator (active volume 1 $cm^2 \times 1$ cm) placed in front of the SDD along the same LOS (see Figure 1) is presented in Fig. 5(b) for the same set of discharges of Fig. 5(a). Again, we find a very good correlation between the two set of data ($R^2 = 0.9986$). The NE213/SDD efficiency ratio, derived from a linear fit to the data, is about 50/1.

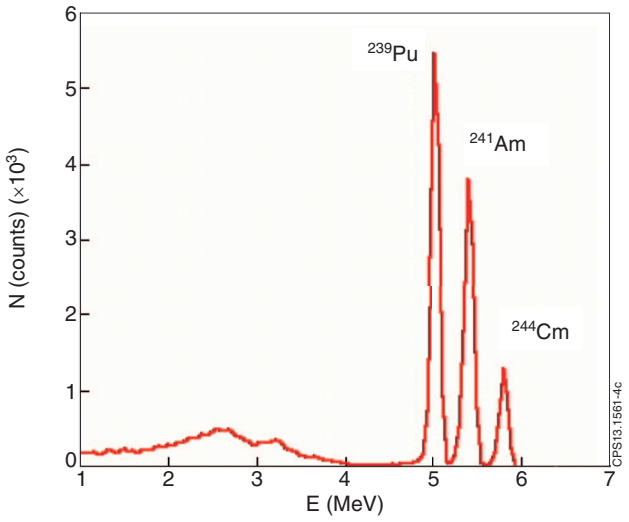

FIG. 4. Energy spectrum of a calibration triple-α source measured with the SDD in the final setup at JET.

The neutron emission time trace measured by SDD is compared with that from the JET fission chambers for a specific JET discharge (#84476) in Fig. 6. The latter is a discharge with average Neutral Beam Injection (NBI) power of about 15 MW. Data for SDD are shown every 0.5 s to mitigate the statistical fluctuations arising from the low (a few hundred Hz) counting rates observed in deuterium plasmas at the detector location. The good agreement between the two set of data confirms the validity of the SDD measurements.

We now move to the analysis of the measured PHS from DD neutrons. This is shown for a single JET discharge (#84476) in Fig 7(a) and for 45 similar discharges in Fig. 7(b) as a function of the charged particle energy released in the detector E_d. All these experiments were deuterium plasmas with NBI power from 12 MW to 20 MW. Qualitatively, the PHS has the characteristic box shape expected from the energy distribution of the ^{12}C recoil ions. The shoulder of the PHS is at 0.69 MeV, which correctly corresponds to the maximum energy deposited by back-scattering of 2.5 MeV neutrons on Carbon.[27] The broadening of the edge is due to the combined contribution of the finite detector energy resolution and of Doppler broadening from plasma kinematics (see Sec. IV).

It can be noted here that a deuterium plasma offers the opportunity to also perform measurements of 14 MeV neutrons. These come from the burn up of tritons on deuterium. Tritons are in turn produced by the $d + d \rightarrow p + t$ reaction, which has about the same cross section as $d + d \rightarrow n + {}^3He$. At JET, the 14 MeV, Triton Burn up Neutron emission (TBN) in deuterium plasmas is estimated to be about 1% of that at 2.5 MeV.[28–30] In order to observe TBN emission we have summed all discharges performed at JET during more than 1 month of operations with the result shown in Fig. 8. The 14 MeV TBN emission is manifested by the appearance of the (n,α) peak which, as stated in the introduction, is the dominant neutron interaction channel for $E_n > 6.2$ MeV. The significant width of the peak (about 2 MeV FWHM) reflects the triton slowing down distribution and is in good agreement

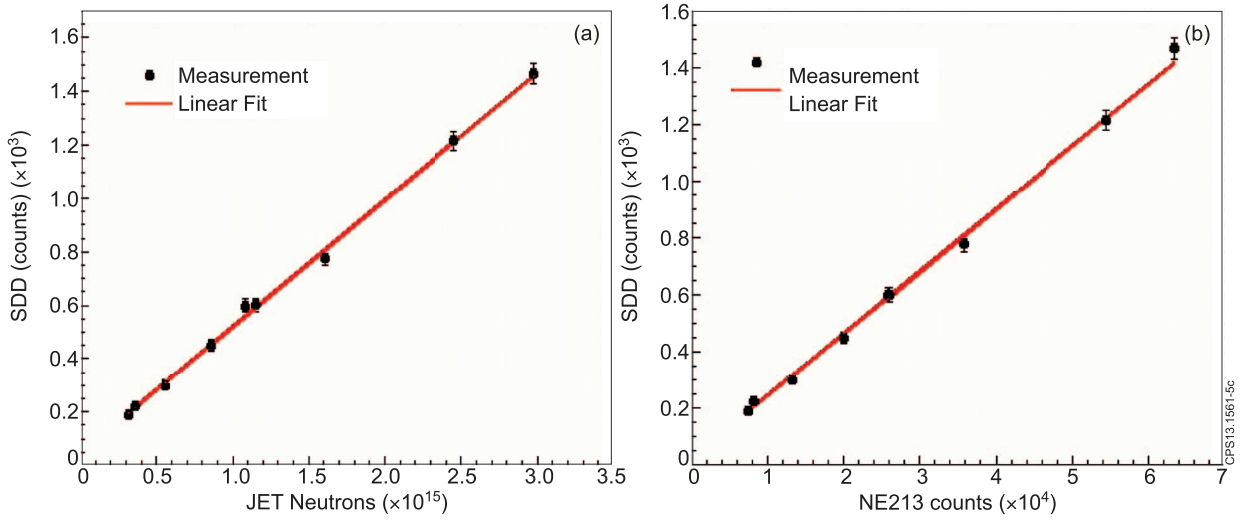

FIG. 5. (a) Neutron counts measured by SDD versus the JET total neutron yield as derived from fission chambers. Each point corresponds to an individual discharge. (b) Neutron counts measured by SDD and by a NE213 liquid scintillator along the same line of sight.

with calculations for JET (see Figure 7 of Ref. 29). The fit is obtained by comparison of a Gaussian function in terms of Cash statistics.[31] It can be noted that a shoulder appears for $E_d < 8$ MeV; this continuous is due to the $^{12}C(n,n)3\alpha$ reaction, as it is discussed in more details in Ref. 11.

IV. QUANTITATIVE ANALYSIS OF THE DEPOSITED ENERGY SPECTRUM

The measured PHS can be analyzed to separate different neutron emission components from the plasma. To this end, one must first determine the background due to the calibration source. This was measured, without plasma emission, for about 130 min with the results shown in Fig. 9.

A MCNP model[18] was developed to simulate the detector response function to mono-energetic neutrons up to 4 MeV with an energy step of 100 keV. The model geometry consisted of the bare diamond volume and aluminum contacts.

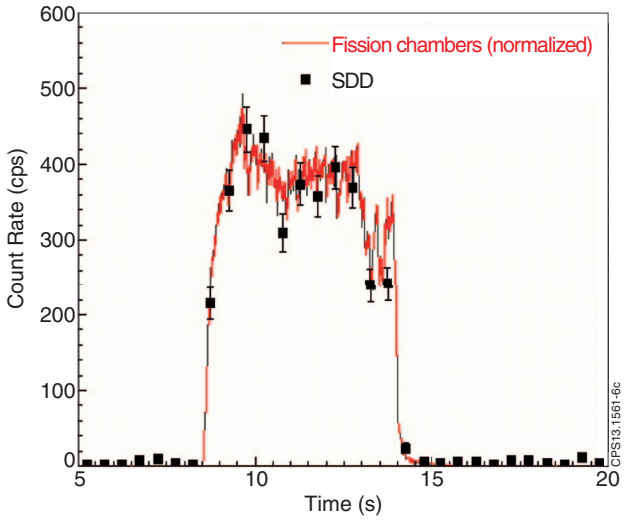

FIG. 6. Time trace of neutron emission measured by SDD and by the JET fission chambers for discharge #84476.

Mono-energetic neutrons at different energies were generated and impinged on the front part of the detector. The same geometry was used to simulate the response to background γ-rays (see below). The resulting response function was convoluted with simulations of increasing complexity of the neutron emission spectrum from the plasma for comparison with measurements, as shown in Fig. 10. As a first step, we assumed the neutron spectrum to uniquely consist of mono-energetic neutrons at E = 2.45 MeV (green dashed curve). This however provided an unsatisfactory description of the measured PHS, both in the flat region corresponding to low recoil energies and for the high energy shoulder.

As a second step, we used a more detailed model for neutron emission from NBI heated plasmas. In this model, neutron emission is described in terms of three components: the thermal, that arises from reaction within the thermal (Maxwellian) plasma population; the beam-plasma, which originates from beam ions reacting with thermal ions; and the beam-beam, that is due to fusion reactions among deuterons of the beam. All of these components were calculated with the Monte Carlo code GENESIS, which can determine the neutron and γ-ray emission spectrum from the plasma using as input the reactant distribution functions.[32–35] A half-box model was adopted to represent the beam population.[36] The output from GENESIS was in turn validated by comparison with measurements from the TOFOR neutron spectrometer for a few discharges.[19–21]

As the summed spectrum of Figure 10 included plasmas with different NBI injection energies (ranging from 80 keV to 120 keV), separate simulations were correspondingly performed and then combined with weights proportional to the actual NBI power mix used in the experiments. The finite energy resolution of the SDD was taken into account by convolution with a Gaussian of FWHM = 8%. This value was extrapolated from the resolution determined experimentally using a ^{137}Cs γ-ray source. The result of the fit is shown by the red curve in Fig. 10. The high energy shoulder is now well described, but there is a significant excess of data in the low

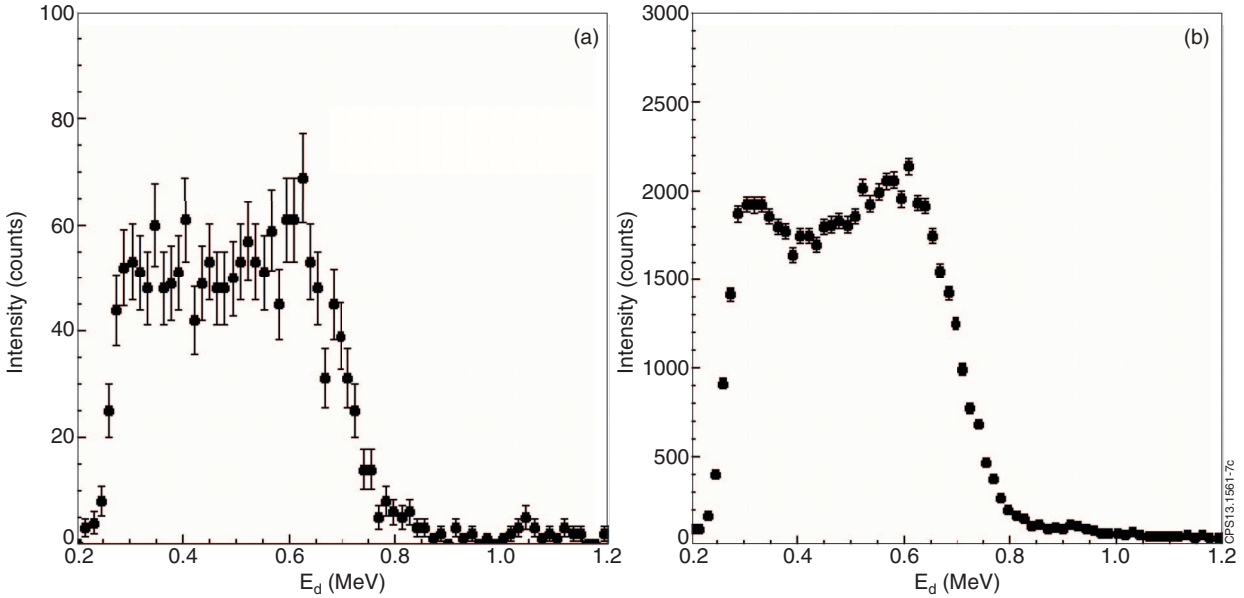

FIG. 7. (a) Pulse height spectrum from DD fusion neutrons measured by SDD in discharge #84476 at JET, as a function of the charged particle energy released in the detector E_d. (b) Pulse height spectrum from the sum of 45 similar JET discharges.

energy part of the spectrum that is not accounted for by the simulation.

This discrepancy can be solved by considering the background contributions from γ-rays and scattered neutrons to the measured spectrum. To this end, the MCNP model for MPRu (Fig. 1) was used to calculate γ-ray production in the beam dump and the scattering of the incoming neutrons along the MPRu line of sight. The contributions of these two background sources are shown in Figure 11 in linear and log scale. Neutron scattering results in an excess of low energy neutrons that show up as a component of significant intensity up to $E_d = 0.5$ MeV, with a rapid fall off at higher energies. Gamma-ray induced events in the SDD have a clear exponential shape.

The complete description of the measured data (solid line of Fig. 11) thus included four contributions: (1) a primary component due to d+d neutrons emitted from the plasma and that reach the detector, as in Fig. 10; (2) scattered neutrons and (3) γ-rays produced by the interaction of the primary neutrons with the MPRu LoS; (4) background events from the triple-α calibration source, normalized to measurement time. Two normalization parameters only were determined by the fit, namely the absolute intensity of the primary neutron component and the amount of scattered neutrons. The scattered neutron/background γ-ray ratio was constrained to the value found by MCNP and confirmed by the NE213 measurements, which can distinguish signals from neutrons and γ-rays from their different pulse shapes. This allows for minimizing the number of free parameters in the fit. The background intensity from the triple-α source was known independently

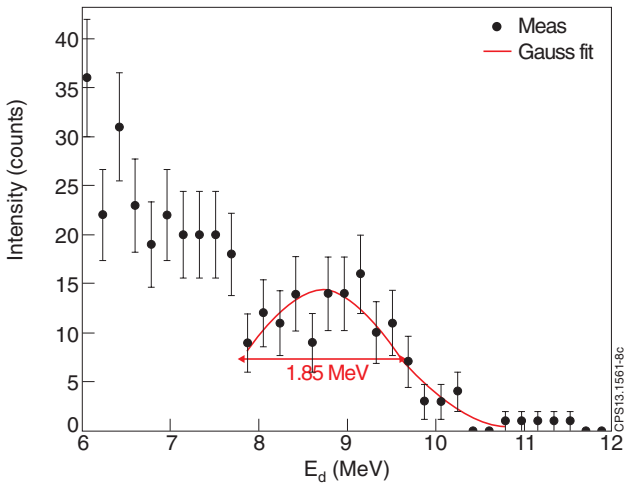

FIG. 8. Measured pulse height spectrum from triton burn up neutrons in deuterium plasmas at JET. Data from all discharges during 1 month of operations at JET were summed. The FWHM of the (n,α) peak is indicated in the figure.

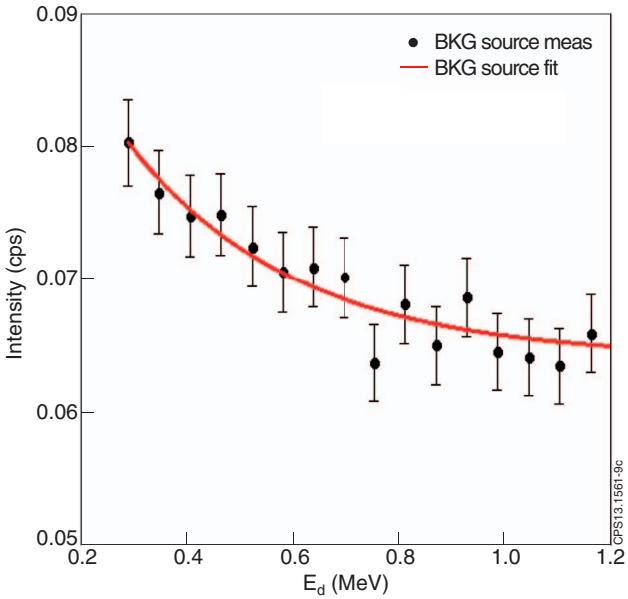

FIG. 9. Background energy spectrum due to the calibration source normalized to the measurement time.

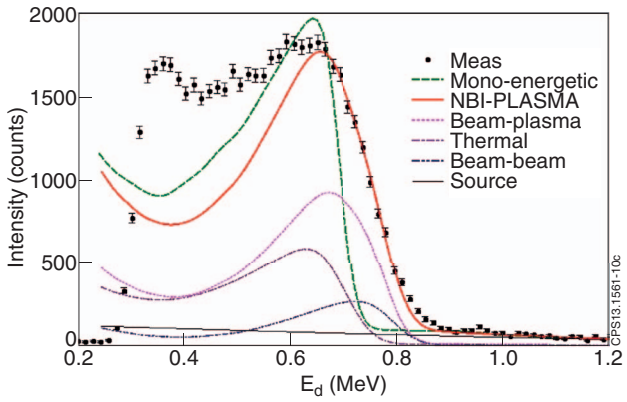

FIG. 10. Measured SDD pulse height spectrum compared to simulations of the expected signal from different neutron emission models. The green dashed curve corresponds to mono-energetic neutrons at E = 2.45 MeV. The solid red curve is instead the result of a neutron emission model for NBI injection, which includes thermal (pink dotted), beam-plasma (violet dotted), and beam-beam (blue dotted) reactions (see text for details). The background counting level from the triple-α calibration source is normalized to the measurement time.

from a separate measurement and re-scaled to the actual measurement time during the plasma discharges. With all four components included, we find a good agreement between measurements and data. In particular, neutron scattering amounts to 35% of the total, with background γ-rays contributing to about 20%. The contribution of the background components is mostly at low energies (say, $E_d < 0.5$ MeV) negligible in the shoulder of the PHS, whose shape is completely determined by direct (primary) d+d neutrons.

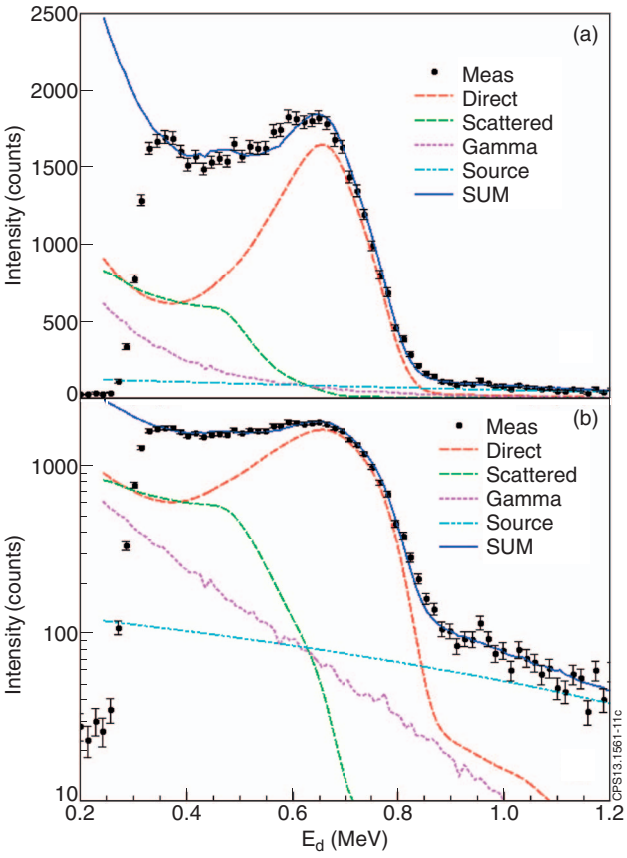

FIG. 11. Measured PHS spectrum from a set of NBI plasmas as compared to simulations in linear (a) and logarithmic (b) scale. The simulated spectrum is the sum of four components: (1) a primary component due to d + d neutrons emitted from the plasma and that reach the detector; (2) scattered neutrons and (3) γ-rays produced by the interaction of the primary neutrons with the MPRu LoS; and (4) background events from the calibration source, normalized to measurement time.

V. DISCUSSION AND OUTLOOK

Artificial diamonds can play a role as compact neutron detectors with spectroscopy capabilities for fusion applications, together with other devices such as NE213 scintillators.[37–39] Compact detectors are of importance for use in camera systems of a burning plasma experiment, where there is limited space for implementation of more complex devices such as dedicated spectrometers for 2.5 and 14 MeV neutrons.[14,19] A few points may be raised here to point out advantages and disadvantages of diamond detectors, also in comparison with NE213 scintillator and with reference to DD and DT experiments:

(i) Both SDD and NE213 feature compact dimensions and high rate capability. The difference in efficiency, which is set by the material volumes commercially available, makes them complementary depending on expected neutron fluxes. The efficiency of SDD can be increased by using a matrix of detectors.

(ii) The SDD does not suffer significant gain drifts at high counting rates[12,40] and strong magnetic fields. These could instead be of major concerns for a scintillator.

(iii) NE213 allows for n-γ pulse shape discrimination[41,42] which is not possible with a SDD, that, nevertheless, is fairly insensitive to γ-rays, as demonstrated by these measurements. Besides, γ-ray events mostly concentrate in the low energy part of the spectrum and can thus be discriminated by setting a proper low energy threshold in the PHS.

(iv) In deuterium plasmas, SDD allows for a good discrimination of direct (primary) and scattered neutrons. For example, setting an energy threshold at $E_d = 0.5$ MeV (see Fig. 11), would reduce the scattered neutron contribution to only 10% of the direct one. Such improvement in the scattered to direct neutron ratio would enhance the imaging capability of a neutron camera system, and ease the interpretation and analysis of neutron calibrations in a tokamak.

(v) In DT plasmas, SDD could allow obtaining spectroscopy information from the peak shape of the (n,α) reaction, providing detailed information on the fuel ion energy distributions. This information could be used for fast ion studies, as demonstrated so far in present tokamaks with dedicated high resolution spectrometers such as MPRu and TOFOR.[43–46] Adding spectroscopy information to a neutron camera system by means of compact detectors would allow for spatially resolved measurements of the fast ion energy distribution in a high performance device.

VI. CONCLUSIONS

First measurements of the neutron spectrum from deuterium plasmas using a single crystal diamond detector were

presented in this paper. The data were taken at JET by equipping the detector with a fast electronic chain designed to combine high count rate capabilities (up to the MHz range) and good energy resolution (≈2% at 5 MeV). The observed neutron count rate was successfully correlated to data from other standard neutron rate diagnostics at JET. The deposited energy spectra were measured for both DD and burn-up DT neutrons. Monte Carlo simulations were used to determine the device response function and to interpret the measured pulse height spectrum in terms of components of neutron emission from NBI plasmas, including background contributions. A good agreement was found between calculations and measurements. The results presented here will be the basis for further developments of diamond detectors for neutron diagnostics of JET DD and DT plasmas and in view of burning plasma experiments of the next generation.

ACKNOWLEDGMENTS

This work was supported by EURATOM and carried out within the framework of the European Fusion Development Agreement. The views and opinions expressed herein do not necessarily reflect those of the European Commission.

[1]C. Tuve, M. Angelone, V. Bellini, A. Balducci, M. G. Donato, G. Faggio, M. Marinelli *et al.*, "Single crystal diamond detectors grown by chemical vapor deposition," Nucl. Instrum. Methods Phys. Res., Sect. A **570**(2), 299–302 (2007).
[2]A. Pietropaolo, C. Andreani, M. Rebai, L. Giacomelli, G. Gorini, E. Perelli Cippo, M. Tardocchi *et al.*, "Single-crystal diamond detector for time-resolved measurements of a pulsed fast-neutron beam," EPL **92**(6), 68003 (2010).
[3]A. Pietropaolo, C. Andreani, M. Rebai, L. Giacomelli, G. Gorini, E. Perelli Cippo, M. Tardocchi *et al.*, "Fission diamond detectors for fast-neutron ToF spectroscopy," EPL **94**(6), 62001 (2011).
[4]M. Rebai, C. Andreani, A. Fazzi, C. D. Frost, L. Giacomelli, G. Gorini, E. Milani *et al.*, "Fission diamond detector tests at the ISIS spallation neutron source," Nucl. Phys. B, Proc. Suppl. **215**(1), 313–315 (2011).
[5]M. Rebai, L. Giacomelli, C. Andreani, A. Fazzi, C. D. Frost, E. Perelli Cippo, A. Pietropaolo *et al.*, "Diamond detectors for fast neutron measurements at pulsed spallation sources," J. Instrum. **7**(05), C05015 (2012).
[6]Günther Lehner and Pohl Frank, "Reaktionsneutronen als hilfsmittel der plasmadiagnostik," Z. Phys. **207**(1), 83–104 (1967).
[7]A. V. Krasilnikov, E. A. Azizov, A. L. Roquemore, V. S. Khrunov, and K. M. Young, "TFTR natural diamond detectors based D–T neutron spectrometry system," Rev. Sci. Instrum. **68**(1), 553–556 (1997).
[8]M. Pillon, M. Angelone, and A. V. Krasilnikov, "14 MeV neutron spectra measurements with 4% energy resolution using a type IIa diamond detector," Nucl. Instrum. Methods Phys. Res. B **101**(4), 473–483 (1995)
[9]M. Angelone, M. Pillon, L. Bertalot, F. Orsitto, M. Marinelli, E. Milani, G. Pucella *et al.*, "Time dependent 14MeV neutrons measurement using a polycrystalline chemical vapor deposited diamond detector at the JET tokamak," Rev. Sci. Instrum. **76**(1), 013506 (2005).
[10]A. Zimbal, L. Giacomelli, R. Nolte, and H. Schuhmacher, "Characterization of monoenergetic neutron reference fields with a high resolution diamond detector," Radiat. Meas. **45**(10), 1313–1317 (2010).
[11]M. Pillon, M. Angelone, A. Krása, A. J. M. Plompen, P. Schillebeeckx, and M. L. Sergi, "Experimental response functions of a single-crystal diamond detector for 5–20.5 MeV neutrons," Nucl. Instrum. Methods Phys. Res. A **640**(1), 185–191 (2011).
[12]M. Rebai, A. Milocco, L. Giacomelli, E. Perelli Cippo, M. Tardocchi, A. Fazzi, A. Pietropaolo, and G. Gorini, "Response of a single-crystal diamond detector to fast neutrons," J. Instrum. **8**(10), P10007 (2013).
[13]M. Angelone, D. Lattanzi, M. Pillon, M. Marinelli, E. Milani, A. Tucciarone, G. Verona-Rinati *et al.*, "Development of single crystal diamond neutron detectors and test at JET tokamak," Nucl. Instrum. Methods Phys. Res. A **595**(3), 616–622 (2008).
[14]H. Sjöstrand, L. Giacomelli, E. A. Sundén, S. Conroy, G. Ericsson, M. G. Johnson, C. Hellesen *et al.*, "New MPRu instrument for neutron emission spectroscopy at JET," Rev. Sci. Instrum. **77**(10), 10E717 (2006).
[15]E. Andersson Sundén, H. Sjöstrand, S. Conroy, G. Ericsson, M. Gatu Johnson, L. Giacomelli, C. Hellesen *et al.*, "The thin-foil magnetic proton recoil neutron spectrometer MPRu at JET," Nucl. Instrum. Methods Phys. Res. A **610**(3), 682–699 (2009).
[16]G. Ericsson, L. Ballabio, S. Conroy, J. Frenje, H. Henriksson, A. Hjalmarsson, J. Källne, and M. Tardocchi, "Neutron emission spectroscopy at JET—results from the magnetic proton recoil spectrometer," Rev. Sci. Instrum. **72**(1), 759–766 (2001).
[17]L. Giacomelli, E. Andersson Sundén, S. Conroy, G. Ericsson, M. Gatu Johnson, C. Hellesen, A. Hjalmarsson *et al.*, "Development and characterization of the proton recoil detector for the MPRu neutron spectrometer," Rev. Sci. Instrum. **77**(10), 10E708 (2006).
[18]See http://mcnpx.lanl.gov/ for MCNPX code.
[19]M. G. Johnson, L. Giacomelli, A. Hjalmarsson, M. Weiszflog, E. A. Sundén, S. Conroy, G. Ericsson *et al.*, "The TOFOR neutron spectrometer and its first use at JET," Rev. Sci. Instrum. **77**(10), 10E702 (2006).
[20]A. Hjalmarsson, S. Conroy, G. Ericsson, L. Giacomelli, G. Gorini, H. Henriksson, J. Källne, M. Tardocchi, and M. Weiszflog, "The TOFOR spectrometer for 2.5 MeV neutron measurements at JET," Rev. Sci. Instrum. **74**(3), 1750–1752 (2003).
[21]M. G. Johnson, L. Giacomelli, A. Hjalmarsson, J. Källne, M. Weiszflog, E. Andersson Sundén, S. Conroy *et al.*, "The 2.5-MeV neutron time-of-flight spectrometer TOFOR for experiments at JET," Nucl. Instrum. Methods Phys. Res. A **591**(2), 417–430 (2008).
[22]See www.cividec.at for CIVIDEC.
[23]See http://www.caen.it/csite/CaenProd.jsp?parent=14&idmod=632 for CAEN — Costruzioni Apparecchiature Elettroniche Nucleari S.p.A., DT5751 2/4 channel 10 bit 2/1 GS/s digitizer.
[24]V. T. Jordanov, G. F. Knoll, A. C. Huber, and J. A. Pantazis, "Digital techniques for real-time pulse shaping in radiation measurements," Nucl. Instrum. Methods Phys. Res. A **353**(1), 261–264 (1994).
[25]D. B. Syme, S. Popovichev, S. Conroy, I. Lengar, and L. Snoj, "Fusion yield measurements on JET and their calibration," Nucl. Eng. Des. **246**, 185–190 (2012).
[26]See http://atom.kaeri.re.kr for Cross Section Database.
[27]G. F. Knoll, *Radiation Detection and Measurements* (John Wiley and Sons, New York, NY, 1979).
[28]J. Frenje, L. Ballabio, S. Conroy, G. Ericsson, M. Tardocchi, E. Traneus, J. Källne, and G. Gorini, "Neutron spectrometry of triton burn-up in plasmas of deuterium," Plasma Phys. Controlled Fusion **40**(7), 1211 (1998).
[29]L. Ballabio, J. Frenje, J. Källne, S. W. Conroy, G. Ericsson, M. Tardocchi, E. Traneus, and G. Gorini, "Measurement and interpretation of the spectrum of the triton burnup neutron emission from deuterium tokamak plasmas," Nucl. Fusion **40**(1), 21 (2000).
[30]H. Sjöstrand, G. Giuseppe, C. Sean, E. Göran, L. Giacomelli, H. Henriksson, A. Hjalmarsson *et al.*, "Triton burn-up neutron emission in JET low current plasmas," J. Phys. D: Appl. Phys. **41**(11), 115208 (2008).
[31]W. Cash, "Parameter estimation in astronomy through application of the likelihood ratio," Astrophys. J. **228**, 939–947 (1979).
[32]M. Tardocchi, M. Nocente, I. Proverbio, V. G. Kiptily, P. Blanchard, S. Conroy, M. Fontanesi *et al.*, "Spectral broadening of characteristic γ-ray emission peaks from C 12 (He 3, p γ) N 14 reactions in fusion plasmas," Phys. Rev. Lett. **107**(20), 205002 (2011).
[33]M. Nocente, M. Tardocchi, V. G. Kiptily, P. Blanchard, I. Chugunov, Sean Conroy, T. Edlington *et al.*, "High-resolution gamma ray spectroscopy measurements of the fast ion energy distribution in JET 4He plasmas" Nucl. Fusion **52**(6), 063009 (2012).
[34]M. Nocente, M. Garcia-Munoz, G. Gorini, M. Tardocchi, A. Weller, S. Akaslompolo, R. Bilato *et al.* "Gamma-ray spectroscopy measurements of confined fast ions on ASDEX Upgrade" Nucl. Fusion **52**(9), 094021 (2012).
[35]Z. Chen, M. Nocente, M. Tardocchi, T. Fan, and G. Gorini, "Simulation of neutron emission spectra from neutral beam-heated plasmas in the EAST tokamak," Nucl. Fusion **53**(6), 063023 (2013).
[36]H. Henriksson, "Neutron spectroscopy studies of heating effects in fusion plasmas," Ph.D. thesis, Acta Universitatis Upsaliensis No. 861 (Faculty of Sciences and Technology, Uppsala University, 2003).
[37]H. Klein, "Neutron spectrometry in mixed fields: NE213/BC501A liquid scintillation spectrometers," Radiat. Prot. dosim. **107**(1–3), 95–109 (2003).
[38]F. Gagnon-Moisan, M. Reginatto, and A. Zimbal, "Results for the response function determination of the Compact Neutron Spectrometer," J. Instrum. **7**(03), C03023 (2012).

[39]L. Giacomelli, S. Conroy, F. Belli, G. Gorini, L. Horton, E. Joffrin, E. Lerche, A. Murari, S. Popovichev, M. Riva, and B. Syme, International Conference on Fusion Reactor Diagnostics, Villa Monastero, Varenna, Italy, 9–13 September 2013, see http://www.iop.org/Jet/fulltext/EFDC130402.pdf.

[40]L. Giacomelli, A. Zimbal, K. Tittelmeier, H. Schuhmacher, G. Tardini, R. Neu, and ASDEX Upgrade Team, "The compact neutron spectrometer at ASDEX Upgrade," Rev. Sci. Instrum. **82**(12), 123504 (2011).

[41]S. Marrone, D. Cano-Ott, N. Colonna, C. Domingo, F. Gramegna, E. M. Gonzalez, F. Gunsing *et al.*, "Pulse shape analysis of liquid scintillators for neutron studies," Nucl. Instrum. Methods Phys. Res. A **490**(1), 299–307 (2002).

[42]L. Giacomelli, S. Conroy, G. Gorini, L. Horton, A. Murari, S. Popovichev, D. B. Syme, and JET EFDA Contributors, "Tomographic analysis of neutron and gamma pulse shape distributions from liquid scintillation detectors at Joint European Torus," Rev. Sci. Instrum. **85**(2), 023505 (2014).

[43]C. Hellesen, M. G. Johnson, E. A. Sundén, S. Conroy, G. Ericsson, J. Eriksson, G. Gorini *et al.* "Measurements of fast ions and their interactions with MHD activity using neutron emission spectroscopy" Nuclear fusion **50**(8), 084006 (2010).

[44]M. Gatu Johnson, C. Hellesen, E. Andersson Sundén, M. Cecconello, S. Conroy, G. Ericsson, G. Gorini *et al.* "Neutron emission from beryllium reactions in JET deuterium plasmas with 3He minority," Nucl. Fusion **50**(4), 045005 (2010).

[45]M. Tardocchi, M. Nocente, and G. Gorini, "Diagnosis of physical parameters of fast particles in high power fusion plasmas with high resolution neutron and gamma-ray spectroscopy," Plasma Phys. Controlled Fusion **55**(7), 074014 (2013).

[46]M. Nocente *et al.*, "Neutron spectroscopy measurements of tritium beam transport at JET," Nucl. Fusion (submitted).

Paper III

Nuclear Instruments and Methods in Physics Research A 751 (2014) 19–22

Contents lists available at ScienceDirect

Nuclear Instruments and Methods in Physics Research A

journal homepage: www.elsevier.com/locate/nima

Thin YAP:Ce and $LaBr_3$:Ce scintillators as proton detectors of a thin-film proton recoil neutron spectrometer for fusion and spallation sources applications

C. Cazzaniga [a,b,*], M. Nocente [a,b], M. Tardocchi [b], A. Fazzi [c], A. Hjalmarsson [d], D. Rigamonti [a], G. Ericsson [d], G. Gorini [a,b]

[a] Dipartimento di Fisica "G. Occhialini", Università di Milano-Bicocca, Piazza della Scienza 3, Milano, Italy
[b] Istituto di Fisica del Plasma, Associazione EURATOM-ENEA-CNR, Via Roberto Cozzi 53, Milano, Italy
[c] Energy Department, Politecnico di Milano, Via Ponzio 32, Milano, Italy
[d] Department of Physics and Astronomy, EURATOM-VR Association, Uppsala University, Uppsala, Sweden

ARTICLE INFO

Article history:
Received 10 February 2014
Received in revised form
28 February 2014
Accepted 7 March 2014
Available online 16 March 2014

Keywords:
Scintillators
Neutron spectroscopy
Fusion plasmas

ABSTRACT

Two thin inorganic scintillators based on YAP and $LaBr_3$ crystals (1 in. diameter × 0.1 in. height) have been used for proton measurements at the Uppsala tandem accelerator in the energy range 4–8 MeV. Measurements show a comparable good energy resolution for the two detectors, better than 2% (FWHM) for 8 MeV protons, which compares to 3.8% (LaBr3) and 3.7% (YAP) obtained at the 1.3 MeV peak of a ^{60}Co γ-ray source. The main advantages of these crystals are a fast scintillation time (less than 30 ns), an excellent light yield and the capability to operate in large neutron background, which make them ideal candidates as proton detectors of a thin-film proton recoil neutron spectrometer for application on fusion experiments and fast neutron spallation sources.

1. Introduction

Neutron spectrometers for measurements in the MeV range have played important roles in spallation sources and fusion plasma devices in recent years [1–7]. The instrumentation used in both cases is of dedicated design that depends on the specific diagnostic needs of each experiment. For example, in fusion plasma applications at JET, a Magnetic Proton Recoil (MPR) spectrometer has been used for 14 MeV neutron measurements at 5% resolution, providing information of unprecedented detail on neutron emission from the plasma [8–10]. The significant dimensions (several tens of meters) and weight (about 80 t) of the instrument, however, do not make the MPR technique particularly suitable for applications where there are space limitations, such as arrays of neutron detectors arranged in a camera system. In this context, a Thin-film Proton Recoil (TPR) spectrometer could be an interesting alternative. The TPR detection principle is based on neutron-to-proton conversion via elastic scattering on hydrogen nuclei at a given angle in a plastic thin foil. The scattered proton energy can be easily measured and converted back to the incoming neutron energy, provided that the recoil angle is known [11]. A preliminary design of a non-magnetic TPR detector for fusion plasma diagnostics has been presented in Ref. [12]. Here it is shown through calculations that TPR could attain an energy resolution close to that of the MPR, combined with an increased efficiency of 2.9 10^{-4} n cm^2 and compact dimensions. The design in Ref. [12] used silicon detectors as proton spectrometers, given their excellent energy resolution and fast signals. In particular, a proton energy resolution better than 2% would be ideal for a TPR system, so that the overall energy resolution of the spectrometer, that gains contributions also from the finite aperture of the recoil solid angle and the thickness of the scattering foil, could still be about 5%.

In this paper we demonstrate that such requirement for the proton energy resolution could be also achieved using fast inorganic scintillators as alternatives to silicon detectors. Their main advantages are the resistance to neutron irradiation and cost effectiveness. In particular $LaBr_3$(Ce) and YAP(Ce) are the proposed scintillator crystals, the latter being the most cost effective one. Besides, the fast scintillation time constants of these crystals would enable their use at high count rates up to few MHz. A prototype of a TPR spectrometer of such design was tested at the ISIS neutron source of the Rutherford-Appleton Laboratory (UK) in a proof-of-principle measurement using YAP scintillators, presented in Ref.[13]. In this experiment neutron spectroscopy in the energy range 30 to 80 MeV was demonstrated and advantage was taken from the fast scintillation time of the crystal, which is needed to cope with the high instantaneous count rate provided

* Corresponding author.
E-mail address: carlo.cazzaniga@mib.infn.it (C. Cazzaniga).

http://dx.doi.org/10.1016/j.nima.2014.03.012
0168-9002/

by the pulsed nature of the ISIS neutron source. However, for this application no strict requirement was set on the overall energy resolution.

In this paper, we report on measurements aimed at the determination of the energy resolution of YAP and $LaBr_3$ to protons in the energy range 4 to 8 MeV. The experiment, performed at the Uppsala Tandem accelerator at low counting rates (a few kHz), is presented in the next section. The results on the energy resolution are then illustrated and compared to laboratory calibrations using γ-ray sources.

2. Experimental setup

Two thin inorganic scintillators based on YAP and $LaBr_3$ crystals (1 in. diameter × 0.1 in. height) have been coupled to two eight dynode Photo Multiplier Tubes (PMTs), model R6231 by Hamamatsu [14]. Special care was taken in the case of $LaBr_3$ which, being hygroscopic, was encapsulated on all sides, with a thin (125 μm) Be entrance window. This is where the proton beam was impinging in the experiment and was needed to minimize energy loss, which would otherwise not be tolerable in the thick encapsulating material. The ^{9}Be window was not needed for YAP, as this crystal is not hygroscopic. In this case, a thin (20 μm) aluminum layer was used for the purpose of light collection optimization only.

An electronic chain devoted to energy resolution measurements and consisting of an ORTEC 570 amplifier and an ORTEC Multichannel Analyzer was prepared [15]. The scintillators were first irradiated with calibration γ-ray ^{137}Cs and ^{60}Co sources at the IFP-CNR spectroscopy laboratory in Milano and then with 4 to 8 MeV protons from a tandem accelerator at Uppsala University. The accelerator features an accelerating voltage up to 5 MV and can produce beams of protons as well as heavy ions. Fig. 1 shows the setup of the experiment in Uppsala inside the proton interaction chamber, i.e. a metal cylinder with a diameter of about 0.5 m. The proton beam enters from the aperture on one side of the chamber, along a diameter and perpendicularly to the chamber s plane. The experiment was performed using a Rutherford scattering configuration [16] on a gold foil target (~3 μm), which was necessary to significantly reduce the proton current in the detector, which would otherwise result in counting rates well beyond the MHz range that can be coped with the device. A proton scattering angle on the gold foil of about 45° with respect to the proton beam was chosen. PMTs were operated with a negative high voltage of 750 V and energy calibration was repeated in situ with ^{137}Cs and ^{60}Co sources.

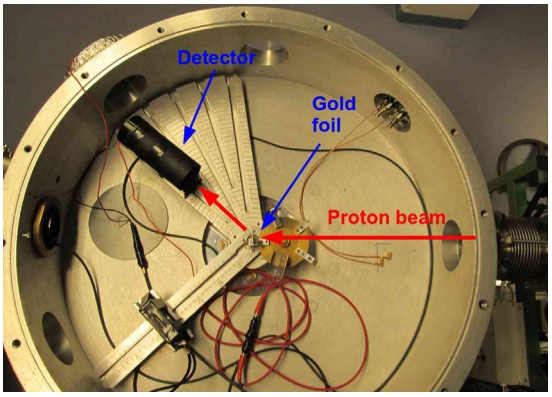

Fig. 1. Experimental setup at the Uppsala tandem accelerator. The position of the detector and target (a gold-foil) for the Rutherford scattering experiment are indicated, together with the proton beam direction.

The spectroscopic chain described above is the reference for energy resolution measurements, but it cannot be used at high rates (MHz), since the shaped signals after the amplifier have a too long time constant (μs). High rate measurements can however still be performed by direct digitization of the signal from the PMT anode using a digital acquisition system (see the experimental setup in Ref. [13]). Count rates up to a few MHz can be handled thanks to the fast scintillation time of YAP and $LaBr_3$ crystals, which is 27 and 16 ns, respectively, with only a moderate degradation in the energy resolution, as demonstrated in Refs. [17,18]. The shapes of YAP and $LaBr_3$ signals after the PMT anode are compared in Fig. 2. In particular, we can notice a clear difference in the falling edges of the two signals, which is due to the different time constant of the crystals. The rising edge is instead similar, as this part of the signal is dominated by the PMT response, which is the same for both scintillators.

3. Detector characterization with laboratory gamma-ray sources

The thickness of the two crystals is optimized to stop protons up to 20 MeV. For this reason the detectors have low efficiency to γ-rays, which are the main background sources during the measurement. Nevertheless, the high density and high effective Z of the crystal allow distinguishing full-energy-peaks when the crystal is irradiated with laboratory γ-ray sources. These measurements are useful to determine the energy resolution of the two crystals to γ-rays in the MeV range, obtained from the FWHM of the full-energy peaks. ^{137}Cs and ^{60}Co sources were used for this scope with the results summarized in Table 1 for YAP and $LaBr_3$. Here we note that the energy resolution found in the two cases does not differ significantly, especially above 1 MeV, where it is practically identical and has a value of 3.8%. This number can be compared to the expected light yield of 63,000 photons-per-MeV

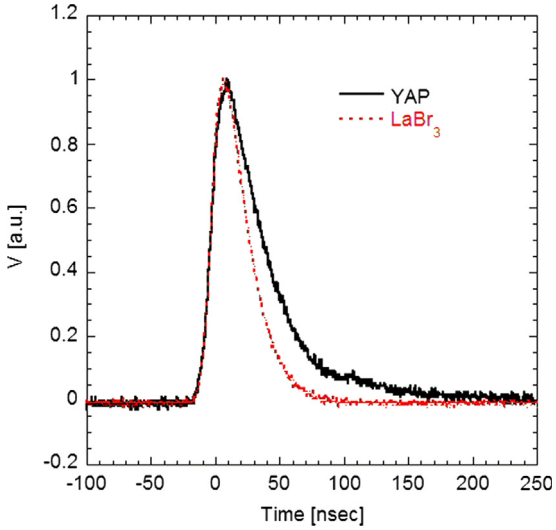

Fig. 2. Measured YAP and $LaBr_3$ signals from the PMT anode.

Table 1
Energy resolution values (FWHM/E) measured with γ-ray sources for the thin $LaBr_3$ and YAP scintillators used in the proton experiment.

Source	Peak energy(MeV)	$LaBr_3$ resolution(%)	YAP resolution (%)
^{137}Cs	0.66	4.2	5.5
^{60}Co	1.17	3.5	3.8
^{60}Co	1.33	3.7	3.8

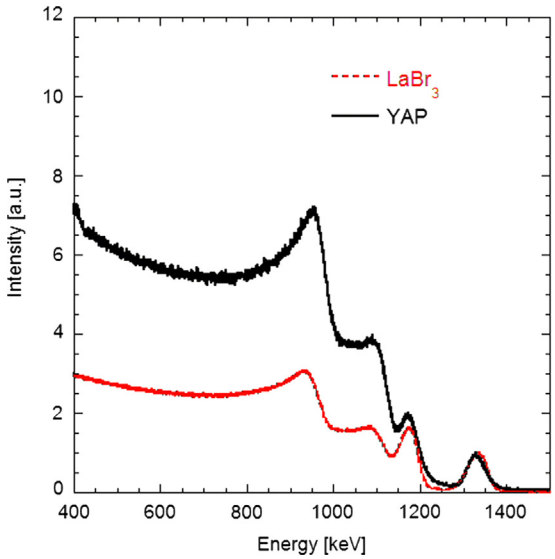

Fig. 3. γ-ray spectra from a ^{60}Co γ-ray laboratory source measured with the thin $LaBr_3$ and YAP scintillators used in the proton measurements at Uppsala.

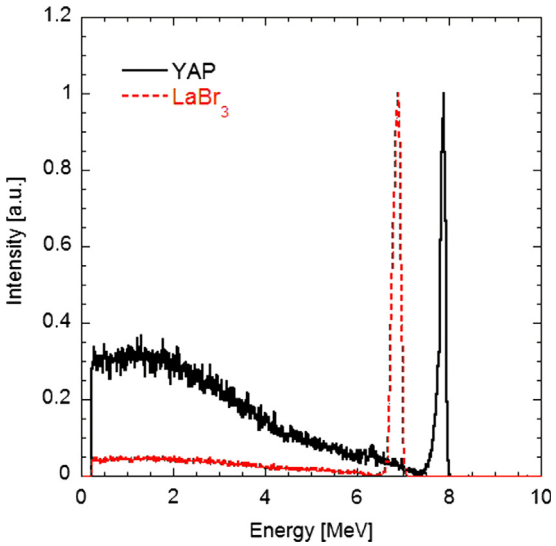

Fig. 4. Proton energy spectra measured with thin $LaBr_3$ and YAP scintillators at the Uppsala tandem accelerator using an 8 MeV beam.

of $LaBr_3$ [19] and 20,000 to 25,000 photons-per-MeV of YAP [20–23], which would imply a much better resolution for $LaBr_3$. The difference can be qualitatively understood based on other contributions to the energy resolution. These are, for instance, variations in the luminescence and transparency characteristics of YAP depending on the concentration of the Ce doping and crystal phases [23]. Besides, the PMT quantum efficiency curve has a 10% decrease when moving from a wavelength of 350 nm (peak emission for YAP) to 380 nm (peak emission for $LaBr_3$). Finally, there can be a further contribution due to non-homogeneous light collection over the crystal volume. This can be minimized by optimizing the coupling of the crystal to PMT.

Fig. 3 shows the measured γ-ray spectrum from a ^{60}Co calibration source using $LaBr_3$ and YAP. The spectra are normalized to unity at the 1.33 MeV peak. In both cases, two full energy peaks corresponding to 1.17 and 1.33 MeV γ-rays from ^{60}Co can be observed, which are used to determine the energy resolution values reported in Table 1. Most of the events lie in the Compton shoulder, as expected from the limited thickness of the scintillators, which provides a peak-to-Compton ratio of about 1/4 for YAP and 1/2 for $LaBr_3$.

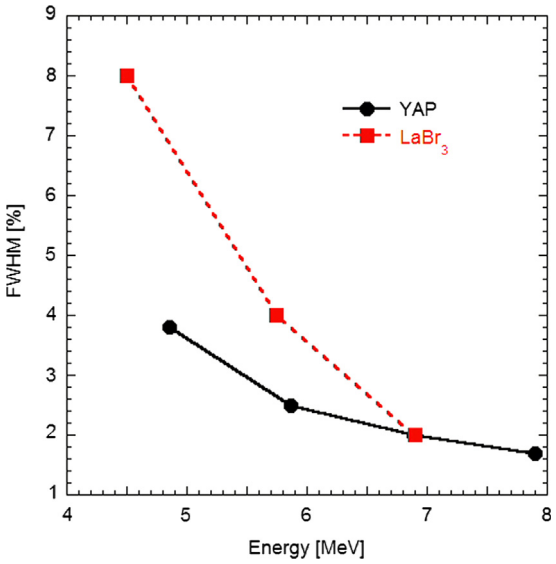

Fig. 5. Energy resolution of thin $LaBr_3$ and YAP scintillators measured at the Uppsala tandem accelerator at different proton beam energies.

4. Proton measurements at the Uppsala tandem accelerator

The light yield of a scintillator crystal under proton irradiation is different from that measured with γ-rays of same energy due to quenching effects. For this reason, dedicated measurements of the crystal energy resolution with protons of known energies were undertaken. Fig. 4 compares proton energy spectra, normalized to peak height, measured with the thin $LaBr_3$ and YAP scintillators at the Uppsala tandem accelerator in the Rutherford scattering experiment described in Section 2 and using an 8 MeV proton beam. The *x*-axis scale corresponds to the known proton beam energy corrected for the energy loss in the entrance window of each detector. This was calculated using MCNPX [24] and was found to be larger (1.1 MeV) for the 125 μm Be window of $LaBr_3$ than in the case of the YAP Al window (0.2 MeV). Different background levels can also be observed for the two measurements, due to different positions of the two detectors in the interaction chamber. In particular, YAP was closer to the proton beam dump.

Besides introducing a correction in the energy scale on the *x*-axis of the spectrum, the entrance windows also give a finite contribution to the detector energy resolution that sums up to those from statistics, electronic noise and intrinsic crystal effects, such as a non-ideal light collection by the PMT. This finite contribution is relevant in the case of the $LaBr_3$ Be entrance window, is derived from proton straggling, and is calculated by MCNPX to range from 8.8% to 1.2% MeV as the energy of the proton beam varies in the range 4 to 8 MeV.

The overall proton energy resolution of thin $LaBr_3$ and YAP scintillators measured for 4 MeV $< E_p <$ 8 MeV are shown in Fig. 5. The energy dependence of the resolution suggests a predominance of straggling effects for the $LaBr_3$ detector below 7 MeV. This is likely to be the reason why YAP outperforms $LaBr_3$ for $E_p < 8$ MeV. Finally, it is worth noticing that, based on our measurements, the energy resolution of both detectors is better than 2% for $E_p > 7$ MeV, which is an excellent value and promising result in

view of the design of a scintillator based TPR spectrometer for applications at fusion devices and spallation sources.

5. Conclusions

Energy resolution measurements have been performed with thin (1 in. × 0.1 in.) $LaBr_3$ and YAP scintillators using protons and γ-rays between 1 and 8 MeV. The measurements show that both crystals are good candidate components for a TPR spectrometer for fusion and spallation source applications as they match the required energy resolution and fast scintillation time. In particular, our measurements show that a proton energy resolution better than 2% can be achieved at 8 MeV. These results extrapolate favorably at $E_p > 8$ MeV, making $LaBr_3$ and YAP an effective alternative to silicon detectors for a TPR neutron spectrometer designed to deliver neutron spectra with an overall neutron energy resolution better than 5%.

References

[1] A. Pietropaolo, et al., Single-crystal diamond detector for time-resolved measurements of a pulsed fast-neutron beam, Europhysics Letters 92.6 (2010) 68003.
[2] M. Rebai, et al., Response of a single-crystal diamond detector to fast neutrons, Journal of Instrumentation 8 (10) (2013) P10007.
[3] Z. Chen, et al., Simulation of neutron emission spectra from neutral beam-heated plasmas in the EAST tokamak, Nuclear Fusion 53 (6) (2013) 063023.
[4] M. Nocente, J. Källne, G. Grosso, M. Tardocchi, G. Gorini, Reaction analysis of neutron emission from D and DT plasmas with/without 3He, Nuclear Fusion 53 (2013) 053010.
[5] M. Nocente, G. Gorini, J. Källne, M. Tardocchi, Calculated neutron emission spectrum with knock-on effects for RF heated (3He)D plasmas, Nuclear Fusion 51 (2011) 063011.
[6] M. Nocente, G. Gorini, J. Källne, M. Tardocchi, Cross section of the d+3He→α+p reaction of relevance for fusion plasma applications, Nuclear Fusion 50 (2010) 055001.
[7] M. Tardocchi, M. Nocente, G. Gorini., Diagnosis of physical parameters of fast particles in high power fusion plasmas with high resolution neutron and gamma-ray spectroscopy, Plasma Physics and Controlled Fusion 55 (7) (2013) 074014.
[8] H. Sjostrand, et al., New MPRu instrument for Neutron Emission Spectroscopy at JET, Review of Scientific Instruments 77 (2006) 10E717.
[9] E. Andersson Sundén, et al., The thin foil magnetic proton recoil neutron spectrometer MPRu at JET, Nuclear Instruments and Methods in Physics Research A 610 (2009) 682.
[10] G. Ericsson, et al., Neutron emission spectroscopy at JET – results from the magnetic proton recoil spectrometer, Review of Scientific Instruments 72 (2001) 759.
[11] G.F. Knoll, Radiation Detection and Measurement, 3rd ed., Wiley, New York (2000) 569 (Chapter 15).
[12] Sean W. Conroy, et al., Neutron spectrometer for ITER using silicon detectors, Review of Scientific Instruments 79 (10) (2008) 10E508.
[13] C. Cazzaniga, et al., First measurement of the VESUVIO neutron spectrum in the 30–80 MeV energy range using a Proton Recoil Telescope technique, Journal of Instrumentation 8.11 (2013) P11008.
[14] Hamamatsu Online Catalogue, ⟨http://www.hamamatsu.com/⟩.
[15] ORTEC Online Catalogue, ⟨http://www.ortec-online.com/⟩.
[16] E. Rutherford, The scattering of α and β particles by matter and the structure of the atom, Philosophical Magazine 21 (1911) 669–688.
[17] M. Nocente, M. Tardocchi, A. Olariu, S. Olariu, R.C. Pereira, I.N. Chugunov, A. Fernandes, et al., High resolution gamma ray spectroscopy at MHz counting rates with LaBr scintillators for fusion plasma applications, IEEE Transactions on Nuclear Science NS60 (2) (2013) 1408–1415.
[18] M. Nocente, M. Tardocchi, I. Chugunov, R.C. Pereira, T. Edlington, A. M. Fernandes, D. Gin, et al., Energy resolution of gamma-ray spectroscopy of JET plasmas with a LaBr scintillator detector and digital data acquisition, Review of Scientific Instruments 81 (2010) 10D321.
[19] E.V.D. Van Loef, P. Dorenbos, C.W.E. Van Eijk, K.W. Krämer, H.U. Güdel., Scintillation properties of LaBr3:Ce3+ crystals: fast, efficient and high-energy-resolution scintillators, Nuclear Instruments and Methods in Physics Research A 486 (1) (2002) 254–258.
[20] M. Moszyhski, et al., Properties of the YAP: Ce scintillator, Nuclear Instruments and Methods in Physics Research A 404 (1998) 157–165.
[21] M. Kapusta, et al., A high-energy resolution observed from a YAP: Ce scintillator, Nuclear Instruments and Methods in Physics Research A 421 (1999) 610–613.
[22] A. Del Guerra, et al., Measurement of absolute light yield and determination of a lower limit for the light attenuation length for YAP:Ce crystal, IEEE Transactions on Nuclear Science NS44 (6) (1997).
[23] T.B. de Queiroz, et al., Luminescence characteristics of YAP:Ce scintillator powders and composites, Optical Materials 32 (2010) 1480–1484.
[24] The MCNPX Website: ⟨http://mcnpx.lanl.gov/⟩.

Paper IV

PUBLISHED BY IOP PUBLISHING FOR SISSA MEDIALAB

RECEIVED: *September 14, 2013*
REVISED: *October 30, 2013*
ACCEPTED: *November 1, 2013*
PUBLISHED: *November 11, 2013*

2013 JINST 8 P11008

First measurement of the VESUVIO neutron spectrum in the 30–80 MeV energy range using a Proton Recoil Telescope technique

C. Cazzaniga,[a,b,1] **M. Tardocchi,**[a] **G. Croci,**[a] **C. Frost,**[d] **L. Giacomelli,**[b] **G. Grosso,**[a] **A. Hjalmarsson,**[c] **M. Rebai,**[a,b] **N.J. Rhodes,**[d] **E.M. Schooneveld**[d] **and G. Gorini**[a,b]

[a] *Istituto di Fisica del Plasma "P. Caldirola", Associazione EURATOM-ENEA/CNR, Milano, Italy*

[b] *Dipartimento di Fisica "G. Occhialini", Università degli Studi di Milano-Bicocca, Milano, Italy*

[c] *Department of Physics and Astronomy, EURATOM-VR Association, Uppsala University, Uppsala, Sweden*

[d] *ISIS Facility, Rutherford Appleton Laboratory, Chilton, Didcot, U.K.*

E-mail: carlo.cazzaniga@mib.infn.it

ABSTRACT: Measurements of the fast neutron energy spectrum at the ISIS spallation source are reported. The measurements were performed with a Proton Recoil Telescope consisting of a thin plastic foil placed in the neutron beam and two scintillator detectors. Results in the neutron energy range 30 MeV $< E_n <$ 80 MeV are in good agreement with Monte Carlo simulations of the neutron spectrum.

KEYWORDS: Instrumentation for neutron sources; Neutron detectors (cold, thermal, fast neutrons)

[1] Corresponding author.

doi:10.1088/1748-0221/8/11/P11008

Contents

2013 JINST 8 P11008

1 Introduction

A fast neutron beam line is under construction at the ISIS spallation source [1]. The beam line, named CHIPIR (for Chip Irradiation), will provide neutrons with an energy spectrum as close as possible to the one of atmospheric neutrons, but with a 10^8 times more intense flux. The beam line will be used for accelerated testing of micro-electronic devices under fast neutron irradiation [2, 3].

Different kinds of detectors are proposed for fast neutron flux monitoring, such as diamond detectors [4]–[7] and gas detectors with a hydrogenated conversion layer (nGEM) [8]–[11]. In order to measure the fast neutron spectrum in the energy range $10\,\text{MeV} < E_n < 100\,\text{MeV}$, the Proton Recoil Telescope (PRT) technique [12] is proposed. In this paper results of test of a prototype PRT spectrometer are reported. Aim of the measurements was a first assessment of the feasibility of PRT neutron spectrometry in the ISIS environment.

2 Experimental setup

The prototype PRT spectrometer was tested on the VESUVIO [13] beam line at the ISIS spallation source. The ISIS neutrons are produced by a proton beam delivering an average current of $200\,\mu\text{A}$ on a Ta-W target and yielding about 15–20 neutrons per incident proton. The 800 MeV proton beam has a repetition frequency of 50 Hz and a double bunch fine structure. The two proton bunches are about 70 ns wide (FWHM) and 322 ns apart. The VESUVIO beam-line is 11 meters long and neutrons, coming from the spallation target are partially moderated by a 300 K water tank. The result is an under-moderated spectrum with an intense flux of neutrons ($5 \cdot 10^4$ neutrons cm^{-2} sec^{-1} with $E_n > 10\,\text{MeV}$) [13, 14].

Figure 1 shows the PRT spectrometer schematics. A 2 mm thick polyethylene foil is used as hydrogenated target for converting neutrons into protons via elastic scattering. The foil is placed

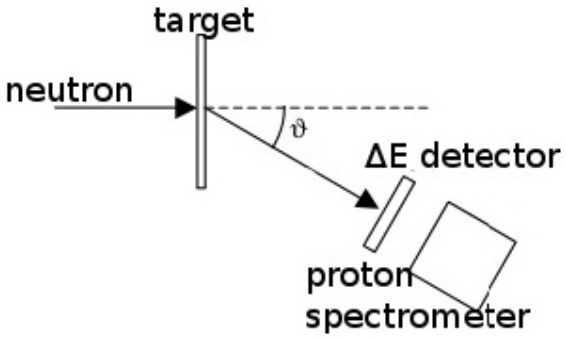

Figure 1. Schematics of the PRT experimental setup (not to scale).

in the neutron beam and intercepts the entire beam cross section (about 5 cm in diameter). The neutron energy E_n is related to the recoil proton energy E_p according to

$$E_p = E_n \cos^2 \theta \tag{2.1}$$

where θ is the recoil angle. The telescope detector for recoil protons is composed by a thin ΔE detector for background suppression and a proton spectrometer, which stops the protons and measures their full energy.

A 1" x 1" (diameter x height) YAP scintillator is used as proton spectrometer. The thickness is enough to stop protons up to 100 MeV. The detector energy resolution is about 8% at the 662 keV γ-ray peak of a ^{137}Cs calibration source. The fast scintillation time (27 ns) of YAP allows for high rate measurements. The crystal is coupled to a Hamamatsu R9420-100-10mod photo-multiplier-tube (PMT) [15]. The YAP spectrometer was previously calibrated with gamma sources of ^{137}Cs and ^{60}Co. The ratio between the proton light yield to photon light yield is assumed to be 60% according to [16]. An energy resolution of 3% for 60 MeV protons using a YAP scintillator was measured [16].

A 500 μm thick lithium glass scintillator [17] was used as ΔE detector. Protons with energy from 10 MeV to 50 MeV can deposit up to 4.8 MeV and 1.3 MeV, respectively. Lithium glass has a fast scintillation time, providing good timing performances for coincidence measurements.

Signals from the two detectors are fed into a CAEN waveform digitizer model DT5751 [18]. This is a 4 channel desktop digitizer with 1 GHz sampling frequency, 0–1 V input range and 10 bit resolution. The board trigger is set on a reference signal (T_0) generated by the proton extraction from the synchrotron. For each ISIS pulse a 3000 ns long waveform is stored for both detectors. All pulses related to fast neutrons fall inside this short time window. This means that, even if the global count rate is relatively low (the machine operates at 50 Hz), the instantaneous count rate can be very high ($>$ 1 MHz): more than one signal pulse is typically present in the time window, and pile-up is an important issue. Off-line analysis is needed for coincidence measurements with the two detectors and for pulse height and Time of Flight (ToF) spectral analysis. Figure 2 shows an example of signal output from the YAP detector. Three main pulses can be seen, which could be due either to recoil protons or to background events. Using a High Voltage value $HV = -600$ V, a pulse with amplitude equal to 7.5 mV corresponds to 1 MeV of γ-equivalent deposited energy. The three main pulses shown in figure 2 have deposited energies above 15 MeV. Such high energy

2013 JINST 8 P11008

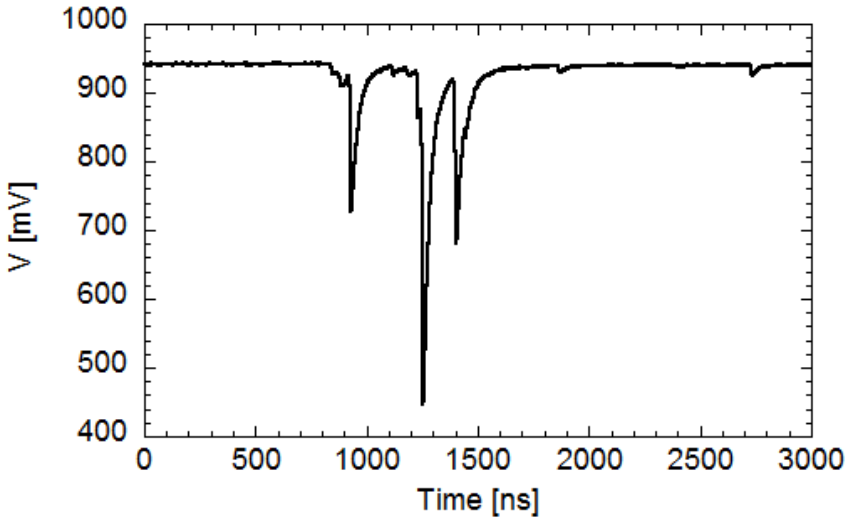

Figure 2. Example of YAP detector signal output.

pulses, if due to background, would not come from nuclear interactions, but rather to Inter-Nuclear-Cascade interactions [19]. Their ToF can not be easily distinguished from the ToF of fast neutrons with energy $E_n > 10\,\text{MeV}$. Coincidence measurements, on the other hand, provide a method for identification of proton signals, but the geometry must be optimized. A 45° recoil angle has been used in the present measurements, since a smaller angle would have brought the YAP detector too close to the beam, with a corresponding increase of the background events. Another background, with a different time structure, is given by γ-rays produced by nuclear interactions of neutrons with the materials in the beam line [20, 21]. Their energy does not exceed 10 MeV, which allows for effective rejection by pulse height discrimination.

3 Efficiency and resolution

Efficiency and energy resolution of the PRT system depend on several parameters that have to be optimized. Here an acceptable efficiency level was obtained at the price of relatively poor energy resolution. A MCNPX [22] model was used to determine the PRT efficiency and energy resolution for mono-energetic neutrons. In the model a collimated neutron beam is directed towards a polyethylene target foil. The system geometry was taken into account with sufficient level of detail, including the ΔE detector with thin entrance and exit aluminum windows and air along the proton flight path. A detector is placed at the YAP position and the proton energy distribution is given as output of the simulations. The proton energy distribution was calculated for several neutron energies; figure 3 shows an example for 50 MeV neutrons. The computed efficiency is defined as the ratio between the number of protons arriving at the detector position and the number of neutrons hitting the target foil. The computed energy resolution is given by the FWHM of the proton energy distribution, using a fit assuming a Gaussian distribution. Figure 4 and figure 5 show the simulated efficiency and resolution as function of neutron energy.

2013 JINST 8 P11008

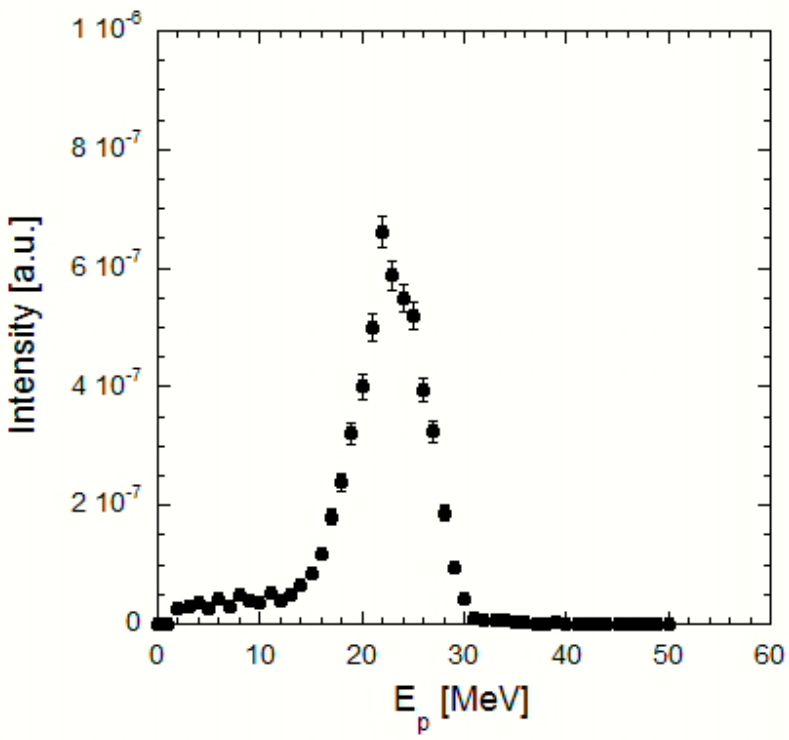

Figure 3. Simulated recoil proton energy distribution at the detector position for 50 MeV mono-energetic neutrons for the setup used in these measurements.

It is worth to notice from figure 4 that the efficiency is vanishing for under-20-MeV neutrons. They correspond to 10 MeV protons (according to eq. (2.1)), which are not energetic enough to reach the YAP detector, and are stopped either by the polyethylene foil itself, by the ΔE detector or by the air. Neutrons above 30 MeV correspond to protons above 15 MeV, which are energetic enough to reach the YAP detector. Efficiency for neutrons in the 30 MeV $< E_n <$ 100 MeV range is dominated by the elastic scattering macroscopic cross section and it ranges (see figure 4) from $7 \cdot 10^{-6}$ to $4 \cdot 10^{-6}$.

In figure 5 one can notice a very poor resolution below 40 MeV. This is due to the fact that in this energy range energy resolution is dominated by the contribution of the thickness of the scattering foil. The resolution is rather flat above 50 MeV and it is about 30%. In this region the dominant effect is due to the detector-foil solid angle contribution.

A significant improvement on the energy resolution is expected if, thanks to a better background reduction, one could choose a smaller scattering angle, because the proton recoil energy would increase according to eq. (2.1).

4 Optimization of coincidence measurements

The acquired raw data (see example in figure 2) are analyzed off-line by a dedicated software based on a trapezoidal filter algorithm [23]. The combined information of pulse height and ToF is recorded for every pulse exceeding a user defined threshold. The time reference (T_0) is the rising

2013 JINST 8 P11008

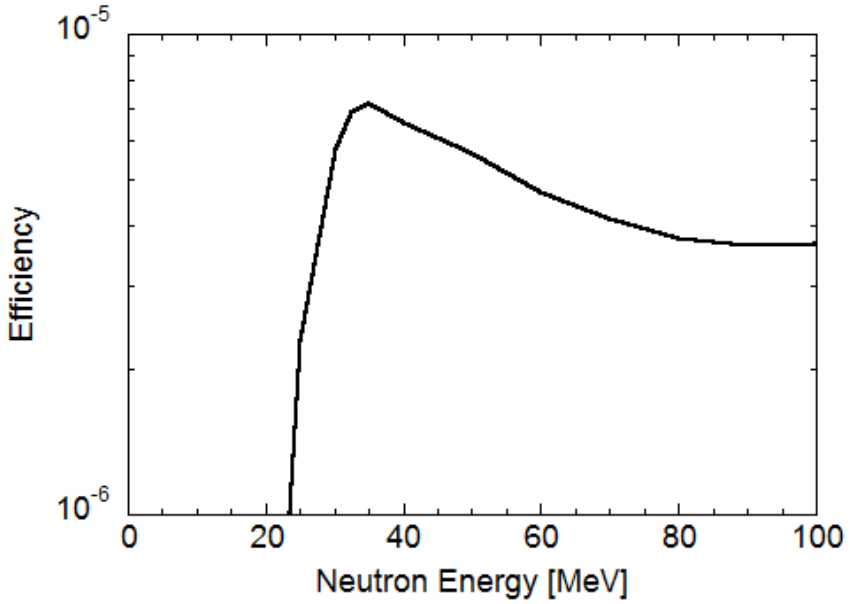

Figure 4. Simulated PRT efficiency for the setup used in these measurements.

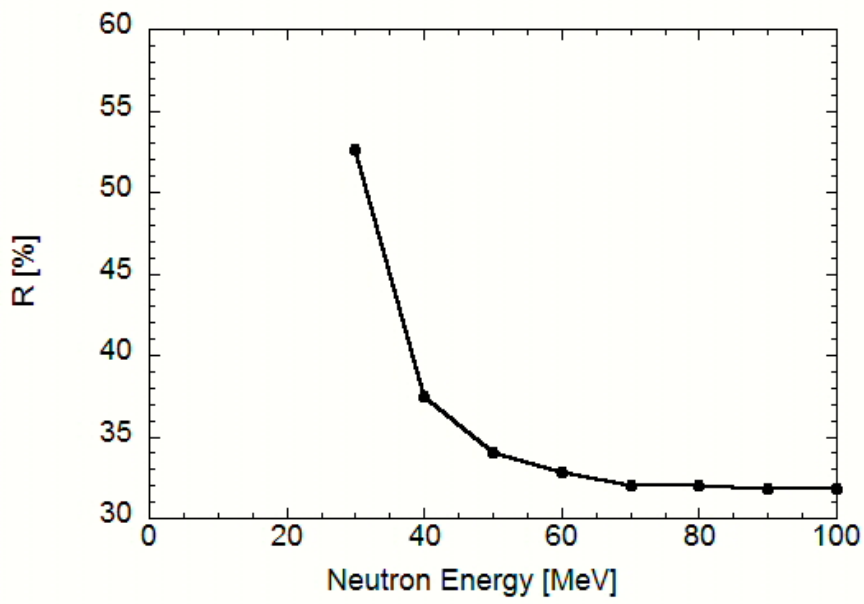

Figure 5. Simulated PRT energy resolution for the setup used in these measurements.

edge of the signal generated by the ISIS proton extraction. ToF calibration is performed knowing the fight path (12 meters) and the time of arrival of the first γ-rays on the YAP detector. The analysis is performed in two steps. First, the signals from the two detectors are analyzed separately and ToF spectra are produced. Second, using the information from the first step, a coincidence analysis is performed. A coincidence event is taken into account if the difference in ToF of the two detectors signals is less than 30 ns. This time window was chosen to be about three times larger than the

2013 JINST 8 P11008

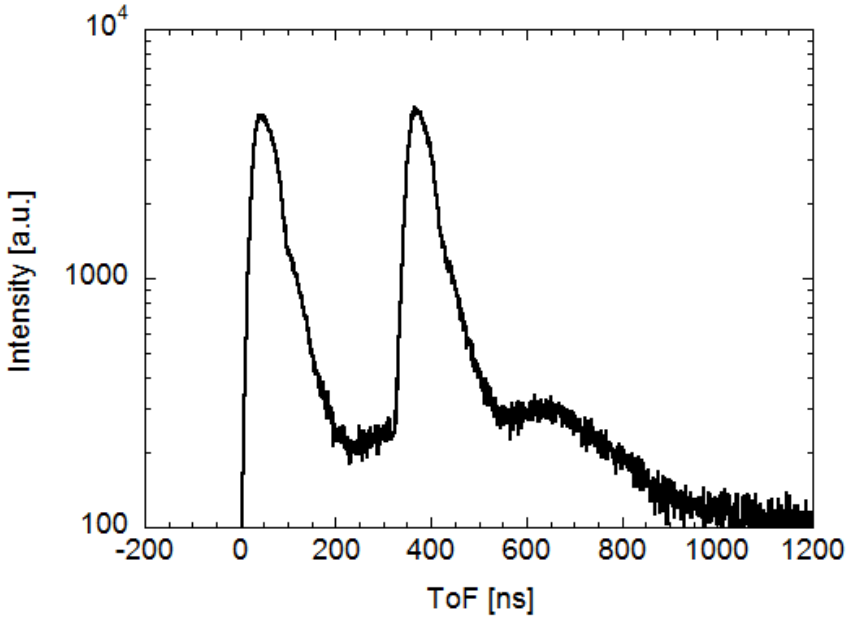

Figure 6. ToF spectrum recorded by the YAP proton spectrometer measured at VESUVIO.

detectors rising time, which is less than 10 ns. A few coincidence events per second are expected based on the combined information of neutron flux and detection efficiency.

Figure 6 shows the ToF spectrum recorded by the YAP scintillator for a pulse height threshold equivalent to 2.5 MeV γ-ray energy. The two peaks reflect the double pulse structure of the ISIS proton beam. Each peak consists of a fast component (mainly photons) and a slower broaden component due neutron induced background and recoil protons admixed. The evaporation peak [24] relative to the second proton bunch can be seen at ToF $\approx$ 650 ns, corresponding to a neutron energy of about 2–3 MeV. The evaporation peak for the first proton bunch is hidden under the second peak. Discrimination of events due to fast neutrons and recoil protons is possible with the coincidence analysis, as described above.

Figure 7 shows the ToF spectrum of the Lithium Glass used as ΔE-detector. A comparison of the measurement with and without the scattering target foil shows the contribution of the recoil protons in the ToF region related to fast neutrons. The spectra are normalized with respect to the ISIS proton current integrated over the measurement time. The difference between the two spectra amounts to a factor ≈ 5 in the ToF window corresponding to $E_n = 50 \pm 30$ MeV. Note that the relation between energy and ToF is uncertain due to the time width of the proton bunches. The excess of events due to recoil protons ends at a ToF value corresponding to $E_n = 15 \pm 5$ MeV, which corresponds to $E_p = 7 \pm 3$ MeV. This is consistent with the fact that protons with $E_p < 5$ MeV can not reach the lithium glass scintillator with enough energy to generate a signal above the pulse height threshold set at about 1 MeV equivalent γ-ray deposited energy.

Although the difference between the two spectra in figure 7, shown in figure 8, is representative of the ToF spectrum due to recoil protons, it can not provide an accurate neutron spectrum due to the ISIS beam pulse width. Coincidence analysis is restricted to ToF windows corresponding to

2013 JINST 8 P11008

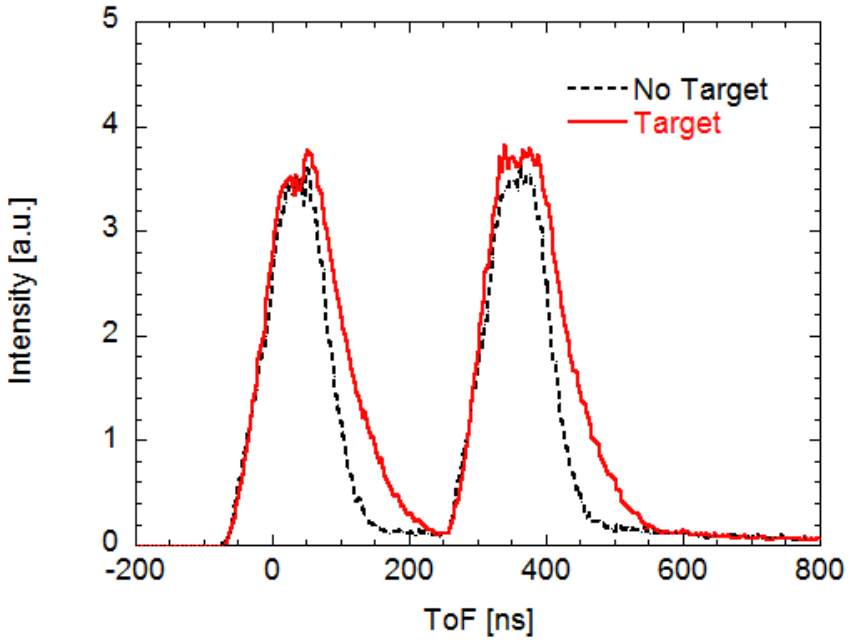

Figure 7. ToF spectrum recorded by the Lithium Glass used as ΔE-detector. The red (continuous) and black (dashed) data correspond to a measurement with and without polyethylene foil target in the beam, respectively.

10–80 MeV energy range. Neutrons above 80 MeV are too close to the gamma-flash, and extending the coincidence analysis above 80 MeV would mean increasing the coincidence background due to random events.

5 Measurement of the neutron spectrum using the PRT technique

A coincidence analysis has been performed to measure the recoil proton pulse height spectrum. A measurement without the scattering foil gives an estimation of the background level, possibly due to random coincidence events. Figure 9 shows the coincidence spectra with and without the scattering foil. Energy calibration is performed using γ-ray sources and assuming that the proton light yield is 60% of the photon light yield. The spectra are normalized to the ISIS proton current integrated over the measurement time.

Figure 10 shows the neutron spectrum derived from the data of figure 9. The following steps were performed for the analysis: (1) the background level, fitted with a polinomial function, was subtracted from the measurement, (2) the calculated [25] energy loss of the protons before arriving to the YAP detector was added, (3) the neutron energy was calculated from the recoil proton energy according to eq. (2.1), (4) the data were divided by the efficiency (see figure 4). The neutron spectrum of VESUVIO [13] simulated with MCNP is shown for comparison. The simulation is normalized so as to give the same area for 30 MeV $< E_n <$ 80 MeV. The analysis was restricted to the 30–80 MeV energy range, since the efficiency drops to zero below 30 MeV (see figure 4) and

2013 JINST 8 P11008

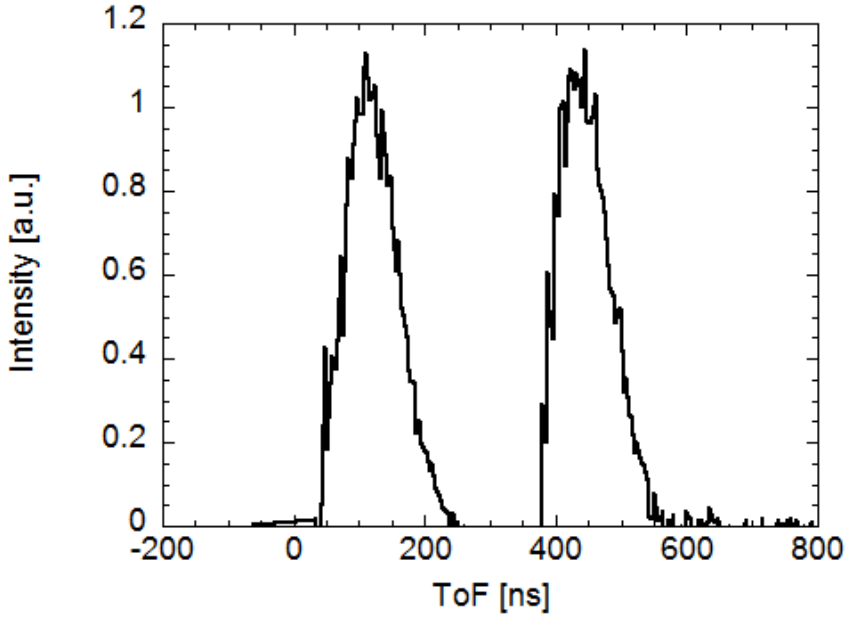

Figure 8. ToF spectrum due to recoil protons recorded by the Lithium Glass used as ΔE-detector.

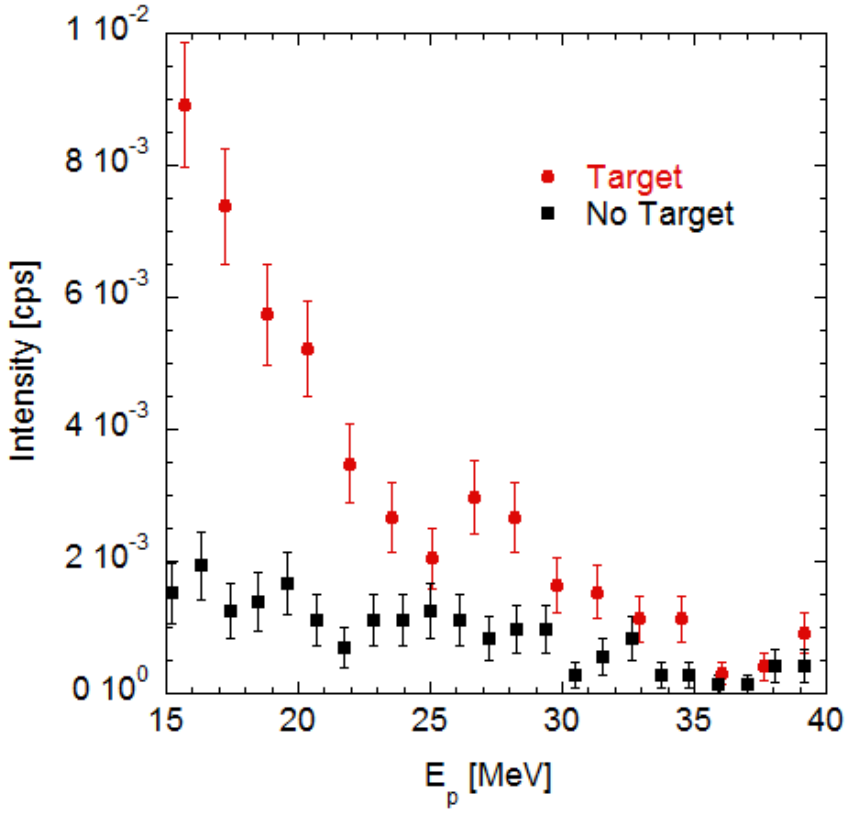

Figure 9. Calibrated spectrum of the recoil protons using off-line coincidence technique.

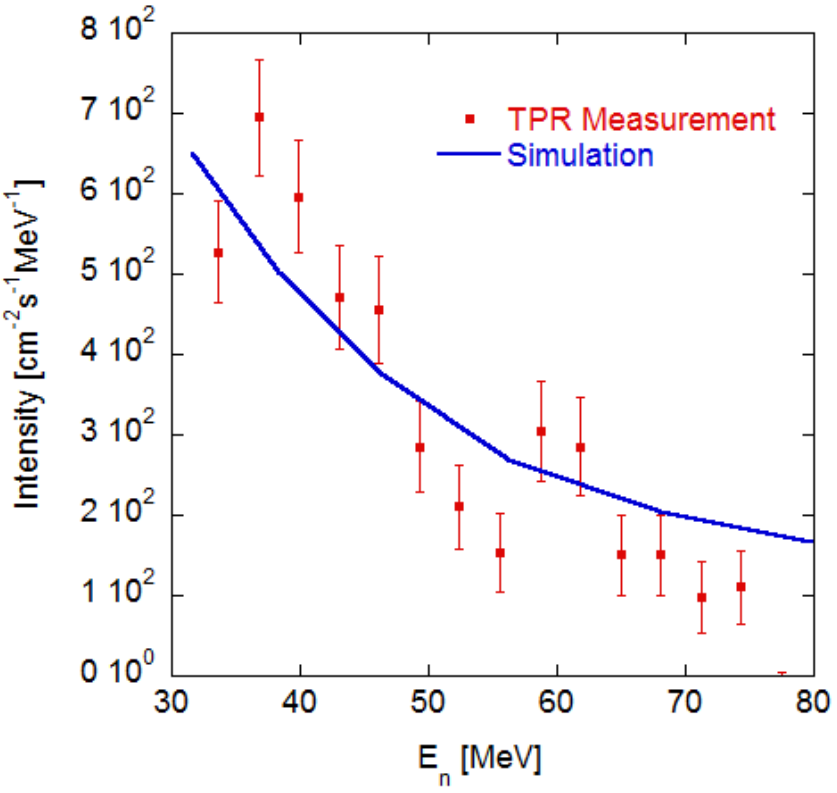

Figure 10. Neutron spectrum measured with the PRT and Monte Carlo simulation for VESUVIO.

coincidence measurements were limited to 80 MeV to avoid contamination due to gamma-flash background. The agreement between measurement and simulation is satisfactory.

6 Outlook

The results presented in this paper are the basis for further studies in order to design a PRT spectrometer with improved energy resolution and background discrimination.

The most important development will be the design of a new ΔE detector. The main requirement are a fast analog signal (FWHM < 20 ns) for good coincidence timing, good energy resolution for background reduction via $\Delta E - E$ correlation, low γ-sensitivity and radiation hardness. The best candidate to meet these requirements is a silicon detector coupled to a fast preamplifier. A better background discrimination will give the possibility to perform measurements at smaller recoil angle, which will result in a higher proton recoil energy and hence a better energy resolution.

The YAP proton spectrometer used in the measurements showed good performance and is a good candidate for the final PRT spectrometer. A possible alternative could be a $LaBr_3$scintillator, which would provide a faster scintillation time (16 ns) that would reflect in a lower pile-up level. Drawbacks of this second choice are a higher cost and the fact that this crystal is hygroscopic and would require an "ad-hoc" casing with thin entrance window.

2013 JINST 8 P11008

The upgraded PRT spectrometer will be used for measurements on VESUVIO in order to test its performance. The results of this work are relevant for CHIPIR and possibly for other fast neutron applications.

7 Conclusions

A PRT spectrometer prototype was installed at the ISIS spallation source for fast neutron measurements. The optimization of the setup and off-line coincidence analysis was mostly devoted to reduce the background and distinguish recoil proton events. This allowed for the first measurements of the neutron spectrum in the 30–80 MeV energy range using a PRT spectrometer on a spallation source beam line. The success of these experiments demonstrates the feasibility of the method and indicates further improvements leading to the design of an upgraded PRT spectrometer that will be used for fast neutron spectroscopy on the CHIPIR beam-line.

References

[1] The ISIS pulsed neutron and muon source at the Rutherford Appleton Laboratory webpage, http://www.isis.stfc.ac.uk/.

[2] E. Normand, *Single event upset at ground level*, *IEEE T. Nucl. Sci.* **43** (1996) 2742.

[3] P.E. Dodd, M.R. Shaneyfelt, J.R. Schwank and G.L. Hash, *Neutron-induced soft errors, latchup, and comparison of SER test methods for SRAM technologies*, in proceedings of *International Electron, Device Meeting*, Albuquerque U.S.A. (2002), pg. 333.

[4] A. Pietropaolo et al., *Single-crystal diamond detector for time-resolved measurements of a pulsed fast-neutron beam*, *Europhys. Lett.* **92** (2010) 68003.

[5] A. Pietropaolo et al., *Fission diamond detectors for fast-neutron ToF spectroscopy*, *Europhys. Lett.* **94** (2011) 62001.

[6] M. Rebai et al., *Fission diamond detector tests at the ISIS spallation neutron source*, *Nucl. Phys.* **B 215** (2011) 313.

[7] M. Rebai et al., *Diamond detectors for fast neutron measurements at pulsed spallation sources*, 2012 *JINST* **7** C05015.

[8] F. Murtas et al., *Triple GEM gas detectors as real time fast neutron beam monitors for spallation neutron sources*, 2012 *JINST* **7** P07021.

[9] G. Croci et al., *nGEM fast neutron detectors for beam diagnostics*, *Nucl. Instrum. Meth.* **A 720** (2013) 144.

[10] G. Croci et al., *nGEM neutron diagnostic concept for high power deuterium beams*, 2012 *JINST* **7** C03010.

[11] G. Croci et al., *Measurements of γ-ray sensitivity of a GEM based detector using a coincidence technique*, 2013 *JINST* **8** P04006.

[12] G.F. Knoll, *Radiation detection and measurement*, Wiley (2010).

[13] C. Andreani et al., *Facility for fast neutron irradiation tests of electronics at the ISIS spallation neutron source*, *Appl. Phys. Lett.* **92** (2008) 114101.

2013 JINST 8 P11008

[14] C. Andreani et al., *CdZnTe detector for deep inelastic neutron scattering on the VESUVIO spectrometer*, *Appl. Phys.* **A 78** (2004) 903.

[15] Hamamatsu webpage, http://www.hamamatsu.com.

[16] N. Randazzo et al., *YAP(Ce) crystal characterization with proton beam up to 60 MeV*, *Nucl. Instrum. Meth.* A 586 (2008) 295.

[17] Quantum Detectors webpage, http://www.quantumdetectors.com/products/isis-neutron-beam-monitor.

[18] CAEN — Costruzioni Apparecchiature Elettroniche Nucleari S.p.A., DT5751 2/4 channel 10 bit 2/1 GS/s digitizer webpage, http://www.caen.it/csite/CaenProd.jsp?parent=14&idmod=632.

[19] G.J. Russell et al., *Introduction to spallation physics and spallationtarget design*, *AIP Conf. Proc.* **346** (1995) 93.

[20] Pietropaolo et al., *Characterization of the γ-background in epithermal neutron scattering measurements at pulsed neutron sources*, *Nucl. Instrum. Meth.* **A 568** (2006) 826.

[21] Pietropaolo et al., *γ-Ray background sources in the VESUVIO spectrometer at ISIS spallation neutron source*, *Nucl. Instrum. Meth.* **A 608** (2009) 121.

[22] MCNPX code website, http://mcnpx.lanl.gov/.

[23] V.T. Jordanov et al., *Digital techniques for real-time pulse shaping in radiation measurements*, *Nucl. Instrum. Meth.* **A 353** (1994) 261.

[24] V. Weisskopf, *Statistics and nuclear Reactions*, *Phys. Rev* **52** (1937) 295.

[25] J.F. Ziegler, *SRIM — The Stopping and Range of Ions in Solids*, http://www.srim.org/.

2013 JINST 8 P11008

Paper V

A Telescope Proton Recoil spectrometer for fast neutron beam-lines

C. Cazzaniga[1,2], M. Rebai[1,2], M. Tardocchi[2], G. Croci[2], M. Nocente[1,2], S. Ansell[3], C. D. Frost[3] and G. Gorini[1,2]

[1]*Università degli Studi di Milano-Bicocca, Dipartimento di Fisica, Piazza della Scienza 3, Milano, Italy*
[2]*Istituto di Fisica del Plasma "P. Caldirola", Associazione EURATOM-ENEA/CNR, Via Cozzi 53, Milano, Italy*
[3]*ISIS Facility, Science and Technology Facilities Council, Rutherford Appleton Laboratory, Didcot OX11 0QX, UK*

carlo.cazzaniga@mib.infn.it

Abstract

Fast neutron measurements were performed on the VESUVIO beam-line at the ISIS spallation source using a new Telescope Proton Recoil spectrometer. Neutrons are converted into protons via elastic scattering on a plastic target. Recoil protons are measured by a proton spectrometer, which use in coincidence a 1" thick YAP scintillator and a 500 μm thick silicon detector, measuring the full proton recoil energy and the partial deposited energy in transmission, respectively.

The VESUVIO fast neutron spectrum was measured up to 120 MeV and results are in good agreement with Monte Carlo simulation of the beam-line.

This instrument is of particular interest for the characterization of the ChipIr beam-line at ISIS, which was designed to feature an atmospheric-like neutron spectrum for the irradiation of micro-electronics.

1. Introduction

The new beam-line ChipIr has been built at the ISIS neutron source of the Rutherford Appleton Laboratory (UK) [1] for neutron irradiation experiments on electronic and avionic devices and systems . ChipIr is designed to feature a fast neutron spectrum that mimics the atmospheric one with approximately 10^8-10^9 times higher intensity at ground level and approximately 300 less at normal flight altitude [2]. Atmospheric radiation is a major concern to the reliability of micro-electronic devices, which, due to their constantly decreasing dimensions and increased functionality, are more susceptible to failures caused by Single Event Effects (SEE) [3-5]. Because of their intense flux and high Linear Energy Transfer, in the terrestrial environment neutrons represent the most important part of cosmic radiation producing single event upsets [6].

The VESUVIO beam-line at ISIS, featuring a 300K water moderator, was designed to have an under-moderated spectrum for studies in the eV energy range. Spallation neutrons, before the moderators, have a wide energy spectrum, ending at the energy of the proton beam (800 MeV). This configuration provides VESUVIO with an intense tail of fast neutrons ($5 \cdot 10^4$ neutrons cm^{-2} sec^{-1} with E_n >10 MeV), which has been exploited in recent years for micro-electronics irradiation [7-10].

The neutron energy spectrum and the flux spatial distribution of fast neutron beam-lines (e.g. ChipIr and VESUVIO) are determined on the basis of Monte Carlo calculations that try to reproduce the complexity of nuclear and intra-nuclear interactions up to 800 MeV. Direct measurements of these quantities are needed for the characterization of the neutron flux, to benchmark the simulations, and for a better understanding of the underlying physics of this kind of facilities.

Different kinds of fast neutron detectors have been used to measure the fast neutron flux [7,9-10] and several are proposed for fast neutron (E_n > 10 MeV) flux monitoring and imaging, such as diamond detectors [11-16] and gas detectors (nGEM) [17-20]. The threshold energy for fast neutrons of interest for SEE studies is commonly taken to be 10 MeV, under the assumption that the contribution of lower energy neutrons to the event rate is small [21]. A Telescope Proton Recoil spectrometer (TPR) was developed for a direct measurement of the fast neutron spectrum in the energy range 10 MeV < E_n < 120 MeV, where one can find SEE thresholds of most systems [21]. We present measurements in the 30 MeV < E_n < 120 MeV, and more experimental work will be needed to extend the masurement to the 10 MeV < E_n < 30 MeV range.

The TPR system is composed by a thin plastic foil to convert neutrons into recoil protons and a high resolution proton spectrometer.
A prototype TPR spectrometer was first tested on the VESUVIO beam line, and results are reported in Ref. [22]. In those preliminary measurements, a lithium glass scintillator was used for the transmission measurements (ΔE measurement), together with a 1" thick YAP crystal was used as proton spectrometer (E measurement) [22].
As a further development, the lithium glass scintillator has been replaced by a silicon detector for ΔE measurements. This solution allows for better background discrimination due to a better energy resolution on the ΔE and fast signals. In this paper the measurements performed with the TPR spectrometer in its final detector configuration on the VESUVIO beam-line are reported. The measured neutron spectrum is then compared to Monte Carlo Simulation.

2. Experimental setup

A TPR neutron spectrometer is composed of a hydrogenated target, to convert neutrons into protons via elastic scattering, and a proton spectrometer. A picture of the experimental setup of the TPR spectrometer on the VESUVIO beam-line is shown in Fig.1. A 2 mm thick polyethylene foil intercepts the entire beam cross section (about 5 cm in diameter). The proton spectrometer is placed clear of the neutron beam at 19 cm from the target and at an angle of 45 deg with respect to the neutron direction. At this angle recoil protons have 1/2 of the corresponding neutron energy, due to the elastic scattering kinematics.
Efficiency and energy resolution of the TPR system depend on several parameters that have to be optimized; the most relevant effects are the contribution of the target thickness and the kinematically smearing effect due to a finite solid angle of the telescope and a finite size of the neutron-beam profile at the polyethylene converter. For a complete discussion we refer to Ref.22, where the calculations of efficiency and energy resolution for this geometry have been presented. In the 30 MeV < E_n < 120 MeV range, an acceptable efficiency level (ranging from $7 \cdot 10^{-6}$ to $4 \cdot 10^{-6}$) was obtained at the price of relatively poor energy resolution (ranging from 40% to 30%).
The efficiency for neutrons in the 30 MeV < E_n < 120 MeV range is dominated by the elastic scattering macroscopic cross section. A review of the world database on np scattering differential cross section data up to 1000 MeV incident neutron energy can be found in Ref.23.
In this configuration of the TPR, the proton spectrometer is composed by a 500 μm thick silicon detector for ΔE measurement and a 2.54 cm thick YAP scintillator for E measurements. The YAP scintillator is thick enough to stop protons up to about 100 MeV [24]. Both detectors have a circular section with a diameter of 2.54 cm. The YAP crystal is coupled to a Hamamatsu R9420-100-10mod photo-multiplier-tube (PMT) [25], where a High Voltage (HV) of -600 V is applied. The Silicon Detector is coupled to a current preamplifier CIVIDEC C2 [26] with a HV of +170 V.
The YAP spectrometer was previously calibrated with gamma sources of ^{137}Cs and ^{60}Co. The ratio between the proton light yield to photon light yield is assumed to be 90% according to measurements performed at proton accelerators [27-29]. The Silicon Spectrometer was calibrated using ^{241}Am alpha source and with protons from 10 to 20 MeV at the Legnaro tandem accelerator [29].
Signals from the two detectors are fed into a 4 channel desktop digitizer with 1 GHz sampling frequency, 0-1 V input range and 10 bit resolution [30]. Since at the ISIS neutron source the beam is pulsed with a repetition frequency of 50 Hz, the board trigger is set on a reference signal (T_0) generated by the proton extraction from the synchrotron. For each T_0 a 3000 ns long waveform is stored for both detectors. Neutrons with E_n > 10 MeV fall inside this short time window. Fig.2 shows an example of the two detectors pulses recorded for the same T_0. The zero of the time scale is defined as the rising edge of the T_0 signal. Neutrons with E_n > 10 MeV are recorded into the "pre-trigger" (i.e. negative time in the figure), because they arrive before the T_0 signal. This is due to the electronics used to extract the T_0 signal at ISIS and it is suited for most of the instruments that work with a Time of Flight (ToF) in the ms time scale.

Due to the pulsed nature of the source, even if the global count rate is relatively low (the machine operates at 50 Hz), the instantaneous count rate is typically very high (> 1 MHz), more than one signal pulse is typically present within 1 μs window and pile-up is an important issue. A fast scintillation time (27 ns for the YAP crystal), a dedicated voltage divider and analysis algorithms are needed to cope with high count rate, keeping a good energy resolution [31-34]. The coincidence analysis is carried out *off-line* and includes Pulse Height (PH) and ToF spectral analysis. In the example of Fig.2, one can notice three E signals with PH > 50 mV (t = -825, -663 and -475 ns). Only the first two of these three have a corresponding ΔE signal from the Silicon detector, and can be associated to a recoil proton event.

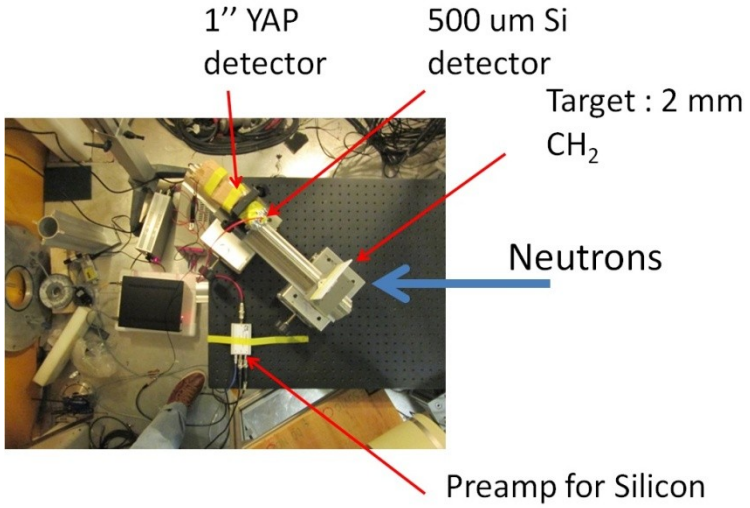

Fig.1: Picture of the experimental setup of a TPR spectrometer on the VESUVIO beam-line of the ISIS spallation source.

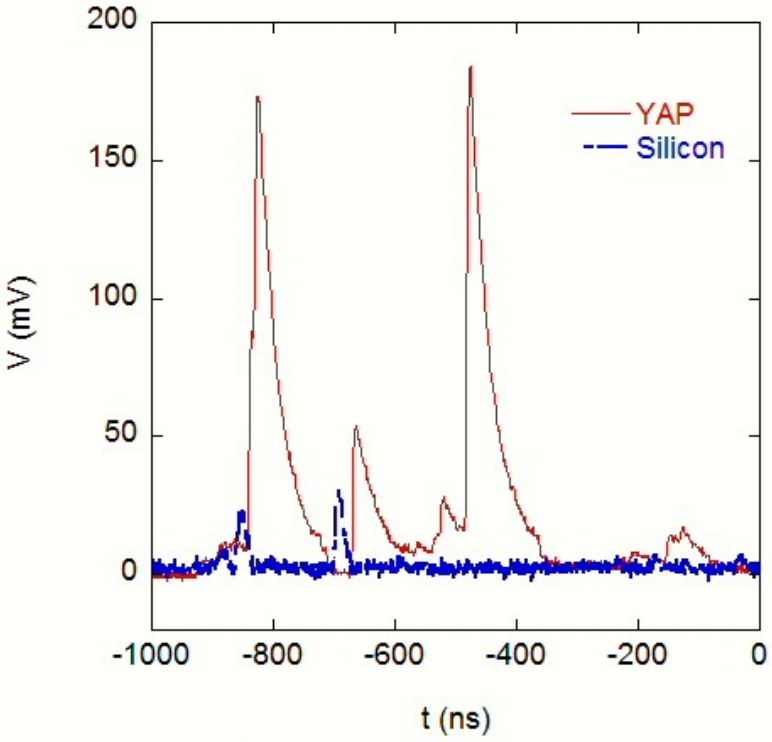

Fig.2: Example of signal pulses from the two detectors composing the TPR. The signal of the YAP is recorded directly after the PMT, while the Silicon signal is recorded after a current preamplifier.

3. Optimization of ΔE-E coincidence of TPR measurements

A proton recoil spectrometer could in principle use a single detector. Multiple detectors are used in coincidence to reduce the background of secondary particles induced by fast neutrons (i.e. γ-rays and charged particles) [35-38]. The coincidence analysis of the TPR was optimized off-line. Two events, E and ΔE, are considered to be in coincidence if the time difference Δt of their maxima falls inside a selected Δt window. Any rising edge in the waveform with amplitude above a *user-defined* threshold is defined as *event*. In order to reduce the probability of random coincidences, the Δt window must be set as short as possible. The Δt window is not centered to zero, since different time delays are introduced by the PMT and the preamplifier. The center of the Δt window was found using a routine that counts the number of coincidence events as a function of Δt. The result is plotted in Fig.3. True coincidence events appear in a peak, which rises over a continuum of random coincidences. According to these results, the Δt window was centered at -27.5 ns with a 10 ns width.

A further tool for data reduction is given by the relation between E and ΔE. Fig.4 shows the ΔE-E contour plot of coincidence events measured by the TPR. Proton related events have the characteristic distribution due to the *Bethe formula* [39]. Energy thresholds are defined accordingly; threshold on E is 8 MeV, which is the minimum energy for a proton to be transmitted by the silicon. Threshold on ΔE is set above the electronic noise. Protons can be measured up to 60 MeV with this system. Above this value the ΔE signal is too small (PH is less than 10 mV).

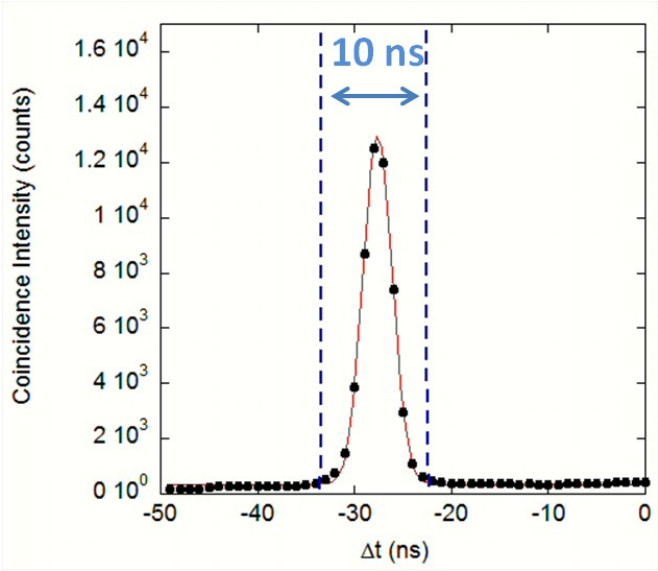

Fig.3: Coincidence events as a function of the time difference of YAP and Si events (E and ΔE). True coincidence events appear in a peak, which rises over a continuum of random coincidences. The continuous line is a Gaussian fit of the data. Dashed lines indicate the limit of the Δt window selected for the TPR measurements.

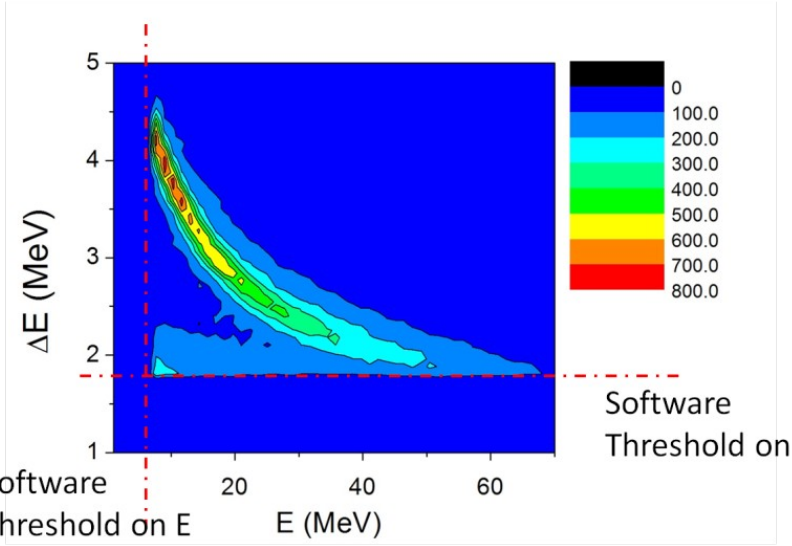

Fig.4: ΔE-E contour plot of coincidence events measured by the TPR. The chromatic scale (colors online) indicates the intensity of counts. Dashed lines indicate software energy threshold used for the off-line analysis.

4. Results

The results of the ToF and PH coincidence analysis are presented in Fig.5 and Fig.6, respectively. A measurement without the scattering target («no target» in Fig.5 and Fig.6) was carried out to estimate the background level and it is shown for comparison normalized to the integrated beam current.

The time distribution of the coincidence counts reflects the double bunch structure of the ISIS proton beam. Every proton bunch is 70 ns wide and for this reason neutron spectroscopy in the MeV range or above is impossible with ToF analysis alone, due to the 11 meters of flight path, because the energy resolution would be too poor. However, it is possible to distinguish a clear difference between measurements with and without the scattering foil. The peaks in the background measurement (no target) are almost symmetric in ToF, centered at a ToF compatible with γ-rays. For this reason, this background is called *γ-flash*, even if it could be due to at least four processes, (1) γ-rays from the target, (2) γ-rays induced by spallation neutrons (hundreds of MeV) with a velocity not distinguishable from light, (3) charged particles (including protons) induced by spallation neutrons and (4) charged particles (including protons) induced by γ-rays via photonuclear reactions. Among those (3) and (4) are the most likely because can produce a coincidence ΔE-E event, while (1) and (2) can contribute only via random coincidences.

The ToF structures are broadened at higher ToF when the scattering target is present. These events are compatible with proton recoil of fast neutrons with energy 20 MeV < E_n < 120 MeV.

In the PH Spectrum, shown in Fig.6, it is possible to notice that the normalized intensity almost doubles with the presence of the target, and the slope of the spectrum is different. The proton energy is defined as ΔE + E.

In order to retrieve the neutron spectrum the data have been analyzed following the step listed here:

i. The background measurement was subtracted from the measured proton energy spectrum.
ii. The proton energy is corrected by adding the calculated energy loss in 19 cm of air [22].
iii. The neutron energy scale is set according to the scattering kinematics (i.e. the proton energy scale is multiplied by a factor of 2 at 45 deg).
iv. The neutron flux is found dividing the counts by the efficiency, which is a function of the neutron energy and by the area illuminated by the beam. The efficiency was calculated with MCNPX as presented in Ref.21.

The resulting neutron spectrum is presented in Fig.7 compared to the simulated neutron spectrum [7]. The intensity of the simulated spectrum was normalized to the measurement. The measured neutron flux in the

energy range 30 MeV < E_n < 120 MeV is (1.5 ± 0.2) · 10^4 n s^{-1} cm^{-2}, considering an average proton current of 160 µA. Extrapolating this result at lower energies, it corresponds to a neutron flux of (7.6 ± 0.9) · 10^4 n s^{-1} cm^{-2} for E_n > 10 MeV, at 180 µA proton current. For comparison, the reference value for VESUVIO, reported in Ref.7, is (5.8 ± 1) · 10^4 n s^{-1} cm^{-2} for E_n > 10 MeV at 180 µA proton current and the neutron flux measured by the TPR is compatible within 2σ. Ref.9 and Ref.10 report measurements of (8.3 ± 0.8) · 10^4 n s^{-1} cm^{-2} and (8.5 ± 1) · 10^4 n s^{-1} cm^{-2}, respectively.

To extrapolate the intensity in the 10 MeV < E_n < 30 MeV range, the simulated neutron spectrum with intensity normalized with respect to the measurement in the 30 MeV < E_n < 120 MeV range has been used.

It has to be reminded that the most important advantage of the TPR technique is the direct measurement of the energy spectrum, without the necessity of deconvolution algorithms. Concerning the spectral information, a good agreement between the measured and simulated neutron energy spectrum is found. As a discussion of the comparison between measurements and simulations, the following points must be addressed:

a. It has to be considered that the flux and spectrum measured by the TPR are an average over the 5 cm wide neutron beam area. The measurement was carried out at the back of the irradiation table (see Fig.1) and not in the center of the beam line tank. A correction for the distance resulting from the R^2 law allows a measurement on the table to be scaled to the centre of the tank [10].
b. The quality of the simulations can be affected by components of the beam line not included in the geometry and by lack of reliable nuclear cross sections above 20 MeV.
c. Errors in the TPR measurement shown in Fig.7 are estimated based on the Poisson counting statistics. The error in the measured neutron flux is considering also an error of 10% in the energy calibration of the proton spectrometer. Future measurements at a proton accelerator can diminish this error.
d. It is worth to notice that the simulation seems to overestimate the measured spectrum (or the measurement may underestimate the simulation) below 40 MeV and the trend seems to show more descripancy as the energy descreases. This can be explained by the fact that the energy resolution is poor when approacing the 30 MeV cut-off (see simulations in Ref.21). This has an effect of spectral broadening.
e. When the scattering target (as any other material) is put into the neutron beam, one can consider a distortion effect to the neutron spectrum, due to the interaction of neutrons with hydrogen and carbon nuclei of the target. This is a second order effect: the probability of interaction of a neutron with the target is in the order of 1%. Therefore, the probability of a double interaction (and similarly the difference in the neutron spectrum before and after the distortion) is in the order of 0.01%.

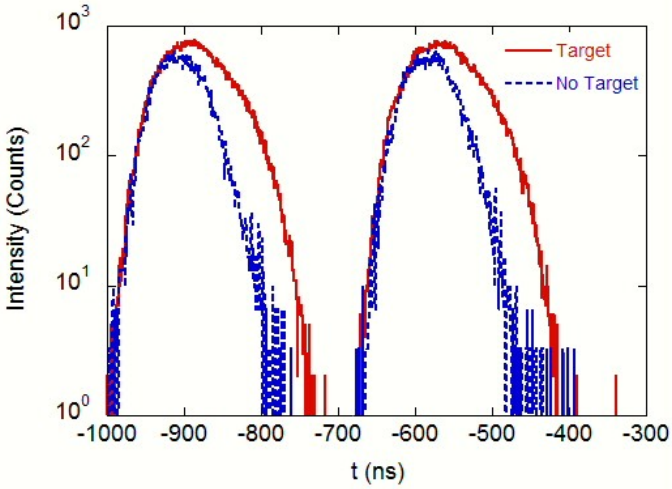

Fig.5: Time distribution of the coincidence counts with respect to the T_0 signal of the accelerator. Comparison with a background measurement without the polyethylene target is shown.

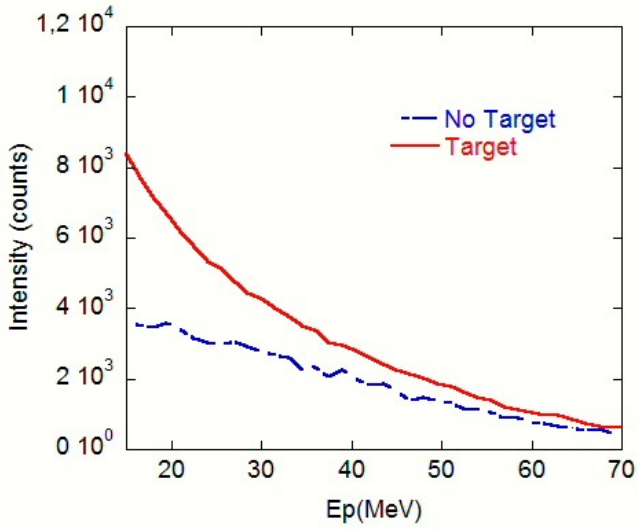

Fig.6: Recoil proton energy distribution of the coincidence counts. Comparison with a background measurement without the polyethylene target is shown.

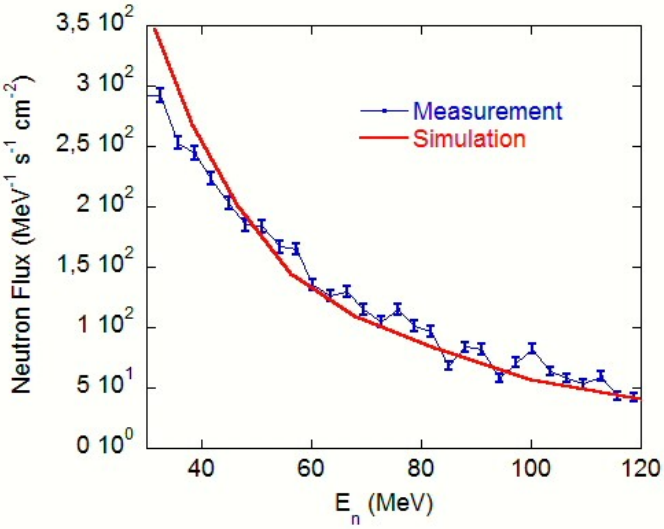

Fig.7: Neutron spectrum measured by the TPR compared to Monte Carlo simulation of the VESUVIO beam-line.

6. Conclusions

A Telescope Proton Recoil spectrometer was optimized for fast neutron measurements at pulsed spallation sources. Good background discrimination was obtained with the present detector configuration, using in coincidence a 500 µm Silicon detector and a 2.5 cm thick YAP scintillator. Measurements of the neutron spectrum of the VESUVIO beam line are presented in the 30 MeV < E_n < 120 MeV energy range, where the neutron flux was measured to be $(1.5 \pm 0.2) \cdot 10^4$ n s^{-1} cm^{-2} at 160 µA proton current. The measured spectrum shows a good agreement with Monte Carlo simulations of the VESUVIO beam line.

References

[1] Frost, Christopher D., Stuart Ansell, and G. Gorini. "A new dedicated neutron facility for accelerated SEE testing at the ISIS facility." *Reliability Physics Symposium, 2009 IEEE International*. IEEE, 2009.

[2] Gordon, M. S., et al. "Measurement of the flux and energy spectrum of cosmic-ray induced neutrons on the ground." *Nuclear Science, IEEE Transactions on* 51.6 (2004): 3427-3434

[3] Normand, Eugene. "Single event upset at ground level." *IEEE transactions on Nuclear Science* 43.6 (1996): 2742-2750.

[4] Taber, A., and E. Normand. "Single event upset in avionics." *IEEE Transactions on Nuclear Science* 40 (1993): 120-126.

[5] Dodd, P. E., et al. "Neutron-induced soft errors, latchup, and comparison of SER test methods for SRAM technologies." *IEDm: international electron devices meeting*. 2002.

[6] Ziegler, James F. "Terrestrial cosmic rays." *IBM journal of research and development* 40.1 (1996): 19-39.

[7] Andreani, C., et al. "Facility for fast neutron irradiation tests of electronics at the ISIS spallation neutron source." *Applied physics letters* 92.11 (2008): 114101-114101.

[8] Platt, Simon, et al. "Charge-collection and single-event upset measurements at the ISIS neutron source." *Nuclear Science, IEEE Transactions on* 55.4 (2008): 2126-2132.

[9] Bedogni, Roberto, et al. "Characterization of the neutron field at the ISIS-VESUVIO facility by means of a bonner sphere spectrometer." *Nuclear Instruments and Methods in Physics Research Section A: Accelerators, Spectrometers, Detectors and Associated Equipment* 612.1 (2009): 143-148.

[10] Smirnov, A. N., et al. "Application of thin-film breakdown counters for characterization of neutron field of the VESUVIO instrument at the ISIS spallation source." *Nuclear Instruments and Methods in Physics Research Section A: Accelerators, Spectrometers, Detectors and Associated Equipment* 687 (2012): 14-22.

[11] Pietropaolo, A., et al. "Single-crystal diamond detector for time-resolved measurements of a pulsed fast-neutron beam." *EPL (Europhysics Letters)* 92.6 (2010): 68003.

[12] Pietropaolo, A., et al. "Fission diamond detectors for fast-neutron ToF spectroscopy." *EPL (Europhysics Letters)* 94.6 (2011): 62001.

[13] Rebai, M., et al. "Fission diamond detector tests at the ISIS spallation neutron source." *Nuclear Physics B-Proceedings Supplements* 215.1 (2011): 313-315.

[14] Rebai, M., et al. "Diamond detectors for fast neutron measurements at pulsed spallation sources." *Journal of instrumentation* 7.05 (2012): C05015.

[15] Cazzaniga, C., et al. "A diamond based neutron spectrometer for diagnostics of deuterium-tritium fusion plasmasa)." *Review of Scientific Instruments* 85.11 (2014): 11E101.

[16] Cazzaniga, C., et al. "Single crystal diamond detector measurements of deuterium-deuterium and deuterium-tritium neutrons in Joint European Torus fusion plasmas." *Review of Scientific Instruments* 85.4 (2014): 043506.

[17] Murtas, F., et al. "Triple GEM gas detectors as real time fast neutron beam monitors for spallation neutron sources." *Journal of instrumentation* 7.07 (2012): P07021.

[18] Croci, G., et al. "nGEM fast neutron detectors for beam diagnostics." *Nuclear Instruments and Methods in Physics Research Section A: Accelerators, Spectrometers, Detectors and Associated Equipment* 720 (2013): 144-148.

[19] Croci, G., et al. "nGEM neutron diagnostic concept for high power deuterium beams." *Journal of instrumentation* 7.03 (2012): C03010.

[20] Croci, G., et al. "Measurements of γ-ray sensitivity of a GEM based detector using a coincidence technique." *Journal of Instrumentation* 8.04 (2013): P04006.

[21] Platt, S. P., A. V. Prokofiev, and X. X. Cai. "Fidelity of energy spectra at neutron facilities for single-event effects testing." Reliability Physics Symposium (IRPS), 2010 IEEE, International. IEEE, 2010.

[22] Cazzaniga, C., et al. "First measurement of the VESUVIO neutron spectrum in the 30–80 MeV energy range using a Proton Recoil Telescope technique." *Journal of instrumentation* 8.11 (2013): P11008.

[23] Blomgren, J., N. Olsson, and J. Rahm. "How strong is the strong interaction? The πNN coupling constant and the shape and normalization of np scattering cross sections." *Physica Scripta* 2000.T87 (2000): 33.

[24] J. F. Ziegler, SRIM - *The Stopping and Range of Ions in Solids*, http://www.srim.org/

[25] Hamamatsu webpage, http://www.hamamatsu.com

[26] CIVIDEC webpage, http://www.cividec.at

[27] Cazzaniga, C., et al. "Thin YAP: Ce and $LaBr_3$: Ce scintillators as proton detectors of a thin-film proton recoil neutron spectrometer for fusion and spallation sources applications." *Nuclear Instruments and Methods in Physics Research Section A: Accelerators, Spectrometers, Detectors and Associated Equipment* 751 (2014): 19-22.

[28] Fazzi, A., et al. "A large area SiPM array coupled to a $LaBr_3$ crystal for a TPR spectrometer." *Nuclear Science Symposium and Medical Imaging Conference (NSS/MIC), 2013 IEEE*. IEEE, 2013.

[29] Perelli Cippo, E., et al. "Light Response of $LaBr_3$ and YAP Scintillators to 5-20 MeV protons for applications to thin-foil proton recoil neutron spectrometer" *poster presented at the 7th International Conference on New Developments in Photodetection*, Tours, France, June 30th to July 4th, 2014

[30] CAEN — Costruzioni Apparecchiature Elettroniche Nucleari S.p.A., DT5751 2/4 channel 10 bit 2/1 GS/s digitizer webpage, http://www.caen.it/csite/CaenProd.jsp?parent=14&idmod=632.

[31] Nocente M., et al. "Energy resolution of gamma-ray spectroscopy of JET plasmas with a LaBr scintillator detector and digital data acquisition." *Review of scientific instruments* 81 (2010): 10D321.

[32] Nocente M., et al. "High-resolution gamma ray spectroscopy measurements of the fast ion energy distribution in JET 4He plasmas." *Nuclear Fusion* 52, no. 6 (2012): 063009.

[33] Nocente M., et al. "High Resolution Gamma Ray Spectroscopy at MHz Counting Rates With LaBr Scintillators for Fusion Plasma Applications." *Nuclear Science, IEEE Transactions on* 60, no. 2 (2013): 1408-1415.

[34] Nocente M., et al. "Experimental investigation of silicon photomultipliers as compact light readout systems for gamma-ray spectroscopy applications in fusion plasmas", *Rev. Sci. Instrum*. 85 (2014) 11E108

[35] Pietropaolo, A., et al. "Characterization of the γ background in epithermal neutron scattering measurements at pulsed neutron sources." *Nuclear Instruments and Methods in Physics Research Section A: Accelerators, Spectrometers, Detectors and Associated Equipment* 568.2 (2006): 826-838.

[36] Pietropaolo, A., et al. "γ-ray background sources in the VESUVIO spectrometer at ISIS spallation neutron source." *Nuclear Instruments and Methods in Physics Research Section A: Accelerators, Spectrometers, Detectors and Associated Equipment* 608.1 (2009): 121-124.

[37] Cazzaniga, C., et al. "Response of $LaBr_3$ (Ce) scintillators to 2.5 MeV fusion neutrons." *Review of Scientific Instruments*, *84*(12), (2013) 123505.

[38] Cazzaniga, C., et al. "$LaBr_3$ scintillator response to admixed neutron and γ-ray fluxes." *Nuclear Instruments and Methods in Physics Research Section A: Accelerators, Spectrometers, Detectors and Associated Equipment*, *732* (2013). 384-387.

[39] M. S. Livingston and H. A. Bethe, Revs. Modern Phys. 9, 285 (1937)

Paper VI

Nuclear Instruments and Methods in Physics Research A 732 (2013) 384–387

Contents lists available at ScienceDirect

Nuclear Instruments and Methods in Physics Research A

journal homepage: www.elsevier.com/locate/nima

$LaBr_3$ scintillator response to admixed neutron and γ−ray fluxes

C. Cazzaniga [a,b,*], G. Croci [b], L. Giacomelli [a], G. Grosso [b], M. Nocente [a,b], M. Tardocchi [b], G. Gorini [a,b], A. Weller [c], ASDEX Upgrade team

[a] Università degli studi di Milano Bicocca, Milano, Italy
[b] Istituto di Fisica del Plasma Piero Caldirola – CNR, Milano, Italy
[c] Max-Planck-Institut fuer Plasmaphysik, IPP-EuratomAssociation, Garching, Germany

ARTICLE INFO

Available online 11 June 2013

Keywords:
X- and γ−ray spectroscopy
Scintillation detectors

ABSTRACT

The γ−ray spectroscopy is a promising method for diagnosing fast ions and confined α particles in a fusion plasma device. This application requires γ−ray detectors with high energy resolution (say a few percent for γ−ray energies in the range 1–5 MeV), high efficiency and high count rate capability, ideally up to a few MHz. Furthermore, the detector will have to withstand the high 14 MeV and 2.45 MeV neutron fluxes produced by the main fusion reactions between deuterium and tritium. Experimental results demonstrate that the requirements on energy resolution, efficiency and count rate can be met with a $LaBr_3$(Ce) scintillator detector equipped with fast digital data acquisition. The measured response of the detector to 2.45 MeV neutrons is presented in this paper and discussed in terms of the interaction mechanism between neutrons and detector.

1. Introduction

A confined thermonuclear plasma is heated by α particles from Deuterium–Tritium (DT) reactions. These particles are produced with an energy of 3.5 MeV, much higher than the plasma bulk temperature (10–20 keV), and must slow down in order to release their energy into the plasma. The study of α−particles and more generally of fast ion confinement is therefore a crucial topic for future thermonuclear plasma experiments, such as ITER. Fast ions induce magneto-hydro-dynamics (MHD) instabilities and can lead to the loss of energetic particles, which are potentially harmful for plasma control and for the integrity of the machine. However, very few diagnostic techniques of fast ions are available today for confined energetic particles in the MeV energy range. Neutron spectroscopy provides diagnostic information on the reactants' energy distribution, and can be used for fast ion studies, as demonstrated with measurements in present day tokamaks [1–5]. More recently, γ−ray spectroscopy demonstrated to be a candidate diagnostics for confined fast ions observations [6–8]. The γ−ray emission is typically relevant for fast ion energies of some hundred keV, as a consequence of the underlying cross-sections. Many γ−ray emitting reactions are possible between fast ions and impurities in the plasma. Beryllium will be naturally present as an impurity in ITER plasmas, since it is the main component of tokamak's first wall. Most promising for diagnosis of α particles is the reaction $n\gamma)^9Be(\alpha, n\gamma)^{12}C$ [9,10].

A spectrometer suited for this application must have a good energy resolution (say a few percent for γ−ray energies in the range 1–5 MeV) and be able to cope with a few MHz count rate. Energy resolution is essential to perform spectral analysis that can provide information on the fast ion energy distribution (e.g. Doppler broadening). High rate capability is necessary for time resolved measurements crucial in order to measure fast transients in the γ−ray counting rate associated to MHD instabilities in the plasma.

First observations of γ−ray spectral broadening in fusion plasmas were reported in Ref. [7]. The measurements were performed in radio-frequency heated (^{3}He)D plasmas of the JET tokamak using a High Purity Germanium (HPGe) spectrometer, which permits high energy resolution (<2.8 keV at 1.33 MeV). The measured γ−ray peak shape was reproduced using a physics model that combined the kinetics of the reacting ions with a detailed description of the nuclear reaction differential cross-sections and branching ratios.

However, the HPGe detector does not allow for high rate measurements in the MHz range, which is required if one wants to study fast ion dynamics on characteristic time scales of MHD instabilities (a few ms). For this reason a spectrometer based on the $LaBr_3$ scintillator has been specifically developed. High energy resolution is made possible by the high scintillation light yield of the crystal (about 63 000 photons per MeV) [11,12]. $LaBr_3$ spectrometers were designed to be able to cope with high counting rate measurements (up to a few MHz), with an ad hoc developed active voltage divider for the photomultiplier tube and a fast digital data acquisition (see [13]).

* Corresponding author at: Istituto di Fisica del Plasma Piero Caldirola – CNR, Milano, Italy. Tel.: +39 0266173458.
E-mail addresses: carlo.cazzaniga@mib.infn.it, cazzaniga.carlo87@gmail.com (C. Cazzaniga).

0168-9002/$ - see front matter © 2013 The Authors. Published by Elsevier B.V. All rights reserved.
http://dx.doi.org/10.1016/j.nima.2013.05.055

2. Performance of the new $LaBr_3$ spectrometer

A 3 in. × 6 in. (diameter × height) $LaBr_3$ scintillator was developed for measurements at the JET tokamak in the United Kingdom. The detector was fully characterized and now regularly takes data during JET plasma experiments. Energy calibration measurements were carried out using radioactive sources, such as ^{137}Cs and ^{60}Co, and were successfully reproduced with Monte Carlo simulations using the MCNPX code [14]. The model used in the simulations included details of the geometry and of the materials surrounding the crystal, such as iron shielding and steel supports, which are important due to the effect of high-Z materials on γ−ray scattering. Fig. 1 shows a comparison between the measured and simulated spectrum for a ^{137}Cs (a) and a ^{60}Co (b) radioactive source. Spectral broadening due to the finite energy resolution of the spectrometer is included in the simulation. The measured energy resolution ($R = FWHM/E$) is 3.3% at the 662 keV peak, 2.5% at the 1173 keV peak and 2.4% at the 1333 keV peak. Spectra are normalized to the full-energy-peak height. There is very good agreement between simulation and data, which holds both at the Compton-edge level and in the low energy back-scattering region. Small differences are ascribed to minor details of the actual experimental setup. This confirms the reliability of the MCNPX model of the detector for determining its response function to γ−rays of different energies. Simulations have been performed using the MCNP model in order to evaluate the efficiency as a function of the γ−ray energy. Full-energy-peak efficiency (ϵ_{peak}) is defined as the number of events in the full-energy-peak divided by the number of photons impinging on the detector. Results are shown in Fig. 2. Every point is obtained with a simulation of 10^6 events, resulting in very low relative errors (< 0.2%). The 3 in. × 6 in. $LaBr_3$ scintillator has a very high efficiency thanks to high effective Z, high density and big volume.

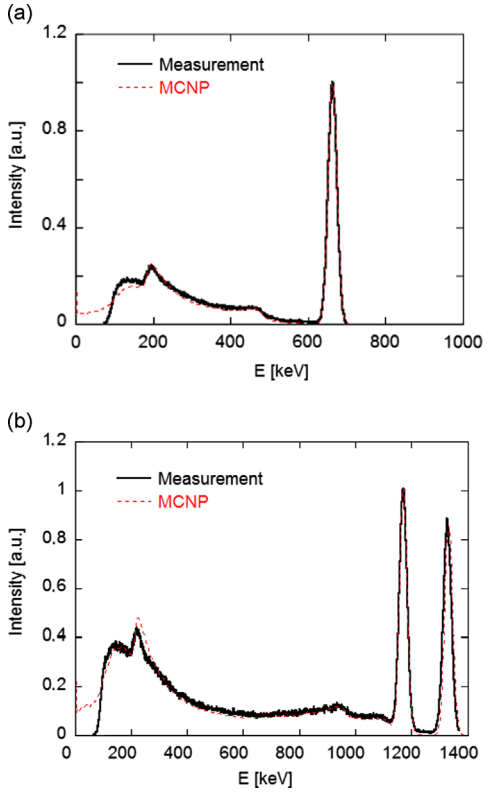

Fig. 1. Simulated and measured energy spectrum using a $LaBr_3$ scintillator for a ^{137}Cs (a) and a ^{60}Co (b) radioactive source.

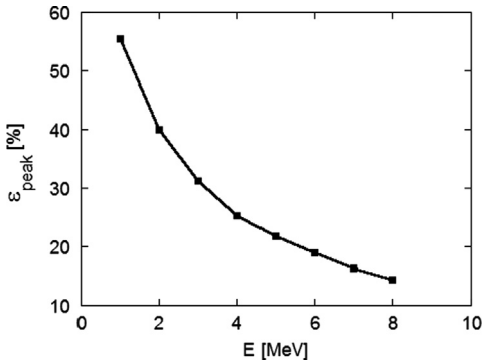

Fig. 2. Simulated full-energy-peak efficiency as a function of the γ−ray energy for a 3 in. × 6 in. $LaBr_3$ scintillator.

Full-energy-peak efficiency is 25% at 4.44 MeV, which is the energy of γ−rays from the reaction $^9Be(\alpha, n\gamma)^{12}C$.

High rate capability was a fundamental goal when the design of the detector was first presented in 2008 [15]. An important hardware component to be carefully optimized is the photo-multiplier-tube (PMT). PMTs are known to be affected by gain drifts when the counting rate of the source varies. This is due to the fact that an increasing mean photoelectric current running between the dynodes results in a voltage drop in the divider chain, which in turn causes a gain modification [16]. A PMT with a custom developed active base, which includes transistors in the last three stages, has been developed and optimized for this application. This PMT is an eight stage Hamamatsu R6233-01 with a length of 223 mm and a diameter of 82 mm. The gain at the nominal High Voltage (HV) of −1000 V is 2.7×10^5. The gain stability was tested as a function of the frequency using a LED source for different values of the HV (see [15]).

The detector's high rate capability was demonstrated in dedicated experiments at nuclear accelerators [17,18]. A not significant degradation in energy resolution was found for count rates up to 2.6 MHz (R=2.0% at $E_\gamma = 3$ MeV), using HV=−800 V. The mean position of the peaks was also unchanged between measurements at 80 kHz and 2.6 MHz, showing that no appreciable variations of the PMT gain occurred (see [18]). High rate capability has been further verified during tokamak discharges. Experiments were performed at the ASDEX Upgrade (AUG) tokamak in Garching (Germany), where the detector was installed on a collimated line of sight, 12 m away from the plasma [19,23]. The detector allowed the first γ−ray spectroscopy measurements of confined fast ions on AUG [20]. AUG operates with deuterium plasmas, which means that the main components of the emitted neutron spectrum are 2.45 MeV neutrons from Deuterium–Deuterium (DD) reactions. Deuterium plasmas with high Neutral Beam Injection (NBI) power have a high neutron yield, mostly from beam–plasma reactions.

At AUG the neutron flux at the detector position was about 1.7×10^4 neutrons/s/cm^2 considering a typical discharge with 7.4 MW of NBI (92 kV deuterons). These kind of plasmas are poor in fast ions in the MeV energy range, which is reflected in a negligible fast ion induced γ−ray emission. However, neutrons produce background γ−rays when they directly interact with the detector or surrounding materials. In Fig. 3 temporal variations in the measured counting rate of the $LaBr_3$ spectrometer for a discharge with 7.4 MW NBI are shown. The counting rate reaches values very close to 1 MHz. One can notice long time scale variations (a), due to modulation of the NBI power and RF power. Fast variations (b) can be attributed instead to changes in the power coupling due to bulk plasma instabilities such as, for instance, sawteeth.

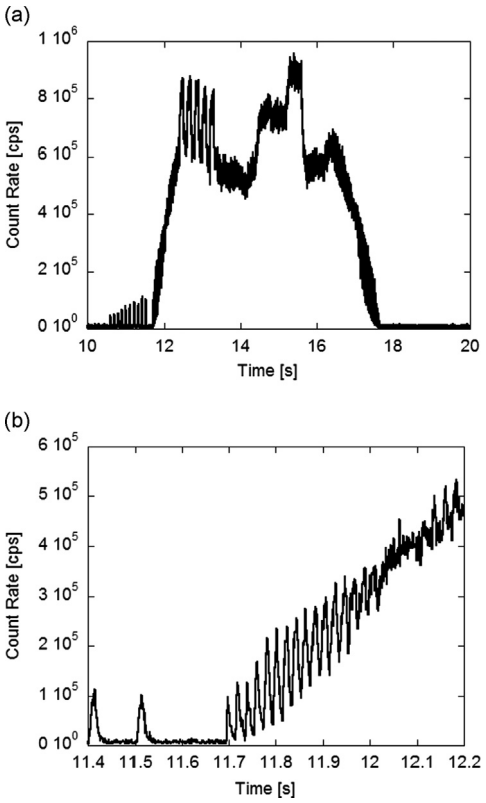

Fig. 3. Temporal evolution of the counting rate of the $LaBr_3$ spectrometer as a function of time for AUG discharge # 26328 (a). In (b) a magnification of (a) for the range 11.4–12.2 s. An offset of about 10 s with respect to the AUG time base is present.

3. $LaBr_3$ response to fusion neutrons

In view of $\gamma-$ray spectroscopy measurements on fusion burning plasmas, one must consider experimental constraints posed by high neutron fluxes, which will be orders of magnitude larger than in today's tokamak experiments (up to 10^8–10^9 neutrons cm^{-2} s^{-1} at the detector position without neutron filters [21]). The 2.45 MeV neutrons emitted from fusion reactions in a deuterium plasma can interact with $LaBr_3$ through nuclear inelastic scattering. As a result of this interaction the constituent nuclei of $LaBr_3$, i.e. ^{139}La, ^{79}Br and ^{81}Br, are left in an excited state that de-excites by emission of (background) $\gamma-$rays [22]; the latter can interfere with the $\gamma-$signal from nuclear reactions induced by α particles or even paralyse the detector if the count rate saturates the detector capabilities. As said before, the measurements from AUG plasmas heated by NBI power were characterized by intense 2.45 MeV neutron fluxes. These data were then compared to preliminary measurements of the response of the $LaBr_3$ $\gamma-$ray spectrometer to 2.45 MeV mono-energetic neutrons performed at the Frascati Neutron Generator (FNG). At FNG a deuteron beam was accelerated on a deuterium target, providing a neutron flux on the detector surface of about 8×10^4 neutrons per second. Fig. 4 shows a comparison between the energy spectra measured at AUG and at FNG. Each spectrum was separately energy-calibrated using radioactive ^{137}Cs and ^{60}Co sources and normalized to a total counting statistics of 1.5×10^4. The measured spectra are fairly similar for $E < 1.5$ MeV. At larger gamma energies, however, the different neutron energy spectra at AUG and FNG play a role. At AUG, high energy NBI deuterons reacting with the bulk plasma thermal D population give rise to neutrons of energy $E_n = 2.45 \pm 0.3$ MeV. At the FNG accelerator with the spectrometer positioned at 90° with respect to the deuteron beam impinging onto the target, the neutron energy spectrum is quite narrow around 2.45 MeV. This is probably the reason for the different

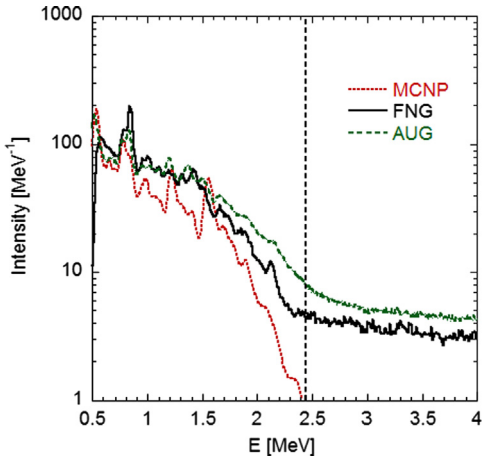

Fig. 4. The $\gamma-$ray energy spectra from 2.45 MeV fusion neutrons interacting on a $LaBr_3$ scintillator, measured at AUG and FNG, and simulated with MCNP. The dashed line indicates the 2.45 MeV energy value.

slopesof the spectra for $1.5 < E < 2.5$ MeV (see Fig. 4). The events with $E > 2.5$ MeV are mostly due to $\gamma-$rays emitted by neutron capture on surrounding materials. This was different in the two experiments, as it depends on details of the specific environment where the experiment is carried out. However, the fact that there are only few neutron induced events for $E > 2.45$ MeV confirms the 2.45 MeV neutron origin and it is promising, as $\gamma-$rays of interest for plasma diagnostics are expected to show up in the energy range $E_\gamma =$ 2–5 MeV.

The role of nuclear inelastic scattering from fusion neutrons was investigated with a preliminary MCNP model in which the interaction process is divided into two steps. In the first one, the energy distribution of $\gamma-$rays born from the interaction of a uniform beam of 2.45 MeV neutrons impinging on the $LaBr_3$ crystal is simulated. In the second step, the resulting neutron-induced $\gamma-$ray spectrum is used as input for a new MCNP simulation aimed at evaluating the interaction of these neutron-induced $\gamma-$rays with the crystal. According to MCNP simulation, an average number of 1.14 $\gamma-$rays per neutron is produced. Due to the large volume of the crystal, it is likely that the same neutron interacts more than once via inelastic scattering. The average probability of an emitted $\gamma-$ray to give a signal, considering the low energy threshold ($E > 100$ keV) is 65%. It is possible to notice in Fig. 4 that the main structure of the measured neutron-induced spectra is only partially reproduced in the region $E < 2.45$ MeV. Differences in single peaks and in details of the spectral structures are explained by the fact that other materials than $LaBr_3$ are not included in the simulation. For the same reason the spectrum region $E > 2.5$ MeV is not reproduced, since it is due to $\gamma-$rays emitted by neutron capture on surrounding materials. A more detailed MCNP model will be implemented in order to reproduce the full spectrum. This model will (1) include surrounding materials and line of sight and (2) consider the complete neutron spectrum emitted by the plasma, rather than just the main 2.45 MeV component. Starting from the understanding of the interaction mechanisms of 2.45 MeV neutrons, one must study the response function of the $LaBr_3$ crystal to 14-MeV neutrons emitted from deuterium–tritium plasmas of a thermonuclear device. Based on cross-section values, reactions of the type (n,2n) are expected to play a significant role, which results in an increased sensitivity of the detector to 14-MeV neutrons [22].

4. Conclusions and outlook

In this paper the energy resolution, efficiency for $\gamma-$rays in the MeV energy range and high rate capability of a $LaBr_3$ scintillator

have been assessed in view of γ−ray measurements on next-step fusion devices. The response of $LaBr_3$ detectors to 2.45-MeV neutrons was presented and compared with a preliminary MCNP simulation. A $LaBr_3$ detector is now installed at the JET tokamak and will collect data with two main goals: (1) γ−ray measurements for confined fast-ion diagnostics at JET and (2) measurements of the $LaBr_3$ response to fusion neutrons. The reported results provide the basis for the conceptual design of optimized $LaBr_3$ detectors for fusion burning plasmas.

References

[1] J. Kaellne, et al., Physical Review Letters 85 (2000) 1246.
[2] M. Nocente, G. Gorini, J. Kallne, M. Tardocchi, Nuclear Fusion 51 (2011) 063011.
[3] C. Hellesen, et al., Nuclear Fusion 50 (2010) 084006.
[4] M. Gatu Johnson, et al., Nuclear Fusion 50 (2010) 045005.
[5] M. Gatu Johnson, et al., Review of Scientific Instruments 81 (2010) 10D336.
[6] I. Proverbio, et al., Review of Scientific Instruments 81 (2010) 10D320.
[7] M. Tardocchi, et al., Physical Review Letters 107 (2011) 205002.
[8] M. Nocente, et al., Nuclear Fusion 52 (2012) 053009.
[9] V.G. Kiptily, et al., Nuclear Fusion 42 (2002) 999.
[10] V.G. Kiptily, et al., Plasma Physics and Controlled Fusion 48 (2006) R59.
[11] R. Nicolini, F. Camera, et al., Nuclear Instruments and Methods in Physics Research Section A 582 (2007) 554.
[12] E.V.D. van Loef, et al., Nuclear Instruments and Methods in Physics Research Section A 486 (2002) 254.
[13] M. Nocente, et al., Review of Scientific Instruments 81 (2010) 10D321.
[14] The MCNPX website: ⟨http://mcnpx.lanl.gov/⟩.
[15] M. Tardocchi, et al., Review of Scientific Instruments 79 (2008) 10E524.
[16] M. Tardocchi, et al., Nuclear Instruments and Methods in Physics Research Section A 485 (2002) 624.
[17] M. Nocente, et al., IEEE Transactions on Nuclear Science, in press.
[18] M. Nocente, et al., in: IEEE Nuclear Science Symposium Conference Record, 2011.
[19] L. Giacomelli, et al., Review of Scientific Instruments 82 (2011) 123504.
[20] M. Nocente, et al., Nuclear Fusion 52 (2012) 094021.
[21] I.N. Chugunov, et al., Nuclear Fusion 51 (2011) 083010.
[22] Cross Section Database ⟨http://atom.kaeri.re.kr/⟩.
[23] M. Tardini, et al, JINST 7 (2012), C03004.

Paper VII

Response of $LaBr_3(Ce)$ scintillators to 2.5 MeV fusion neutrons

C. Cazzaniga,[1,2,a)] M. Nocente,[1,2] M. Tardocchi,[2] G. Croci,[2] L. Giacomelli,[1] M. Angelone,[3] M. Pillon,[3] S. Villari,[3] A. Weller,[4] L. Petrizzi,[5] G. Gorini,[1,2] ASDEX Upgrade Team,[b)] and JET-EFDA Contributors[c)]

JET-EFDA, Culham Science Centre, Abingdon OX14 3DB, United Kingdom
[1]*University of Milano Bicocca, Piazza della Scienza 3, Milano 20125, Italy*
[2]*Istituto di Fisica del Plasma, Associazione EURATOM-ENEA-CNR, Via Roberto Cozzi 53, Milano 20125, Italy*
[3]*ENEA, C. R. Frascati, P.O. Box 65, I-00044 Frascati, Italy*
[4]*Max-Planck-Institut fuer Plasmaphysik, IPP-Euratom Association, Boltzmann str. 2, D-85748 Garching, Germany*
[5]*IAEA Representative at OECD Nuclear Energy Agency 12, Boulevard des Îles, F-92130 Issy-les-Moulineaux, France*

(Received 31 October 2013; accepted 28 November 2013; published online 19 December 2013)

Measurements of the response of $LaBr_3(Ce)$ to 2.5 MeV neutrons have been carried out at the Frascati Neutron Generator and at tokamak facilities with deuterium plasmas. The observed spectrum has been interpreted by means of a Monte Carlo model. It is found that the main contributor to the measured response is neutron inelastic scattering on ^{79}Br, ^{81}Br, and ^{139}La. An extrapolation of the count rate response to 14 MeV neutrons from deuterium-tritium plasmas is also presented. The results are of relevance for the design of γ-ray diagnostics of fusion burning plasmas. [http://dx.doi.org/10.1063/1.4847056]

I. INTRODUCTION

One of the primary goals of next step magnetic fusion devices is the understanding and control of a burning plasma. There is wide consensus among plasma physicists that the dynamics of a plasma close to ignition is largely dominated by the behavior of suprathermal particles,[1] which can be generated as products of the main fusion reactions (such as α particles from the $d + t \rightarrow n + \alpha$ reaction) or by external auxiliary heating. For this reason, the distribution function of the energetic ions, which are confined by the magnetic field in the plasma, needs to be measured. γ-ray spectroscopy is one of the few diagnostic techniques proposed for this scope.[2] Gamma-ray emission results from interactions between the energetic ions and impurities that are naturally found in the plasma.[2–4] Recently, γ-ray measurements at low counting rates and high energy resolution in present tokamak devices[5,6] have shown that other parameters of the fast ion energy distribution can be obtained by combining information on the intensity and shape of characteristic peaks of γ-ray reactions occurring in the plasma.[7–10] A review on neutron and gamma-ray measurements in tokamak plasmas for fast ion studies has been recently published in Ref. 3.

Unlike present devices, γ-ray measurements in next step tokamaks, such as ITER, will have to be performed at MHz counting rates, still with high-energy resolution, and under significant irradiation from 2.5 and 14 MeV neutrons produced by the main fusion reactions, $d + d \rightarrow n + {}^3He$ in deuterium plasmas and $d + t \rightarrow n + \alpha$ in deuterium-tritium. Dedicated solutions therefore need to be developed. A new scintillator material, $LaBr_3(Ce)$,[11,12] meets many of the requirements for γ-ray measurements at ITER. This detector is resilient to neutron damage, and first measurements at low counting rates at tokamak devices have been demonstrated.[10,13] High counting rate γ-ray measurements up to a few MHz were also shown at nuclear accelerators without any significant degradation of the energy resolution.[9] The effect of 2.5 and 14 MeV neutron irradiation on the detector has not yet been studied in detail. One study where the response of a 1.5 in. $LaBr_3(Ce)$ detector to neutrons produced by a conventional $^{241}Am/^9Be$ source was presented.[14] However, this result cannot be easily extrapolated for applications in fusion plasmas, due to the very different neutron spectrum of $^{241}Am/^9Be$ from that of deuterium and deuterium-tritium reactions.

In this paper we present dedicated measurements of the $LaBr_3(Ce)$ response to 2.5 MeV neutrons. The experiments were carried out at neutron accelerators and at tokamak devices with deuterium plasmas. The results are analyzed using a MCNP model to identify the main processes contributing to the observed response. Implications of the results for γ-ray measurements in a deuterium-tritium plasma of ITER are finally discussed.

II. $LaBr_3(Ce)$ RESPONSE TO 2.5 MeV MONO-ENERGETIC NEUTRONS

Measurements of the $LaBr_3(Ce)$ response to 2.45 MeV mono-energetic neutrons were performed at the Frascati Neutron Generator (FNG).[15] The crystal has a cylindrical shape with 3 in. diameter and 6 in. height. At FNG a deuteron beam was accelerated on a deuterium target, providing a neutron yield of 2×10^8 neutrons/s during the measurements. This figure was given by the standard neutron counting

a)carlo.cazzaniga@mib.infn.it
b)See authors list of U. Stroth *et al.*, "Overview of ASDEX Upgrade results," Nucl. Fusion **53**(10), 104003 (2013).
c)See the Appendix of F. Romanelli *et al.*, Proceedings of the 24th IAEA Fusion Energy Conference 2012, San Diego, USA.

diagnostics of FNG, which is based on calibrated organic scintillators. The detector was placed at about 1 m from the target, which resulted in a neutron fluence on the detector front surface of approximately 8×10^4 neutrons/s. The light produced by neutron interactions with the crystal was detected by an eight stage Hamamatsu R6233-01 photo multiplier tube (PMT). The PMT was equipped with a custom developed active base for gain shift minimization at high counting rates[16] and was operated at a high voltage $V_{HV} = 800$ V (for reference, the PMT nominal gain at $V_{HV} = 10^3$ V is 2.7×10^5). A commercially available 1 Gsample/s, 12 bit digitizer was used to record individual pulses from the PMT. The corresponding pulse height spectrum (PHS) was reconstructed off-line using dedicated software.[13]

The spectrum measured at FNG is shown in Figure 1 and can be compared with that of Figure 2. The latter is the spectrum measured by the same detector in the absence of neutron irradiation and entirely due to its intrinsic radioactivity. $LaBr_3(Ce)$ has an intrinsic background due to the radioactive ^{138}La isotope (present in trace concentrations of about 0.09%) and to actinides. These are manifested as distinctive structures in the spectrum from combined α, β, and γ decays.[12] In the presence of 2.45 MeV neutron irradiation (Figure 1), the intrinsic background spectrum cannot be anymore distinguished as neutron interactions with the crystal dominate the response. Figure 1 reveals a rather complex structure, where peaks at several energies appear, the most significant being at $E \approx 800$ keV. All structures are found in the region $E < 2.5$ MeV, whose area is about 90% of the whole spectrum. In the region $E > 2.5$ MeV, there is only a rough exponential tail of events, at a much lower amplitude. These high energy events are likely due to radiative capture of neutrons on the surrounding materials and on the detector itself.

The observed difference between the regions $E < 2.5$ MeV and $E > 2.5$ MeV can be qualitatively understood on the basis of the processes contributing to the measured response. The 2.5 MeV neutrons can interact with the crystal through radiative capture, inelastic, and elastic scattering. Of these three mechanisms, only radiative capture and inelastic scattering are of practical importance, as the recoil energy left behind by 2.45 MeV neutron elastic scattering on the heavy ^{139}La, ^{79}Br, and ^{81}Br isotopes ($\approx$100 keV at most) is well below the experimental energy threshold of our measurements ($\approx$500 keV). The cross section for neutron inelastic scattering on these three $LaBr_3$ isotopes is presented in Figure 3. Here we do not separate the individual curves corresponding to $LaBr_3$ isotopes left in different excited states after scattering, but we rather show their sum.

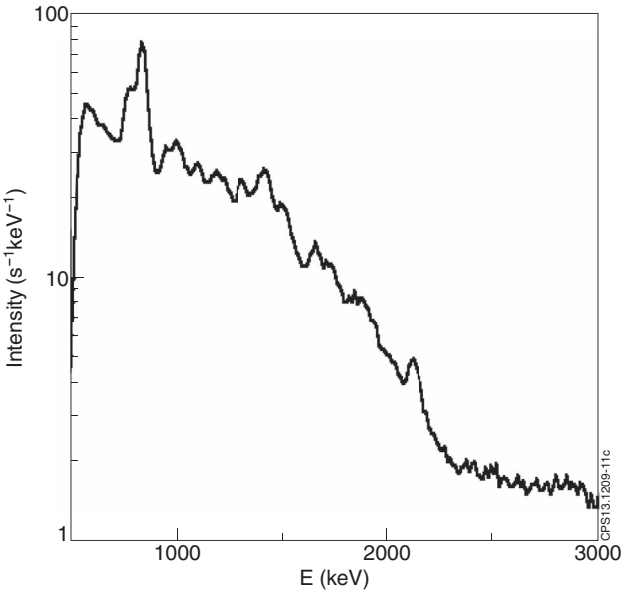

FIG. 1. Energy spectrum measured by a 3 in. × 6 in. $LaBr_3(Ce)$ detector from mono-energetic 2.5 MeV neutron irradiation at FNG.

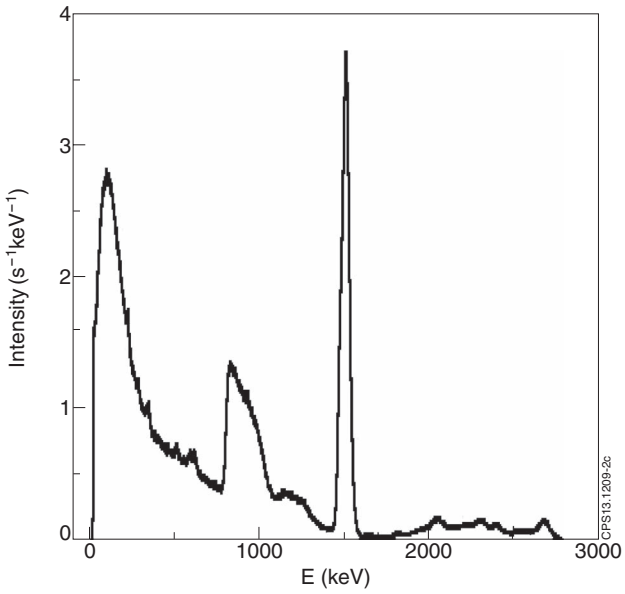

FIG. 2. Measured energy spectrum of the intrinsic background of a 3 in. × 6 in. $LaBr_3(Ce)$ scintillator.

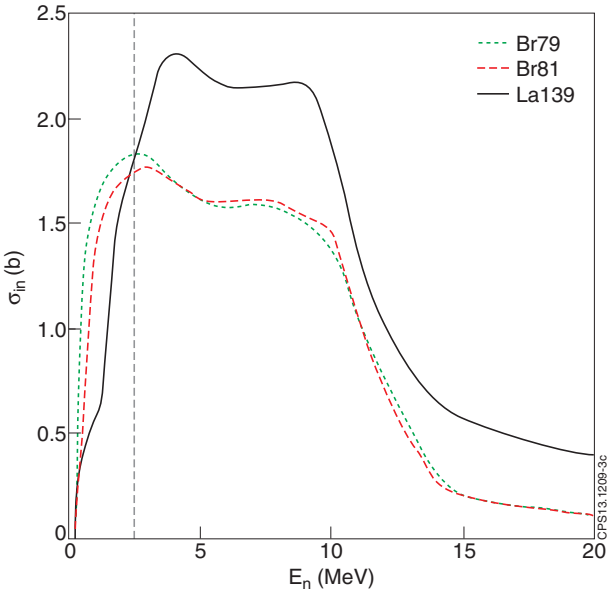

FIG. 3. Neutron inelastic scattering cross section on the three $LaBr_3$ isotopes ^{79}Be, ^{81}Br, and ^{139}La.[17] For each isotope, the summed curve for excitation into any level after neutron scattering is shown. The dashed line corresponds to 2.5 MeV.

At $E_n = 2.5$ MeV, inelastic scattering on ^{79}Br, ^{81}Br, and ^{139}La is equal likely, with a cross section $\sigma \approx 2$ b. For comparison, the cross section for radiative capture is $\sigma \approx 10$ mb at $E_n = 2.5$ MeV, which makes this process of relevance only in the presence of a significant amount of thermalized neutrons. Further processes involving neutron capture with production of charged particles in the exit channel (such as ^{79}Br(n,p)^{79}Se) are negligible at all neutron energies, due to their cross sections.

The spectrum of Figure 1 is compared with MCNP simulations in Sec. IV. Here we finally note that neutron inelastic scattering would explain why, as reported by Roberts *et al.*,[14] no neutron/gamma discrimination can be performed with $LaBr_3$(Ce). Neutron interactions with this scintillating material also result in γ-rays. The corresponding pulse shapes could not be thus distinguished from those of external γ-rays traversing the detector.

III. 2.5 MeV NEUTRON MEASUREMENTS AT TOKAMAKS WITH $LaBr_3$(Ce)

The $LaBr_3$ response to 2.5 MeV from d + d reactions was further measured at two different tokamaks, the Joint European Torus (JET) and ASDEX Upgrade (AUG), using the same measurement setup of FNG. Measurements of the scintillator response to fusion neutrons at the AUG tokamak have been first presented in Ref. 18. In both cases, deuterium plasmas were heated with deuterium neutral beam injection (NBI) at different power levels. In these conditions, the plasma is a good neutron source, where neutron emission mostly arises from reactions between deuterons in the beam and those in the plasma (beam-target reactions). The resulting neutron spectrum is roughly monoenergetic, with an energy spread of about 300 keV around the mean neutron energy $E_n = 2.45$ MeV.[19] This makes the experimental conditions of the measurements at JET and AUG comparable to those at FNG. The difference between the two measurements was the position of the detector with respect to the plasma. At AUG, $LaBr_3$(Ce) was placed 12 m from the plasma, along a collimated horizontal line of sight,[20] providing a neutron flux at the detector position of 1.7×10^4 neutrons s^{-1} cm^{-2}. At JET, instead, the distance from the plasma was 23 m, with a collimated vertical view. The neutron flux (0.8×10^4 neutrons s^{-1} cm^{-2}) was here reduced by a factor 2 only with respect to AUG. These are average values determined using AUG and JET neutron yield diagnostics information combined with a transport factor for the line of sights, presented in Refs. 20 and 21, respectively. In both cases, the detector was directly exposed to the 2.5 MeV neutron flux, with no shielding.

In order to verify that the measured signals are dominated by 2.5 MeV d + d neutron interactions with $LaBr_3$ (and not, for instance, by nuclear radiation of different origin emitted from the plasma), we can compare the measured counting rate as function of time with variations of the plasma neutron yield, measured by fission chambers (Figure 4). The strong correlation between the two traces is a clear indication of the 2.5 MeV neutron origin of the signal. Time variations in the measured traces are due to the specific plasma conditions of the measurements: slower variations can be ascribed to changes in the plasma temperature/density and NBI power; faster variations originate from plasma instabilities, such as sawteeth.

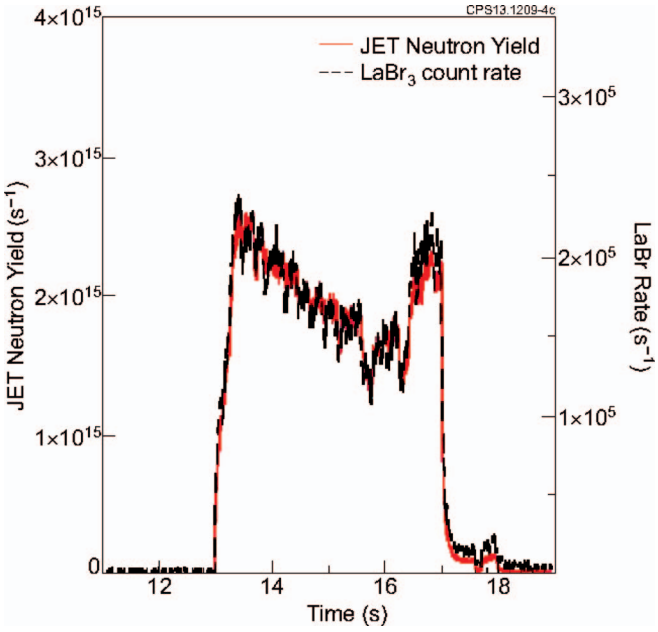

FIG. 4. Time evolution of the counting rate of the $LaBr_3$(Ce) spectrometer (dashed line) and JET total neutron yield measured with fission chambers for discharge #82539 (solid line).

The energy spectra measured at the JET and AUG tokamaks can be compared to the one measured at the FNG neutron source (see Fig. 5). Each spectrum was separately calibrated in energy using radioactive ^{137}Cs and ^{60}Co sources and normalized to an equivalent 150 kHz count rate. The JET and AUG spectra are acquired during single plasma discharges.

The three spectra show remarkable similarities in terms of peak positions and structures. In each case the main

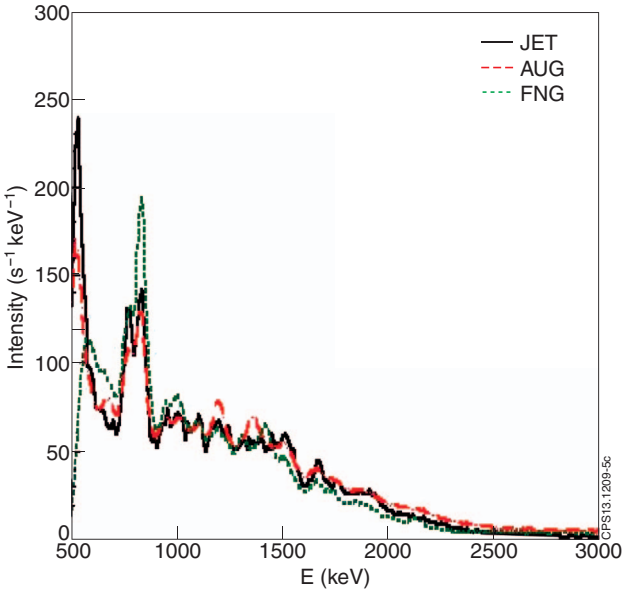

FIG. 5. Energy spectra induced by 2.5 MeV fusion neutrons on a $LaBr_3$(Ce) scintillator, measured at AUG (dashed), JET (solid), and FNG (dotted).

component of the spectrum presents counts recorded in the region $E < 2.5$ MeV, while there are only few events at $E > 2.5$ MeV. This fact confirms that the response is mainly dominated by 2.5 MeV inelastic neutron scattering. The differences between the three spectra can be ascribed to the following effects. The first is the additional contribution of γ-rays produced by neutrons that interact with materials surrounding the detector. This further background source was different in the three experiments, as it depends on details of the specific environment where the experiment was carried out. A second effect comes from the differences in the neutron energy spectra among the three measurements. At JET and AUG, high energy NBI deuterons reacting with the bulk plasma give rise to neutrons of energy $E_n = 2.45 \pm 0.3$ MeV. At the FNG accelerator, instead, the neutron energy spectrum is narrower around $E_n = 2.45$ MeV. Moreover, the scattered and moderated components of the neutron spectrum are different depending on details of the line of sight of each experiment. In spite of these differences, the similarity between the measurements indicates that the contribution from 2.5 MeV neutrons interacting with the detector is the dominant one. Finally, we note that neutron induced events mostly lie in the region $E < 2.5$ MeV, which is promising for γ-ray observations in deuterium plasmas, as most of the γ-ray emission from fast ions is expected in the range 2 MeV $< E <$ 6 MeV.

IV. DATA ANALYSIS

The role of nuclear inelastic scattering from fusion neutrons as the main contributor to the measured response has been investigated in detail using a MCNP[22] model. The interaction process has been divided into two steps, according to the optimal use of the F8 tally, i.e., the energy distribution of pulses created in a detector by radiation. In the first step, the energy distribution of γ-rays born from the interaction of a uniform, mono-energetic beam of 2.5 MeV neutrons impinging on the crystal is simulated. In the second step, the resulting neutron induced gamma-ray spectrum is used as input for a new MCNP simulation aimed at evaluating the interaction of these neutron born γ-rays with the crystal. The continuous-energy neutron data libraries ENDF62MT[23] are used to simulate γ-rays emitted by neutron interactions with lanthanum and bromine nuclei. The model used in the simulation includes a uniform beam of 2.45 MeV mono-energetic neutrons impinging on the front side of a 3 in. × 6 in. $LaBr_3$ crystal. No other material is included in the simulation. Figure 6 separately shows the γ-ray energy spectrum emitted by each individual isotope ^{139}La, ^{79}Br, and ^{81}Br. The number of excited levels, and therefore the number of corresponding γ-ray energies from de-excitation, is considerably high. Some of these lines are expected to be overlapped in the measured spectrum, due to the finite energy resolution of the spectrometer, thus appearing as complex structures. A second MCNP simulation was then carried out to take into account the efficiency of the crystal to neutron born γ-rays of different energy. In this case the output γ-rays of the first simulation are used and are assumed to be uniformly distributed in the whole crystal volume. The simulation of the detector response to mono-energetic γ-rays was benchmarked with measurements as presented in Ref. 18. Table I summarizes the main results of the simulations. On average, $N_\gamma = 1.14$ γ-rays per neutron are produced. The fact that N_γ is larger than 1 is due to multiple inelastic neutron scattering. In fact, the mean free path of a 2.5 MeV neutron in $LaBr_3$ is about 7 cm, which is about half of the crystal length (15.24 cm = 6 in.). The probability for an emitted γ-ray to give a count, i.e., the number of γ-rays that deposit in the crystal an energy above a certain threshold divided by the number of histories is 0.7 when the threshold on deposited energy is $E_{th} = 2$ keV. This value decreases for higher thresholds; for instance, it becomes 0.65 at $E > 100$ keV. Therefore, we can calculate the detection efficiency to 2.5 MeV neutrons by combining N_γ with the γ-ray detection probability. The result is 0.76 counts per neutron in the region $E > 2$ keV.

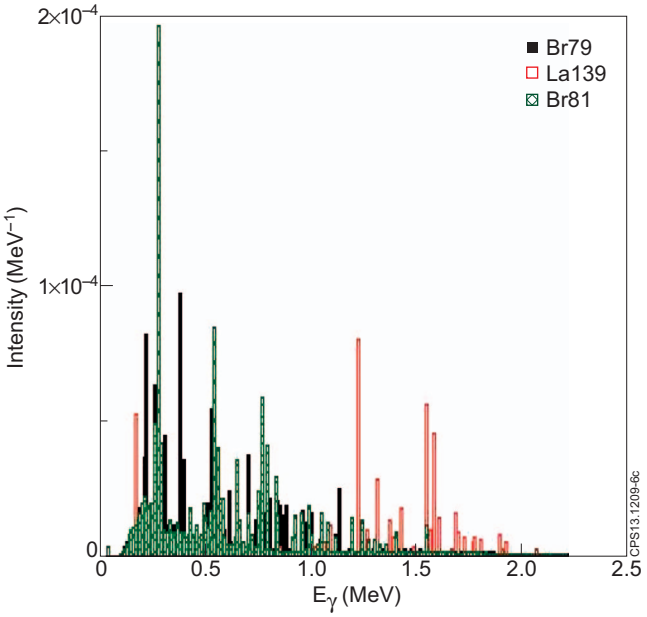

FIG. 6. Energy distribution of γ-rays induced by 2.5 MeV mono-energetic neutrons simulated with MCNP for a 3 in. × 6 in. $LaBr_3$ detector. The contribution of each individual isotope is shown separately.

The spectrum obtained with MCNP simulations can be compared to that measured from JET deuterium plasmas (Figure 7). An experimental energy broadening has been added to the MCNP simulation for comparison with measurements at JET. Both spectra in Figure 7 are normalized to same height. Simulation and measurements are consistent, as the same peaks and structures are found. The small differences observed are due to the following reasons. First of all, we have not included any other material in the simulation but the $LaBr_3$ crystal. Background gamma rays induced by neutron interactions with the tokamak main components and materials surrounding the detector are therefore not accounted for by

TABLE I. Summary of the MCNP simulation results for 2.5 MeV neutrons impinging on a 3 in. × 6 in. $LaBr_3$ detector.

Emitted γ-rays per neutron	1.14
Counts per emitted γ-ray	0.7
Counts per neutron	0.76

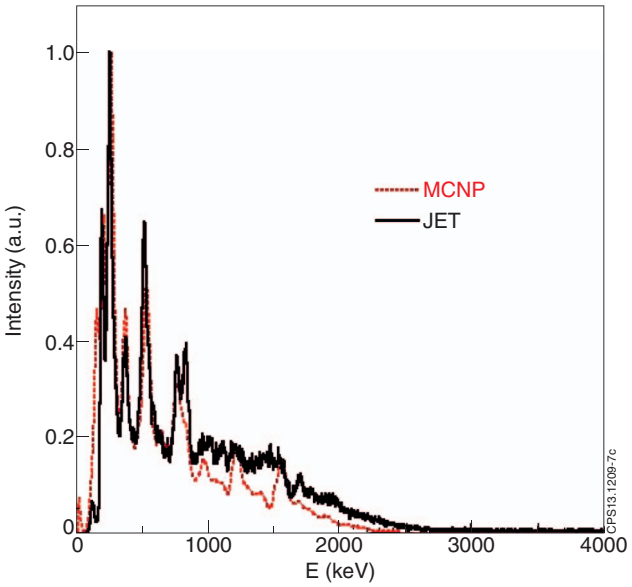

FIG. 7. Response spectrum of a $LaBr_3$(Ce) detector to 2.5 MeV neutrons simulated with MCNP and measured at JET.

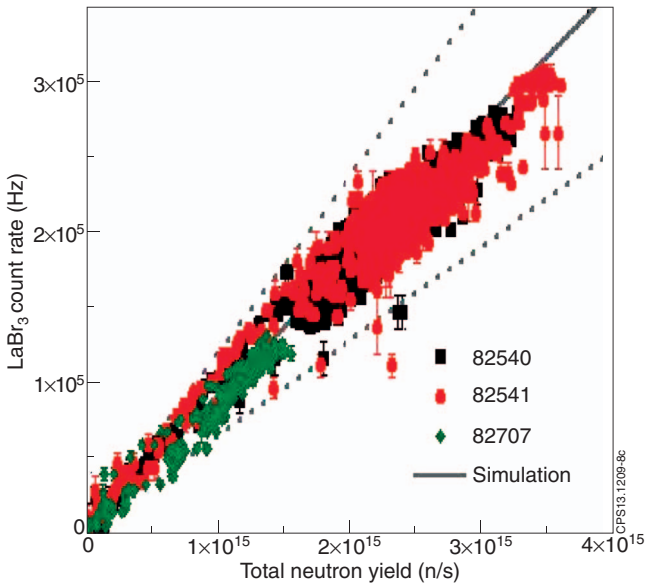

FIG. 8. $LaBr_3$(Ce) detector count rate as a function of the JET total neutron yield. Scattered points are from different JET discharges. The dashed lines correspond to the uncertainty on the slope for the linear relation between the $LaBr_3$(Ce) counting rate and the JET neutron yield, as predicted by simulations.

the MCNP result. For example, the peak at 0.8 MeV can be attributed to the interaction of fast neutrons on iron, an abundant element in most tokamak structures. Similarly, we expect that environmental γ-rays induced by neutron interactions can fill the gaps in the energy region 1–1.5 MeV of the simulated spectrum. The second reason that could explain such differences is that the simulation considers only 2.5 MeV monoenergetic neutrons, and does not include other components of the neutron spectrum. For example, a deuterium plasma can also generate the so-called triton burn up neutrons.[24,25] These are 14 MeV neutrons born from deuterium-tritium reactions (here, tritium is generated in the plasma by $d + d \rightarrow p + t$) and constitute about 1% of the total neutron emission. The corresponding contribution to the $LaBr_3$ signal can be estimated to be about 2%, using the results that are presented later in Sec. V. A more detailed MCNP model could be developed to account for these effects. This goes however beyond the level of accuracy needed for our applications.

As a final test of the MCNP model, we can compare the predicted detector count rate as a function of the total neutron yield of JET with that measured (see Fig. 8). Three different discharges have been considered with NBI powers up to 17 MW, corresponding to neutron yields as high as 4×10^{15} neutrons/s. Measurements have been integrated on time windows of 0.04 s. Errors are from counting statistics.

Simulations of neutron transport from the plasma along the detector line of sight[21] predict the ratio of neutron fluence on the detector to the total neutron yield of JET to be $(1.36 \pm 0.4) \times 10^{-10}$. This value is known with 30% uncertainty as it can vary depending on plasma shapes and neutron emission profiles. According to the MCNP simulation, the number of counts on the detector per incoming neutron is 0.76, of which 88% are above the 200 keV threshold used in the measurement. For this reason the predicted linear function relating the $LaBr_3$(Ce) count rate to the total JET neutron yield has a slope of $0.76 \times 0.88 \times (1.36 \pm 0.4) \times 10^{-10} = (0.9 \pm 0.3) \times 10^{-10}$, while the predicted intercept is the intrinsic background count rate 1.5×10^3 of the $LaBr_3$(Ce) crystal.

Table II compares the parameters of the linear function predicted by the simulations to the same parameters obtained from a linear fit of the experimental data in Figure 8. Results are in good agreement. The scattering of the data points around the best fit line is mostly due to neutron transport to the detector, that depends on plasma shapes and neutron emission profiles (see details in Ref. 21). The dashed lines in the figure correspond to the ±30% uncertainty on the predicted slope of the $LaBr_3$(Ce) count rate as a function of the total JET neutron yield. The scattering of the experimental data lies within these limits.

V. $LaBr_3$(Ce) RESPONSE TO 14 MeV NEUTRONS FROM DT REACTIONS

Based on the results for 2.5 MeV neutrons, we can discuss the expected $LaBr_3$(Ce) response to 14 MeV neutrons from deuterium-tritium plasmas. More nuclear processes play a role at this neutron energy. Although inelastic scattering cross sections are reduced for 14 MeV neutrons with respect to 2.45 MeV neutrons by a factor 3 (see Fig. 3), Fig. 9 shows that (n,2n) reactions can occur at 14 MeV. These are threshold reactions that are active above 9 MeV, 10 MeV, or 11 MeV for

TABLE II. Parameters of the linear function relating the $LaBr_3$(Ce) count rate to the total JET neutron yield, as obtained from measurements (left) and simulations (right).

	Measurements (linear fit)	Predicted from simulations
Slope	0.88×10^{-10}	$(0.9 \pm 0.3) \times 10^{-10}$
Intercept	2×10^3	1.5×10^3

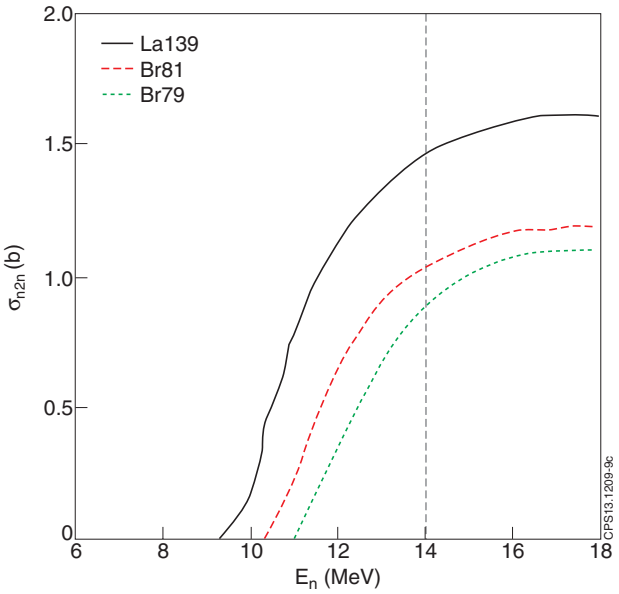

FIG. 9. (n,2n) reaction cross sections for the three isotopes of $LaBr_3$.[17] The dashed line corresponds to 14 MeV.

^{139}La, ^{81}Br, and ^{79}Br, respectively, with an increasing cross section as a function of the mass number A. The two neutrons resulting from each (n,2n) reaction can themselves be a source of signal, since they have enough energy to undergo inelastic scattering reactions with the other nuclei into the large crystal volume. The nuclei left behind by (n,2n) process, which are produced at mass number A-1, are generated in an excited state and, in turn, de-excite by emission of γ-rays. For this reason, a higher counting rate can be expected from 14 MeV neutrons than from 2.5 MeV. Besides, the A-1 nuclei ^{78}Br and ^{80}Br bred by (n,2n) reactions are unstable and undergo a β decay with a half life of 6 and 17 min, respectively. Their activity can be ignored for short discharges (say, a few seconds), such as those at JET, but will give a large contribution to the background counting rate for long tokamak discharges, like those expected at ITER.

Preliminary MCNP simulations have been performed for 14 MeV neutrons using the same method and simplifications discussed for 2.5 MeV. In the model, 14 MeV neutrons are impinging on the front side of a 3 in. $\times$ 6 in. $LaBr_3$ crystal. A first simulation is carried out to determine the number of photons emitted per impinging neutron via inelastic scattering or following a (n,2n) reaction. The number of neutrons that undergo (n,2n) reactions also gives the number of radioactive nuclei produced. The results of these simulations are presented in Table III. Using these values we can make a first prediction of the detector-counting rate. Here we note that, when the neutron flux is not constant as a function of time, the corresponding $LaBr_3$(Ce) counting rate is not necessarily proportional to the instantaneous flux. The reason is that the amount of radiation from β decays of ^{78}Br and ^{80}Br at time t depends on the number of radioactive A-1 nuclei produced at time $t - \Delta t$ and is thus proportional to the neutron flux at that time. For the sake of clarity, we shall here assume a constant neutron flux and we limit the estimation of the counting rate to the cases of a very short pulse ($t \ll 1$ min) and a very long one ($t \gg 20$ min). The numbers of counts we obtain per 14 MeV neutrons are 1.3 and 1.7 in the two cases, respectively. An energy threshold of $E_\gamma = 2$ keV in the γ-ray spectrum is assumed.

TABLE III. Summary of MCNP simulation results considering 14 MeV neutrons on a 3 in. $\times$ 6 in. $LaBr_3$(Ce) detector.

(n,2n) reactions per neutron	0.70
Emitted γ-rays per neutron	1.87
Radioactive ^{78}Br nuclei produced per neutron	0.23
Radioactive ^{80}Br nuclei produced per neutron	0.23
Counts per neutron ($t \ll 1$ min)	1.3
Counts per neutron ($t \gg 20$ min)	1.7

Preliminary experiments at FNG were also dedicated to measurements of background induced by 14 MeV neutrons. The fluence to the detector was 3.8×10^5 neutrons s^{-1}. This figure was given by the standard neutron counting diagnostics of FNG, which is based on a calibrated alpha detector, which measures alpha particles from the target deuterium-tritium reaction. The measured detector count rate was 5.2×10^5 s^{-1}, in the limit case of a short pulse. This yields 1.4 counts per 14 MeV neutron, which is in agreement with the predicted value (1.3) within 10%.

The measured energy spectrum of a 3 in. $\times$ 6 in. $LaBr_3$(Ce) detector is shown in Fig. 10. The calibration was obtained from ^{60}Co and ^{137}Cs laboratory sources. Several structures are observed, which are the result of γ-rays induced by neutron interactions. The spectrum is however rather flat at high energies ($E_\gamma > 3$ MeV). This is again promising in view of γ-ray measurements for fusion plasma diagnostics, as γ-rays from plasma reactions are mostly expected in the range 2 MeV $< E_\gamma <$ 6 MeV.

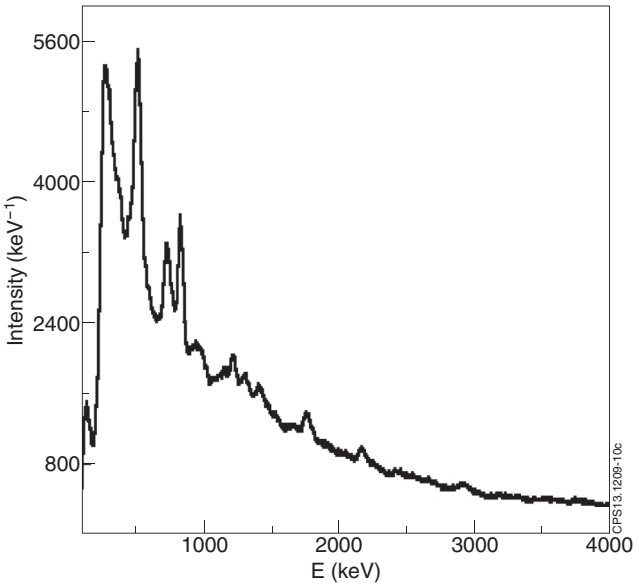

FIG. 10. Energy spectrum measured at FNG using 14 MeV fusion neutrons on a $LaBr_3$(Ce) scintillator.

VI. OUTLOOK AND IMPLICATIONS FOR ITER

At ITER, γ-ray spectroscopy has been proposed for fast ion diagnostics in high power plasmas and, in particular, for α particle diagnosis. $LaBr_3$(Ce) is currently the most promising scintillator given its high rate capability and resistance to neutron damage. The possibility to implement a γ-ray camera system composed of an array of $LaBr_3$(Ce) crystals is currently under study for ITER.[26] One of the main challenges is the background on the detector produced by high neutron fluxes up to 10^8–10^9 neutrons cm^{-2} s^{-1} at the possible detector position without neutron filters. The present work aims at contributing to that particular problem. The fact that, as shown in Figure 1, neutron induced background is mostly distributed on the low energy part of the spectrum, is promising for γ-ray observations from fast ions. However, the overall background count rate of the detector must also be kept sufficiently low, in order not to exceed its few MHz total count rate capability, leading to paralysis. Further work needs to be addressed to the design of neutron attenuators that can reduce the overall detector load at an acceptable level to enable measurements. A promising candidate is ^{6}LiH, as both ^{6}Li and H, being light nuclei, are good neutron moderators. Besides, ^{6}Li is also a neutron absorber, with a capture cross section of 3×10^3 b for thermalized neutrons. Clearly, a deeper understanding of the $LaBr_3$(Ce) response to 14 MeV neutrons is a preliminary requirement for the attenuator design.

VII. CONCLUSION

The response of a 3 in. $\times$ 6 in. $LaBr_3$(Ce) detector to 2.5 MeV neutrons has been measured to understand the relevance of neutron induced background in view of γ-ray measurements at ITER.

The experiments were carried out at the FNG neutron source and, with deuterium plasmas, at the ASDEX Upgrade and JET tokamaks, showing a remarkable similarity. A simple MCNP model has been implemented that can reproduce the experimental data both in terms of the main features of the pulse height spectrum and expected counting rate. The model reveals that inelastic scattering of 2.5 MeV neutrons with lanthanum and bromine nuclei gives the most important contribution to the response. Based on the results for 2.5 MeV neutrons, first extrapolations to 14 MeV neutrons show that (n,2n) reactions will play a significant role at this energy, yielding an increased contribution to the background. The presented results are of relevance for the design of γ-ray diagnostics of fusion burning plasmas, such as ITER.

ACKNOWLEDGMENTS

This work was supported by EURATOM and carried out within the framework of the European Fusion Development Agreement. The views and opinions expressed herein do not necessarily reflect those of the European Commission.

[1] A. Fasoli, C. Gormenzano, H. L. Berk, B. Breizman, S. Briguglio, D. S. Darrow, N. Gorelenkov *et al.*, "Physics of energetic ions," Nucl. Fusion **47**(6), S264 (2007).

[2] V. G. Kiptily, F. E. Cecil, and S. S. Medley, "Gamma ray diagnostics of high temperature magnetically confined fusion plasmas," Plasma Phys. Controlled Fusion **48**(8), R59 (2006).

[3] M. Tardocchi, M. Nocente, and G. Gorini, "Diagnosis of physical parameters of fast particles in high power fusion plasmas with high resolution neutron and gamma-ray spectroscopy," Plasma Phys. Controlled Fusion **55**(7), 074014 (2013).

[4] V. G. Kiptily, F. E. Cecil, O. N. Jarvis, M. J. Mantsinen, S. E. Sharapov, L. Bertalot, S. Conroy *et al.*, "γ-ray diagnostics of energetic ions in JET," Nucl. Fusion **42**(8), 999 (2002).

[5] M. Tardocchi, M. Nocente, I. Proverbio, V. G. Kiptily, P. Blanchard, S. Conroy, M. Fontanesi *et al.*, "Spectral broadening of characteristic γ-ray emission peaks from ^{12}C (^{3}He, pγ)^{14} N reactions in fusion plasmas," Phys. Rev. Lett. **107**(20), 205002 (2011).

[6] M. Nocente, M. Tardocchi, V. G. Kiptily, P. Blanchard, I. Chugunov, S. Conroy, T. Edlington *et al.*, "High-resolution gamma ray spectroscopy measurements of the fast ion energy distribution in JET ^{4}He plasmas," Nucl. Fusion **52**(6), 063009 (2012).

[7] F. E. Cecil and D. E. Newman, "Diagnostics of high temperature deuterium and tritium plasmas by spectrometry of radiative capture reactions," Nucl. Instrum. Methods Phys. Res. **221**(2), 449–452 (1984).

[8] I. Proverbio, M. Nocente, V. G. Kiptily, M. Tardocchi, G. Gorini, and JET-EFDA Contributors, "The ^{12}C (^{3}He, pγ) ^{14}N reaction cross section for γ-ray spectroscopy simulation of fusion plasmas," Rev. Sci. Instrum. **81**(10), 10D320 (2010).

[9] M. Nocente, M. Tardocchi, A. Olariu, S. Olariu, R. C. Pereira, I. N. Chugunov, A. Fernandes *et al.*, "High resolution gamma ray spectroscopy at MHz counting rates with $LaBr_3$ scintillators for fusion plasma applications," IEEE Trans. Nucl. Sci. **60**(2), 1408–1415 (2013).

[10] M. Nocente, M. Garcia-Munoz, G. Gorini, M. Tardocchi, A. Weller, S. Akaslompolo, R. Bilato *et al.*, "Gamma-ray spectroscopy measurements of confined fast ions on ASDEX Upgrade," Nucl. Fusion **52**(9), 094021 (2012).

[11] E. V. D. Van Loef, P. Dorenbos, C. W. E. Van Eijk, K. W. Krämer, and H. U. Güdel, "Scintillation properties of $LaBr_3$:Ce^{3+} crystals: Fast, efficient and high-energy-resolution scintillators," Nucl. Instrum. Methods Phys. Res. A **486**(1), 254–258 (2002).

[12] R. Nicolini, F. Camera, N. Blasi, S. Brambilla, R. Bassini, C. Boiano, A. Bracco *et al.*, "Investigation of the properties of a 1″ × 1″ $LaBr_3$:Ce scintillator," Nucl. Instrum. Methods Phys. Res. A **582**(2), 554–561 (2007).

[13] M. Nocente, M. Tardocchi, I. Chugunov, R. C. Pereira, T. Edlington, A. M. Fernandes, D. Gin *et al.*, "Energy resolution of gamma-ray spectroscopy of JET plasmas with a $LaBr_3$ scintillator detector and digital data acquisition," Rev. Sci. Instrum. **81**, 10D321 (2010).

[14] O. Roberts, P. Joshi, D. Jenkins, B. Wadsworth, and A. Tuff, "Neutron response of 1.5″ $LaBr_3$:Ce crystal scintillators for PARIS," http://paris.ifj.edu.pl/documents/detectors/Ce.pdf (2008).

[15] M. Martone, M. Angelone, and M. Pillon, "The 14 MeV Frascati neutron generator," J. Nucl. Mater. **212–215**, 1661–1664 (1994).

[16] M. Tardocchi, L. I. Proverbio, G. Gorini, G. Grosso, M. Locatelli, I. N. Chugonov, D. B. Gin *et al.*, "Gamma ray spectroscopy at high energy and high time resolution at JET," Rev. Sci. Instrum. **79**(10), 10E524 (2008).

[17] See http://atom.kaeri.re.kr/ for cross section database.

[18] C. Cazzaniga, G. Croci, L. Giacomelli, G. Grosso, M. Nocente, M. Tardocchi, and G. Gorini, "$LaBr_3$ scintillator response to admixed neutron and γ-ray fluxes," Nucl. Instrum. Methods Phys. Res. A **732**, 384–387 (2013).

[19] C. Hellesen, M. Albergante, E. A. Sundén, L. Ballabio, S. Conroy, G. Ericsson, M. G. Johnson *et al.*, "Neutron spectroscopy measurements and modeling of neutral beam heating fast ion dynamics," Plasma Phys. Controlled Fusion **52**(8), 085013 (2010).

[20] G. Tardini, A. Zimbal, B. Esposito, F. Gagnon-Moisan, D. Marocco, R. Neu, H. Schuhmacher, and the ASDEX Upgrade Team, "First neutron spectrometry measurements in the ASDEX Upgrade tokamak," J. Instrum. **7**(03), C03004 (2012).

[21] M. G. Johnson, S. Conroy, M. Cecconello, E. A. Sundén, G. Ericsson, M. Gherendi, C. Hellesen *et al.*, "Modelling and TOFOR measurements of scattered neutrons at JET," Plasma Phys. Controlled Fusion **52**(8), 085002 (2010).

[22] The MCNPX website, see http://mcnpx.lanl.gov/.

[23] M. B. Chadwick *et al.*, "ENDF/B-VII. 0: Next generation evaluated nuclear data library for nuclear science and technology," Nucl. Data Sheets **107**(12), 2931–3060 (2006).

[24]L. Ballabio, J. Frenje, J. Källne, S. W. Conroy, G. Ericsson, M. Tardocchi, E. Traneus, and G. Gorini, "Measurement and interpretation of the spectrum of the triton burnup neutron emission from deuterium tokamak plasmas," Nucl. Fusion **40**(1), 21 (2000).
[25]H. Sjöstrand, G. Gorini, S. Conroy, G. Ericsson, L. Giacomelli, H. Henriksson, A. Hjalmarsson *et al.*, "Triton burn-up neutron emission in JET low current plasmas," J. Phys. D **41**(11), 115208 (2008).
[26]I. N. Chugunov, A. E. Shevelev, D. B. Gin, V. G. Kiptily, G. Gorini, M. Nocente, M. Tardocchi, D. N. Doinikov, V. O. Naidenov, and E. M. Khilkevitch, "Development of gamma-ray diagnostics for ITER," Nucl. Fusion **51**(8), 083010 (2011).

Paper VIII

Response of $LaBr_3$(Ce) scintillators to 14 MeV fusion neutrons

C. Cazzaniga[1,2], M. Nocente[1,2], M. Tardocchi[2], M. Rebai[1], M. Pillon[3], F. Camera[4], A. Giaz[4], L.Pellegri[4] and G. Gorini[1,2]

[1]*University of Milano Bicocca, Departement of Physics, Piazza della Scienza 3, Milano 20125, Italy*
[2]*Istituto di Fisica del Plasma, Associazione EURATOM-ENEA-CNR, via Roberto Cozzi 53, Milano 20125 , Italy*
[3]*Associazione EURATOM-ENEA sulla Fusione ENEA C.R. Frascati, Via E. Fermi, 45, 00044 Frascati (Roma), Italy*
[4]*University of Milano, Departement of Physics, Via Celoria 16, Milano 1-20133 Italy*
carlo.cazzaniga@mib.infn.it

ABSTRACT
The response of a 3"x3" $LaBr_3$(Ce) scintillator to 14 MeV neutron irradiation has been measured at the Frascati Neutron Generator and simulated by means of a dedicated MCNP model. Several reactions are found to contribute to the measured response, with a key role played by neutron inelastic scattering and (n,2n) reactions on ^{79}Br, ^{81}Br and ^{139}La isotopes. An overall 43% efficiency to 14 MeV neutron detection above an experimental threshold of 0.35 MeV is calculated and confirmed by measurements. Post irradiation activation of the crystal has been also observed and is explained in terms of nuclear decays from the short lived ^{78}Br and ^{80}Br isotopes produced in (n,2n) reactions. The results presented in this paper are of relevance for the design of γ-ray detectors in burning plasma fusion experiments of the next generation, such as ITER, where capability to perform measurements in an intense 14 MeV neutron flux is required.

1. Introduction

Gamma-ray spectroscopy is among the diagnostics proposed to measure confined energetic ions in a high performance burning plasma, where the plasma behaviour is dominated by suprathermal ions [1]. Energetic particles in the MeV range are naturally present in a burning deuterium-tritium plasma due to the main fusion reaction t(d,n)α and to auxiliary heating schemes. In a high power fusion device, γ-ray emission results from interactions between the energetic ions and impurities that are naturally found in the plasma [2-4]. Parameters of the fast ion energy distribution can be obtained by combining information on the intensity and shape of characteristic peaks of γ-ray reactions occurring in the plasma [5-7] as demonstrated with high energy resolution measurements in present tokamak devices [8-10].
Instrumentation for γ-ray spectroscopy measurements in a burning plasma (eg. ITER [11]) requires, in addition to good energy resolution, high counting rate capabilities (>MHz).
$LaBr_3$(Ce) scintillators [12,14] are good candidates to meet these requirements, thanks to their fast scintillation time, high light yield and resilience to neutron damage. First measurements at low counting rates (kHz) at present tokamak devices have been recently performed [8,15]. Dedicated tests at nuclear accelerators demonstrated high counting rate performances up to 4 MHz without any significant degradation of the γ-ray energy resolution [7].
In a high power fusion device, besides coping with high counting rates, the detector will have to measure in a harsh environment at high neutron fluxes. A detailed study of the scintillator response to neutron irradiation is thus needed for the design of suitable line of sights, neutron filters and to aid in the measurement interpretation.
In a previous work, we presented the response of $LaBr_3$(Ce) scintillators to 2.5 MeV neutron irradiation [16], which is the dominant component in a deuterium plasma. Measurements were performed at the Frascati Neutron Generator (FNG) with 2.5 MeV mono-energetic neutrons and at tokamak devices run in deuterium. A dedicated MCNP model was used to interpret the results.

In this paper, we complete our previous investigation by presenting the response of $LaBr_3$(Ce) scintillators to 14 MeV neutron irradiation, which is most interesting for operations in deuterium-tritium plasmas. Measurements were carried out at FNG using a tritium doped target, rather than the deuterium doped target employed for 2.5 MeV neutron irradiation.
Similarly to our previous investigation, an MCNP model is used to aid in the interpretation of the results and, in particular, to identify the most relevant processes determining the measured response.

2. 14 MeV neutron measurements at FNG

At the Frascati Neutron Generator (FNG) 14 MeV neutron emission is obtained by reactions between a 300 keV deuterium beam impinging onto a tritium doped titanium target [17]. In our experiment, a 3"x3" (diameter x height) $LaBr_3$(Ce) scintillator was placed at 90 degrees with respect to the incoming deuterium beam, at the same height of the target. The distance from the target (1.25 m) was chosen so to obtain a neutron flux of about $2.4 \cdot 10^3$ n/(cm^2·s) on the detector front surface for a neutron yield of $5 \cdot 10^8$ n/s generated by the machine. The latter was measured by the standard neutron counting diagnostic of FNG, which consists of an absolutely calibrated detector measuring alpha particles produced by deuterium-tritium reactions in the target. The impinging neutron energy spectrum at the detector position was centred at 14 MeV, with an estimated 1% (FWHM) energy spread.
The light emitted by the scintillator was collected by a photo-multiplier tube and signals were fed directly into a 12 bit - 250 Msample/s CAEN DT5720 digitizer. Each waveform above a selectable threshold was stored and processed off-line using a dedicated algorithm based on pulse fitting [7]. The pulse height spectrum was energy calibrated with laboratory ^{137}Cs and ^{60}Co radioactive sources. An energy resolution of 3.2% was measured at the 0.662 MeV line of ^{137}Cs, which is close to the nominal value expected for $LaBr_3$ crystals (about 3%). In the following, the letter E indicates the γ-ray (or electron equilavent) energy; a subscript is otherwise used to indicate the energy of a different particle.
Fig. 1 shows the measured energy spectrum during 14 MeV neutron irradiation. Data were integrated over a time of 120 seconds. Gamma-rays peaks at distinctive energies and more complex structures can be clearly observed in the figure, with most of the events in the region E<3 MeV, where the detection efficiency to gamma-rays is known to be higher [18]. There is however a clear tail of events extending to energies up to about E=14 MeV, with an estimated uncertainty of 500 keV on the end point, due to the non-linearity of the crystal. An average counting rate of $8 \cdot 10^4$ cps above the experimental E=0.35 MeV threshold was observed during measurements. After about 1 h of 14 MeV neutron irradiation, the FNG beam was switched off, and a post-irradiation measurement was started. Fig. 1 shows the spectrum measured 10 minutes after irradiation, which can be compared to that obtained during irradiation, for the same experiment time. There is a clear difference in magnitude and shape between the two spectra. No events are found above E=4 MeV in the post-irradiation spectrum. Many of the structures observed during irradiation have also disappeared and the shape of the spectrum is now dictated by the superposition of beta decays of different short lived unstable isotopes (see section 5). An intense 511 keV annihilation peak still remains, together with a second peak at E=0.8 MeV. The post irradiation spectrum can also be compared to that due to the crystal intrinsic radioactivity (figure 1, dotted line). The latter was measured at FNG right before irradiation and also shows a 662 keV peak due to a ^{137}Cs calibration source. Again, we find no similarity between the two spectra, both in terms of structure and magnitude, which indicates that the post-irradiation spectrum must be dominated by decays of unstable isotopes generated by 14 MeV neutron irradiation. The contribution of intrinsic radioactivity to the counting rate before neutron irradiation was 700 cps, a value much lower than the (average) $2.5 \cdot 10^4$ cps measured 10 minutes after neutron irradiation.

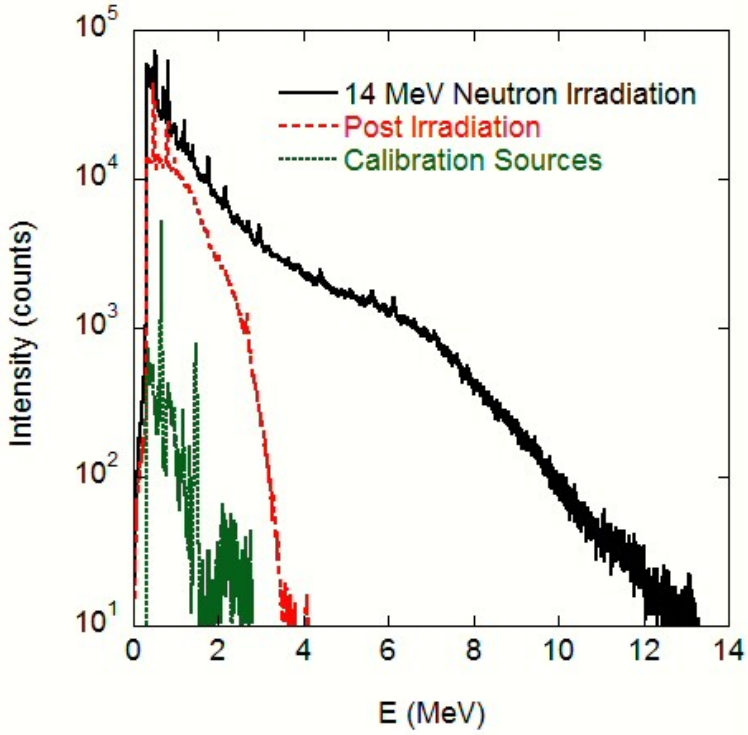

Fig.1: Energy spectrum measured at FNG with a 3''x3'' $LaBr_3$ detector during 14 MeV neutron irradiation (solid line). The spectrum is compared to that taken post (dashed) and before (dotted) irradiation. In all cases, measurements are integrated for 120 seconds.

3. Monte Carlo simulation of the $LaBr_3$ response

As discussed in our previous paper on 2.5 MeV neutrons [16], nuclear interactions between 14 MeV neutrons and lanthanum and bromine isotopes dominate the measured response. ^{79}Br and ^{81}Br are the Bromine isotopes in the crystal, with approximately the same abundance, while ^{139}La is the only stable isotope of Lanthanum. Few other isotopes are also present, but only in trace concentrations and were not considered in the analysis. Besides inelastic scattering, the main neutron interaction mechanism with these isotopes is the production of secondary particles (neutrons, protons, deuterons, alpha particles) which in turn deposit their energy into the crystal, resulting in recordable pulses. The cross sections for the most relevant reactions are shown in figure 2. It is worth noticing here that there is a clear difference between the dominant neutron interaction channels with $LaBr_3$ at E_n=2.5 MeV and E_n=14 MeV: while at E_n=2.5 MeV inelastic scattering dominates the response [16], secondary particle production is the most important process at E_n > 10 MeV and, particularly, (n,2n) reactions. The latter have a multiplicative effect on the detector response: secondary neutrons generated in the crystal can in turn undergo nuclear inelastic scattering, which generates excited nuclear states decaying by γ-ray emission, that adds up to the detector gamma-ray load due to inelastic scattering of the primary (14 MeV) neutrons. Among the reactions leading to charge particle production, proton generation due to n+^{79}Br interactions is the most relevant.

A MCNP [19] model was implemented to interpret the experimental results, assuming a beam of mono-energetic 14 MeV neutrons directed onto a 3"x3" $LaBr_3$ and tracking all the processes listed in Figure 2. A summary of the results of this simulation is presented in Table 1, where numbers are normalized per 14 MeV neutron history. Of most interest is γ-ray production, that exceeds unity with 1.17 γ-rays produced per 14 MeV neutron. This result can be explained by the large additional contribution of secondary neutrons generated in the crystal (0.45), a fraction of which also undergoes inelastic scattering. Here we note that γ-rays born in the crystal volume have a significant detection probability (about 40%), given the large volume, high density and high Z of the scintillator, and are thus of relevance to understand the measured crystal response. Charged particle production

is less important, mostly because of the smaller cross sections of the associated processes, although, on the other hand, positive ions have a detection probability approaching 100%. For comparison, the simulation was also run for a 3"x6" crystal, which is the size of the scintillator currently in use at JET [15]. As noted from Table 1, doubling the crystal volume determines a 55% increase in secondary neutron production, which is turn enhances gamma-ray creation by almost the same amount. Charged particle production remains small.

The contribution of secondary neutron/ gamma-rays and other particles to the crystal response was also analysed in terms of spectral shapes, as shown in Fig.3 for the 3"x3" case. γ-rays dominate in the region E < 5 MeV, while proton production contributes most to the spectral shape at E > 5 MeV, leading to a change of slope in this region. Alpha particle and deuterium generation introduces two additional structures centred around E=6 and E=10 MeV respectively, which are however an order of magnitude lower that that due to protons and would be hard to distinguish in the overall detector response, without using pulse shape discrimination algorithms as investigated in recent studies [20]. By summing up all the different contributions, we can determine a 43% detection efficiency to 14 MeV neutrons above the experimental threshold of 0.35 MeV, based on the MCNP results.

In order to compare the simulated response with that measured, a separated calculation of the (external) neutron/gamma-ray background in the FNG hall at the detector position was performed, which was finally added to the (intrinsic) response described above. In fact, the radiation field impinging on the detector in the FNG hall is a complex admixture of neutron and gamma-rays. Of these two, the neutron field has a dominant 14 MeV (direct) component, with an additional scattering contribution at the 50% level, the latter arising from direct neutrons that degrade their energy by interacting with materials in the experimental hall. Gamma-ray background originates from inelastic scattering of the direct neutrons. For the calculation of the scattered neutron and gamma-ray fields, we relied on an existing MCNP model of the FNG facility [22]. Its results were in turn used as input to separately determine the crystal response to such background for comparison with measurement.

Table 2 summarizes the output of the calculations, with numbers normalized per 14 MeV neutron history. Scattered neutrons are responsible of about 50% of the detector load due to the primary component. Gamma-ray background contributes to a further 30% fraction. In terms of energy spectrum (Fig. 4), the scattered neutron component has an exponential shape without clear structures, while gamma-rays are manifested as distinctive peaks and dominate the E > 4.5 MeV region. Figure 4 also shows the response to direct 14 MeV neutrons (presented in figure 3) and which can be here compared to background. In order to obtain the γ-ray equivalent energy for the direct component, quenching effects were taken into account [23-25]. The finite energy resolution of the detector was included in Fig. 4 by convolution of the simulated spectra with a Gaussian function of energy dependent width. This was obtained from the measured value of 3.2% (FWHM/E) at 662 keV and assumed to follow the Poisson law, i.e. to scale as $E^{-½}$.

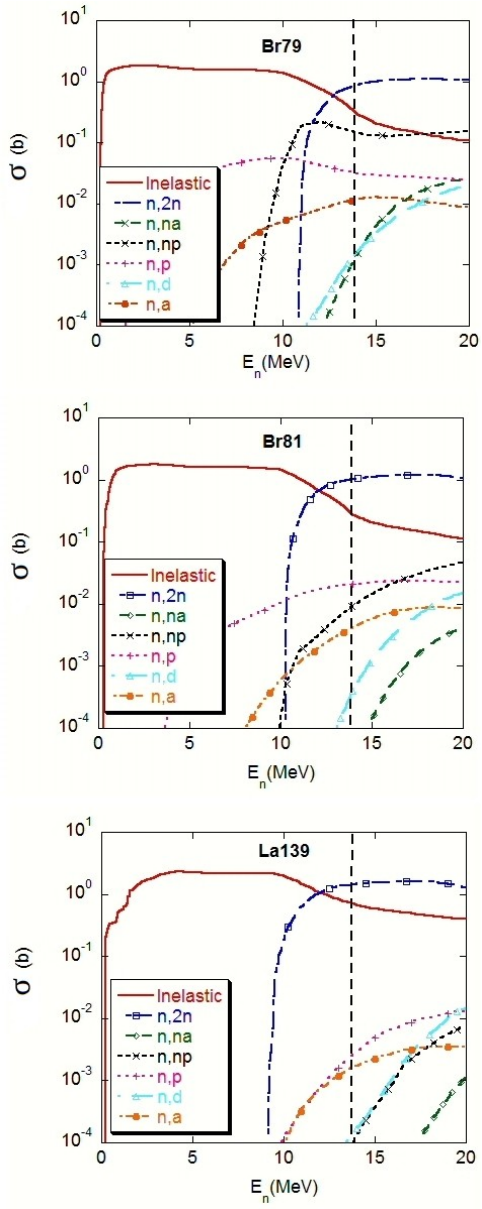

Fig.2: Cross sections for neutron reactions with ^{79}Br, ^{81}Br and ^{139}La isotopes leading to neutron, alpha particle, proton and deuteron production in the final states. The continuous line indicates the nuclear inelastic scattering cross section. Data taken from [20].

	$LaBr_3$ 3"x6"	$LaBr_3$ 3"x3"
gamma creation	1.868	1.178
neutron creation (n,2n)	$6.982 \cdot 10^{-1}$	$4.513 \cdot 10^{-1}$
proton creation	$1.53 \cdot 10^{-2}$	$9.54 \cdot 10^{-3}$
deuteron creation	$1.13 \cdot 10^{-3}$	$7.63 \cdot 10^{-4}$
alpha creation	$1.58 \cdot 10^{-3}$	$1.10 \cdot 10^{-3}$

Table 1: Summary of MCNP simulations of the $LaBr_3$ response to 14 MeV neutrons. Simulations were performed for two different crystal dimensions (3"x3" and 3"x6"). Results are normalized per 14 MeV neutron history.

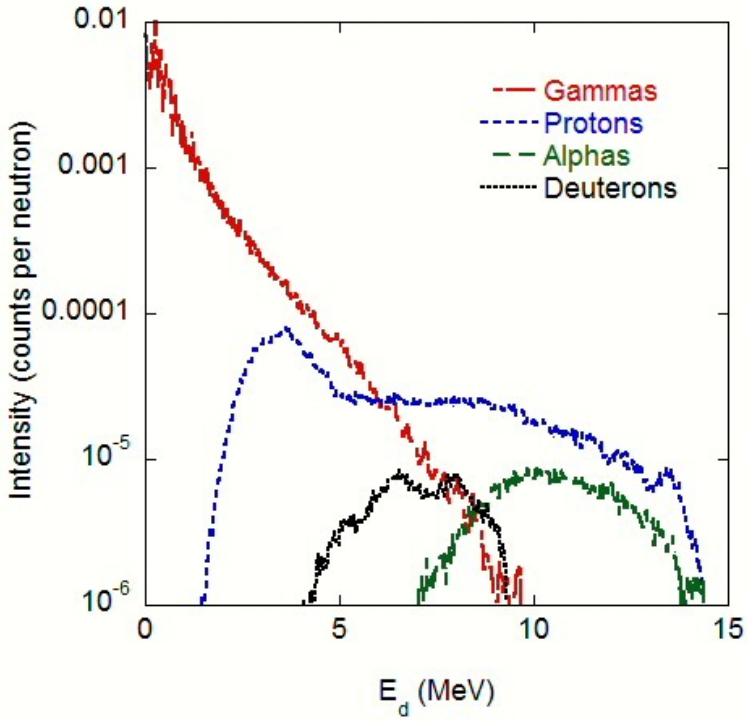

Fig.3: Deposited energy spectrum from secondary particles produced by uniform irradiation of a 3"x3" LaBr3 crystal with 14 MeV neutrons, as calculated by MCNP.

Counts from direct 14 MeV neutrons	0.432
Counts from scattered neutrons at FNG	0.206
Counts from gamma background at FNG	0.138
Sum	0.776

Table 2: Summary of MCNP simulations of primary and background radiation (above a threshold of 350 keV) recorded by $LaBr_3$ in the 14 MeV irradiation experiment at FNG, at the detector position. Results are normalized per 14 MeV neutron history.

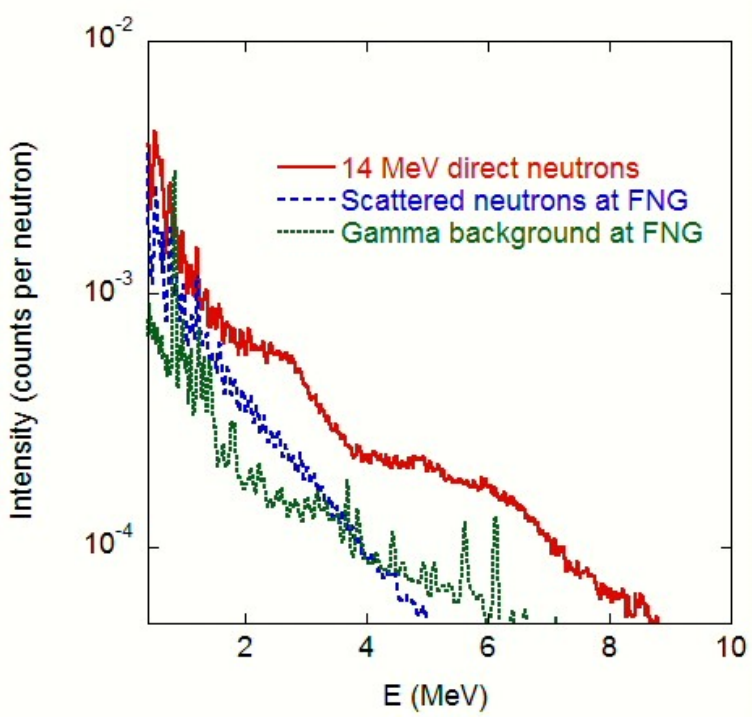

Fig.4: Simulated pulse height spectra from direct 14 MeV neutrons, scattered neutrons and gamma-ray background recorded at the detector position in the FNG irradiation experiment. Energies are electron equivalent and take into account quenching effect.

4. Data analysis

The results of the MCNP simulations are compared to the measured spectrum in Fig. 5. To this extent, the three components of Fig. 4 (direct and scattered neutrons, gamma-ray background) were summed to obtain the expected measured spectrum during the FNG irradiation experiment. The comparison is limited to 3 orders of magnitude below the most intense spectral structures, a range that well exceeds the accuracy needs for the use of $LaBr_3$ in gamma-ray spectroscopy applications at ITER. In terms of counting rates above the 0.35 MeV experimental threshold, we find that measurement and simulation agree within 5%. A similar good level of agreement also holds as far as the overall shape of the spectrum is concerned. In particular, when shown in logarithmic scale, the measured spectrum exhibits the change of slope predicted by MCNP in the region 5 - 10 MeV and due to the contribution of secondary charged particles (see section 3). At a more detailed level, we find that most of the gamma-ray peaks observed in the measurement are also reproduced by the simulation, although, at times, there is a mismatch in terms of intensity. In few cases only, peaks predicted in the simulation do not appear in the measurement, and vice versa. We ascribe these minor differences to uncertainties in the cross sections used by MCNP, especially since they are derived by statistical models, which may not accurately depict reality [26]. A second source of uncertainty arises from the FNG model, which may not specify the material composition of the experimental hall at a level of detailed necessary to explain all peaks found in the measurement. Although these minor discrepancies, we consider the level of agreement between simulation and measurement as satisfactory, given the capability of the simulation to match well the experimental counting rate and spectral shape, which are of most interest to design filters for neutron background reduction on the scintillator at ITER [11]. In this context, we note in particular that the measured spectrum is rather structureless in the range E=3 to 5 MeV, i.e. where gamma-ray lines from plasma reactions of principal interest in thermonuclear fusion applications occur.

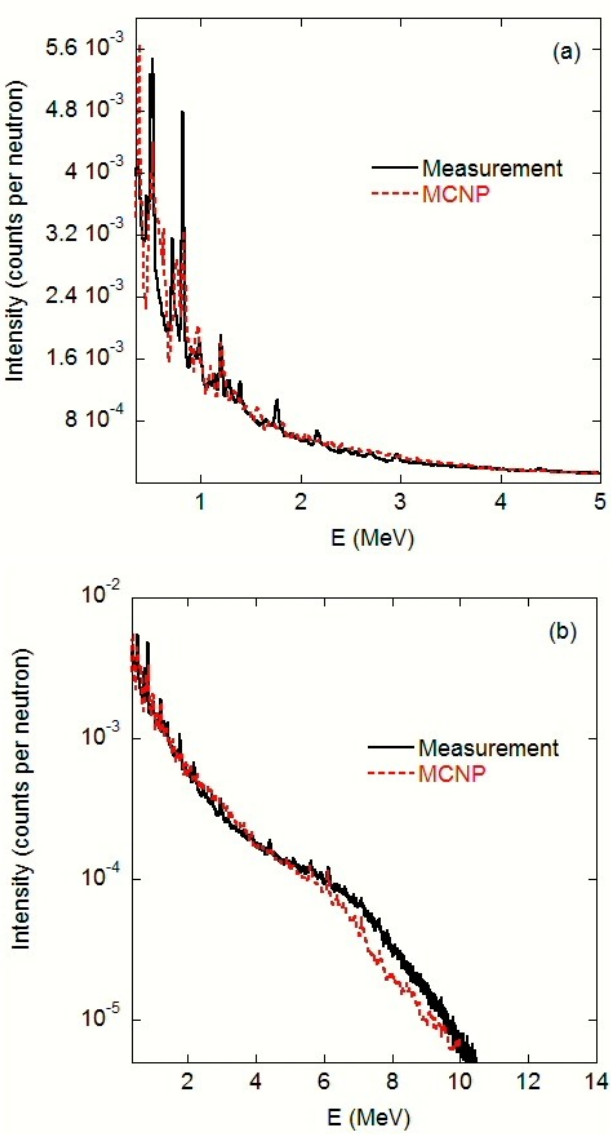

Fig.5: Measured and simulated energy spectrum (linear and log scale) of the $LaBr_3$ response to 14 MeV neutrons at FNG. The simulated spectrum is the sum of the three components (direct and scattered neutrons, gamma-ray background) shown separately in Fig. 4. The direct component also includes events from secondary charged particles, as discussed with reference to Fig. 3.

5. Short lived activation induced by 14 MeV neutrons

Activation of the $LaBr_3$ crystal is of interest in view of ITER for two reasons. First, a significant activation level requires some special care when handling the crystal after an extended irradiation period. Secondly, the activation itself is a background source that interferes with the measured signal and is thus of relevance for signal-to-noise ratio considerations in view of measurements at ITER. In order to investigate the activation of the crystal induced by 14 MeV neutrons, post-irradiation measurements were carried out at FNG. $LaBr_3$(Ce) was first irradiated for about 1.5 h at a total neutron yield of $1.5 \cdot 10^{10}$ neutrons per second, corresponding to a flux on the detector front surface of approximately $5.4 \cdot 10^5$ neutrons/(s·cm^2). A measurement of the residual counting rate, as a function of time, due to the crystal activation was then started immediately after FNG had been

switched off, with the results shown in Fig. 6. Data points were acquired every second, for 30 minutes.
Based on our previous analysis [16], short lived activation is expected to be due to ^{78}Br and ^{80}Br isotopes, which have a decay time of 540 s and 1500 s, respectively. ^{78}Br and ^{80}Br are produced by (n,2n) reactions on ^{79}Br and ^{81}Br. On the other hand, the (n,2n) reaction on ^{139}La produces ^{138}La, which has a half life of billions of years, and is therefore practically stable on the time scale of minutes.
The conclusions of our previous analysis are experimentally confirmed by a fit to the measurement of Fig.6 using the following equation

$$I = A \cdot exp\left(-\frac{t}{\tau_1}\right) + B \cdot exp\left(-\frac{t}{\tau_2}\right) + C \qquad (1)$$

where I indicates the intensity (counting rate) and t is the time. In equation 1 the time constants τ_1 and τ_2 were fixed and set to the decay times of ^{78}Br (540 s) and ^{80}Br (1500 s). The free fit parameters A, B are proportional to the initial number of ^{78}Br and ^{80}Br nuclei produced by 14 MeV irradiation. C is a fit parameter that takes into account long lived (τ >> 30 min) activation, such as that due to materials of the FNG hall that were also activated by 14 MeV neutrons.
As seen from Fig. 6, the fit reproduces very well the measurements, confirming the role of ^{78}Br and ^{80}Br as main responsible of the crystal post-irradiation activity. The values obtained for the fit parameters A,B and C are summarized in Table 3.

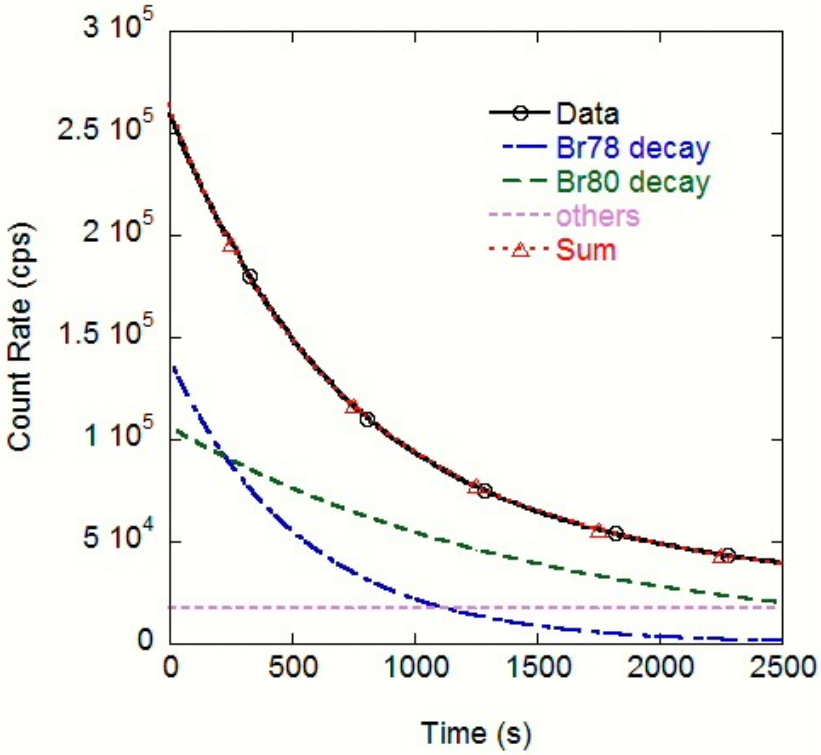

Fig.6: $LaBr_3$ counting rate as a function of time measured after 1.5 h of 14 MeV neutron irradiation at FNG. The measurement was started immediately after the machine switch off. A fit with eq. 1 is also shown (dashed line with symbols), together with individual curves for the three sources (^{78}Br, ^{80}Br and others) contributing to the measured activation (see text for details).

Fit Parameter	Value (cps)	Error (cps)
A	$1.279 \cdot 10^5$	$\pm 1.6 \cdot 10^2$
B	$1.005 \cdot 10^5$	$\pm 1.6 \cdot 10^2$
C	$1.794 \cdot 10^4$	$\pm 5 \cdot 10^1$

Table 3. Values of the fit parameters A,B and C as obtained by fitting data in Fig. 6 with Eq. 1

6. Conclusions

The response of a 3"x3" $LaBr_3$ crystal to 14 MeV neutron irradiation was measured at FNG in a dedicated experiment. The results were interpreted by means of a MCNP model of 14 MeV neutron interactions with $LaBr_3$, including background contributions from scattered neutrons and gamma-rays generated in the FNG experimental hall. A good overall agreement between simulation and measurements was found. The simulations revealed that (n,2n) reactions and nuclear inelastic scattering on ^{79}Br, ^{81}Br and ^{139}La isotopes are the dominant interaction processes between 14 MeV neutrons and the crystal. Reactions leading to the production of secondary charged particles are of relevance to explain events at deposited energies higher than 5 MeV. The overall efficiency of the 3"x3" detector to 14 MeV neutrons was found to be 43%, above an experimental threshold of 0.35 MeV. Measurements of the residual crystal activation after irradiation were also performed and were found to be dominated by decays of short lived ^{78}Br and ^{80}Br isotopes produced by (n,2n) reactions. The results presented in this paper are of relevance for the design of γ-ray detectors in burning plasma fusion experiments of the next generation, such as ITER, where capability to perform measurements in an intense 14 MeV neutron flux is required.

Acknowledgement

This project has received funding from the European Union's Horizon 2020 research and innovation programme under grant agreement number 633053. The views and opinions expressed herein do not necessarily reflect those of the European Commission.

References

[1] Fasoli, A., C. Gormenzano, H. L. Berk, B. Breizman, S. Briguglio, D. S. Darrow, N. Gorelenkov et al. "Physics of energetic ions." *Nuclear Fusion* 47, no. 6 (2007): S264.

[2] Kiptily, V. G., F. E. Cecil, and S. S. Medley. "Gamma ray diagnostics of high temperature magnetically confined fusion plasmas." *Plasma physics and controlled fusion* 48, no. 8 (2006): R59.

[3] Tardocchi, M., M. Nocente, and G. Gorini. "Diagnosis of physical parameters of fast particles in high power fusion plasmas with high resolution neutron and gamma-ray spectroscopy." *Plasma Physics and Controlled Fusion* 55.7 (2013): 074014.

[4] Kiptily, V. G., F. E. Cecil, O. N. Jarvis, M. J. Mantsinen, S. E. Sharapov, L. Bertalot, S. Conroy et al. "γ-ray diagnostics of energetic ions in JET." *Nuclear Fusion* 42, no. 8 (2002): 999.

[5] Cecil, F. E., and David E. Newman. "Diagnostics of high temperature deuterium and tritium plasmas by spectrometry of radiative capture reactions." *Nuclear Instruments and Methods in Physics Research* 221, no. 2 (1984): 449-452.

[6] Proverbio, I., M. Nocente, V. G. Kiptily, M. Tardocchi, G. Gorini, and JET-EFDA Contributors. "The ^{12}C (^{3}He, pγ) ^{14}N reaction cross section for γ-ray spectroscopy simulation of fusion plasmas." *Review of scientific instruments* 81, no. 10 (2010): 10D320-10D320.

[7] Nocente, M., M. Tardocchi, A. Olariu, S. Olariu, R. C. Pereira, I. N. Chugunov, A. Fernandes et al. "High Resolution Gamma Ray Spectroscopy at MHz Counting Rates With LaBr Scintillators for Fusion Plasma Applications." *Nuclear Science, IEEE Transactions on* 60, no. 2 (2013): 1408-1415.

[8] Nocente, M., M. Garcia-Munoz, G. Gorini, M. Tardocchi, A. Weller, S. Akaslompolo, R. Bilato et al. "Gamma-ray spectroscopy measurements of confined fast ions on ASDEX Upgrade." *Nuclear Fusion* 52, no. 9 (2012): 094021.

[9] Tardocchi, Marco, M. Nocente, I. Proverbio, V. G. Kiptily, P. Blanchard, Sean Conroy, M. Fontanesi et al. "Spectral Broadening of Characteristic γ-Ray Emission Peaks from ^{12}C (^{3}He, pγ)^{14} N Reactions in Fusion Plasmas." *Physical review letters* 107, no. 20 (2011): 205002.

[10] Nocente, Massimo, Marco Tardocchi, V. G. Kiptily, Patrick Blanchard, I. Chugunov, Sean Conroy, T. Edlington et al. "High-resolution gamma ray spectroscopy measurements of the fast ion energy distribution in JET 4He plasmas." *Nuclear Fusion* 52, no. 6 (2012): 063009.

[11] I.N. Chugunov, A.E. Shevelev, D.B. Gin, V.G. Kiptily, G. Gorni, M. Nocente, M. Tardocchi, D.N. Doinikov, V.O. Naidenov and E.M. Khilkevitch " Development of gamma-ray diagnostics for ITER", *Nucl. Fusion* 51 (2011) 083010

[12] Van Loef, E. V. D., P. Dorenbos, C. W. E. Van Eijk, K. W. Krämer, and H. U. Güdel. "Scintillation properties of $LaBr_3:Ce^{3+}$ crystals: fast, efficient and high-energy-resolution scintillators." *Nuclear Instruments and Methods in Physics Research Section A: Accelerators, Spectrometers, Detectors and Associated Equipment* 486, no. 1 (2002): 254-258.

[13] Nicolini, R., F. Camera, N. Blasi, S. Brambilla, R. Bassini, C. Boiano, A. Bracco et al. "Investigation of the properties of a 1 ″× 1 ″ $LaBr_3$:Ce scintillator." *Nuclear Instruments and Methods in Physics Research Section A: Accelerators, Spectrometers, Detectors and Associated Equipment* 582, no. 2 (2007): 554-561.

[14] Giaz, A., Pellegri, L., Riboldi, S., Camera, F., Blasi, N., Boiano, C., ... & Wieland, O. (2013). Characterization of large volume 3.5 ″× 8 ″$LaBr_3$: Ce detectors. *Nuclear Instruments and Methods in Physics Research Section A: Accelerators, Spectrometers, Detectors and Associated Equipment*, *729*, 910-921.

[15] Nocente, M., M. Tardocchi, I. Chugunov, R. C. Pereira, T. Edlington, A. M. Fernandes, D. Gin et al. "Energy resolution of gamma-ray spectroscopy of JET plasmas with a LaBr scintillator detector and digital data acquisition." *Review of scientific instruments* 81 (2010): 10D321.

[16] Cazzaniga, C., Nocente, M., Tardocchi, M., Croci, G., Giacomelli, L., Angelone, M., ... & Contributors, J. E. (2013). Response of $LaBr_3$ (Ce) scintillators to 2.5 MeV fusion neutrons. *Review of Scientific Instruments*, *84*(12), 123505.

[17] Martone, M., M. Angelone, and M. Pillon. "The 14 MeV frascati neutron generator." *Journal*

of nuclear materials 212 (1994): 1661-1664.

[18] Cazzaniga, C., Croci, G., Giacomelli, L., Grosso, G., Nocente, M., Tardocchi, M., ... & Weller, A. (2013). $LaBr_3$ scintillator response to admixed neutron and γ-ray fluxes. *Nuclear Instruments and Methods in Physics Research Section A: Accelerators, Spectrometers, Detectors and Associated Equipment*, *732*, 384-387.

[19] The MCNPX website: http://mcnpx.lanl.gov/

[20] Cross Section Database http://atom.kaeri.re.kr/

[21] Crespi, F. C. L., Camera, F., Blasi, N., Bracco, A., Brambilla, S., Million, B., ... & Owens, A. (2009). Alpha–gamma discrimination by pulse shape in $LaBr_3$: Ce and $LaCl_3$: Ce. *Nuclear Instruments and Methods in Physics Research Section A: Accelerators, Spectrometers, Detectors and Associated Equipment*, *602*(2), 520-524.

[22] Angelone, M., Pillon, M., Batistoni, P., Martini, M., Martone, M., & Rado, V. (1996). Absolute experimental and numerical calibration of the 14 MeV neutron source at the Frascati neutron generator. *Review of scientific instruments*, *67*(6), 2189-2196.

[23] Cazzaniga, C., Nocente, M., Tardocchi, M., Fazzi, A., Hjalmarsson, A., Rigamonti, D., ... & Gorini, G. (2014). Thin YAP: Ce and $LaBr_3$: Ce scintillators as proton detectors of a thin-film proton recoil neutron spectrometer for fusion and spallation sources applications. *Nuclear Instruments and Methods in Physics Research Section A: Accelerators, Spectrometers, Detectors and Associated Equipment*, *751*, 19-22.

[24] Fazzi, A., Nocente, M., Tardocchi, M., Varoli, V., Gorini, G., Lorenzoli, M., ... & Cazzaniga, C. (2013, October). A large area SiPM array coupled to a $LaBr_3$ crystal for a TPR spectrometer. In *Nuclear Science Symposium and Medical Imaging Conference (NSS/MIC), 2013 IEEE* (pp. 1-4). IEEE.

[25] M. Nocente, A. Fazzi, M. Tardocchi, C. Cazzaniga, M. Lorenzoli, C. Pirovano, M. Rebai, C. Uboldi, V. Varoli and G. Gorini, "Experimental investigation of silicon photomultipliers as compact light readout systems for gamma-ray spectroscopy applications in fusion plasmas", *Rev. Sci. Instrum*. 85 (2014) 11E108

[26] A.J. Koning, S. Hilaire, M.C. Duijvestijn, 〈http://www.talys.eu/tendl-2008/〉